National Library of Canada
Bibliothèque nationale du Canada

Canadian Theses Service
Service des thèses canadiennes

Ottawa, Canada
K1A 0N4

NOTICE

The quality of this microform is heavily dependent upon the quality of the original thesis submitted for microfilming. Every effort has been made to ensure the highest quality of reproduction possible.

If pages are missing, contact the university which granted the degree.

Some pages may have indistinct print especially if the original pages were typed with a poor typewriter ribbon or if the university sent us an inferior photocopy.

Reproduction in full or in part of this microform is governed by the Canadian Copyright Act, R.S.C. 1970, c. C-30, and subsequent amendments.

AVIS

La qualité de cette microforme dépend grandement de la qualité de la thèse soumise au microfilmage. Nous avons tout fait pour assurer une qualité supérieure de reproduction.

S'il manque des pages, veuillez communiquer avec l'université qui a conféré le grade.

La qualité d'impression de certaines pages peut laisser à désirer, surtout si les pages originales ont été dactylographiées à l'aide d'un ruban usé ou si l'université nous a fait parvenir une photocopie de qualité inférieure.

La reproduction, même partielle, de cette microforme est soumise à la Loi canadienne sur le droit d'auteur, SRC 1970, c. C-30, et ses amendements subséquents.

NL-339 (r. 88/04) c

Canada

UNIVERSITY OF ALBERTA

OXIDATION OF CARBON MONOXIDE ON PLATINUM CATALYSTS: KINETIC MODEL DISCRIMINATION USING EXPERIMENTAL STEADY-STATE MULTIPLICITY AND FEED COMPOSITION CYCLING

BY

WILLIAM REGINALD CHOATE GRAHAM ©

A THESIS

SUBMITTED TO THE FACULTY OF GRADUATE STUDIES AND RESEARCH IN PARTIAL FULFILLMENT OF THE REQUIREMENTS FOR THE DEGREE OF DOCTOR OF PHILOSOPHY

DEPARTMENT OF CHEMICAL ENGINEERING

EDMONTON, ALBERTA

SPRING 1990

National Library of Canada
Bibliothèque nationale du Canada

Canadian Theses Service
Service des thèses canadiennes

Ottawa, Canada
K1A 0N4

NOTICE

The quality of this microform is heavily dependent upon the quality of the original thesis submitted for microfilming. Every effort has been made to ensure the highest quality of reproduction possible.

If pages are missing, contact the university which granted the degree.

Some pages may have indistinct print especially if the original pages were typed with a poor typewriter ribbon or if the university sent us an inferior photocopy.

Reproduction in full or in part of this microform is governed by the Canadian Copyright Act, R.S.C. 1970, c. C-30, and subsequent amendments.

AVIS

La qualité de cette microforme dépend grandement de la qualité de la thèse soumise au microfilmage. Nous avons tout fait pour assurer une qualité supérieure de reproduction.

S'il manque des pages, veuillez communiquer avec l'université qui a conféré le grade.

La qualité d'impression de certaines pages peut laisser à désirer, surtout si les pages originales ont été dactylographiées à l'aide d'un ruban usé ou si l'université nous a fait parvenir une photocopie de qualité inférieure.

La reproduction, même partielle, de cette microforme est soumise à la Loi canadienne sur le droit d'auteur, SRC 1970, c. C-30, et ses amendements subséquents.

ISBN 0-315-60216-3

NL-339 (r. 88/04) c

Canada

UNIVERSITY OF ALBERTA

RELEASE FORM

NAME OF AUTHOR: William Reginald Choate Graham

TITLE OF THESIS: Oxidation of Carbon Monoxide on Platinum Catalysts: Kinetic Model Discrimination Using Experimental Steady-State Multiplicity and Feed Composition Cycling

DEGREE: Doctor of Philosophy

YEAR THIS DEGREE GRANTED: 1990

Permission is hereby granted to THE UNIVERSITY OF ALBERTA LIBRARY to reproduce single copies of this thesis and to lend or sell such copies for private, scholarly or scientific research purposes only.

The author reserves other publication rights, and neither the thesis nor extensive extracts from it may be printed or otherwise reproduced without the author's written permission.

.....

Box 1843

Deep River, Ontario, K0J 1P0

Date: April 24, 1990

UNIVERSITY OF ALBERTA

FACULTY OF GRADUATE STUDIES AND RESEARCH

The undersigned certify that they have read, and recommend to the Faculty of Graduate Studies and Research for acceptance, a thesis entitled OXIDATION OF CARBON MONOXIDE ON PLATINUM CATALYSTS: KINETIC MODEL DISCRIMINATION USING EXPERIMENTAL STEADY-STATE MULTIPLICITY AND FEED COMPOSITION CYCLING submitted by William Reginald Choate Graham in partial fulfillment of the requirements for the degree of DOCTOR OF PHILOSOPHY.

David T. Lynch

Dr. D. T. Lynch

I. G. Dalla Lana

Dr. I. G. Dalla Lana

S. E. Wanke

Dr. S. E. Wanke

Thomas Rogers

Dr. T. D. Rogers

R. R. Hudgins

Dr. R. R. Hudgins

Date: April 19, 1990

Dedication

This thesis is dedicated to Candace.

Abstract

The oxidation of carbon monoxide on platinum catalysts was studied using a recycle reactor. Multiple steady states were found in a cusp-shaped region of the feed concentration ($CO-O_2$) phase plane. The bifurcation behavior was used to discriminate among five proposed mathematical models, including a new surface island formation model, for CO oxidation. Only an elementary-step model which invoked self-exclusion of CO from surface sites could describe the observed multiplicity.

To test the validity of the model, a series of feed-composition cycling experiments was carried out. Reaction rate resonance was found. The model selected with steady-state data, while able to predict resonance, was not capable of describing the magnitude of resonance which was found. A new model, combining CO self-exclusion with a surface-phase transformation mechanism in which the platinum surface undergoes adsorbate-induced transformations between two surface phases of very different catalytic activity, was found to be capable of describing both the steady-state and the dynamic data.

Feed-composition cycling experiments were carried out in which the phasing of the CO and oxygen feed streams was varied. It was found that the phase angle between the input forcing functions is an important parameter in determining the time-average conversion.

Acknowledgements

I would like to take this opportunity to acknowledge the assistance and support I have received during the past several years. Bruce Russell wrote some of the computer programs for finding steady-state solutions of the kinetic equations. Bob Barton of the DACS Center provided valuable assistance in setting up and trouble-shooting the data acquisition programs I used. Don Sutherland and his staff in the Instrument Shop were able to make the equipment I wanted and somehow managed to keep it working.

I would like to thank Dr. Lynch for suggesting I tackle the CO oxidation problem - it has been a most interesting challenge. I do not believe I could have completed the work without his direction.

I wish to acknowledge the Province of Alberta for a Graduate Fellowship.

I would like to thank all of the Chemical Engineering Graduate Students I have known for their friendship, and for all the beer we spilled in the Power Plant. I am grateful to all of them, but especially to Will Cluett, John Carroll, Ray Tomcej, Bill Pick, Bruce Russell, and Rosalynn MacGregor.

I wish to thank my family for their support over the past years. Finally, I wish to thank Candace, my wife, for all her love, patience, and support over the past eight years. Without her this work would never have been completed.

Table of Contents

Chapter Page

1. Introduction 1

1.1 Outline 1

1.2 References 3

2. Literature Survey 4

2.1 Nomenclature 4

2.2 Introduction 4

2.2.1 Steady-State Multiplicity 5

2.2.2 Reaction Rate Enhancement During Feed Cycling 8

2.2.3 Oscillatory Behavior 10

2.3 Basic Reaction Mechanism 10

2.4 CO Surface Island Formation Model 13

2.5 Surface Oxidation-Reduction Model 14

2.6 Surface Phase Transformation Model 14

2.7 References 16

3. Island Models and the Catalytic Oxidation of Carbon Monoxide 22

3.1 Nomenclature 22

3.2 Introduction 23

3.3 Model Derivation 23

3.4 Model Comparison 28

3.5 References 33

4. Experimental Equipment and Materials 35

4.1 Reactor Systems 36

4.1.1 Reactor I 36

4.1.2 Reactor II 38

4.2 Feed Gas System 40

4.3 Gas Analysis System 41
4.4 References 42
5. Steady-State Behavior 43
5.1 Nomenclature 43
5.2 Introduction 47
5.3 Review 47
5.4 Experimental Steady-State Behavior 49
5.5 Mathematical Models 57
5.5.1 Langmuir-Hinshelwood Model 59
5.5.2 Surface Oxidation-Reduction Model 67
5.5.3 CO Surface Island Formation Model 71
5.5.4 Modified Surface Island Model 75
5.5.5 CO Self-Exclusion Model 78
5.6 Summary of Steady-State Analysis 87
5.7 References 88
6. Behavior During Forced Feed Cycling 92
6.1 Nomenclature 92
6.2 Introduction 95
6.3 Definition of Oxygen Phase Lead 96
6.4 Experimental Behavior 99
6.4.1 Out-of-Phase Feed Cycling 101
6.4.2 Effect of Oxygen Phase Lead on Time-Average Conversion 111
6.5 Model Details 115
6.6 Model Predictions 119
6.7 Conclusions 125
6.8 References 126
7. Oscillations and Multiplicity 129

7.1 Predicted Behavior 129

7.2 Experimental Behavior 132

7.3 References 142

8. The Effect of Model Assumptions on Predicted Bifurcation Behavior 143

8.1 Nomenclature 143

8.2 Introduction 145

8.3 Reaction Model 146

8.4 Bifurcation Behavior in a CSTR with Equilibrium 149

8.5 Recycle Reactor Bifurcation Behavior (CO Adsorption at Equilibrium) 152

8.6 Bifurcation Behavior in a CSTR without Equilibrium 163

8.7 References 170

9. Summary and Recommendations 172

9.1 CO Oxidation 172

9.2 Feed Composition Cycling 176

9.3 Recommendations for Future Work 179

9.4 References 180

Appendix A 181

Appendix B 208

Appendix C 237

Appendix D 244

Appendix E 252

List of Tables

Table Page

3.1 Model Parameters.....30

5.1 Model-Dependent Parameter Values.....61

5.2 Model-Dependent Rate Parameters.....70

6.1 Reactor Operating Conditions.....99

7.1 Summary of Platinum Gauze Behavior.....133

List of Figures

Figure Page

2.1 Steady-State Multiplicity.....6

2.2 Reaction Rate Enhancement During Feed Cycling.....9

2.3 Reaction Rate Oscillations.....11

3.1 Island Model Comparison.....29

4.1 Overall Experimental Schematic.....36

4.2 Reactor I Schematic.....37

4.3 Reactor II Schematic.....39

4.4 Feed System Schematic.....41

5.1 Steady-State CO Conversion Multiplicity.....50

5.2 Multiplicity Boundaries for Three Catalyst Charges...52

5.3 Effect of Temperature on the Multiplicity Boundaries.53

5.4 Dependence of Bifurcation Points on Temperature.....54

5.5 Effect of Flow Rate on the Multiplicity Boundaries...55

5.6 Dependence of Bifurcation Points on Flow Rate.....56

5.7 Effect of Flow Rate on Predicted Bifurcation Points..71

5.8 Predicted CO Conversions.....72

6.1 Feed Cycling Strategies.....98

6.2 Steady-State Bifurcation Behavior.....100

6.3 Instantaneous CO Conversion.....102

6.4 Effect of Frequency on Time-Average Conversion.....106

6.5 Effect of Phase Angle on Time-Average Conversion....113

6.6 Effect of CO Coverage on Rate Constants.....116

6.7 Comparison of Predicted Time-Average Conversions....120

6.8 Predicted Dynamic Behavior.....123

7.1 Transition from Multiplicity to Oscillations.....130

7.2 Region of Oscillations.....135

7.3 Multiplicity and Oscillations with Different Catalyst Charges.....137

7.4 Experimental Transition from Multiplicity to Oscillations.....139

8.1 Multiplicity Behavior in a CSTR with Equilibrium....150

8.2 Bifurcation Behavior in a CSTR with Equilibrium.....151

8.3 Recycle Reactor Bifurcation Behavior (Step 1 and 2 at Equilibrium).....154

8.4 Effect of Recycle Ratio on Bifurcation Behavior: Equilibrium Assumption.....155

8.5 Ratio of Bifurcation Points.....157

8.6 Falsification of Surface Rate Constant.....158

8.7 Effect of Recycle Ratio on Falsification of Surface Rate Constant.....159

8.8 Effect of Recycle Ratio on Falsification of Equilibrium Constant.....160

8.9 Effect of Recycle Ratio on Falsification of Surface Rate Constant.....162

8.10 Bifurcation Behavior in a CSTR without Equilibrium..165

8.11 Effect of Equilibrium Assumption on Bifurcation Behavior in a CSTR.....166

8.12 Falsification of Surface Rate Constant.....167

8.13 Effect of Equilibrium Assumption on Falsification of Surface Rate Constant.....168

8.14 Effect of Equilibrium Assumption on Falsification of Equilibrium Constant.....169

1. Introduction

1.1 Outline

In recent years there have been many reports addressing the catalytic oxidation of carbon monoxide on platinum. One reason for this interest is the need to reduce automotive emissions. However, platinum-catalyzed CO oxidation has also proven to be a sufficiently interesting reaction to merit investigation in its own right. This reaction displays many complex dynamic and steady-state phenomena that cannot easily be explained. Among these phenomena are steady-state multiplicity, reaction rate enhancement during feed cycling, self-sustained oscillations, and chaos. These phenomena have been reviewed by Razon and Schmitz (1986), Sheintuch and Schmitz (1977), and Slin'ko and Slin'ko (1978). Although there has been much study of this reaction in the past two decades, there is still not universal agreement as to the causes of the complex phenomena. Several different mechanisms have been proposed, but typically these mechanisms have been concerned with explaining only a single aspect of the complex behavior. Thus, a single, consistent explanation for the behavior of CO oxidation has yet to be presented.

A primary goal of this work is to develop a mechanism which can explain the complex behavior observed during CO oxidation. In the following chapters, several proposed mechanisms for CO oxidation on platinum will be examined.

The ability of these mechanisms to describe various types of complex behavior will be assessed using experimental data from laboratory reactors. From these comparisons it will be seen if any of the mechanisms can quantitatively describe the observed complex phenomena.

A secondary goal of this work is to examine the effect of operating conditions on reaction rate enhancement during forced feed cycling.

The introductory chapter of this thesis is followed by a brief survey of some of the mechanisms that have been proposed for CO oxidation on platinum. In the third chapter a mathematical model based on one of these mechanisms, the surface island model, is examined. Some alternative formulations of the classical surface island model are also discussed in Chapter 3. In Chapter 4 the experimental equipment is described. The steady-state behavior of an alumina-supported platinum catalyst is described in Chapter 5. The effect of operating parameters on multiplicity behavior are presented and these data are used to discriminate among several kinetic mechanisms which have been proposed to describe the behavior. In Chapter 6 a study of feed composition cycling is used to discriminate further among rival kinetic mechanisms. Resonant behavior, i.e. the time-average reaction rate passing through a maximum as the cycling frequency varies, is described. It is shown that time-average rate behavior can be used to discriminate effectively between kinetic models with identical

steady-state behavior. Predictions made with the final model of Chapter 6 were used to design an experiment to test the model. The results of this experiment are presented in Chapter 7. In Chapters 5 and 6 it is assumed that a tubular reactor with a high rate of recycle can be modeled as a well-mixed reactor, or CSTR. The effects of this assumption are examined in Chapter 8. Finally, the conclusions of this thesis and recommendations for future work are made in Chapter 9.

1.2 References

Razon, L. F., and R. A. Schmitz, "Intrinsically Unstable Behavior during the Oxidation of Carbon Monoxide on Platinum", Catal. Rev.-Sci. Eng. 28, 89-164 (1986).

Sheintuch, M., and R. A. Schmitz, "Oscillations in Catalytic Reactions", Catal. Rev.-Sci. Eng. 15, 107-172 (1977).

Slin'ko, M. G., and M. M. Slin'ko, "Self-Oscillations of Heterogeneous Catalytic Reaction Rates", Catal. Rev.-Sci. Eng. 17, 119-153 (1978).

2. Literature Survey

2.1 Nomenclature

[CO] = gas phase CO concentration

k_a = CO adsorption equilibrium constant

k_r = surface reaction rate constant

$[O_2]$ = gas phase oxygen concentration

r_{CO} = rate of CO oxidation

2.2 Introduction

The catalytic oxidation of carbon monoxide has become an important reaction in the past twenty years. Although the product, carbon dioxide, has a limited market, increasingly stringent automotive emissions requirements and an increased public awareness of environmental issues have combined to force industries to reduce the release of carbon monoxide. Accompanying the increased industrial interest has been a large volume of research published in the scientific literature addressing the catalytic oxidation of CO. A commonly used catalyst for CO oxidation is platinum deposited on a high surface area support such as alumina or silica. Reviews by Engel and Ertl (1979) and by Razon and Schmitz (1986) have summarized much of the recent literature concerning this reaction.

One of the earliest reported studies of CO oxidation on platinum catalysts was by Langmuir (1922), who postulated that adsorbed CO molecules reacted with adsorbed oxygen

atoms. Langmuir also showed that the reaction is inhibited by CO at low temperatures.

2.2.1 Steady-State Multiplicity

Voltz *et al.* (1973) studied the kinetics of CO and propylene oxidation on Pt catalysts between 200 and 375°C. They found that oxidation rates increased with increasing oxygen concentration and were inhibited by CO, C_3H_6 and NO. They presented rate equations to describe the experimental data. For $CO-O_2-N_2$ mixtures, the rate function they presented can be written as:

$$r_{CO} = \frac{k_r[CO][O_2]}{\{1+k_a[CO]\}^2} \tag{2.1}$$

At low CO concentrations with a large excess of oxygen the reaction rate is first order in CO, and at high CO concentrations the rate varies inversely with CO concentration. When Eqn. (2.1) is incorporated into the steady state equations for a CSTR, rate multiplicity, similar to that shown in Figure 2.1, can result. The first report of steady-state rate multiplicity during CO oxidation on platinum was apparently by Padberg and Wicke (1967).

The occurrence of multiple steady states in the operation of chemical reactors has been recognized for over seventy years (Liljenroth, 1918). While the operation of an industrial reactor in a multiple steady-state region is usually avoided, multiplicity behavior can provide valuable insight into reaction mechanisms. The causes of

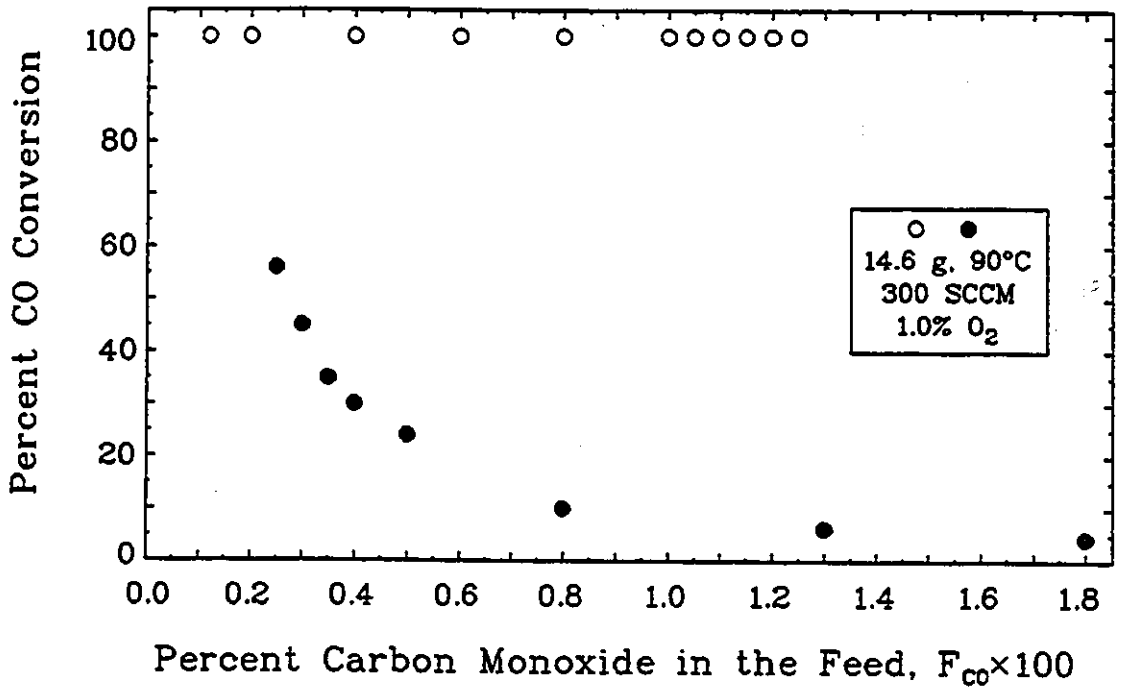

Figure 2.1 Steady-State Multiplicity

steady-state multiplicity include autothermicity (Van Heerden, 1953), reaction rate inhibition due to competitive adsorption (Matsuura and Kato, 1967; Beusch *et al.*, 1972), diffusion-reaction interactions (Hegedus *et al.*, 1977) and autocatalysis (Gray and Scott, 1983).

Reaction rate multiplicity has often been observed for the oxidation of carbon monoxide over noble metal catalysts. The catalyst most often studied has been platinum. For isothermal reactor operation, this reaction displays conversions of CO near 100% at low CO feed concentrations, and low conversions (less than 10%) at high CO feed concentrations.

At intermediate CO feed concentrations both high- and low-conversion steady states can occur, as shown in Figure 2.1. This behavior has been observed in CSTRs (Cutlip, 1979) and tubular reactors (Hegedus *et al.*, 1977) using Pt wires, gauze and foils, and supported platinum catalysts. Although there are many suggested explanations for CO oxidation multiplicity behavior, there is a dearth of detailed studies of the effect of reactor parameters; such as temperature, feed flow rate, feed composition, and size of catalyst charge, on multiplicity behavior. Cutlip (1979) examined the effect of temperature and composition on the region of multiple steady states. Oh *et al.* (1979) investigated the effect of catalyst particle size on multiplicity behavior, and showed that hysteresis was eliminated when catalyst particle size became sufficiently small. Chakrabarty *et al.* (1984) examined the effect of diluent gases on the region of multiplicity and concluded that the reaction-sorption interference explanation cannot be overlooked. Herskowitz and Kenney (1983) examined the effects of temperature and feed composition on multiplicity behavior. They used three Langmuir-Hinshelwood Hougen-Watson (LHHW) models to describe the reaction system, and found that two of them could accurately predict the transition from the low-conversion steady-state rate branch to the high-conversion rate branch. However, no comparisons were made concerning the high-to-low conversion bifurcation point. Mukesh *et al.* (1984) have used an elementary-step Langmuir-Hinshelwood model incorporating CO surface island

formation to describe the low-conversion branch of the steady-state rate curve. This model was also able to describe the dynamic response of a CSTR to step changes in feed composition.

2.2.2 Reaction Rate Enhancement During Feed Cycling

The first demonstration of reaction rate enhancement for CO oxidation over platinum was by Cutlip (1979), who found that periodic switching between carbon monoxide and oxygen feed streams to a gradientless reactor significantly increased the time-average reaction rate as compared to the steady-state rate. The rate enhancement was attributed to the attainment of more desirable surface concentrations on the platinum catalyst. An example of reaction rate enhancement is shown in Figure 2.2. Cutlip *et al.* (1983) and Lynch (1983, 1984) have demonstrated that the large rate enhancements which occur for CO oxidation in a gradientless reactor can be explained by elementary-step models, while Cho (1983) has shown in a modeling study of a single pellet reactor that chromatographic effects can have a major influence on the rate enhancement. Concerning the forced cycling of tubular reactors, Barshad and Gulari (1985) claim that rate enhancement is due to a maximization of the total perimeter-to-area ratio for CO surface islands, while Oh *et al.* (1978) have shown that a diffusion-reaction model which accounts for surface accumulation can adequately describe the rate enhancement that was observed.

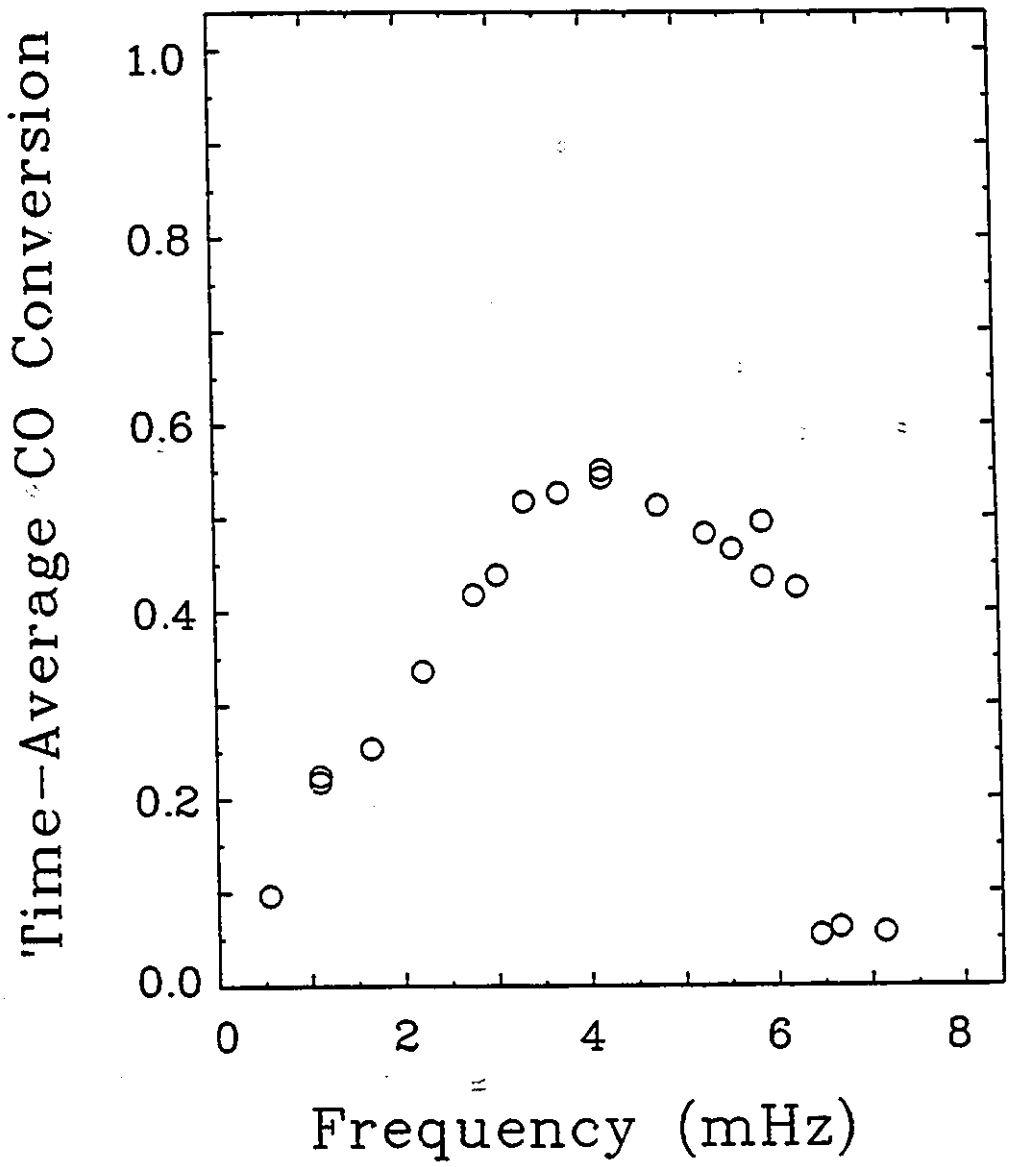

Figure 2.2 Reaction Rate Enhancement During Feed Cycling

With the exception of the work of Cho (1983) all of the above studies have been concerned with 180 degree out-of-phase cycling, that is, the CO stream was turned off when the oxygen stream was turned on, and vice versa. Cho

examined in-phase cycling and 90 degree out-of-phase cycling as well as 180 degree out-of-phase cycling in a numerical investigation of rate enhancement, and suggested that the best performance can be obtained when the CO and O_2 feed concentrations change in opposite directions (180 degrees out-of-phase) during cycling. Barshad and Gulari (1985) examined the effects of frequency and of duty fraction, but used only out-of-phase square-wave cycling for their experiments.

2.2.3 Oscillatory Behavior

Self-sustained oscillatory behavior was first reported for CO oxidation by Beusch *et al.* (1972). Oscillations are typically of the relaxation type, similar to those shown in Figure 2.3. Since the initial observations, many reports of similar findings have been published. Reviews of oscillatory behavior during CO oxidation can be found in Sheintuch and Schmitz (1977), Slin'ko and Slin'ko (1978), and Razon and Schmitz (1986). Chaotic oscillations were first reported by Plichta and Schmitz (1979). Razon *et al.* (1986) showed that the oscillations they observed were chaotic by demonstrating a Hausdorff-Bescovitch dimension of 3.4.

2.3 Basic Reaction Mechanism

It is generally agreed (Engel and Ertl, 1979) that the elementary steps for CO oxidation on platinum can be represented as follows:

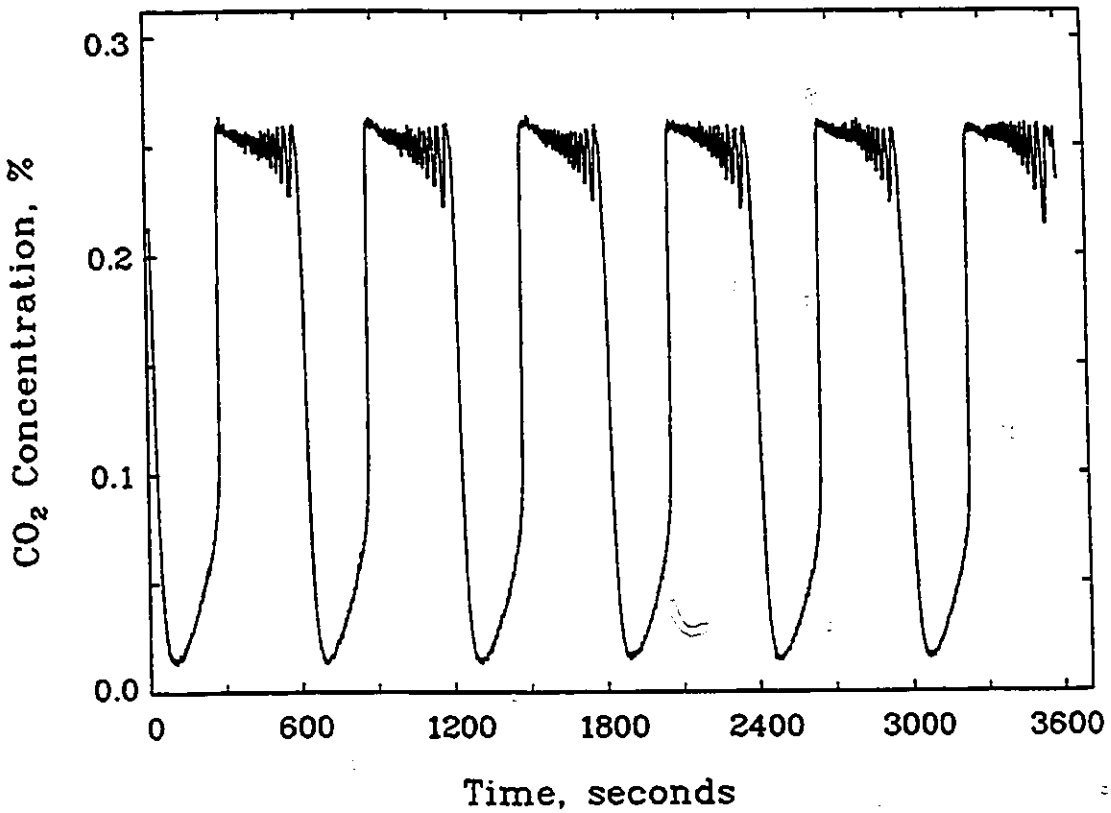

Figure 2.3 Reaction Rate Oscillations

$$CO(g) + S \underset{k_{-1}}{\overset{k_1}{\rightleftharpoons}} CO\text{-}S \qquad (2.2)$$

$$O_2(g) + 2\ S \underset{k_{-2}}{\overset{k_2}{\rightleftharpoons}} 2\ O\text{-}S \qquad (2.3)$$

$$CO\text{-}S + O\text{-}S \xrightarrow{k_3} CO_2(g) + 2\ S \qquad (2.4)$$

$$CO(g) + O\text{-}S \xrightarrow{k_4} CO_2(g) + S \qquad (2.5)$$

CO and oxygen adsorb reversibly on the platinum surface. At temperatures below 600 K the desorption of oxygen can be

neglected (Engel and Ertl, 1979). Reaction mechanisms incorporating Steps (2.2) and (2.3) and the bimolecular surface reaction (Step 2.4) will be referred to as Langmuir-Hinshelwood (LH) mechanisms. Mechanisms incorporating gas phase attack by CO on the adsorbed oxygen species (Step 2.5) will be referred to as Eley-Rideal (ER) mechanisms.

In early attempts to model CO oxidation on platinum it was usually assumed that either the LH or the ER mechanism was predominant and that one of Steps (2.2)-(2.5) was rate determining. Then, by assuming the other steps were at equilibrium or at a pseudo-steady state, an analytical expression for the reaction rate could usually be derived in terms of the gas-phase concentrations. However, such an expression would typically be valid only in the relatively narrow range of gas-phase concentrations where the equilibrium or pseudo-steady-state assumptions applied, and could not describe the full range of phenomena that has been observed for CO oxidation on platinum. Another problem with rate expressions derived using equilibrium or pseudo-steady-state assumptions is that the conservation equations can be violated if transient results are modeled using these rate expressions.

There have been numerous models proposed for CO oxidation on platinum, and most of these have been reviewed by Razon and Schmitz (1986). Three of the more successful models are the surface island model, in which it is postulated that "islands" of adsorbates form on the surface,

the surface oxide model, in which it is believed that a strongly adsorbed oxygen species exists, and the surface phase transformation model, in which the key assumption is that the metal surface switches between states with different sticking probabilities. For a model of CO oxidation to be accepted as adequate, it should be capable of describing the many complex phenomena exhibited by the reaction. These models will be reviewed in the following pages.

2.4 CO Surface Island Formation Model

Infrared spectroscopy results indicate that both carbon monoxide and oxygen form single species "patches" or "islands" on platinum (Bonzel and Ku, 1972). Low Energy Electron Diffraction (LEED) results indicate that adsorbed atomic oxygen forms islands for surface concentrations greater than about 0.4×10^{14} atoms/cm^2 (about one tenth of the maximum oxygen coverage) and suggest that CO forms islands when it is adsorbed on surfaces containing adsorbed oxygen (Gland and Kollin, 1983). It should be noted that there need not be favourable thermodynamics for surface islands to form; Monte Carlo studies show that there is a tendency for separate clusters of two adsorbed reactants A and B to form when reaction removes adjacent AB pairs (Wicke *et al.*, 1980). Mukesh *et al.* (1984) presented several mathematical models of CO oxidation incorporating adsorbate island formation. These models were used to describe steady-state and dynamic rates of reaction on supported platinum

catalysts. The surface island model can also predict oscillatory behavior, although there is little resemblance between the predicted rates and those which have been observed experimentally (Mukesh *et al.*, 1984). The surface island model will be examined in more detail in Chapter 3.

2.5 Surface Oxidation-Reduction Model

Platinum forms an oxide which is theoretically stable up to 579°C(Yao *et al.*, 1981). There is evidence that a surface or subsurface oxide may form during the oxidation of CO on platinum. A model of CO oxidation, incorporating surface oxidation and reduction, was developed by Sales *et al.* (1982). This model was able to describe relaxation oscillations that were observed on polycrystalline platinum wires. A nonisothermal form of this model was presented by Yeates *et al.* (1986). This latter form was able to describe many of the features of the oscillations. Aluko and Chang (1986) presented a nonisothermal oxidation-reduction model which was able both to quantitatively describe the transitions from oscillatory behavior to multiple steady states and to describe the shape and frequency of the oscillations.

2.6 Surface Phase Transformation Model

Ertl and co-workers (Behm *et al.*, 1983; Thiel *et al.*, 1983) found from single-crystal LEED studies that a clean Pt(100) surface spontaneously transforms from a quasi-hexagonal (hex) structure to a (1×1) structure on

exposure to CO. The empty sites on the (1×1) platinum surface have an oxygen sticking probability several orders of magnitude higher than empty sites on the clean reconstructed (hex) surface. Ertl *et al.* (1982) and Cox *et al.* (1983) observed that surface transformations occurred in phase with reaction rate oscillations and showed that the low-rate part of the oscillations occurred on the (1×1) surface while the high-rate part occurred on the hex surface. A mathematical model based on surface phase transformations was used successfully by Lynch *et al.* (1986) to quantitatively describe the effects of several reactor operating parameters on the oscillations reported by Lynch and Wanke (1984a, 1984b). At first glance it might appear that assigning single-crystal properties to highly dispersed supported metal catalysts is not justifiable. However, transmission electron microscopy results by Wang *et al.* (1985) show that platinum supported on silica and γ-alumina forms rectangular crystallites which have a predominance of (100) faces. Thus, it may not be unreasonable to assign single-crystal properties to supported platinum catalysts.

Schwartz and Schmidt (1987) showed that spontaneous oscillations in the NO + CO reaction on clean Pt(100), or on clean polycrystalline platinum, are caused by the hex to (1×1) transition. They suggested that many of the observed rate oscillations on platinum surfaces may arise from adsorbate-induced hex to (1×1) surface phase transitions on Pt(100). They further suggested that the mechanism may also

be operative on polycrystalline wires and foils and on supported platinum particles because in many reactive gases all crystallographic orientations tend to a predominance of the (100) plane.

In the following chapters the surface island model, the oxidation reduction model, and the surface phase transformation model will be examined. An assessment will be made of the ability of these models to describe the complex phenomena observed during CO oxidation.

2.7 References

Aluko, M., and H.-C. Chang, "Dynamic Modelling of a Heterogeneously Catalysed System with Stiff Hopf Bifurcations", Chem. Eng. Sci. 41, 317-331 (1986).

Barshad, Y., and E. Gulari, "A Dynamic Study of CO Oxidation on Supported Platinum", AIChE J. 31, 649-658, (1985).

Behm, R. J., P.A. Thiel, P. R. Norton, and G. Ertl, "The Interaction of CO and Pt(100). I. Mechanism of Adsorption and Pt Phase Transition", J. Chem. Phys. 78, 7437-7447 (1983).

Beusch, H., P. Fieguth, and E. Wicke, "Thermisch und kinetisch verursachte Instabilitäten im Reaktionsverhalten einzelner Katalysatorkörner", Chem. Ing. Tech. 44, 445-451 (1972).

Bonzel, H. P., and R. Ku, "Mechanisms of the Catalytic Carbon Monoxide Oxidation on Pt(110)", Surface Sci. 33, 91-106, (1972).

Chakrabarty, T., P. L. Silveston, and R. R. Hudgins, "Hysteresis Phenomena in CO Oxidation over Platinum-Alumina Catalyst", Can. J. Chem. Eng. 62, 651-660 (1984).

Cho, B. K., "Dynamic Behavior of a Single Catalyst Pellet. 1. Symmetric Concentration Cycling during CO oxidation of Pt/Al_2O_3", Ind. Eng. Chem. Fundam. 22, 410-420 (1983).

Cox, M. P., G. Ertl, R. Imbihl, and J. Rustig, "Non-Equilibrium Surface Phase Transitions during the Catalytic Oxidation of CO on Pt(100)", Surface Sci. 134 L517-523 (1983).

Cutlip, M. B., "Concentration Forcing of Catalytic Surface Rate Processes, Part 1. Isothermal Carbon Monoxide Oxidation Over Supported Platinum", AIChE J. 25, 502-508 (1979).

Cutlip, M. B., C. J. Hawkins, D. Mukesh, W. Morton, and C. N. Kenney, "Modelling of Forced Periodic Oscillations of Carbon Monoxide Oxidation over Platinum Catalyst", Chem. Eng. Commun. 22, 329-344 (1983).

Engel, T., and G. Ertl, "Elementary Steps in the Catalytic Oxidation of Carbon Monoxide on Platinum Metals", Adv. Catal. 28, 1-78 (1979).

Ertl, G., P. R. Norton, and J. Rustig, "Kinetic Oscillations in the Platinum-Catalyzed Oxidation of CO", Phys. Rev. Letters 49, 177-180 (1982).

Gland, J. L., and E. B. Kollin, "Carbon Monoxide Oxidation on the Pt(111) Surface: Temperature Programmed Reaction of

Coadsorbed Atomic Oxygen and Carbon Monoxide", J. Chem. Phys. 78, 963-974 (1983).

Gray, P., and S. K. Scott, "Autocatalytic Reactions in the Isothermal, Continuous Stirred Tank Reactor: Isolas and Other Forms of Multistability", Chem. Eng. Sci. 38, 29-43 (1983).

Hegedus, L. L., S. H. Oh, and K. Baron, "Multiple Steady States in an Isothermal, Integral Reactor: The Catalytic Oxidation of Carbon Monoxide over Platinum-Alumina", AIChE J. 23, 632-642 (1977).

Herskowitz, H., and C. N. Kenney, "CO Oxidation on Pt Supported Catalysts. Kinetics and Multiple Steady States", Can. J. Chem. Eng. 61, 194-199 (1983).

Langmuir, I., "The Mechanism of the Catalytic Action of Platinum in the Reactions $2CO + O_2 = 2CO_2$ and $2H_2 + O_2 = 2H_2O$", Trans. Faraday Soc. 17, 621-654 (1922).

Liljenroth, F. G., "Starting and Stability Phenomena of Ammonia-Oxidation and Similar Reactions", Chem. Metall. Eng. 19, 287-293 (1918).

Lynch, D. T., "Modelling of Resonant Behavior During Forced Cycling of Catalytic Reactors", Can. J. Chem. Eng. 61, 183-188 (1983).

Lynch, D. T., "On the Use of Adsorption/Desorption Models to Describe the Forced Periodic Operation of Catalytic Reactors", Chem. Eng. Sci. 39, 1325-1328 (1984).

Lynch, D. T., and S. E. Wanke, "Oscillations during CO Oxidation over Supported Metal Catalysts: I. Influence of

Catalyst History on Activity", J. Catal. 88, 333-344 (1984a)

Lynch, D. T., and S. E. Wanke, "Oscillations during Carbon Monoxide Oxidation over Supported Metal Catalysts: II. Effects of Reactor Operating Conditions on Oscillatory Behavior for a Pt-Pd/Al_2O_3 Catalyst", J. Catal. 88, 345-354 (1984b).

Lynch, D. T., G. Emig, and S. E. Wanke, "Oscillations during CO Oxidation over Supported Metal Catalysts: III. Mathematical Modeling of the Observed Phenomena", J. Catal. 97, 456-468 (1986).

Matsuura, T., and M. Kato, "Concentration Stability of the Isothermal Reactor", Chem. Eng. Sci. 22, 171-184 (1967).

Mukesh, D., W. Morton, C. N. Kenney, and M. B. Cutlip, "Island Models and the Catalytic Oxidation of Carbon Monoxide and Carbon Monoxide-Olefin Mixtures", Surface Sci. 138, 237-257 (1984).

Oh, S. E., K. Baron, J. C. Cavendish, and L. L. Hegedus, "Carbon Monoxide Oxidation in an Integral Reactor: Transient Response to Concentration Pulses in the Regime of Isothermal Multiplicities", ACS Symp. Ser. 65, 461-474 (1978).

Oh, S.H., K. Baron, E. M. Sloan, and L. L. Hegedus, "Effects of Catalyst Particle Size on Multiple Steady States", J. Catal. 59, 272-277 (1979).

Padberg, G., and E. Wicke, "Stabiles und instabiles Verhalten eines adiabatischen Rohrreaktors am Beispiel der

katalytischen CO-Oxydation", Chem. Eng. Sci. 22, 1035-1051 (1967).

Plichta, R. T., and R. A. Schmitz, "Oscillations in the Oxidation of Carbon Monoxide on a Platinum Foil", Chem. Eng. Commun. 3, 387-398 (1979).

Razon, L. F., S.-M. Chang, and R. A. Schmitz, "Chaos During the Oxidation of Carbon Monoxide on Platinum - Experiments and Analysis", Chem. Eng. Sci. 41, 1561-1576 (1986).

Razon, L. F., and R. A. Schmitz, "Intrinsically Unstable Behavior during the Oxidation of Carbon Monoxide on Platinum", Catal. Rev.-Sci. Eng. 28, 89-164 (1986).

Sales, B. C., J. E. Turner, and M. B. Maple, "Oscillatory Oxidation of CO over Pt, Pd and Ir Catalysts: Theory", Surface Sci. 114, 381-394 (1982).

Schwartz, S. B., and L. D. Schmidt, "Is There a Single Mechanism of Catalytic Rate Oscillations on Pt?", Surface Sci. 183, L269-278 (1987).

Sheintuch, M., and R. A. Schmitz, "Oscillations in Catalytic Reactions", Catal. Rev.-Sci. Eng. 15, 107-172 (1977).

Slin'ko, M. G., and M. M. Slin'ko, "Self-Oscillations of Heterogeneous Catalytic Reaction Rates", Catal. Rev.-Sci. Eng. 17, 119-153 (1978).

Thiel, P. A., R. J. Behm, P. R. Norton, and G. Ertl, "The Interaction of CO and Pt(100). II. Energetic and Kinetic Parameters", J. Chem. Phys. 78, 7448-7458 (1983).

van Heerden, C., "Autothermic Processes: Properties and Reactor Design", Ind. Eng. Chem. 45, 1242-1247 (1953).

Voltz, S. E., C. R. Morgan, D. Liederman, and S. M. Jacob, "Kinetic Study of Carbon Monoxide and Propylene Oxidation on Platinum Catalysts", Ind. Eng. Chem. Prod. Res. Dev. 12, 294-301 (1973).

Wang, T., C. Lee, and L. D. Schmidt, "Shape and Orientation of Supported Pt Particles", Surface Sci. 163, 181-197 (1985).

Wicke, E., P. Kummann, W. Keil, and J. Schiefler, "Unstable and Oscillatory Behavior in Heterogeneous Catalysis", Ber. Bunsenges. Phys. Chem. 84, 315-323 (1980).

Yao, H. C., P. Wynblatt, M. Sieg, and H. K. Plummer, Jr., "Sintering, Redispersion and Equilibrium of Platinum Oxide on γ-Alumina", *in* "Sintering Processes", G. C. Kuczynski, (Ed.), Materials Science Research 13, 561-571 (1983).

Yeates, R. C., J. E. Turner, A. J. Gellman, and G. A. Somorjai, "The Oscillatory Behavior of the CO Oxidation Reaction at Atmospheric Pressure over Platinum Single Crystals: Surface Analysis and Pressure Dependent Mechanisms", Surface Sci. 149, 175-190 (1985).

3. Island Models and the Catalytic Oxidation of Carbon Monoxide

3.1 Nomenclature

a_c = catalyst surface area

[CO] = gas phase CO concentration

k_1 = CO adsorption rate constant

k_{-1} = CO desorption rate constant

k_2 = oxygen adsorption rate constant

k_{-2} = oxygen desorption rate constant

k_3 = surface reaction rate constant

$[O_2]$ = gas phase oxygen concentration

$R_{CO,ads}$ = rate of CO adsorption

$R_{CO,des}$ = rate of CO desorption

$R_{O_2,ads}$ = rate of O_2 adsorption

$R_{O_2,des}$ = rate of O_2 desorption

R_1 = net rate of CO adsorption

R_2 = net rate of O_2 adsorption

R_3 = rate of CO oxidation

X_1 = CO concentration

X_2 = oxygen concentration

Z_0 = ratio of surface capacity to volume

Greek Symbols

θ_{CO} = fractional CO coverage on the metal surface

A version of this chapter has been published.
Graham, W. R. C., and D. T. Lynch, "Island Models and the Catalytic Oxidation of Carbon Monoxide", Surface Sci. 187 L633-638 (1987).

θ_o = fractional oxygen coverage on the metal surface

3.2 Introduction

In this chapter an examination is made of the effect of surface island formation on the mathematical representation of rates of adsorption, desorption and surface reaction. It will be shown that for adsorbates requiring more than one catalytic site per gas-phase molecule (e.g. oxygen), the presence of surface islands enhances the rates of adsorption, relative to surfaces with uniform adsorbate concentrations, because of an increased concentration of empty sites in the region of the surface which is free of islands. It will be seen that a model incorporating this effect is superior to existing elementary-step Langmuir-Hinshelwood and surface-island models for describing steady-state multiplicity and rate behavior during the oxidation of carbon monoxide on supported platinum catalysts.

3.3 Model Derivation

Kenney and co-workers have extensively studied the oxidation of carbon monoxide on platinum catalysts (Mukesh *et al.*, 1983, 1984; Herskowitz and Kenney, 1983; Cutlip *et al.*, 1983; Herskowitz *et al.*, 1982; Goodman *et al.*, 1982). In a recent study, Mukesh *et al.* (1984) examined several simple kinetic models in which account was taken of the formation of islands of adsorbate on the catalyst

surface. They found that the island models could better describe steady-state rate data than an elementary-step Langmuir-Hinshelwood kinetic model. In describing the steady-state reaction rates, Mukesh *et al.* (1984) restricted themselves to examining the effect of adsorbate surface islands on the rate of the surface reaction between adsorbed carbon monoxide and adsorbed oxygen. If it is assumed that only CO forms surface islands, the simplest form of the island model entails modifying the rate of the reaction step to make it proportional to the perimeter of the CO surface islands, i.e.:

$$R_3 \propto \theta_O\sqrt{\theta_{CO}} \tag{3.1}$$

instead of proportional to the fractional CO surface coverage,

$$R_3 \propto \theta_O\theta_{CO} \tag{3.2}$$

as employed in standard elementary-step Langmuir-Hinshelwood models.

A potentially more important effect of the formation of surface islands, which was not included in the models examined by Mukesh *et al.* (1984), is the effect of surface islands on the adsorption rates of species which require more than a single site for adsorption. This effect is due to localized increases in the surface concentrations which occur when one or more surface species form islands. For

example, if only CO islands are formed such that the average fractional coverage for the entire surface is θ_{CO}, then the total catalyst area, a_c, can be divided into two portions: the area, $\theta_{CO}a_c$, covered with CO islands on which the fractional coverage of CO is unity, and the area, $(1-\theta_{CO})a_c$, which has a fractional coverage of CO of zero. If the average fractional coverage of oxygen on the entire catalyst surface is θ_O, then the surface coverage of oxygen in the CO island region will be zero, but it will be $\theta_O/(1-\theta_{CO})$ in the region which has an area of $(1-\theta_{CO})a_c$. Thus, the formation of CO surface islands not only results in an increased local CO concentration in the island region, but also results in an increased local oxygen concentration (and empty site concentration) in the region free of CO islands. If oxygen adsorption can only occur in the region where empty sites are present, then the rate of oxygen adsorption will be proportional to the product of the area of the CO-free region, the square of the empty site concentration in the CO-free region, and the gas-phase oxygen concentration, i.e.:

$$R_{O_2,ads} \propto (1-\theta_{CO})a_c \left[1-\frac{\theta_O}{1-\theta_{CO}}\right]^2 [O_2] = a_c[O_2]\frac{(1-\theta_{CO}-\theta_O)^2}{(1-\theta_{CO})} \quad (3.3)$$

Since, for a standard Langmuir-Hinshelwood model, the rate of oxygen adsorption is proportional to $a_c[O_2](1-\theta_{CO}-\theta_O)^2$, then the existence of CO islands will produce larger rates of oxygen adsorption due to the increased probability of finding neighboring empty surface sites when the surface is divided into the two types of regions. In a similar

fashion, the rate of oxygen desorption will also be enhanced, since it will be proportional to the product of the area of the CO-free region and the square of the oxygen surface concentration in the CO-free region, i.e.:

$$R_{O_2,des} \propto (1-\theta_{CO})a_c \left[\frac{\theta_O}{1-\theta_{CO}}\right]^2 = \frac{a_c\theta_O^2}{(1-\theta_{CO})} \tag{3.4}$$

Thus, the net rate of oxygen adsorption will be given by:

$$R_2 = k_2 Z_o^2 X_2 \frac{(1-\theta_{CO}-\theta_O)^2}{(1-\theta_{CO})} - k_{-2} Z_o^2 \frac{\theta_O^2}{(1-\theta_{CO})} \tag{3.5}$$

whereas in Mukesh *et al.* (1984), as well as in the standard Langmuir-Hinshelwood kinetic model, this rate is given by:

$$R_2 = k_2 Z_o^2 X_2 \ (1-\theta_{CO}-\theta_O)^2 - k_{-2} Z_o^2 \theta_O^2 \tag{3.6}$$

This effect of surface islands on adsorption and desorption rates only occurs when surface concentrations enter the rate expressions in a nonlinear manner. Thus, for CO adsorption, a similar analysis to the preceding gives that:

$$R_{CO,ads} \propto (1-\theta_{CO})a_c \ (1-\frac{\theta_O}{1-\theta_{CO}})[CO] = a_c[CO](1-\theta_{CO}-\theta_O) \tag{3.7}$$

$$R_{CO,des} \propto \theta_{CO}a_c(1) = a_c\theta_{CO} \tag{3.8}$$

The net rate of CO adsorption will then be given by:

$$R_1 = k_1 Z_o X_1 \ (1-\theta_{CO}-\theta_O) - k_{-1} Z_o \theta_{CO} \tag{3.9}$$

which is identical to that used both in Mukesh *et al.* (1984)

and in the standard Langmuir-Hinshelwood kinetic model.

A secondary effect of the increased local concentrations is that the island-model reaction rate expression in Mukesh *et al.* (1984),

$$R_3 = k_3 Z_o \sqrt{\theta_{co}} \theta_o \tag{3.10}$$

should be modified to:

$$R_3 = k_3 Z_o \sqrt{\theta_{co}} \frac{\theta_o}{(1-\theta_{co})} \tag{3.11}$$

in order to include the effect of the increased local oxygen surface concentration.

The effect of these increased local surface concentrations can be determined by comparing the predictions of the following three models: Model 1, a standard Langmuir-Hinshelwood kinetic model consisting of Eqns. (3.6), (3.9) and

$$R_3 = k_3 Z_o^2 \theta_{co} \theta_o \tag{12}$$

for the surface reaction rate; Model 2, an island model (labelled 1a by Mukesh *et al.*, 1984) composed of Eqns. (3.6), (3.9) and (3.10); and Model 3, an island model incorporating the effect of increased local surface concentrations, composed of Eqns. (3.5), (3.9) and (3.11). It should be noted that all of the models have the same number of kinetic parameters.

3.4 Model Comparison

In order to estimate the parameters, and compare the predictive abilities of the models, the data of Herskowitz and Kenney (1983) for CO oxidation on supported platinum are used (1.17% Pt on SiO_2 powder, 437.4 K, 3.1% O_2 inlet concentration). These data, shown in Figure 3.1, are particularly useful for model discrimination and parameter estimation due to the existence of a CO feed concentration region (2.1% CO - 5.8% CO) over which multiple steady states occur. Also shown in Figure 3.1 are the predictions of Models 1, 2 and 3 in which the parameters, given in Table 3.1, are minimum sum-of-squares estimates subject to the constraint that the region of multiple steady-state behavior be correctly predicted. In addition, oxygen desorption is assumed to be negligible ($k_{-2}=0$) in agreement with experimental observations (Engel and Ertl, 1979). The algebraic equations were solved using a differential arclength homotopy-continuation method (Kubicek, 1976). A finite difference approximation of the Jacobian matrix was used as a check of the stability of the steady-state solution. A sample program is listed in Appendix A.

In Figure 3.1, it is seen that the predictions of Models 1 and 2 are essentially identical. While both of these models can correctly describe the feed %CO interval over which multiplicity exists, they both consistently predict conversions which are much too low in the low-conversion region. While Model 3 also predicts conversions

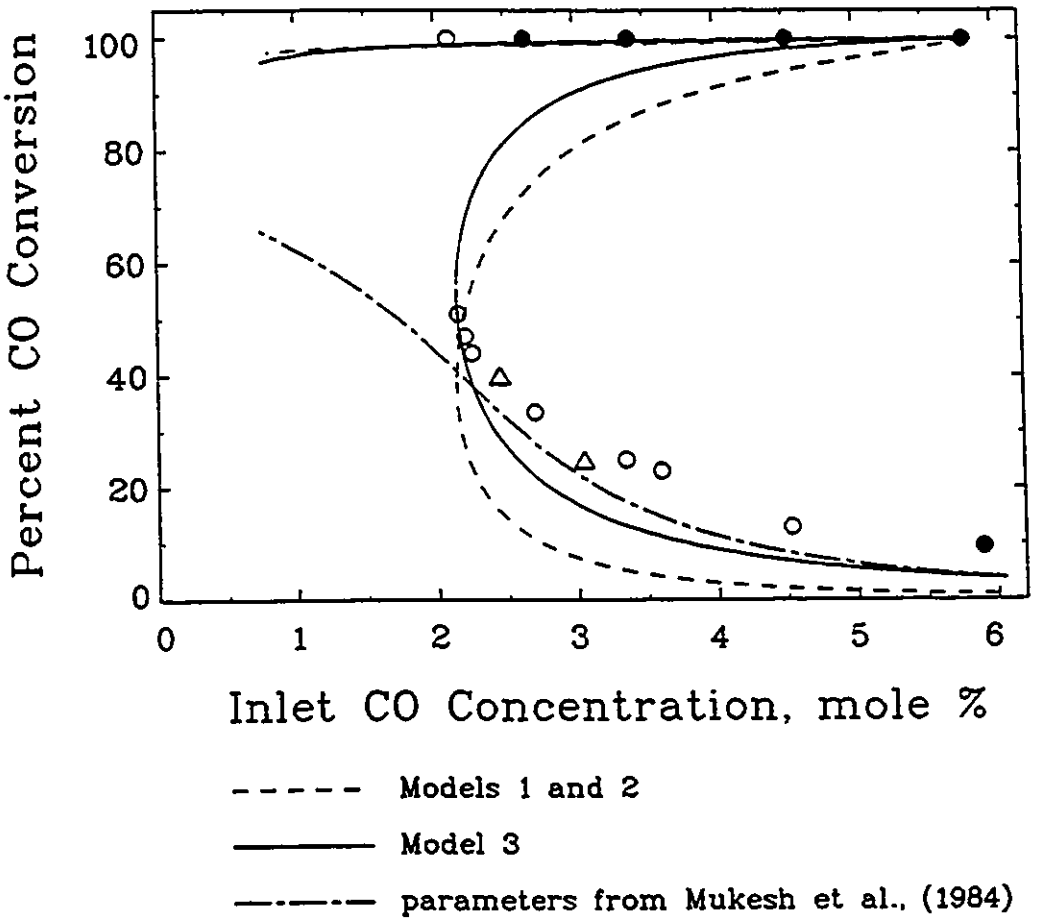

Figure 3.1 Island Model Comparison

which are too low, it is seen that the Model 3 predictions are in much closer agreement with the experimental data. For the predictions in the low-conversion region, the difference between Model 3 and either Model 1 or 2 is statistically significant at the 4.6% level, which is less than the 5% level customarily used in hypothesis testing. The superior performance of Model 3 relative to Models 1 and

Table 3.1 Model Parameters

	Model 1 (LH Model)	Model 2 Mukesh *et al.* (1984)	Model 3
k_1	2.75×10^4	2.16×10^5	2.75×10^5
k_{-1}	40	283	41
k_2	7.0×10^4	8.5×10^4	7.1×10^4
k_{-2}	0	0	0
k_3	2.0×10^8	1.2×10^4	9.1×10^3
Z_o	0.0146	0.0146	0.0146

2 results from oxygen adsorption being the rate-limiting step in the low-conversion region. In this region, the surface is mainly covered with CO, and thus the $(1-\theta_{CO})$ divisor in Eqn. (3.5) produces markedly greater rates of oxygen adsorption when compared to Eqn. (3.6). An interesting consequence of this finding is that the modifications to the surface reaction rate expression, Eqn. (3.11), are not very important. The superior predictive ability of Model 3 results almost entirely from the differences between Eqns. (3.5) and (3.6), and not from the differences between Eqns. (3.11) and (3.12).

It is possible using Model 2 (or Model 1) to obtain higher conversion predictions in the low-conversion region, and thus obtain closer agreement between Model 2 and the experimental data. However, this improvement in conversion prediction is invariably accompanied by a severe reduction

in width, or total elimination, of the region of multiple steady states. In their attempts at describing this data, Mukesh *et al.* (1984) found that Model 2 was superior to Model 1 in describing the low-conversion behavior. However, for the parameters used by Mukesh *et al.* (1984) it is seen in Figure 3.1 that Model 2 does not predict the occurrence of multiple steady states, at total variance with the experimental observations. Thus, from Figure 3.1, it is seen that, of the surface-island models, only Model 3 is superior to the elementary-step Langmuir-Hinshelwood model when both bifurcation and conversion behavior are taken into account.

The approach, embodied in Model 3, in which account is taken of the increased local concentrations of all surface species resulting from the formation of CO surface islands, can be readily extended to cover the case of oxygen island formation. If only oxygen surface islands are formed, then

$$R_2 = k_2 Z_o^2 X_2 \frac{(1-\theta_{CO}-\theta_O)^2}{(1-\theta_O)} - k_{-2} Z_o^2 \theta_O \tag{3.13}$$

$$R_3 = k_3 Z_o \sqrt{\theta_O} \frac{\theta_{CO}}{(1-\theta_O)} \tag{3.14}$$

whereas if both carbon monoxide and oxygen form surface islands, then

$$R_2 = k_2 Z_o^2 X_2 (1-\theta_{CO}-\theta_O) - k_{-2} Z_o^2 \theta_O \tag{3.15}$$

$$R_3 = k_3 \sqrt{\theta_O \theta_{CO}} \tag{3.16}$$

In both cases, Eqn. (3.9) describes the net rate of CO

adsorption. The situation in which both carbon monoxide and oxygen form surface islands has been examined by Dumont *et al.* (1986) through the use of Monte Carlo simulations. They found that the best-fit kinetic equations issuing from their simulations resulted in the oxygen adsorption expression being of the form:

$$R_2 \propto (1-\theta_{CO}-\theta_O)^{\gamma} \tag{3.17}$$

where $1.5 < \gamma < 2$ for the parameters used in their experiments. The development presented herein, which results in R_2 being given by one of Eqns. (3.5), (3.13) or (3.15) provides an explanation for these findings from the Monte Carlo simulations.

With respect to the surface reaction rate, Dumont *et al.* (1986) found that the best fit expression did not have a square-root dependence on the fractional surface coverages, but instead was of the form:

$$R_3 \propto \theta_{CO}(1-\theta_{CO})\theta_O(1-\theta_O) \tag{3.18}$$

They showed that Eqn. (3.18) can be viewed as the product of the total dual perimeters of the oxygen and carbon monoxide islands. This form of the surface reaction rate is certainly superior to the square root dependence used in Eqn. (3.16) since Eqn. (3.18) can account for decreasing island perimeters due to coalescence when fractional coverages become large. However, use of an R_3 term with the

functional dependence of Eqn. (3.18) in a model with Eqns. (3.9) and (3.15) results in predictions which are essentially identical to that from Model 3, when used with the data in Figure 3.1. This occurs because, as already pointed out, in the low-conversion region the oxygen adsorption step, and not the surface reaction, is limiting when agreement with the multiplicity boundaries is obtained. Thus, the functional dependence of R_3 on the fractional coverages has little effect on the predictions of the various models.

Although the preceding formulation of the surface-island model is superior to either the elementary-step LH model or the surface-island model proposed by Mukesh *et al.* (1984), it still predicts reaction rates which are too low when compared to experimental data for the low-conversion branch of the rate curve. In Chapter 5 it will be shown that a CO self-exclusion model is superior to any of the surface island models for describing steady-state multiplicity of CO oxidation.

3.5 References

Cutlip, M. B., C. J. Hawkins, D. Mukesh, W. Morton, and C. N. Kenney, "Modelling of Forced Periodic Oscillations of Carbon Monoxide Oxidation over Platinum Catalyst", Chem. Eng. Commun. 22, 329-344 (1983).

Dumont, M., M. Poriaux and R. Dagonnier, "On Surface Reaction Kinetics in the Presence of Islands", Surface

Sci. 169 L307-310 (1986).

Engel, T., and G. Ertl, "Elementary Steps in the Catalytic Oxidation of Carbon Monoxide on Platinum Metals", Adv. Catal. 28, 1-78 (1979).

Goodman, M. G., M. B. Cutlip, C. N. Kenney, W. Morton, and D. Mukesh, "Transient Studies of Carbon Monoxide Oxidation Over Platinum Catalyst", Surface Sci. 120, L453-460 (1982).

Herskowitz, M., R. Holliday, M. B. Cutlip and C. N. Kenney, "Effect of Metal Dispersion in CO Oxidation on Supported Pt Catalysts", J. Catal. 74 , 408-410, (1982).

Herskowitz, H., and C. N. Kenney, "CO Oxidation on Pt Supported Catalysts. Kinetics and Multiple Steady States", Can. J. Chem. Eng. 61, 194-199 (1983).

Kubicek, M., "Algorithm 502: Dependence of Solutions of Nonlinear Systems on a Parameter", A. C. M. Trans. Math. Software 2, 98-107 (1976).

Mukesh, D., M. Goodman, C. N. Kenney and W. Morton, "Oscillatory Phenomena in Heterogeneous Catalysed Oxidation Reactions", A Specialist Periodical Report: Catalysis 6, 1-26 (1983).

Mukesh, D., W. Morton, C. N. Kenney, and M. B. Cutlip, "Island Models and the Catalytic Oxidation of Carbon Monoxide and Carbon Monoxide-Olefin Mixtures", Surface Sci. 138, 237-257 (1984).

4. Experimental Equipment and Materials

In order to resolve some of the questions concerning CO oxidation on platinum, an experimental investigation of this system was carried out. A schematic of the experimental setup used in this study is shown in Figure 4.1. Two reactors were used; the first was used previously by Lynch (1981), whereas the second was built specifically for this study. Both reactors were fixed bed recycle reactors. The catalysts used were either lightly loaded (0.5%) platinum on alumina or circular sheets of platinum gauze. The same feed system was used for both reactors, and it evolved throughout the course of this study as progressively greater demands were placed upon it. The feed system was computer controlled. Gas analysis was performed with an infrared spectrophotometer which was interfaced to a computer for real-time data acquisition.

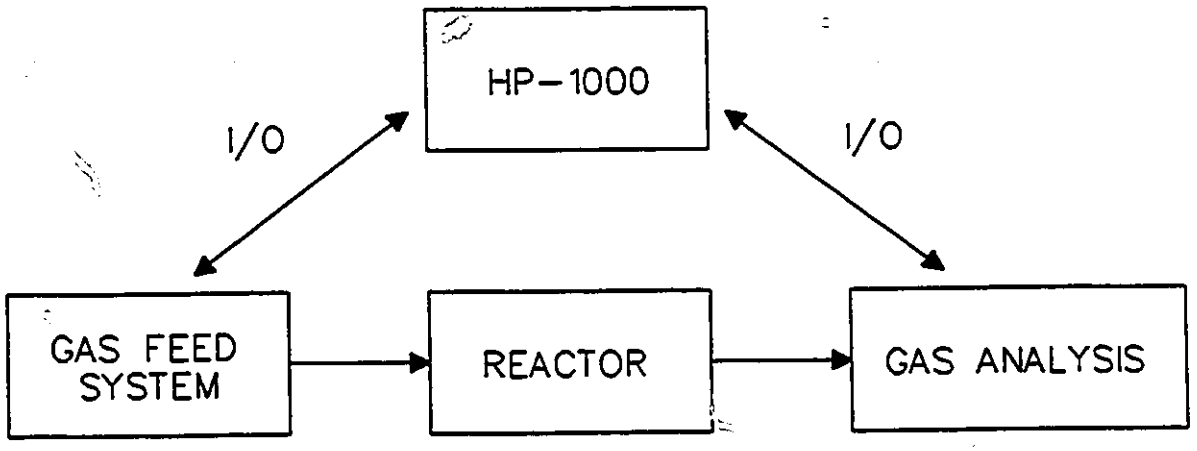

Figure 4.1 Overall Experimental Schematic

The first reactor and the gas analysis system have been described in detail by Lynch (1981), thus only a general description of this reactor system will be given here. Modifications and additions to the equipment used by Lynch, as well as the second reactor system, will be described in detail.

The experimental equipment can be divided into three main sections. These are: the reactors, the feed gas system, and the gas analysis system. These systems will be described in the following sections of this chapter.

4.1 Reactor Systems

4.1.1 Reactor I

The first reactor used in this study, shown schematically in Figure 4.2, has been described in detail by Lynch (1981) and by Lynch and Wanke (1984). The reactor consisted of a 2.54 cm ID stainless steel tube immersed in a heated fluidized sandbath, and a metal bellows recycle pump in a heated airbath. The total reactor volume, including the recycle pump and associated tubing, was determined to be 245 cm^3. The effective reactor volume, when the reactor was packed with 50 g of catalyst, was approximately 190 cm^3. The gas stream temperature was measured immediately upstream and downstream of the catalyst bed. The inlet temperature was used to control the heat input to the sandbath. The reactor operated essentially isothermally, with a maximum

recorded temperature difference across the catalyst bed of 2 K. The temperature difference across the reactor was typically less than 1 K.

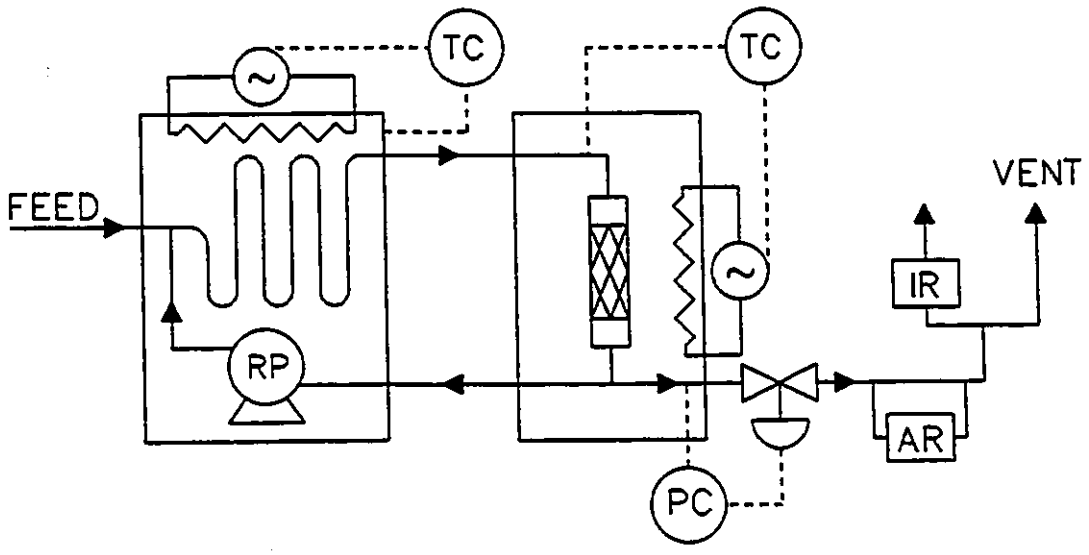

TC Temperature Controller RP Recycle Pump
IR Infrared Spectrometer AR Auxiliary Reactor
PC Pressure Controller

Figure 4.2 Reactor I Schematic

The catalyst used in the first reactor was purchased from Aldrich and contained 0.5 wt% platinum supported on γ-Al_2O_3. A platinum dispersion of approximately 0.5 to 0.6 was calculated from hydrogen adsorption measurements. The catalyst support had a BET surface area of 108 m^2/g and an average pore radius of 3 nm. The cylindrical pellets were approximately 3 mm by 3 mm in size, with the platinum deposited in a thin layer on the exterior portion of the pellets, a so-called egg-shell catalyst. The size of the

reactor limited the maximum catalyst charge to 50 g. For catalyst charges of less than 50 g, the bed was diluted with 3 mm inert glass or Pyrex spheres so that the effective bed volume was approximately constant at 55 cm^3 for all catalyst charges. Catalyst charges of 4.95, 14.6 and 43.6 g were used in this reactor.

Flow rates of 100 to 900 cm^3/min (measured at 21°C and 101 kPa) were used with this reactor. The recycle flow rate was determined to be approximately 500 cm^3/s, thus the recycle ratio was always between 30 and 300. The recycle pump was housed in a temperature controlled box for preheating of the feed gases. The exit stream from the reactor usually was routed directly to an infrared spectrophotometer for analysis of the reactor products. However, the reactor effluent could alternatively be diverted through an auxiliary reactor, loaded with 10 g of 4% platinum on alumina catalyst, to fully oxidize the carbon compounds to carbon dioxide. This facilitated the determination of the total carbon content in the effluent stream.

4.1.2 Reactor II

The second reactor system used in this study is shown schematically in Figure 4.3. This system was designed for use with 2.5 cm disks of platinum gauze. The reactor was a 10 cm section of 2.5 cm ID stainless steel. The reactor was in a temperature controlled airbath. The reactant gas stream was heated between the recycle pump (Metal Bellows

model MB-158) and the reactor, and cooled in a shell and tube heat exchanger upon exit from the reactor airbath. The temperature of the cooling water on the shell side of the heat exchanger was maintained at approximately 20°C. The recycle loop was constructed of 1/4-inch stainless steel tubing between the recycle pump and the exit of the heat exchanger, with 1/8-inch stainless steel tubing used elsewhere. The recycle flow rate was determined to be 193 cm^3/s, and the volume of the empty reactor was approximately 125 cm^3.

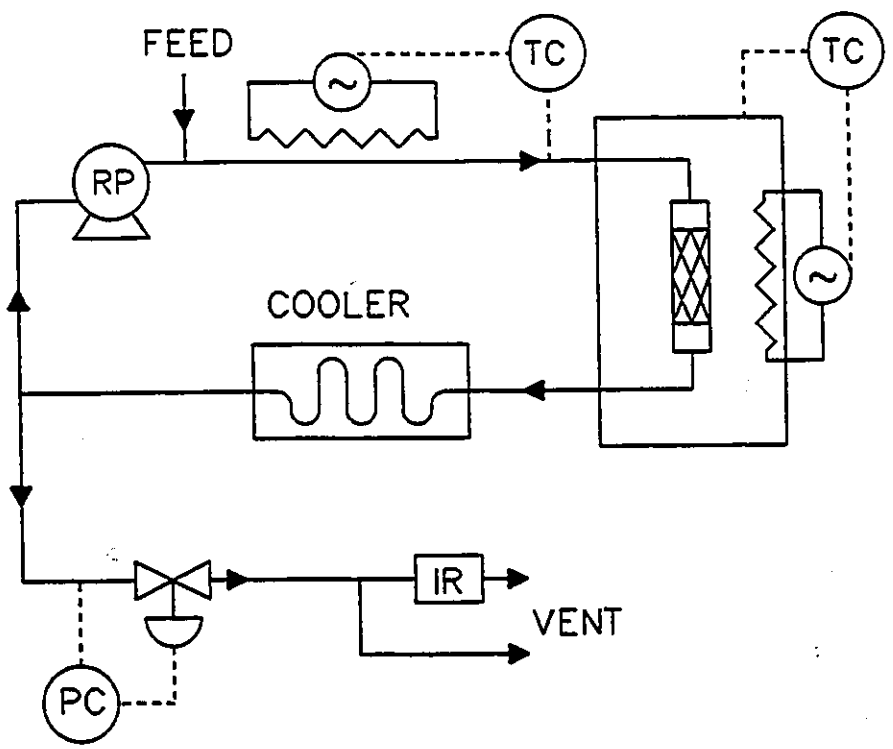

Figure 4.3 Reactor II Schematic

The catalyst used in the second reactor was platinum gauze consisting of 146 disks of gauze (2.5 cm diameter),

with a combined mass of 51.95 g and an estimated platinum surface area of 0.1 m^2. The gauze disks were stacked tightly in the reactor. Ring spacers 2 mm thick were placed immediately above and below the stacked gauze to minimize bypass flow along the reactor walls. The top and bottom sections of the reactor were filled with 3 mm Pyrex beads. Thermocouples were located 2.5 cm from the top and bottom of the reactor. The thermocouple tips were placed along the central axis of the reactor.

4.2 Feed Gas System

The feed system is shown schematically in Figure 4.4. All gases used in this study were either Matheson ultra-high purity grade, or equivalent, or were specialty mixtures of O_2/N_2 and CO/N_2 prepared by Matheson. The feed composition and flow rate were controlled by three Matheson model 8250 series flow controllers which were interfaced to a Hewlett-Packard 1000-MXE minicomputer. The computer could be used to manipulate the set-points of the three flow controllers, or they could be set manually. Reactant flow rates between 6 and 3000 cm^3/min could be accurately set. Standard conditions of 101 kPa and 21°C were used for all flow measurements.

With the valve arrangement shown in Figure 4.4 it was possible to operate a reactor with constant feed mixtures of any desired flow rate or composition of CO, O_2 and N_2 for steady-state rate measurements. Alternatively a reactor

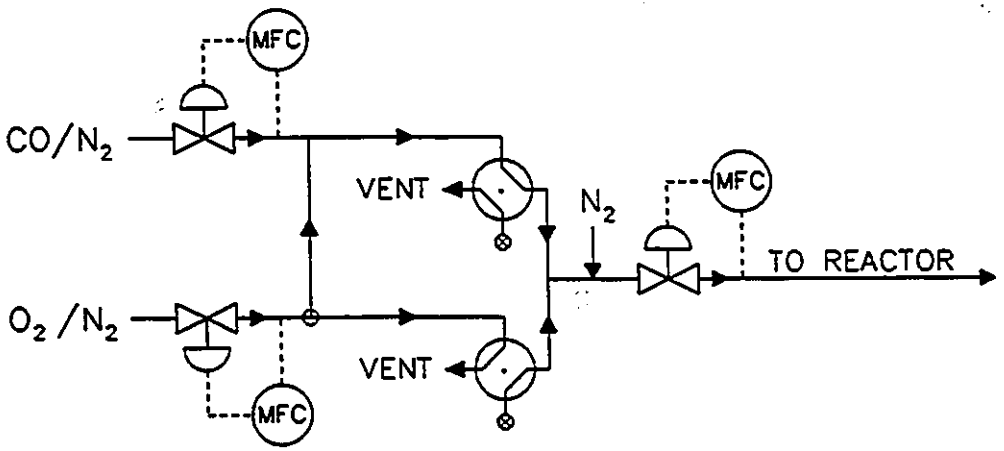

MFC Mass Flow Controller

Figure 4.4 Feed System Schematic

could be operated with the feed composition varied in a cyclic fashion. Square wave composition cycling was achieved by routing the CO and O_2 feed streams through air-actuated four-way valves, the timing of which was independently controlled with digital outputs from a HP minicomputer. It was found that using four-way valves produced composition square waves which were much more precise in form than those generated by periodically changing the setpoints of the mass flow controllers.

4.3 Gas Analysis System

Gas analysis was performed with a Pye Unicam SP3-200 ratio recording infrared spectrophotometer, equipped with an SP3-050 data analysis unit. The IR was interfaced to the HP minicomputer to facilitate real-time data acquisition and

analysis. The link was made through the data analysis unit with an RS-232 interface. The data acquisition program included a calibration function to convert absorbance (at 2355 cm^{-1}) to CO_2 concentration. (During feed cycling the control program also integrated the CO_2 concentration to obtain the cycle-average conversion.)

4.4 References

D. T. Lynch, "Oscillatory Behavior in Catalytic Reactions: A Mathematical and Experimental Investigation", Ph.D. Thesis, University of Alberta (1981).

Lynch, D. T., and S. E. Wanke, "Oscillations during CO Oxidation over Supported Metal Catalysts: I. Influence of Catalyst History on Activity", J. Catal. 88, 333-344 (1984)

5. Steady-State Behavior

5.1 Nomenclature

a_m = total surface area of the supported catalyst, 3.17 m^2 for 4.95 g charge, 9.36 m^2 for 14.6 g charge, 27.8 m^2 for 43.6 g charge (based on Pt dispersion of 0.5)

C_1 = parameter in Eqn. (5.17), $2F_{O_2}k_2a_mL_m^2(k_{-1}RT/k_1P)^2(PT_{ref}/P_{ref}T)$

C_2 = parameter defined in Eqn. (5.49), $1.88\times10^{-4}\sqrt{T}\ e^{(8100/T)}[CO]$, $m^2/mol\cdot s$

C_3 = parameter defined in Eqn. (5.49), $3.18\times10^{3}\sqrt{T}[O_2]$, $m^2/mol\cdot s$

C_4 = parameter defined in Eqn. (5.49), $2.44\times10^{-16}\sqrt{T}\ e^{(13900/T)}[CO]$

C_5 = parameter in Eqn. (5.30), $L_m\sqrt{2F_{O_2}k_2a_mPT_{ref}/P_{ref}T}$

C_6 = parameter in Eqn. (5.42), $4F_{O_2}k_2a_mL_m^2(k_{-1}RT_{ref}/k_1P_{ref})$

[CO] = reactor, and exit, CO concentration, mol/m^3

$[CO]_o$ = time-average feed CO concentration, $F_{CO}P/RT$, mol/m^3

$[CO_2]$ = reactor, and exit, CO_2 concentration, mol/m^3

E_{ox}/R = activation energy for surface oxidation, 1100 K

E_{red}/R = activation energy for surface reduction, 5100 K

E_{-1}/R = activation energy for CO desorption, K

A portion of this chapter was presented at the AIChE Annual Meeting, Chicago, Nov. 1985, "Forced Composition Cycling During CO Oxidation on Platinum", paper 132a.
A version of this chapter has been published.
Graham, W. R. C. and D. T. Lynch, "CO Oxidation on Pt: Model Discrimination Using Experimental Bifurcation Behavior", AIChE J., 33, 792-800 (1987).

E_3/R = activation energy for surface reaction, K

F_{CO} = time-average fraction CO in feed

F_{O_2} = time-average fraction O_2 in feed

k_{ox} = surface oxidation rate constant, $k^o_{ox} \cdot \exp(-E_{ox}/RT)$, $m^2/mol \cdot s$

k^o_{ox} = surface oxidation pre-exponential factor, 1×10^{-5} $m^2/mol \cdot s$

k_{red} = surface reduction rate constant, $k^o_{red} \cdot \exp(-E_{red}/RT)$, $m^2/mol \cdot s$

k^o_{red} = surface reduction pre-exponential factor, 50 $m^2/mol \cdot s$

k_1 = CO adsorption rate constant, 6.87 $S_{CO}\sqrt{T}/L_m$, $m^3/mol \cdot s$

k_{-1} = CO desorption rate constant, $k^o_{-1} \cdot \exp(-E_{-1}/RT)$, s^{-1}

k^o_{-1} = CO desorption pre-exponential factor, s^{-1}

k_2 = O_2 adsorption rate constant, 6.43 $S_{O_2}\sqrt{T}/L_m^2$, $m^5/mol^2 \cdot s$

k_3 = surface reaction rate constant, $k^o_3 \cdot \exp(-E_3/RT)$, $m/mol^{0.5} \cdot s$ for surface island models, $m^2/mol \cdot s$ for other models

k^o_3 = surface reaction pre-exponential factor, $m/mol^{0.5} \cdot s$ for surface island models, $m^2/mol \cdot s$ for other models

K_{ox} = dimensionless surface oxidation rate constant, $a_m L_m^2 k_{ox}/Q_o[CO]_o$

K_{red} = dimensionless surface reduction rate constant, $a_m L_m^2 k_{red}/Q_o[CO]_o$

K_1 = dimensionless CO adsorption rate constant, $a_m L_m k_1/Q_o$

K_{-1} = dimensionless CO desorption rate constant, $a_m L_m k_{-1}/Q_o[CO]_o$

K_2 = dimensionless O_2 adsorption rate constant, $a_m L_m^2 k_2/Q_o$

K_3 = dimensionless surface reaction rate constant, $a_m L_m^n k_3/Q_o[CO]_o$, n=1.5 for surface island models, n=2 for other models

L_m = adsorption capacity of the metal surface, 2×10^{-5} mol/m^2

N_{CO} = CO self-exclusion factor

$[O_2]$ = reactor, and exit, O_2 concentration, mol/m^3

$[O_2]_o$ = time-average feed O_2 concentration, $F_{O_2}P/RT$, mol/m^3

P = reactor pressure, 0.1 MPa absolute

P_{ref} = reference pressure, 0.101 MPa absolute

Q_n = ratio of exit to feed volumetric flow rates

Q = feed volumetric flow rate at standard conditions, m^3/s

Q_o = feed volumetric flow rate at reactor conditions, m^3/s

r_{CO_2} = rate of CO_2 formation, mol/(m^2 of Pt)·s

R = gas constant, 8.314 m^3·Pa/mol·K

$R_{CO,ads}$ = dimensionless rate of CO adsorption

R_{ox} = dimensionless rate of surface oxidation

R_{red} = dimensionless rate of surface reduction

R_1 = dimensionless rate of Step (5.1)

R_2 = dimensionless rate of Step (5.2)

R_3 = dimensionless rate of Step (5.3)

S_{CO} = CO sticking probability on catalyst

S_{O_2} = O_2 sticking probability on catalyst

t = time, s

T = reactor temperature, Kelvin

T_{ref} = reference temperature, 294 K

V = effective free volume of reactor, 1.9×10^{-4} m^3

X = dimensionless reactor CO concentration, $[CO]/[CO]_o$

X_o = instantaneous dimensionless feed CO concentration (1 in this chapter)

Y = dimensionless reactor O_2 concentration, $[O_2]/[O_2]_o$

Y_o = instantaneous dimensionless feed O_2 concentration (1 in this chapter)

Z = dimensionless reactor CO_2 concentration, $[CO_2]/[CO]_o$

Z_o = instantaneous dimensionless feed CO_2 concentration (0 in this chapter)

Greek Symbols

α_m = ratio of bulk volume to metal surface capacitances, $[CO]_oV/a_mL_m$

ϵ = variable defined in Eqn. (5.48), $(1-N_{CO}\theta_{CO})/(1-\theta_{CO})$

θ_{CO} = fractional CO surface coverage on the metal surface

θ_o = fractional oxygen surface coverage on the metal surface

θ_{Ox} = fractional oxide surface coverage on the metal surface

τ = dimensionless time based on the reactor residence time, Q_ot/V

Subscripts

a = adsorbed species

5.2 Introduction

In this chapter an experimental determination of the steady-state behavior for carbon monoxide oxidation in a recycle reactor is presented. Steady-state multiplicity was observed. The effects of the size of catalyst charge, feed flow rate, feed composition, and reactor temperature on the location of the boundaries of the steady-state multiplicity region were determined. The sensitivity of these bifurcation points to variations in reactor parameters was used to discriminate among five reaction mechanisms. Only an elementary-step model incorporating carbon monoxide self-exclusion from the catalyst surface could quantitatively describe all observed steady-state data. An explicit rate function based on this model is presented.

5.3 Review

Conrad and Treguer-Seguda (1984) have investigated how the knowledge of a bifurcation point can lead to parameter estimates. They presented an algorithm for estimating parameters and demonstrated its use through examples concerned with thermal ignition and enzymatic diffusion-reaction. As demonstrated by Herskowitz and Kenney (1983), a knowledge of the bifurcation behavior of a physical system

can also aid in discrimination among rival models. Aluko and Chang (1986) utilized the effect of temperature and composition on the bifurcation behavior of the CO oxidation reaction in order to obtain rate parameter estimates for a kinetic model based on oxidation and reduction of the surface platinum.

In this chapter, it will be shown that a knowledge of the effect of operating parameters on the multiplicity behavior of a reaction can be used to discriminate among rival kinetic models. This will be done by systematically examining the effects of reactor temperature, feed flow rate, feed composition and size of catalyst charge on the steady-state multiplicity behavior of the carbon monoxide oxidation reaction on a supported platinum catalyst in a recycle reactor. In particular, the sensitivity of the location of the bifurcation points to the reactor operating parameters will be determined. The data will be used to discriminate among five steady-state kinetic models which have been proposed for this reaction. All of the models examined are of the elementary-step Langmuir-Hinshelwood form. It will be shown that the classical LH mechanism is incapable of quantitatively describing both the reaction rates and the location of the bifurcation points. However, a model which incorporates CO self-exclusion from the catalyst surface is able to quantitatively describe all observed steady-state data.

5.4 Experimental Steady-State Behavior

The experimental work was concerned with determining the effects of the reactor temperature, feed flow rate, and size of catalyst charge on the rate and multiplicity behavior. Particular attention was paid to determining the feed compositions at which bifurcations occurred (both high-to-low-conversion transitions and low-to-high-conversion transitions). In the following, the term "location of a bifurcation point" refers to the fraction CO in the reactor feed, F_{CO}, at which a bifurcation occurs. The bifurcation point locations depend in a very nonlinear fashion on the reactor operating parameters (temperature, flow rate, etc.). Thus, they are very useful for model discrimination and parameter estimation.

In this study, the exact values of the bifurcation points were not determined, rather their values were bracketed by the following procedure. The total feed flow rate, reactor temperature, and oxygen feed composition were set at desired levels. The CO feed concentration was set at about twice the oxygen concentration. The near stoichiometric mixture invariably led to a low-conversion steady state. When steady state was achieved the CO concentration was decreased slightly. In this manner the reaction rate curve was determined for decreasing CO feed concentration. The rate curve was also determined for increasing CO feed concentration. The adsorption and desorption of CO_2 from the catalytically inert Al_2O_3 support made the quantitative

determination of the low-conversion steady states difficult. Operating times of greater than 24 h were on occasion required to achieve a reproducible low-conversion steady state.

In Figure 5.1 the results of this procedure are summarized for 1.0% O_2, 14.6 g of catalyst, a feed flow rate of 300 cm^3/min and a reactor temperature of 90°C.

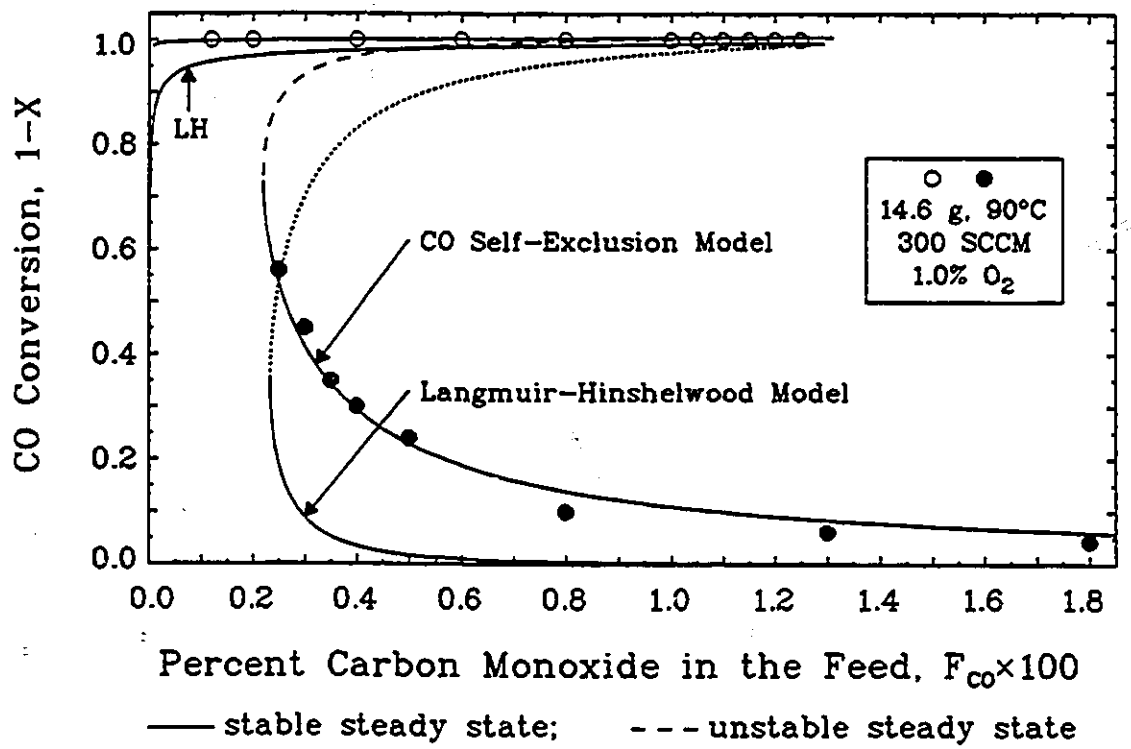

Figure 5.1 Steady-State CO Conversion Multiplicity

At high CO feed concentrations the reactor operated at a low-conversion steady state, shown here as solid circles. Decreasing the CO in the feed caused the conversion to increase gradually from 5% at 1.8% CO to 55% at 0.25% CO.

Further decreases in feed CO below 0.25% caused the rate to increase to a steady state with a conversion of 100%, represented with open circles in Figure 5.1. The reactor remained in a high-conversion steady state when the CO feed concentration was decreased further. Subsequent increases in the percentage CO in the feed resulted in the reactor operating at a high-conversion steady state. The reactor remained in a high-conversion steady state until 1.25% CO in the feed was reached. Increasing the CO in the feed beyond 1.25% caused the reaction rate to drop to the low-conversion steady state. Thus, as shown in Figure 5.1, this reaction displays multiplicity behavior over an intermediate range of values of the %CO in the feed (constant $\%O_2$). In the multiplicity region, the starting conditions determine whether the reactor will operate at a low-conversion or at a high-conversion steady state.

The multiplicity behavior was also determined for O_2 concentrations other than that used in Figure 5.1, and these results are summarized in Figure 5.2 where the transition points are shown as functions of the reactor feed composition. The pairing of a half-filled symbol with an empty symbol brackets the low-conversion to high-conversion transition conditions, while the pairing of a half-filled symbol with a filled symbol brackets the high-conversion to low-conversion transition conditions. Thus, the leftmost region in Figure 5.2 is the high-conversion region, while the rightmost part is the low-conversion region. The cusp

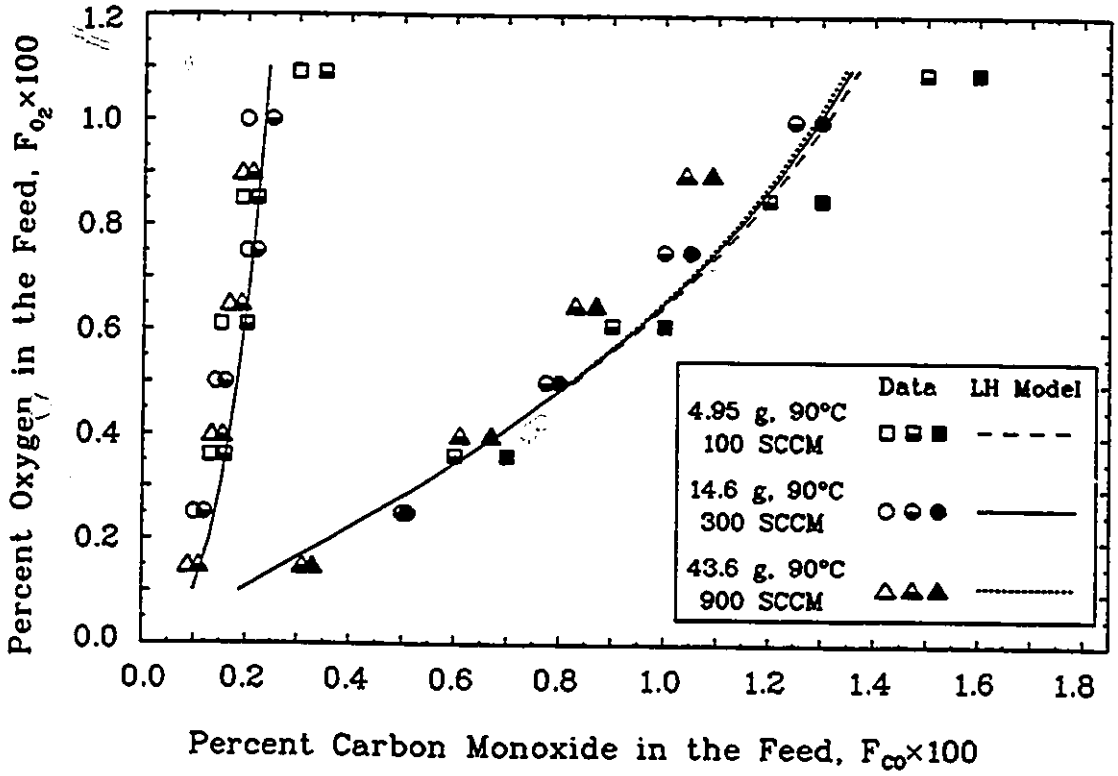

Figure 5.2 Multiplicity Boundaries for Three Catalyst Charges

shaped region delimits the conditions under which multiple steady states occur.

Additional experimental data on the variation of the steady-state bifurcation boundaries have been collected to enable discrimination among kinetic models. Shown in Figure 5.3 are the effects of bulk temperature on the bifurcation boundaries. The boundaries at 90°C from Figure 5.2 are reproduced in Figure 5.3 (circles) to facilitate comparison between the figures. From Figure 5.3 it is seen that both the lower and upper experimental bifurcation boundaries shifted to progressively higher CO concentrations as the

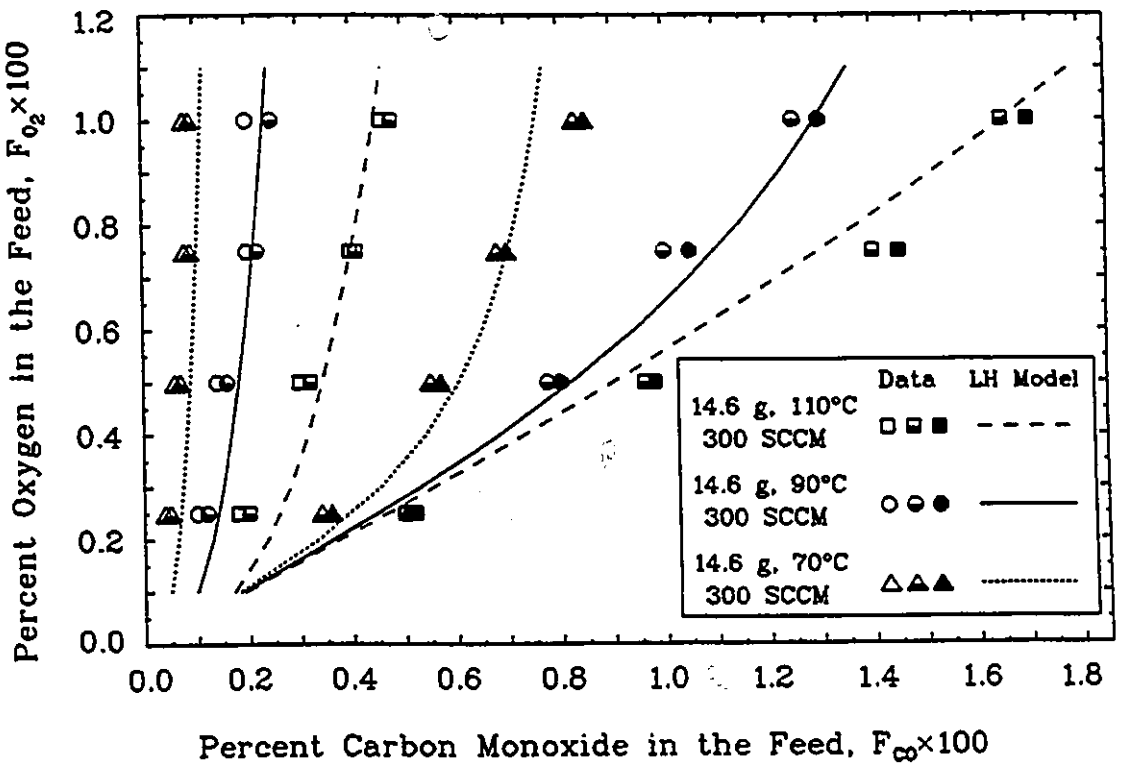

Figure 5.3 Effect of Temperature on the Multiplicity Boundaries

temperature was increased from 70°C to 110°C. An Arrhenius-type plot of the bifurcation points is shown in Figure 5.4. The fraction of CO in the feed at the bifurcation point, normalized with respect to that for the bifurcation point at 90°C, is plotted versus inverse temperature. The low-to-high-conversion bifurcation points have an apparent activation energy of E/R = 5130 K. The high-to-low-conversion bifurcation points have a slope corresponding to E/R = 2200 K in the low-temperature region. At higher temperatures the high-to-low-conversion bifurcation points approach stoichiometric mixtures, and the activation energy

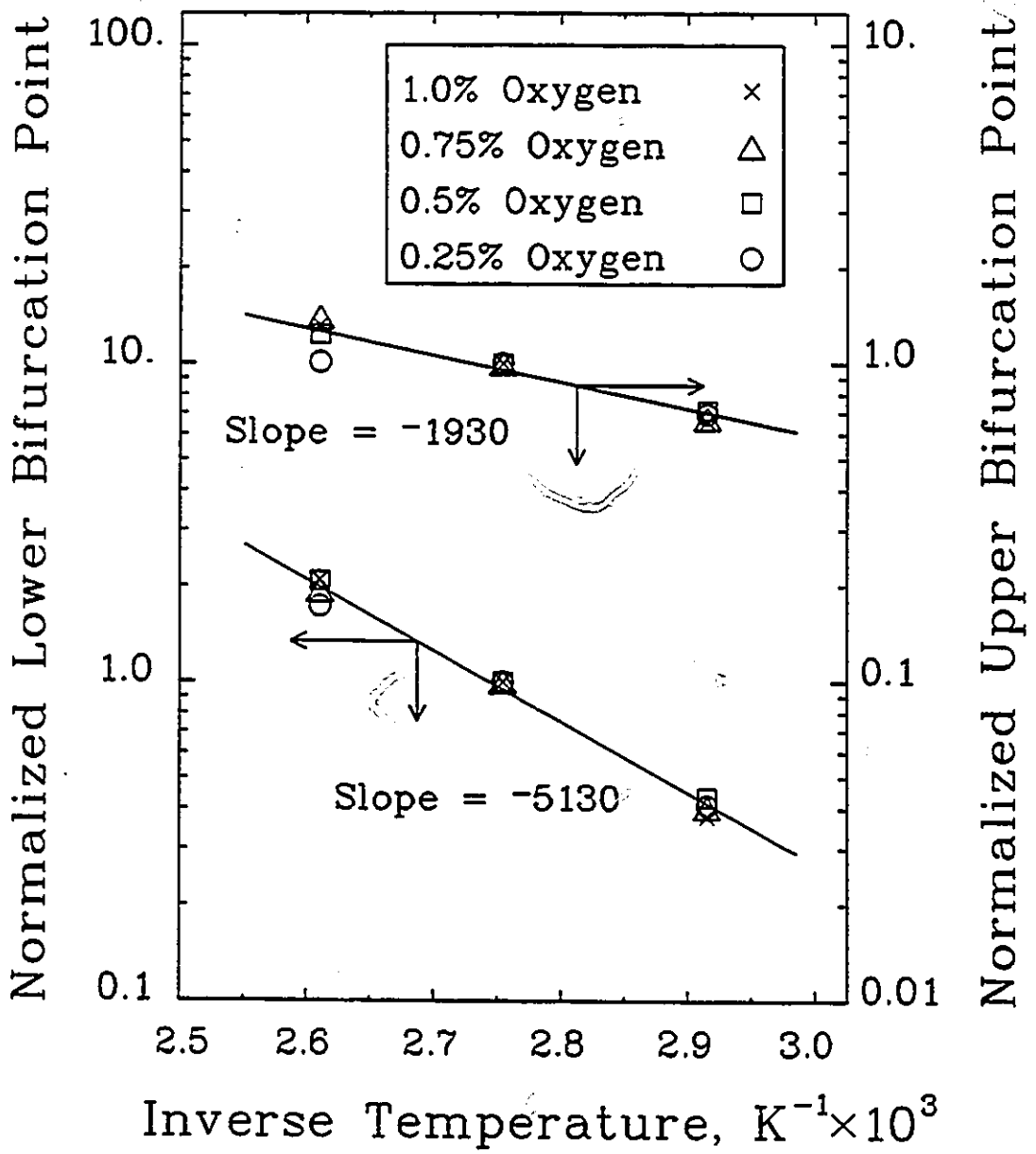

Figure 5.4 Dependence of Bifurcation Points on Temperature

decreases so that the average value over the entire temperature region is E/R = 1930 K as shown in Figure 5.4.

The steady-state behavior of the reactor was also examined for flow rates of 100, 300 and 900 cm^3/min. In

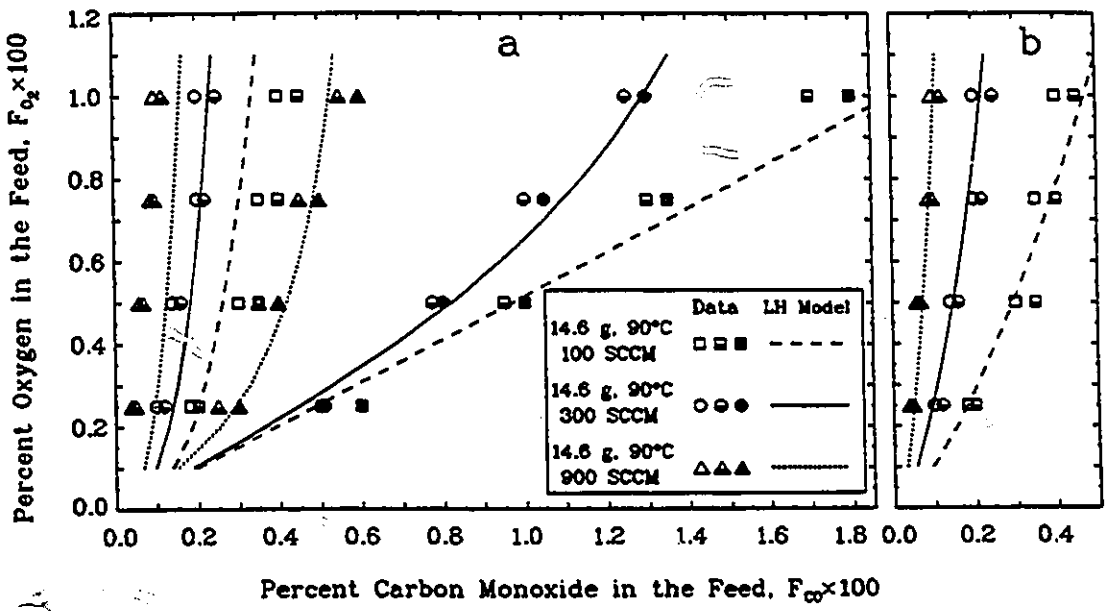

Figure 5.5 Effect of Flow Rate on the Multiplicity Boundaries

Figure 5.5 is shown the effect of flow rate on the bifurcation behavior of the system. As the flow rate was increased, both the upper and lower bifurcation boundaries moved to lower CO concentrations. The relationship between the normalized bifurcation point locations and flow rate is shown in Figure 5.6. (The fraction of CO in the feed at the bifurcation points has been normalized with respect to that for the bifurcation point at 300 cm^3/s.) All of the low-to-high-conversion bifurcation points varied inversely with the 0.66 power of flow rate ($\propto Q^{-0.66}$). However, this was not the case with the high-to-low-conversion bifurcation

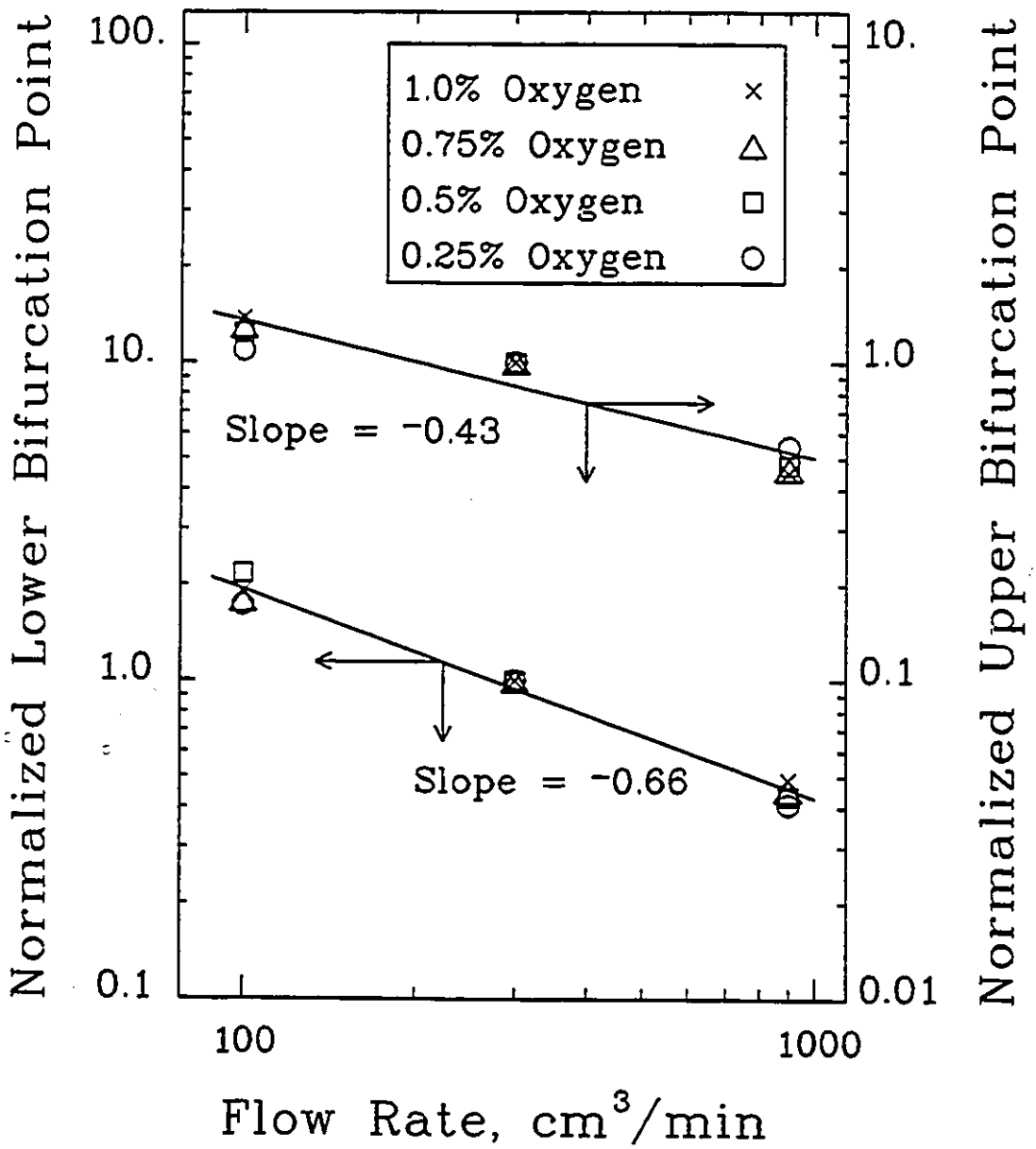

Figure 5.6 Dependence of Bifurcation Points on Flow Rate

points. At low flow rates, these bifurcation points occurred at conditions corresponding to near-stoichiometric mixtures, and the locations of the bifurcation points were nearly independent of the flow rate. For large flow rates,

the high-to-low-conversion bifurcation points depended inversely on flow rate to the 0.72 power. Thus, as shown in Figure 5.6, over the range of flow rates examined, the high-to-low-conversion bifurcation points varied according to $Q^{-0.43}$ on average.

The experimental effects of temperature and feed flow rate on the bifurcation point locations will be used, in the following, as the basis for discrimination among several models for this reaction.

5.5 Mathematical Models

It is generally accepted that, at the temperatures studied, the catalytic oxidation of CO on platinum occurs via the following steps:

$$CO(g) + M \underset{k_{-1}}{\overset{k_1}{\rightleftharpoons}} CO\text{-}M \qquad (5.1)$$

$$O_2(g) + 2\ M \xrightarrow{k_2} 2\ O\text{-}M \qquad (5.2)$$

$$CO\text{-}M + O\text{-}M \xrightarrow{k_3} CO_2(g) + 2\ M \qquad (5.3)$$

CO adsorbs reversibly on a single platinum surface site. Oxygen adsorbs dissociatively and irreversibly. The two surface species undergo a bimolecular reaction forming CO_2, which immediately desorbs, freeing two surface metal sites.

The reactor used in this study can be modeled as a CSTR due to the high recycle ratios which were employed. In the

absence of inter- and intrapellet heat and mass transfer limitations, mass balances on the various gas and surface phase species produce the following five ordinary differential equations:

$$\frac{dX}{d\tau} = X_o - Q_n X - R_1 \tag{5.4}$$

$$\frac{dY}{d\tau} = Y_o - Q_n Y - R_2 \tag{5.5}$$

$$\frac{dZ}{d\tau} = Z_o - Q_n Z + R_3 \tag{5.6a}$$

$$\frac{d\theta_{co}}{d\tau} = \alpha_m \{R_1 - R_3\} \tag{5.7a}$$

$$\frac{d\theta_o}{d\tau} = \alpha_m \{\frac{2F_{o_2}}{F_{co}} R_2 - R_3\} \tag{5.8a}$$

where $Q_n = 1 - F_{co}R_1 - F_{o_2}R_2 + F_{co}R_3$ (5.9a)

The terms R_1, R_2 and R_3 refer to the net rates of Steps (5.1), (5.2), and (5.3), respectively. The forms of the R_i terms depend on the details of the various mechanisms. Equations (5.4) to (5.8a) have been written in differential, rather than algebraic, form so that they may readily be used in conjunction with studies concerned with reaction dynamics. However, since steady-state behavior is the focus of the present chapter, these equations were normally used in algebraic form by setting the derivatives equal to zero. For steady-state operation the normalized CO and O_2 feed concentrations, X_o and Y_o, are equal to unity. The steady-state models examined in detail herein include: 1) elementary-step LH model, 2) surface oxidation-reduction

model, 3) CO surface island model, 4) modified CO surface island model with oxygen adsorption based on the island-free area, and 5) CO self-exclusion model.

5.5.1 Langmuir-Hinshelwood Model

The first mechanism used to describe the reactor behavior was a classical elementary-step Langmuir-Hinshelwood model. Herskowitz and Kenney (1983) showed that a classical LH model, with the surface reaction controlling the overall reaction rate, and both CO and O_2 at equilibrium, was unable to predict most of their experimental bifurcation points. Goodman *et al.* (1982), however, have used an elementary-step LH model to describe the response of the $CO-O_2-Pt$ system to step changes in reactant concentrations. They did not discuss the ability of the model to predict the bifurcation behavior of the system. For the LH model the reaction rates for Steps (5.1) to (5.3) are as follows:

$$R_1 = K_1X(1-\theta_{CO}-\theta_O) - K_{-1}\theta_{CO} \tag{5.10a}$$

$$R_2 = K_2Y(1-\theta_{CO}-\theta_O)^2 \tag{5.11a}$$

$$R_3 = K_3\theta_{CO}\theta_O \tag{5.12}$$

At steady state the time derivatives in Eqns. (5.4) to (5.8a) are set equal to zero. These algebraic equations were solved using a differential arclength homotopy-continuation method (Kubicek, 1976) as in Chapter 3.

Examination of the definitions of the dimensionless rate constants of the LH model (see Nomenclature section) shows that wherever the metal surface area, a_m, appears it is divided by the volumetric feed flow rate, Q_o. This suggests a first test of the proposed model. If the ratio of the mass of catalyst to the volumetric flow rate is constant, then a_m/Q_o is constant, and thus identical values of the dimensionless rate constants are obtained for each catalyst charge. The data in Figure 5.2 are for catalyst charges of 4.95 g, 14.6 g and 43.6 g. The multiplicity bounds are approximately the same in each case because the total volumetric flow rates, 100 cm^3/min, 300 cm^3/min, and 900 cm^3/min, respectively, were adjusted so that the ratio of the mass of catalyst to volumetric flow rate was approximately constant for each charge. The slight differences between the three sets of data are due to the small variations in this ratio. The fact that experimentally the multiplicity boundaries are almost the same for all three sets of data is a first, and very important, point of agreement with the proposed model.

The second test for the model is to determine if it can describe the experimentally observed multiplicity behavior shown in Figures 5.2, 5.3 and 5.5. The predicted multiplicity boundaries of the elementary-step LH model for a particular set of parameter values (values given in Table 5.1) are shown by the curves in Figures 5.2, 5.3 and 5.5, where in Figure 5.2 the different curves are for the slightly

Table 5.1 Model-Dependent Parameter Values

	Langmuir-Hinshelwood	95% Confidence Interval	CO Self-Exclusion	95% Confidence Interval
S_{CO}	3.53×10^{-6}	$(2.4-6.0)\times10^{-6}$	7.6×10^{-5}	$(4.0-20.0)\times10^{-5}$
k^{o}_{-1}	1.01×10^{7}	$(0.61-1.52)\times10^{7}$	7.5×10^{15}	$(2.7-14.5)\times10^{15}$
S_{O_2}	1.38×10^{-7}	$(0.85-2.2)\times10^{-7}$	9.9×10^{-8}	$(7.0-14.0)\times10^{-8}$
k^{o}_{3}	7.46×10^{9}	$(5.91-9.33)\times10^{9}$	5.4×10^{10}	$(4.3-6.7)\times10^{10}$
E_{-1}/R	6950	(2900-10100)	13900	(6000-19300)
E_3/R	5150	(3500-7000)	5800	(4000-7700)
N_{CO}	1.0	———	1.07	(1.06-1.08)*

*based on low-conversion rate behavior, all other confidence intervals based on bifurcation point locations.

different values of the a_m/Q_o ratio which were used experimentally. The parameter values were arrived at by minimizing the sum of the squares of the errors between the predicted and the experimental locations of the 40 bifurcation points presented in Figures 5.3 and 5.5, i.e., minimizing SSE in Eqn. (5.13).

$$SSE = \sum_{i=1}^{40} [(F_{CO})_{BP,PRE} - (F_{CO})_{BP,EXP}]^2 \tag{5.13}$$

It was not possible to use traditional optimization/search techniques because some parameter values fail to predict multiplicity behavior. It was necessary to interactively guide the parameter estimation process in order to keep the model in a region where multiple steady states exist.

In the process of estimating the parameters, it was found that if only the 24 bifurcation points shown in Figure 5.3 were used, then many sets of parameters (with quite different values) could all lead to the quantitative prediction of the 24 bifurcation points. This is partially due to the effects of the values of E_{-1} and E_3 being essentially decoupled. The variation of the location of the boundaries for the transition from low to high conversions (leftmost boundaries in Figures 5.2 and 5.3) is mainly affected by the value of E_{-1}, while the value of E_3 is the most important parameter in determining the manner in which the high-to-low-conversion boundaries shift under the influence of temperature. Reasonably precise parameter estimates only occurred when all 40 bifurcation points were

used. The values of the parameters are given in Table 5.1. The parameter set given in Table 5.1 is not unique: other sets of parameters can give nearly equivalent agreement with the steady-state data. The confidence intervals listed in Table 5.1 are based on varying a single parameter at a time, while other parameters are kept constant at their nominal values.

From Figures 5.2, 5.3 and 5.5 it is seen that excellent prediction of the bifurcation point locations occurs, with the one exception that the LH model significantly underpredicts the effect of flow rate on the location of the low-to-high-conversion bifurcation curve (leftmost curves in Figure 5.5). Experimentally the bifurcation points varied as $Q^{-0.66}$ while the LH model predicts they will vary as $Q^{-0.33}$. The inability of the LH model to predict the effect of flow rate on the location of the low-to-high-conversion bifurcation points can be understood by examining a simplified form of the model.

At steady state, the rates of the various reaction steps are identical, thus, from Eqns. (5.4) to (5.12):

$$1 - Q_n X = R_1 = R_3 = \frac{2F_{O_2}}{F_{CO}} R_2 = \frac{2F_{O_2}}{F_{CO}} K_2 Y (1-\theta_{CO}-\theta_O)^2 \qquad (5.14)$$

The CO adsorption and desorption steps in (5.1) proceed very rapidly. Thus, for the situation of low conversions, the CO adsorption/desorption will be essentially at equilibrium. Thus, from (5.10a), the fraction of empty sites will approximately be given by:

$$(1-\theta_{CO}-\theta_O) = \frac{K_{-1}\theta_{CO}}{K_1 X} \tag{5.15}$$

However, in order to obtain agreement between the experimental and predicted bifurcation points it was necessary for K_1 to be much greater than K_{-1}, which results in θ_{CO} being approximately unity. Also, since oxygen is in excess, and the CO conversion is very low, the oxygen composition in the reactor will be negligibly different from that of the feed, i.e. $Y = Y_o = 1$. In addition, because of the low conversion, and the large amount of inerts in the feed, there will be a negligible change in the volumetric flow rate (Q_n=1). Thus, in light of the above, combining Eqns. (5.14) and (5.15) yields:

$$1 - X = \frac{2F_{O_2}}{F_{CO}} K_2 \left[\frac{K_{-1}}{K_1 X}\right]^2 \tag{5.16}$$

Due to the dimensionalization which was used, K_1, K_{-1} and K_2 depend on the flow rate and the feed composition. Since the issue to be resolved is the inability of the LH model to accurately predict the effect of flow rate on the value of F_{CO} at which a low-to-high-conversion bifurcation occurs, it is necessary to explicitly relate X to F_{CO} and Q. Equation (5.16) becomes:

$$X^3 - X^2 + \frac{C_1}{F_{CO}^3 Q} = 0 \tag{5.17}$$

where C_1 is a constant defined in the Nomenclature section. In addition to Eqn. (5.17), the bifurcation points must

satisfy the condition that the derivative of F_{co} with respect to X vanishes:

$$\frac{dF_{co}}{dX} = (3X^2 - 2X)\left[\frac{F_{co}^4 Q}{3C_1}\right] = 0 \tag{5.18}$$

Solving Eqns. (5.17) and (5.18) simultaneously gives $X = \frac{2}{3}$ and,

$$F_{co} = \left[\frac{27\ C_1}{4\ Q}\right]^{0.33} \tag{5.19}$$

Thus, the conversion of the simplified model at the bifurcation points is 33%, which compares favorably with the full model predictions of 35%. Furthermore, Eqn. (5.19) leads to the bifurcation points varying as $Q^{-0.33}$, which matches exactly the predictions of the full LH model. For the values of the parameters specified in Table 5.1, the predicted locations of the bifurcation points from Eqn. (5.19) are within 5% of the values determined by the full LH model. Equation (5.19) may also be used to predict the effect of temperature on the location of the low-to-high-conversion bifurcation points. From Eqn. (5.19), and the definition of C_1, it is seen that

$$F_{co} \propto \exp\left[\frac{-E_{-1}}{RT}\right]^{0.67} \tag{5.20}$$

Thus, the value of F_{co} at the bifurcation point will have an apparent activation energy of $0.67E_{-1}$. In the full LH model, a value of $E_{-1}/R = 6950$ K was needed in order to describe the effect of temperature on the location of the

low-to-high-conversion bifurcation points. Thus, Eqn. (5.19) predicts that the apparent activation energy of the low-to-high-conversion bifurcation points should be 6950(2/3) or 4633 K. This is in agreement with the experimental value of E/R = 5130 K determined from Figure 5.4.

In addition to its inability to correctly predict the effect of flow rate on the bifurcation point locations, the LH model is also unable to correctly predict the reaction rates. This is shown in Figure 5.1, where predictions of conversion are presented. In the low-conversion region, it is seen that the predicted conversions are always much lower than the experimental observations. It is possible to choose model parameters which result in a closer match between the experimental and predicted conversions. However, in so doing the predicted bifurcation points no longer agree with the experimental values, and the predicted conversions on the high-conversion curve become significantly less than the experimentally observed value which was greater than 99%. In some cases the predicted region of multiplicity disappears when the kinetic parameters are adjusted to increase the conversion of the low-rate branch.

For the LH model the reactor was assumed to be an isothermal CSTR with no inter- or intrapellet mass transfer limitations. (Lynch and Wanke, 1984) The effects of these assumptions were examined individually to determine if any of the assumptions could be responsible for the mismatch between experimental data and model predictions, and it was

concluded that the inability of the LH model to describe the experimental observations was not due to the existence of nonisothermal behavior, imperfect mixing or significant mass transfer limitations.

5.5.2 Surface Oxidation-Reduction Model

There has recently been much interest in self-sustained oscillations in the platinum catalyzed oxidation of CO. Postulating that platinum forms stable oxides in the temperature ranges where oscillations have been observed, Sales *et al.* (1982) proposed a model incorporating oxidation and reduction of the platinum surface. This model was used with success to describe the observed oscillatory behavior and has recently been presented in a nonisothermal form (Yeates *et al.*, 1985; Aluko and Chang, 1986). Sales *et al.* (1982) included three surface concentrations in their model: adsorbed CO, adsorbed oxygen, and platinum oxide. In their model adsorbed oxygen undergoes a slow, irreversible reaction to form platinum oxide. The oxide reacts slowly with adsorbed CO to form CO_2.

$$\text{O-M} \xrightarrow{k_{ox}} \text{Ox-M} \tag{5.21}$$

$$\text{CO-M} + \text{Ox-M} \xrightarrow{k_{red}} CO_2(g) + 2\ \text{M} \tag{5.22}$$

where Ox-M represents the surface oxide complex. In the model of Sales *et al.* (1982) the surface oxidation and

reduction reactions have the rate functions:

$$R_{ox} = K_{ox}\theta_o(1-\theta_{ox}) \tag{5.23}$$

$$R_{red} = K_{red}\theta_{co}\theta_{ox} \tag{5.24}$$

The equation describing the surface oxide species is:

$$\frac{d\theta_{ox}}{d\tau} = \alpha_m \{R_{ox} - R_{red}\} \tag{5.25}$$

Equations (5.6a) to (5.9a) are also modified by adding R_{red}, $-\alpha_m R_{red}$, $-\alpha_m R_{ox}$ and $F_{co}R_{ox}$ to these equations, respectively.

$$\frac{dZ}{d\tau} = Z_o - Q_n Z + R_3 - R_{red} \tag{5.6b}$$

$$\frac{d\theta_{co}}{d\tau} = \alpha_m \{R_1 - R_3 - R_{red}\} \tag{5.7b}$$

$$\frac{d\theta_o}{d\tau} = \alpha_m\{\frac{2F_{o_2}}{F_{co}}R_2 - R_3 - R_{ox}\} \tag{5.8b}$$

where $Q_n = 1 - F_{co}R_1 - F_{o_2}R_2 + F_{co}R_3 + F_{co}R_{ox}$ (5.9b)

Equations (5.10a) and (5.11a) must be modified to account for the surface oxide species by including θ_{ox} in the term for the fraction of empty sites.

$$R_1 = K_1X(1-\theta_{co}-\theta_o-\theta_{ox}) - K_{-1}\theta_{co} \tag{5.10b}$$

$$R_2 = K_2Y(1-\theta_{co}-\theta_o-\theta_{ox})^2 \tag{5.11b}$$

Sales *et al.* (1982) only wrote equations for the surface species, because their gas phase concentrations were assumed constant during oscillations. In the present study the

experimental conversions of CO were often greater than 99%, thus the model presented here, Eqns. (5.4), (5.5), (5.6b)-(5.11b) and (5.25), includes the three gas phase concentrations in addition to the three surface species.

Predictions of the oxidation-reduction model were similar to those of the LH model. The use of the oxidation-reduction model had very little effect on the location of the low-to-high-conversion bifurcation points. In general, for fixed values of the other parameters, increasing k_{ox} shifted the high-to-low-conversion bifurcation curve to lower values of F_{CO}, but had negligible effect on the location of the low-to-high-conversion bifurcation curve. For fixed values of the other parameters, and a constant ratio of (k_{ox}/k_{red}), increasing both k_{ox} and k_{red} moved the high-to-low-conversion bifurcation curve to higher values of F_{CO}. When rate parameters were chosen to match the base case bifurcation diagram (Figure 5.2), the oxidation-reduction model was no better than the elementary-step LH model at predicting the effect of operating parameters on the bifurcation behavior. Using the parameters listed in Table 5.2, the oxidation-reduction model correctly described the effect of temperature on the bifurcation diagram, but underpredicted the effect of flow rate on the low-to-high-conversion bifurcation points, as shown in Figure 5.7a, and consistently gave predictions of the low conversion reaction rates which were much lower than the experimental observations, as shown in Figure 5.8a. An

analysis identical to that performed for the LH model in Eqns. (5.14) to (5.19) showed that the oxidation-reduction model predicts a $Q^{-0.33}$ dependence for the location of the low-to-high-conversion bifurcation points. This analysis also predicted a conversion of 33% at the bifurcation point. These results showed that the oxidation-reduction model is incapable of describing the observed steady-state behavior of the CO oxidation reaction, where the location of the low-to-high-conversion bifurcation point varied as $Q^{-0.66}$ and had a conversion of about 55%. For modeling steady-state multiplicity behavior of CO oxidation on supported platinum it is concluded that the oxidation-reduction model is no better than the elementary-step LH model.

Table 5.2 Model-Dependent Rate Parameters

	Oxidation Reduction	Standard Surface Island	Modified Surface Island
S_{CO}	2×10^{-5}	2×10^{-5}	9×10^{-5}
k^{o}_{-1}	4×10^{8}	5.6×10^{8}	2×10^{10}
S_{O_2}	1.2×10^{-7}	6.2×10^{-8}	5×10^{-8}
k^{o}_{3}	1.7×10^{9}	2.8×10^{8}	2.8×10^{8}
E_{-1}/R	7700	7700	9100
E_3/R	4600	6000	6000

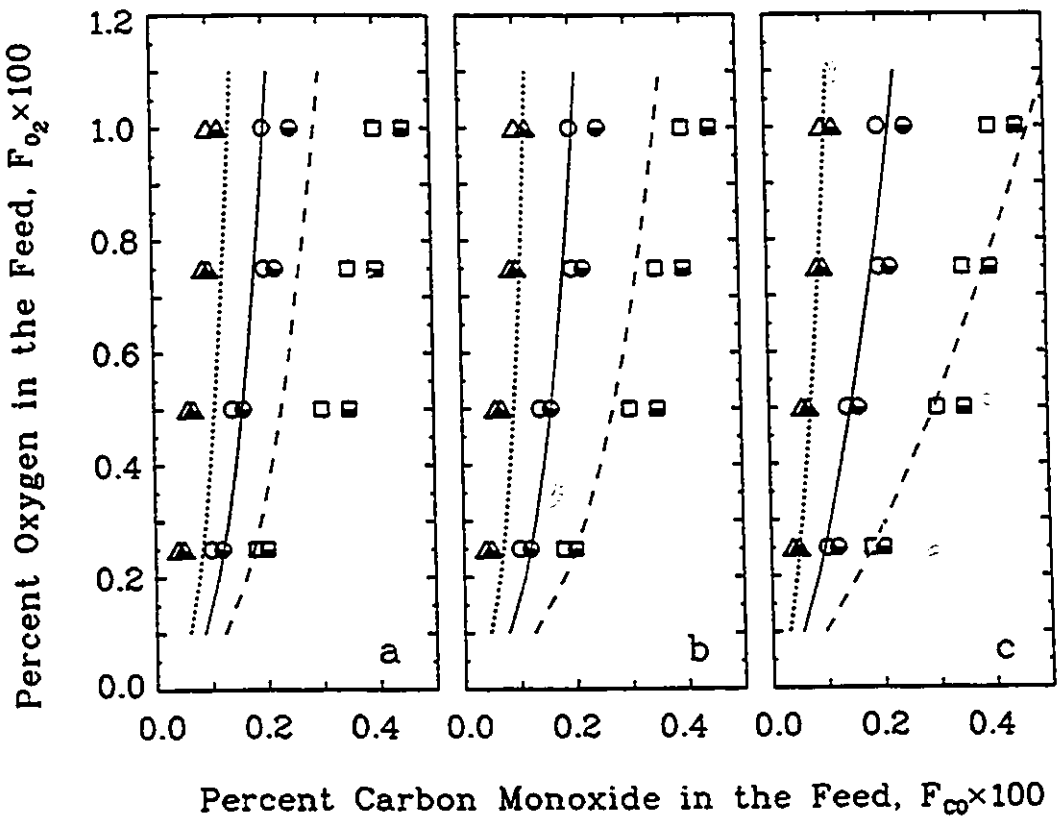

a) Oxidation–Reduction Model

b) Modified Surface Island Model

c) CO Self–Exclusion Model

(Symbols as in Figure 5.5)

Figure 5.7 Effect of Flow Rate on Predicted Bifurcation Points

5.5.3 CO Surface Island Formation Model

The next model examined was a surface island model used by Mukesh *et al.* (1984) to model the dynamic response of CO oxidation on platinum. Mukesh *et al.* (1984) reported that both a model based on CO surface island formation, and a model based on both CO and oxygen surface island formation,

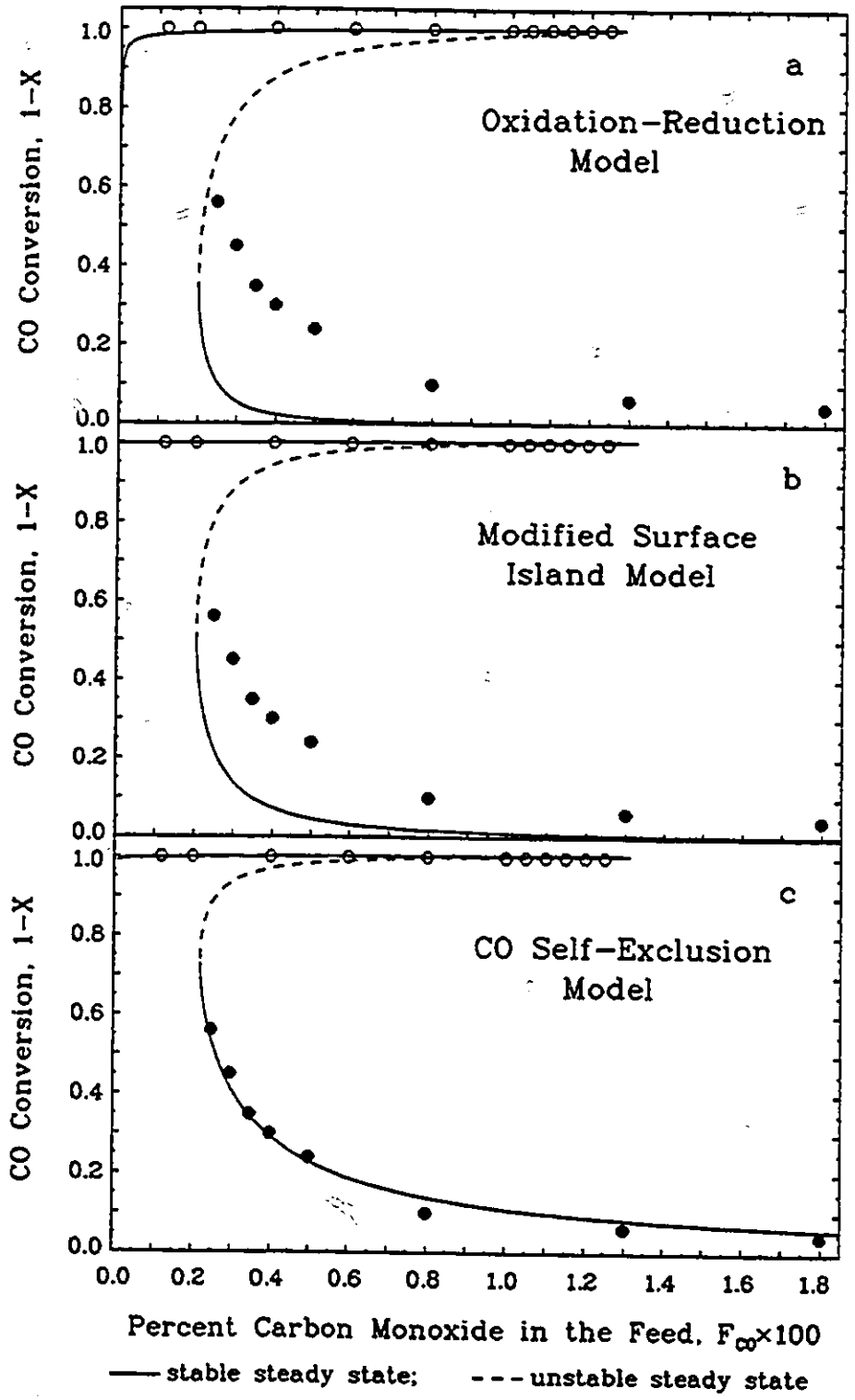

Figure 5.8 Predicted CO Conversions

provided predictions of the dynamic response of their system which were equivalent to those made by an elementary-step Langmuir-Hinshelwood model, but these surface island models gave superior predictions of the steady-state rate in the low-conversion region. They did not discuss the ability of either model to match the bifurcation behavior of the system. They found that including oxygen surface island formation gave no significant improvement over only CO surface island formation, and concluded that the important feature in the low-rate, high CO coverage portion of the curve is the formation of CO islands.

In the CO surface island model it is assumed that adsorbed CO migrates on the surface to form islands. Only the CO at the perimeter of the islands can come into contact with surface oxygen and react. The rate of Step (5.3) is proportional to the concentration of perimeter CO molecules, which is assumed to be proportional to the square root of the surface coverage. The rate expression for Step (5.3) thus becomes:

$$R_3 = K_3\sqrt{\theta_{CO}}\theta_O \tag{5.26}$$

The surface island model consists of Eqns. (5.4) to (5.9a) with rate expressions (5.10a), (5.11a), and (5.26). Surface oxide formation is not included in this model.

The predictions of this island formation model were found to be similar to those of the elementary-step LH model and the oxidation-reduction model. This model could

describe the base case bifurcation behavior correctly, and could account for temperature variation, but underpredicted the effect of variations in flow rate. The predicted reaction rate for the low conversion branch of the rate curve was also too low. As Mukesh *et al.* (1984) have shown, it was possible to match the reaction rate of the low-conversion branch of the rate curve. However, in so doing the same effects encountered with the elementary-step LH model have been found, namely, the bifurcation points are predicted incorrectly, and the predicted conversion of the high-reaction-rate branch becomes significantly less than 100%.

The surface island model and the LH model behave similarly in the low-conversion region. Oxygen adsorption is rate controlling and the surface island model has the same oxygen adsorption rate function as the LH model. Thus, when the analysis presented in Eqns. (5.14) to (5.19) is applied to the surface island model, the results are identical to that for the LH model and thus Eqn. (5.19) applies. The simplified surface island model predicts a variation of low bifurcation points with $Q^{-0.33}$ and a conversion of 33% at the low-to-high-conversion bifurcation points. Thus, the model has the same features as the LH model in the low-conversion region, and as such is incapable of quantitatively describing the behavior of the CO oxidation reaction.

5.5.4 Modified Surface Island Model

The fourth model examined was a modified CO surface island model, which was developed in Chapter 3. Typical surface island models, such as that used by Mukesh *et al.* (1984), examine only the effect of islands on the rate of Step (5.3). However, if all CO on the surface is present in the form of islands, the rate of O_2 adsorption will not be as shown in Eqn. (5.11). The rate of oxygen adsorption becomes:

$$R_2 = K_2 Y \frac{(1-\theta_{CO}-\theta_O)^2}{(1-\theta_{CO})} \tag{5.27}$$

as shown in Chapter 3. The rates of Steps (5.1) to (5.3) in the modified surface island model will be represented by Eqns. (5.10a), (5.27), and (5.26), respectively.

The predictions of the modified surface island model were improvements over the elementary-step LH model. The base case bifurcation behavior, the effect of temperature and the effect of flow rate on the high-to-low-conversion bifurcation curve were described as well by this model as by the LH model. In Figure 5.8b the predicted conversions of the modified surface island model are compared with the experimentally determined values. It is seen that the modified surface island model is in better agreement with the data than the elementary-step LH model. In Figure 5.7b are shown the effects of flow rate on the low-to-high conversion bifurcation curve. The modified surface island model is again better than the elementary-step LH model.

The explanation for the higher conversions predicted by the modified surface island model is straightforward. On the low-conversion branch of the rate curve, the LH model predicted that the CO fractional coverage should be higher than 0.99. This causes the rate controlling step of oxygen adsorption to proceed at a very low rate. In the modified surface island model the rate of oxygen adsorption in the high CO coverage branch is larger by a factor of $(1-\theta_{co})^{-1}$. This causes the rate of oxygen adsorption, and hence the overall reaction rate, to be at least two orders of magnitude greater than for the LH model.

As Figure 5.7b illustrates, the modified surface island model could describe the effect of flow rate on the lower bifurcation points better than either the LH model or the oxidation-reduction model. As shown earlier, the LH model predicts that the low bifurcation point will vary as $Q^{-0.33}$. A similar analysis can be performed for the modified surface island model. At steady state, the rates of the various reaction steps are again identical; thus, from Eqns. (5.4) to (5.12):

$$1 - Q_n X = R_1 = R_3 = \frac{2F_{o_2}}{F_{co}} R_2 = \frac{2F_{o_2}}{F_{co}} K_2 Y \frac{(1-\theta_{co}-\theta_o)^2}{(1-\theta_{co})} \qquad (5.28)$$

As in the previous analysis, the CO adsorption and desorption steps proceed very rapidly. Thus, for low conversions, CO adsorption/desorption will again be nearly at equilibrium. Thus, from (5.10a), the fraction of empty sites will again be given by:

$$(1-\theta_{CO}-\theta_O) = \frac{K_{-1}\theta_{CO}}{K_1 X} \tag{5.15}$$

In order to obtain agreement between the experimental and predicted bifurcation points it was again necessary for K_1 to be much greater than K_{-1}, which results in θ_{CO} being approximately unity. Oxygen is in excess, and the CO conversion is very low, so the oxygen composition in the reactor will be negligibly different from that of the feed, i.e. $Y = Y_o = 1$. There will once again be a negligible change in the volumetric flow rate (Q_n=1). In addition, the oxygen surface coverage will be low due to the high coverage of CO and the moderate value of the surface-reaction rate constant. Thus, in light of the above, combining Eqns. (5.28) and (5.15) yields:

$$1 - X = \frac{2F_{O_2}}{F_{CO}} K_2 \left[\frac{K_{-1}}{K_1 X}\right] \tag{5.29}$$

The issue to be resolved by this analysis is the inability of the modified surface island model to accurately predict the effect of flow rate on the value of F_{CO} at which a low-to-high-conversion bifurcation occurs. Thus it is necessary to explicitly relate X to F_{CO} and Q. Equation (5.29) becomes:

$$X^2 - X + \frac{C_5}{F_{CO}^2 Q} = 0 \tag{5.30}$$

where C_5 is a constant defined in the Nomenclature section. In addition to Eqn. (5.30), the bifurcation points must

satisfy the condition that the derivative of F_{CO} with respect to X vanishes:

$$\frac{dF_{CO}}{dX} = (2X - 1) \left[\frac{F_{CO}^3 Q}{2C_5}\right] = 0 \tag{5.31}$$

Solving Eqns. (5.30) and (5.31) simultaneously gives $X = \frac{1}{2}$ and,

$$F_{CO} = \left[\frac{4\ C_5}{Q}\right]^{0.5} \tag{5.32}$$

Thus, a conversion of 50% is predicted at the low-conversion bifurcation point and the location of the lower bifurcation points will vary as the inverse of the square root of flow rate. However, while these values are much closer to the experimental values of $Q^{-0.66}$ and 55% conversion than the predictions of the three previously examined models, significant underprediction still occurs.

5.5.5 CO Self-Exclusion Model

In the previous models, it has been assumed that the number of sites available for O_2 adsorption is equal to the number available for CO adsorption. This is not necessarily the case. Adsorption studies of oxygen on Pt (Wilson and Hall, 1970; Freel, 1972) indicate that saturation coverage of oxygen can vary between a fractional coverage of about one-half and unity. Herz and Marin (1980) have used a model which excludes oxygen from one-half of the surface to describe the steady-state oxidation of CO on supported

platinum catalysts. Lynch (1984) used a similar oxygen self-exclusion model to describe CO oxidation during forced composition cycling. The main effect of oxygen self-exclusion is to maintain the CO conversion at close to 100% as CO concentration approaches zero. The oxygen self-exclusion model also eliminates the zero-conversion steady state corresponding to complete oxygen surface coverage which otherwise occurs when the oxygen adsorption process is irreversible. However, simulations (Lynch, 1984) have shown that oxygen self-exclusion affects the bifurcation behavior negligibly. Thus, this phenomenon cannot be used to eliminate the discrepancies between the model predictions and the experimental observations.

Studies using CO, analogous to those using oxygen, have shown that a self-exclusion effect also occurs for CO adsorbed on platinum. Freel (1972), Dorling and Moss (1967), and Yao *et al.* (1979) have determined that, for supported Pt with small average particle sizes (<5 nm), the maximum ratio of CO molecules adsorbed per Pt surface atom is 0.87 ± 0.07. Gruber (1962) determined that the ratio of CO molecules adsorbed per surface Pt atom varied from unity to 0.7. In a mathematical model, this effect can be described by requiring that an adsorbed CO molecule excludes other CO from an area equivalent in size to N_{CO} ($1 \leq N_{CO} \leq 1.25$) surface Pt atoms. In the classical LH model $N_{CO}=1$. In the CO self-exclusion model the following assumptions are made. (This derivation is similar to that

of Herz and Marin (1980) for the oxygen self-exclusion model.)

1) A CO_a excludes other CO_a from an area on the surface equivalent in size to the area occupied by N_{CO} ($1 \leq N_{CO} \leq 1.25$) surface Pt atoms.
2) An O_a excludes other O_a from an area on the surface equivalent in size to the area occupied by one surface Pt atom.
3) CO_a excludes O_a from one surface Pt atom.
4) O_a excludes CO_a from one surface Pt atom.

The fraction of surface sites available for CO adsorption is $(1-N_{CO}\theta_{CO}-f\theta_O)$. The term $N_{CO}\theta_{CO}$ represents the fraction of surface sites from which CO adsorption is prohibited by CO_a. The term $f\theta_O$ represents the fraction of surface sites (not accounted for by the $N_{CO}\theta_{CO}$ term) which are unavailable for CO adsorption due to the presence of O_a. The term $f\theta_O$ will include the oxygen surface coverage, but subtracted from θ_O will be the sites already accounted for by the $N_{CO}\theta_{CO}$ term. The portion of θ_O already accounted for by the $N_{CO}\theta_{CO}$ term will be the product of the oxygen surface coverage and that fraction of the CO-free surface from which CO adsorption is inhibited by CO_a. Thus,

$$f\theta_O = \theta_O - \frac{(N_{CO}-1)\theta_{CO}\theta_O}{(1-\theta_{CO})} = \frac{(1-N_{CO}\theta_{CO})}{(1-\theta_{CO})}\theta_O \qquad (5.33)$$

The rate of CO adsorption is proportional to the fraction of surface sites available for CO adsorption,

$$R_{CO,ads} \propto (1-N_{CO}\theta_{CO}-f\theta_o) \tag{5.34}$$

Substituting Eqn. (5.33) into (5.34) and rearranging yields

$$R_{CO,ads} \propto (1-\theta_{CO}-\theta_o)\ \frac{(1-N_{CO}\theta_{CO})}{(1-\theta_{CO})} \tag{5.35}$$

which readily leads to

$$R_1 = K_1X(1-\theta_{CO}-\theta_o)\ \frac{(1-N_{CO}\theta_{CO})}{(1-\theta_{CO})} - K_{-1}\theta_{CO} \tag{5.36}$$

In the CO self-exclusion model, Eqns. (5.36), (5.11a), and (5.12) are used to describe the rates of Steps (5.1) to (5.3). Using the parameters shown in Table 5.1, the CO self-exclusion model gave an excellent description of the steady-state behavior of the CO oxidation reaction. Predictions of the effect of temperature and flow rate on the bifurcation behavior of the system match the experimental behavior exceedingly well. The superiority of the CO self-exclusion model over the LH model is most clearly seen by comparing Figure 5.5a with 5.5b. For the twelve bifurcation points in Figure 5.5b, the sum of the squares of the errors (SSE) is 4.37×10^{-7} when using the CO self-exclusion model. However, in Figure 5.5a, the SSE is 3.03×10^{-6} when using the LH model. This difference is statistically significant at the 0.7% level which easily satisfies the 5% level normally used when testing hypotheses. For the other bifurcation points, the predictions of the two models are essentially equivalent. The improvement occurs because the CO self-exclusion model, unlike the LH model, is not

restricted to a $Q^{-0.33}$ variation of the low-to-high-conversion bifurcation points. A procedure similar to that used for the LH model is followed in order to determine for the CO self-exclusion model the dependence of the location of the bifurcation points on the flow rate. At a low CO conversion steady state, with negligible change in volumetric flow rate (Q_n=1), and negligible change in oxygen concentration between feed and exit streams ($Y=Y_o=1$), Eqn. (5.14) yields:

$$1 - X = \frac{2F_{O_2}}{F_{CO}} K_2 \ (1-\theta_{CO}-\theta_O)^2 \tag{5.37}$$

For low conversions with rapid CO adsorption and desorption steps, the gas- and surface-phase CO will be at near-equilibrium conditions; thus, from (5.36) the fraction of empty sites will be given by:

$$(1-\theta_{CO}-\theta_O) = \frac{K_{-1}\theta_{CO}}{K_1 X} \frac{(1-\theta_{CO})}{(1-N_{CO}\theta_{CO})} \tag{5.38}$$

If, in addition, oxygen adsorption (and not surface reaction) is the rate controlling step, then there will be negligible oxygen surface coverage. Thus, solving for θ_{CO} from Eqn. (5.38) gives:

$$\theta_{CO} = \frac{K_1 X}{N_{CO}K_1 X+K_{-1}} \tag{5.39}$$

Substituting this into (5.37) with the assumption of negligible oxygen coverage yields:

$$1 - X = \frac{2F_{O_2}}{F_{CO}} K_2 \left[\frac{(N_{CO}-1)K_1X + K_{-1}}{N_{CO}K_1X + K_{-1}} \right]^2 \tag{5.40}$$

As previously explained, values of K_1 much greater than K_{-1} were always required in order for the model to predict multiplicity with approximately total conversion at the high-conversion state, thus Eqn. (5.40) becomes:

$$1 - X = \frac{2F_{O_2}}{F_{CO}} K_2 \left[\frac{N_{CO}-1}{N_{CO}} + \frac{K_{-1}}{N_{CO}K_1X} \right]^2 \tag{5.41}$$

This can be rewritten as:

$$X + \frac{C_5^2}{F_{CO}Q}\left[\frac{N_{CO}-1}{N_{CO}}\right]^2 + \frac{C_6(N_{CO}-1)}{F_{CO}^2QN_{CO}^2X} + \frac{C_1}{F_{CO}^3QN_{CO}^2X^2} = 1 \tag{5.42}$$

where C_1, C_5, and C_6 are as defined in the Nomenclature section. The low-to-high-conversion bifurcation points must satisfy both Eqn. (5.42) and the condition that the derivative of F_{CO} with respect to X is equal to zero. Differentiating Eqn. (5.42) gives:

$$X^3 - \frac{C_6(N_{CO}-1)X}{QF_{CO}^2N_{CO}^2} - \frac{2C_1}{QF_{CO}^3N_{CO}^2} = 0 \tag{5.43}$$

One limiting case of Eqn. (5.43) is when $N_{CO}=1$. In this case Eqns. (5.42) and (5.43) can be used to derive Eqn. (5.19). Another limiting case of Eqn. (5.43) is for N_{CO} sufficiently large that the last term of Eqn. (5.43) is negligible compared to the second term. This gives

$$X = \left[\frac{C_6(N_{CO}-1)}{QF_{CO}^2N_{CO}^2}\right]^{1/2} \tag{5.44}$$

Substituting (5.44) into (5.42) gives

$$F_{CO} = 2\left[\frac{C_6(N_{CO}-1)}{QN_{CO}^2}\right]^{1/2} + \frac{C_5^2(N_{CO}-1)^2}{QN_{CO}^2} + \frac{C_1}{C_6(N_{CO}-1)} \qquad (5.45)$$

For $N_{CO} >> 1$, Eqn. (5.45) predicts an inverse relationship between bifurcation points and flow rate.

$$F_{CO} = C_5^2/Q \qquad (5.46)$$

Thus, the location of the bifurcation points will vary as $Q^{-\gamma}$, where γ is in the range 0.33 to 1.0 for $N_{CO} \geq 1$. It is also noted that the conversion at the bifurcation point increases from 33% to 100% as N_{CO} increases from 1.

Using the parameters shown in Table 5.1, the CO self-exclusion model was able to match the experimentally observed value of γ=0.66.

The CO self-exclusion model was also able to better describe the rate behavior for the low-conversion branch of the steady-state rate curve, as shown in Figure 5.1. The SSE for the reaction rates is 3.9×10^{-3} from the CO self-exclusion model, compared to 4.9×10^{-1} for the LH model. This difference is statistically significant at the 0.02% level. The value of N_{CO} in Table 5.1 was arrived at by minimizing the SSE for the low-conversion rate behavior, with the constraint that the SSE for the bifurcation points also be a minimum. This procedure was used because it was found that the low-conversion rate behavior was particularly sensitive to the choice of N_{CO}. The estimation of all other

parameters was based solely on minimizing the SSE for the bifurcation point locations.

The CO self-exclusion model is the only model examined herein that was able to quantitatively predict the bifurcation behavior as a function of flow rate. The CO self-exclusion model is also the only model that predicts conversions for the low-conversion branch as high as those observed experimentally. For these reasons the CO self-exclusion model is the only kinetic model of those examined that can quantitatively describe all of the observed steady-state multiplicity and rate behavior for CO oxidation on supported platinum.

The predictions, shown in Figures 5.1 and 5.5b, for the CO self-exclusion model were calculated by determining the steady-state solution(s) of Eqns. (5.4) to (5.9a) with the rates for Steps (5.1) to (5.3) determined from Eqns. (5.36), (5.11a) and (5.12a). This calculation can be quite involved because the roots must be determined for a system of simultaneous nonlinear algebraic equations. However, this involved calculation is not always necessary because the reaction rate of the CO self-exclusion model can be expressed explicitly in terms of CO and O_2 concentrations by assuming that CO adsorption/desorption is at equilibrium, and oxygen surface coverage is at its steady state value. These two assumptions are implemented by setting Eqns. (5.36) and (5.8) equal to zero and solving for θ_{CO} and θ_O.

$$r_{CO_2} = k_3 L_m^2 \theta_{CO} \theta_O = \frac{2L_m^2 k_2 (k_3 k_1/k_{-1})^2 \epsilon^2 [CO]^2 [O_2]}{\{2k_2[O_2] + k_3(k_1/k_{-1})\epsilon[CO] + k_3(k_1/k_{-1})^2 \epsilon^2 [CO]^2\}^2} \tag{5.47}$$

where

$$\epsilon = \left[\frac{1-N_{CO}\theta_{CO}}{1-\theta_{CO}} \right] = \frac{(C_2-C_3) + \sqrt{(C_2+C_3)^2 + 4C_2C_3C_4}}{2C_2(1+C_4)} \tag{5.48}$$

$$C_2 = k_3(k_1/k_{-1})[CO]; \quad C_3 = 2k_2[O_2];$$
$$C_4 = (N_{CO}-1)(k_1/k_{-1})[CO] \tag{5.49}$$

For the particular values of rate constants listed in Table 5.1, the rate function becomes

$$r_{CO_2} = \frac{4.50\times10^{-14} T^{1.5} e^{(16200/T)} \epsilon^2 [CO]^2 [O_2]}{\left[3.18\times10^3 \sqrt{T}[O_2] + 1.88\times10^{-4}\sqrt{T}\, e^{(8100/T)} \epsilon [CO] + 6.54\times10^{-19}\, T\, e^{(22000/T)} \epsilon^2 [CO]^2 \right]^2} \tag{5.50}$$

where ϵ is determined using Eqn. (5.48) with the values of C_2, C_3, and C_4 given in the Nomenclature section. When this rate expression is used in the design equation (component balance) for a CSTR,

$$Q_o([CO]_o - Q_n[CO]) - r_{CO_2}\, a_m = 0 \tag{5.51}$$

it is found that excellent quantitative predictions result for both the steady-state rate behavior and the locations of the bifurcation points. The use of Eqn. (5.47) is strongly

recommended whenever it is desired to fit a rate function to steady-state data for CO oxidation on platinum. In the fitting procedure, it is only necessary to estimate values for the quantities k_1/k_{-1}, k_2, k_3 and N_{CO}. A rate function of this form should also prove to be useful for describing steady-state CO oxidation on many of the other noble metals.

Unfortunately, the results presented in this chapter do not provide the final word concerning the modeling of CO oxidation on platinum. This is because none of the models described in this chapter can quantitatively describe the complex reaction dynamics, such as chaos, self-sustained oscillations, and rate enhancement during forced composition cycling of the feed, which have often been observed during CO oxidation on supported platinum. Since of the models examined, only the CO self-exclusion model can quantitatively describe the steady-state behavior, it is this model which will be used as the basis for further development in subsequent attempts to describe the dynamic phenomena.

5.6 Summary of Steady-State Analysis

A systematic study of the effects of reactor temperature, feed composition, feed flow rate, and catalyst charge on multiplicity and rate behavior was conducted for the catalytic oxidation of carbon monoxide on Pt/Al_2O_3 in a recycle reactor. It was found that multiple steady states occur in a cusp-shaped region on a $CO-O_2$ feed composition diagram. Multiple steady states were found only when oxygen was in

excess. As oxygen concentration or reactor temperature was increased, or as feed flow rate was decreased, the boundaries of the region of multiple steady states moved to higher carbon monoxide concentrations. An elementary-step Langmuir-Hinshelwood model was able to quantitatively describe the boundaries of the multiple steady state region for temperature variations. The LH mechanism could not quantitatively describe either the effect of feed flow rate on the multiplicity region boundary, or the absolute CO conversion of the low-conversion steady state.

Several other models were examined and gave results comparable to the LH model. These included a surface oxidation-reduction model, and a standard CO surface island formation model. A CO surface island model with a modified oxygen adsorption term gave better predictions than the LH model. The behavior predicted by this model was about midway between that of the LH model and the experimental observations. An elementary-step Langmuir-Hinshelwood model for which CO is excluded from a small fraction of surface sites was the only model which was able to quantitatively predict all observed steady-state phenomena.

5.7 References

Aluko, M., and H.-C. Chang, "Dynamic Modelling of a Heterogeneously Catalysed System with Stiff Hopf Bifurcations", Chem. Eng. Sci. 41, 317-331 (1986).

Conrad, F., and V. Treguer-Seguda, "Parameter Estimation in

Some Diffusion and Reaction Models: An Application of Bifurcation Theory", Chem. Eng. Sci. 39, 705-711 (1984).

Dorling, T. A., and R. L. Moss, "The Structure and Activity of Supported Metal Catalysts II. Crystallite Size and CO Chemisorption on Platinum/Silica Catalyst", J. Catal. 7, 378-385 (1967).

Freel, J., "Chemisorption on Supported Platinum II. Stoichiometry for Hydrogen, Oxygen and Carbon Monoxide", J. Catal. 25, 149-160 (1972).

Goodman, M. G., M. B. Cutlip, C. N. Kenney, W. Morton, and D. Mukesh, "Transient Studies of Carbon Monoxide Oxidation Over Platinum Catalyst", Surface Sci. 120, L453-460 (1982).

Gruber, H. L., "Chemisorption Studies on Supported Platinum", J. Phys. Chem. 66, 48-54 (1962).

Heinemann, R. F., K. A. Overholser, and G. W. Reddien, "Multiplicity and Stability of Premixed Laminar Flames: An Application of Bifurcation Theory", Chem. Eng. Sci. 34, 833-840 (1979).

Herskowitz, H., and C. N. Kenney, "CO Oxidation on Pt Supported Catalysts. Kinetics and Multiple Steady States", Can. J. Chem. Eng. 61, 194-199 (1983).

Herz, R. K., and S. P. Marin, "Surface Chemistry Models of Carbon Monoxide on Supported Platinum Catalysts", J. Catal. 65, 281-296 (1980).

Kubicek, M., "Algorithm 502: Dependence of Solutions of Nonlinear Systems on a Parameter", A. C. M. Trans. Math.

Software 2, 98-107 (1976).

Lynch, D. T., "On the Use of Adsorption/Desorption Models to Describe the Forced Periodic Operation of Catalytic Reactors", Chem. Eng. Sci. 39, 1325-1328 (1984).

Lynch, D. T., and S. E. Wanke, "Oscillations during Carbon Monoxide Oxidation over Supported Metal Catalysts: II. Effects of Reactor Operating Conditions on Oscillatory Behavior for a Pt-Pd/Al_2O_3 Catalyst", J. Catal. 88, 345-354 (1984).

Mukesh, D., W. Morton, C. N. Kenney, and M. B. Cutlip, "Island Models and the Catalytic Oxidation of Carbon Monoxide and Carbon Monoxide-Olefin Mixtures", Surface Sci. 138, 237-257 (1984).

Sales, B. C., J. E. Turner, and M. B. Maple, "Oscillatory Oxidation of CO over Pt, Pd and Ir Catalysts: Theory", Surface Sci. 114, 381-394 (1982).

Wilson, G. R., and W. K. Hall, "Studies of the Hydrogen Held by Solids XVIII. Hydrogen and Oxygen Chemisorption on Alumina- and Zeolite-Supported Platinum", J. Catal. 17, 190-206 (1970).

Yao, H. C., M. Sieg, and H. K. Plummer, Jr., "Surface Interactions in the Pt/γ-Al_2O_3 System", J. Catal. 59, 365-374 (1979).

Yeates, R. C., J. E. Turner, A. J. Gellman, and G. A. Somorjai, "The Oscillatory Behavior of the CO Oxidation Reaction at Atmospheric Pressure over Platinum Single Crystals: Surface Analysis and Pressure Dependent

Mechanisms", Surface Sci. 149, 175-190 (1985).

6. Behavior During Forced Feed Cycling

6.1 Nomenclature

a_m = total surface area of the supported catalyst, 2.34 m^2 for 4.95 g charge, 6.92 m^2 for 14.6 g charge, 20.6 m^2 for 43.6 g charge

$[CO]$ = reactor, and exit, CO concentration, mol/m^3

$[CO]_o$ = time-average feed CO concentration, $F_{CO}P/RT$, mol/m^3

$[CO_2]$ = reactor, and exit, CO_2 concentration, mol/m^3

E_{-1}/R = activation energy for CO desorption, 13900 K

E_3/R = activation energy for surface reaction, 5800 K

F_{CO} = time-average fraction CO in feed

F_{O_2} = time-average fraction O_2 in feed

k_1 = CO adsorption rate constant, $6.87\ S_{CO}\sqrt{T}/L_m$, $m^3/mol \cdot s$

k_{-1} = CO desorption rate constant, $k^o_{-1} \cdot \exp(-E_{-1}/RT)$, s^{-1}

k^o_{-1} = CO desorption pre-exponential factor, $5 \times 10^{15}\ s^{-1}$

k_2 = O_2 adsorption rate constant, $6.43\ S_{O_2}\sqrt{T}/L_m^2$, $m^5/mol^2 \cdot s$

k_3 = surface reaction rate constant, $k^o_3 \cdot \exp(-E_3/RT)$, $m^2/mol \cdot s$

k^o_3 = surface reaction pre-exponential factor, $8.1 \times 10^{10}\ m^2/mol \cdot s$

K_1 = dimensionless CO adsorption rate constant, $a_m L_m k_1/Q_o$

A portion of this chapter was presented at the AIChE Annual Meeting, Chicago, Nov. 1985, "Forced Composition Cycling During CO Oxidation on Platinum", paper 132a.
A version of this chapter has been published.
Graham, W. R. C. and D. T. Lynch, "Forced Cycling of Catalytic Reactors: Systems with Two Inputs", Stud. Surf. Sci. and Cat. 38, 693-703 (1988).

K_{-1} = dimensionless CO desorption rate constant, $a_m L_m k_{-1}/Q_o[CO]_o$

K_2 = dimensionless O_2 adsorption rate constant, $a_m L_m^2 \psi k_2/Q_o$

K_3 = dimensionless surface reaction rate constant, $a_m L_m^2 \psi k_3/Q_o[CO]_o$

K_4 = dimensionless CO_2 adsorption rate constant, 1720 for case VI conditions

K_{-4} = dimensionless CO_2 desorption rate constant, 108 for case VI conditions

L_m = adsorption capacity of the metal surface, 2×10^{-5} mol/m^2

N_{CO} = CO self-exclusion factor, 1.004

$[O_2]$ = reactor, and exit, O_2 concentration, mol/m^3

$[O_2]_o$ = time-average feed O_2 concentration, $F_{O_2}P/RT$, mol/m^3

P = reactor pressure, 0.1 MPa absolute

Q_n = ratio of exit to feed volumetric flow rates

Q_o = feed volumetric flow rate at reactor conditions, m^3/s

r_{SS} = steady state conversion for a feed composition of 1% CO and 0.5% O_2

r_{TA} = time-average rate, as conversion of CO_2

R = gas constant, 8.314 m^3·Pa/mol·K

S_{CO} = CO sticking probability on catalyst, 1×10^{-3}

S_{O_2} = O_2 sticking probability on catalyst, 1.22×10^{-7}

t = time, s

T = reactor temperature, Kelvin

V = effective free volume of reactor, 1.9×10^{-4} m^3

X = dimensionless reactor CO concentration, $[CO]/[CO]_o$

X_o = instantaneous dimensionless feed CO concentration

Y = dimensionless reactor O_2 concentration, $[O_2]/[O_2]_o$

Y_o = instantaneous dimensionless feed O_2 concentration

Z = dimensionless reactor CO_2 concentration, $[CO_2]/[CO]_o$

Z_o = instantaneous dimensionless feed CO_2 concentration (0 in this study)

Greek Symbols

α_m = ratio of bulk volume to metal surface capacitances, $[CO]_o V/a_m L_m$

α_s = ratio of bulk volume to support surface capacitances, 0.023 for case VI conditions

θ_{CO} = fractional CO surface coverage on the metal surface

θ_o = fractional oxygen surface coverage on the metal surface

τ = dimensionless time based on the reactor residence time, $Q_o t/V$

ϕ_{CO_2} = fractional CO_2 surface coverage on the support surface

ψ = enhancement factor for oxygen adsorption and surface reaction, 1 for surface phase 1, 250 for surface phase 2

ω = frequency of the forcing function, Hz

6.2 Introduction

Early work by Douglas (1967, 1972), Douglas and Rippin (1966), and Bailey (1973, 1977) showed that by operating catalytic reactors in a periodic manner it is possible to achieve large improvements in reaction rate, selectivity, or both. Not only can periodic operation of reactors result in enhanced reactor performance, but it can also be used to gain information concerning the fundamental processes occurring on the catalyst surface. Reaction models which are indistinguishable in their ability to describe steady-state behavior will often differ significantly when predicting forced composition cycling behavior. Thus, it is sometimes possible to use forced feed cycling behavior to discriminate among different models which have identical steady-state behavior.

In recent experimental studies (Behm *et al.*, 1983; Thiel *et al.*, 1983) it has been shown that, during CO adsorption, platinum can undergo surface phase transformations with resultant large variations in the oxygen sticking probability. A mathematical model which takes account of this phenomenon has been developed (Lynch *et al.*, 1986) and it has been found that this model is in quantitative agreement with a comprehensive set of observations of oscillatory behavior for CO oxidation. In particular, the model can correctly account for the transitions from stable to oscillatory behavior, as well as describe the variations of the frequency and the changes in the fine details of the shape

of the oscillations as a function of reactor operating conditions.

In this chapter the effect of reactor operating parameters on rate enhancement during forced feed composition cycling will be determined. In particular, the effect of the phase angle between inputs, as well as the frequency of the input, will be examined for forced feed composition cycling during CO oxidation on a platinum catalyst. It will be shown that the phase angle has a significant effect on the time-average reaction rate. These data will be used to evaluate a model combining the surface phase transformation model (Lynch *et al.*, 1986) and the CO self-exclusion model presented in Chapter 5. It will be shown that the combined model is capable of quantitatively describing the experimental observations. Thus, this will result in a single, consistent, explanation for three commonly observed complex phenomena, namely, reaction rate resonance during feed composition cycling, steady-state multiplicity, and self-sustained oscillations, that occur during CO oxidation on supported platinum.

6.3 Definition of Oxygen Phase Lead

In the work reported in this chapter, the reactant feed composition was not maintained at a constant value. Instead, the feed concentration of each reactant was switched periodically between two values. Feed cycling was carried out with the equipment described in Chapter 4.

During cycling the CO feed mole fraction alternated between 2% for one-half of each cycle and 0% for the other half, with an average composition of 1%. The oxygen feed mole fraction alternated between 1% for half of each cycle and 0% for the other half, so that the average feed mole fraction of O_2 was 0.5%. With the equipment described in Chapter 4 (see Figure 4.4), it was possible for the oxygen half-cycle to overlap with the CO half-cycle as much, or as little, as was desired. Different ways of cycling the reactants are shown in Figure 6.1. The overlap between the oxygen and CO half-cycles will be defined using the term "oxygen phase lead". Defining one complete feed cycle as having 360 degrees, the oxygen phase lead will refer to the fraction of a cycle, in degrees, between the start of an oxygen half-cycle (1% O_2) and the start of a carbon monoxide half-cycle (2% CO). Hence, as shown in Figure 6.1a, if the CO is switched off when the oxygen is switched on, and vice versa, an oxygen phase lead of 180 degrees results and the inputs are said to be out-of-phase. If the CO and O_2 are switched on and off simultaneously, as shown in Figure 6.1b, then the phase lead is zero degrees (or 360 degrees; in-phase cycling). If oxygen is turned on one-quarter of a cycle after the CO is turned on, as shown in Figure 6.1c, then the oxygen phase lead is 270 degrees. If the CO is turned on after the oxygen has been flowing to the reactor for one-quarter of a cycle, as shown in Figure 6.1d, then the oxygen phase lead is 90 degrees.

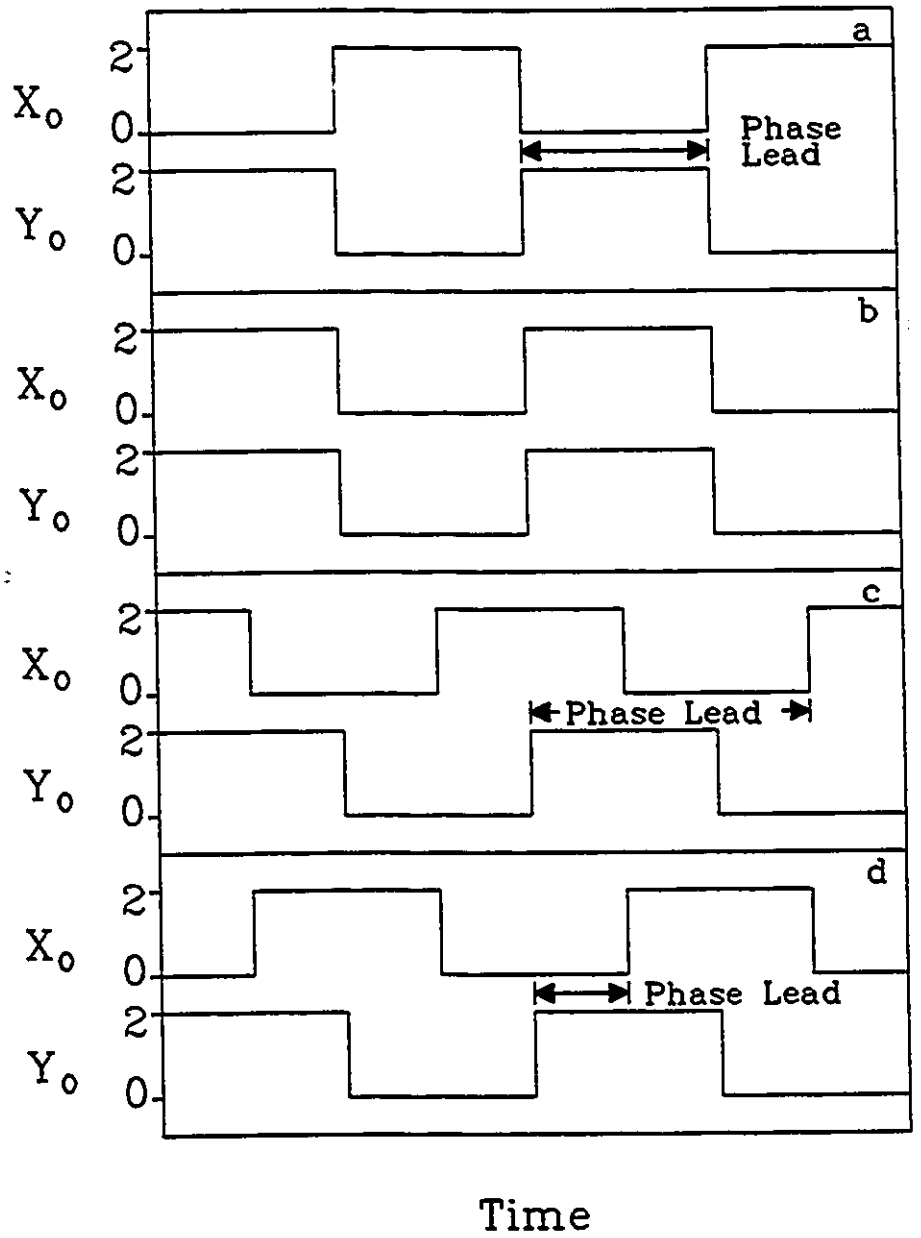

a) 180 degree oxygen phase lead
b) Zero degree oxygen phase lead
c) 270 degree oxygen phase lead
d) 90 degree oxygen phase lead
(X_o = CO, Y_o =O_2)

Figure 6.1 Feed Cycling Strategies

6.4 Experimental Behavior

The operating conditions used in this study were as in the previous chapter and are summarized in Table 6.1. The steady-state bifurcation behavior of the system for these operating conditions is described in Chapter 5 and is summarized in Figure 6.2. In the cusp shaped regions of Figure 6.2, multiple steady states exist. To the left of the multiplicity region only high-conversion steady states occur, while to the right of the multiplicity region only low-conversion steady states are present.

Table 6.1 Reactor Operating Conditions

Case	Mass of catalyst (g)	Temperature (°C)	Flow rate (mol/s)
I	14.6	90	205×10^{-6}
II	4.95	90	68×10^{-6}
III	43.6	90	615×10^{-6}
IV	14.6	70	205×10^{-6}
V	14.6	110	205×10^{-6}
VI	14.6	90	68×10^{-6}
VII	14.6	90	615×10^{-6}

In the first part of this study, the oxygen phase lead was maintained constant at 180 degrees, i.e., the inputs were out-of-phase. The effects of size of catalyst charge,

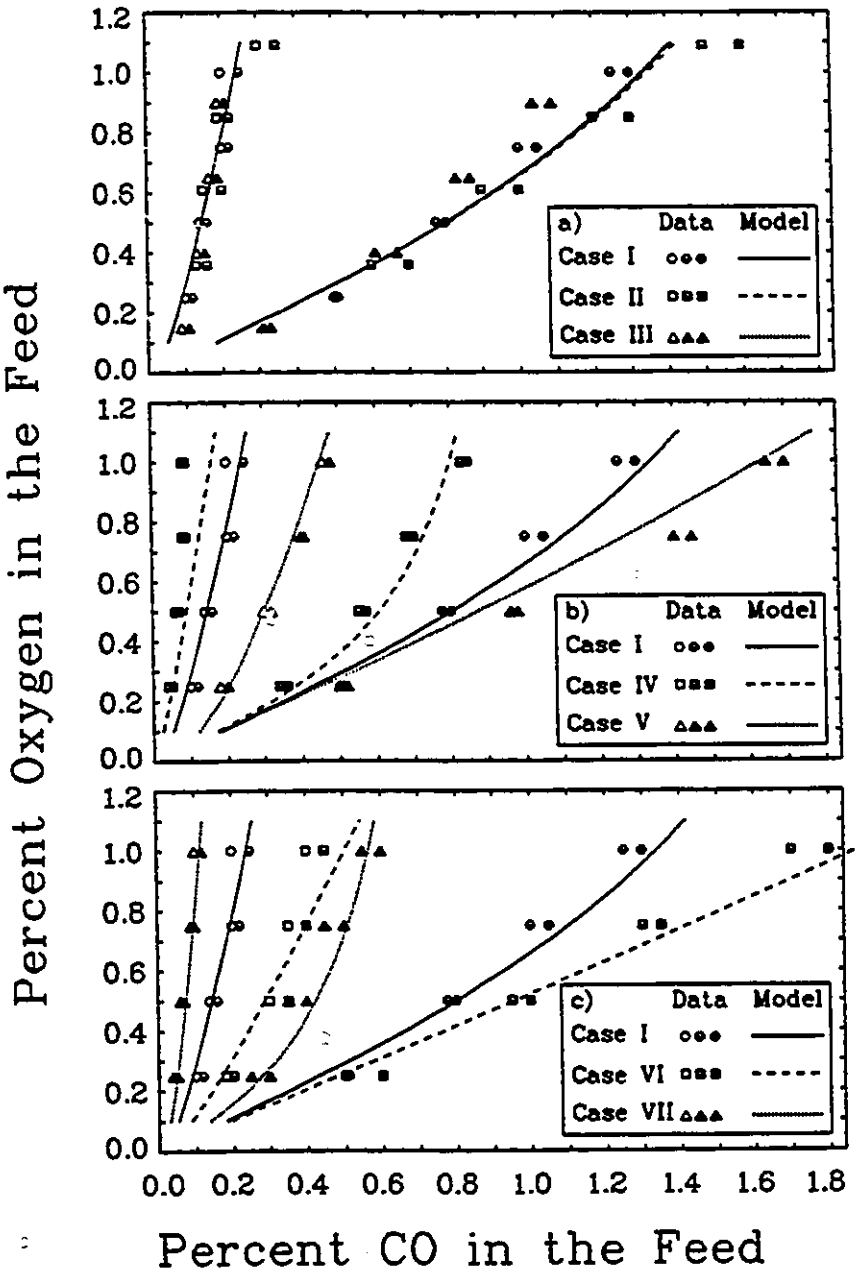

a) effect of mass of catalyst
b) effect of temperature
c) effect of flow rate

Figure 6.2 Steady-State Bifurcation Behavior

temperature, flow rate, and frequency on the average conversion were examined. For out-of-phase feed switching the (CO,O_2) feed composition alternates between (0%,1%) for the first half-cycle, and (2%,0%) for the second half-cycle. The average feed composition of (1%,0.5%) is in the unique low-conversion region in Figure 6.2. For cycling in this manner, the feed alternates between the high and low conversion sides of the multiplicity region.

In the second part of this study, the effect on the average conversion of the phase angle between inputs was examined for the base case (Case I in Table 6.1) operating conditions. For cycling of this type, the (CO,O_2) feed composition switched sequentially from (0%,1%) to (2%,1%), (2%,0%), and (0%,0%) for oxygen phase leads between 0 and 180 degrees, and from (0%,1%) to (0%,0%), (2%,0%), and (2%,1%) for phase leads between 180 and 360 degrees.

6.4.1 Out-of-Phase Feed Cycling

The initial experiments determined the reaction behavior during 180° out-of-phase feed switching. The dynamic CO_2 exit composition during out-of-phase cycling is shown in Figure 6.3 for Case VI operating conditions. At low frequencies (e.g. in Figure 6.3a for ω = 0.56 mHz) there are seven distinct regions of interest during a single cycle. These regions are labelled in Figure 6.3a and are characterized as follows:

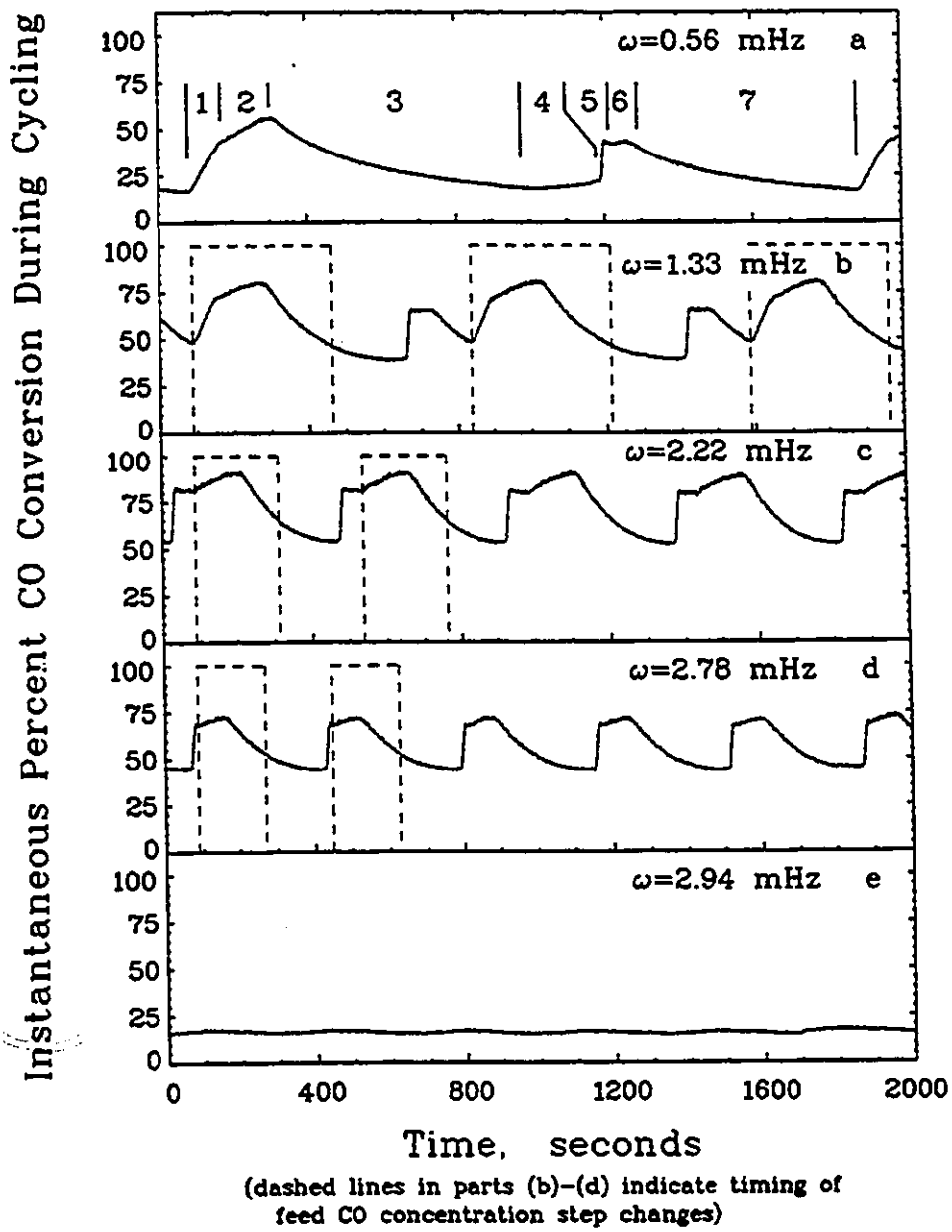

Figure 6.3 Instantaneous CO Conversion

1) There is a rapid increase in CO_2 concentration as soon as the CO is switched on. At the start of this region the catalyst surface is almost entirely covered with oxygen and the reactor oxygen composition is approximately 1%. During this period, almost all the CO entering the reactor adsorbs on the surface and reacts with adsorbed oxygen, which is being replenished from the gas phase. This period lasts until there is no gas-phase oxygen left in the reactor.
2) The rate of increase in CO_2 concentration decreases after the gas-phase oxygen has been depleted. During this interval the CO entering the reactor adsorbs on the catalyst surface and cleans the surface of the remaining oxygen.
3) The CO_2 concentration falls as the reaction rate goes to zero. The gas-phase CO_2 concentration is not a direct indication of the reaction rate, because the alumina support has a large capacity for CO_2 adsorption-desorption. During this interval the metal surface becomes saturated with CO.
4) When the CO feed is switched off, and O_2 is switched on, the reaction rate does not immediately rise because the surface is almost entirely covered with CO, leaving very few pairs of empty sites for oxygen adsorption. The gas-phase CO concentration decrease is accompanied by a decrease in the surface coverage of CO due to CO desorption and reaction.

5) When sufficient pairs of active sites become available for significant oxygen adsorption, there is a very sharp rise in the CO_2 concentration as most of the surface CO is eliminated by reaction with adsorbing oxygen.

6) There is an apparent break in reaction activity, possibly related to a reduced oxygen sticking probability (which will be discussed later), during which the CO_2 concentration briefly falls and then rises again. As the oxygen concentration in the reactor increases, the remainder of the surface CO reacts to form CO_2.

7) In the final region, the CO_2 concentration falls as the oxygen surface coverage increases. The desorption of CO_2 from the alumina support again (as in region 3) prevents the reactor CO_2 concentration from falling to zero.

As the frequency increases from that in Figure 6.3a, the peaks in the CO_2 concentration begin to merge, and the different regions start to overlap or disappear. The double peak per cycle becomes a single peak per cycle, and, above a critical frequency, the high-rate behavior disappears altogether. These features are all shown in Figure 6.3.

Feed switching experiments were performed for several frequencies for each of the cases in Table 6.1. The CO_2 exit concentration was integrated over each cycle to obtain the time-average conversion, which is shown in Figure 6.4.

For example, the integration of the CO_2 concentrations in Figure 6.3 produces the left-most results in Figure 6.4c. The curves represent model predictions which will be discussed later. An examination of the data in Figure 6.4 reveals several interesting facts. At very low frequencies, the time-average conversion increases almost linearly from zero. As the frequency increases, the time-average conversion increases to a maximum and then decreases until the critical frequency is reached, where the time-average conversion drops to a low value which is approximately the steady-state conversion for a 1.0% CO, 0.5% O_2, feed.

Shown in Figure 6.4a is the effect of the mass of catalyst on the time-average conversion (with the ratio of feed flow rate to catalyst mass held constant). Although the steady-state bifurcation behavior was identical for cases I, II and III (see Figure 6.2a), the time-average behavior is seen to be quite different. It is seen that large catalyst charges lead to higher maximum average conversions during forced cycling, and that the cycling frequency at which the maximum average conversion occurs increases with increasing catalyst mass. In Figure 6.4b it is seen that increasing temperature increases the maximum time-average conversion, while the data in Figure 6.4c show that decreasing the flow rate will increase the maximum time-average conversion. The cycling frequency at which the maximum time-average conversion occurs is lower for low flow rates than for high flow rates.

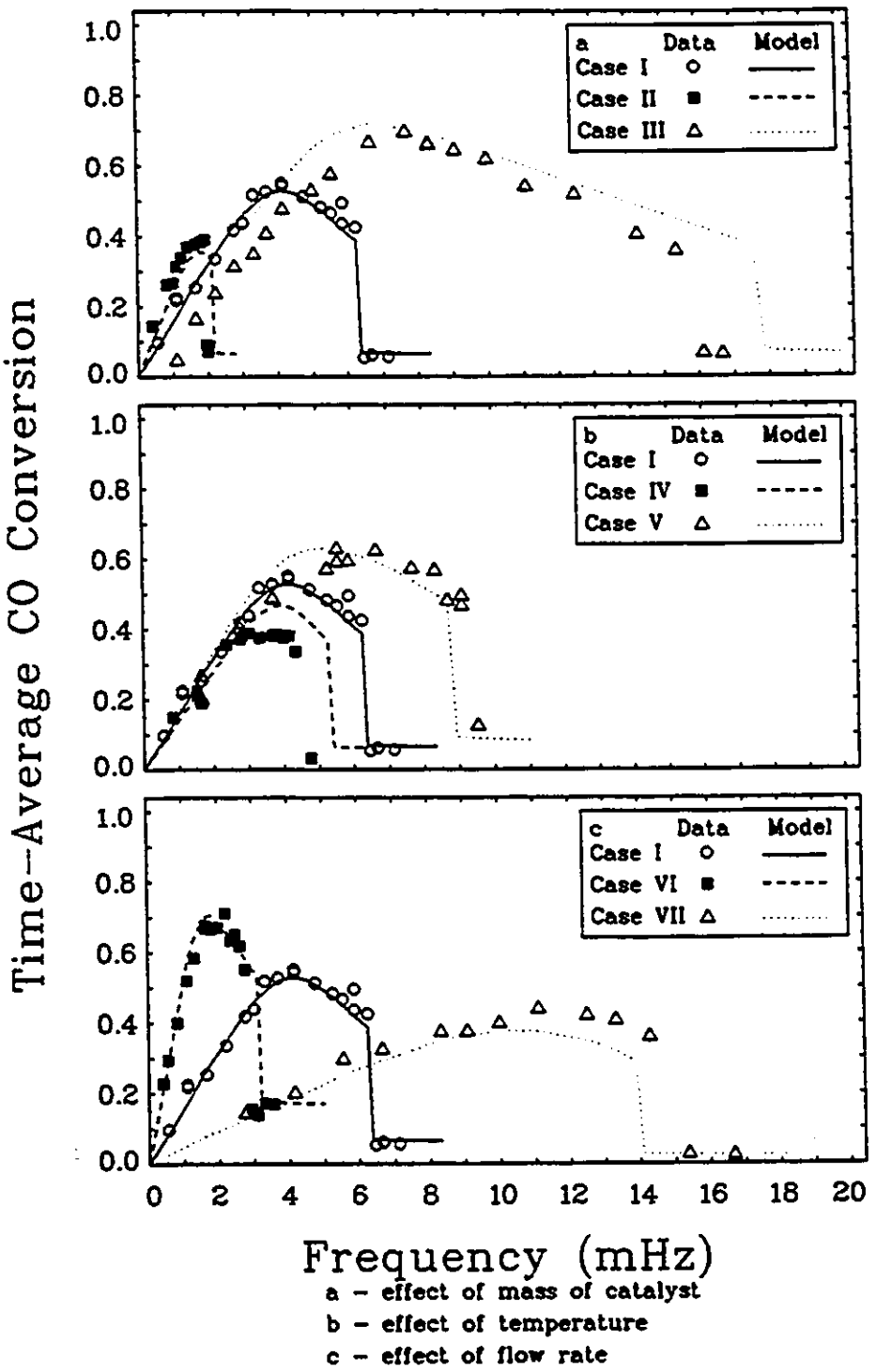

Figure 6.4 Effect of Frequency on Time-Average Conversion

The critical frequency above which significant rate enhancement does not occur is determined primarily from mixing considerations and the steady-state bifurcation diagram (Figure 6.2). In the low-conversion steady-state region, the reaction rate does not significantly affect the reactant concentrations (conversion < 10%, except for Case VI). If it is assumed that the reactor concentration is not affected by the reaction, then for square-wave feed cycling to a CSTR the reactant concentrations will alternately increase and decrease in an exponential manner. For a cycling frequency ω, switching between 0% and 2% CO in the feed, the extreme points of CO reactor composition will be $2/(1+\exp(\frac{-1}{2\omega\tau_v}))$ and $2/(1+\exp(\frac{1}{2\omega\tau_v}))$, where $\tau_v = V/Q_o$. The reactor (CO,O_2) composition will remain on a line between (0%,1%) and (2%,0%) during cycling. As long as the reactor compositions stay to the right of the low-to-high-conversion bifurcation curve, the reactor will remain in a low-conversion state. If, however, the reactor crosses to the left of the low-to-high-conversion; bifurcation curve, the possibility of increased reaction rates will exist. However, in order to reach the high conversion branch of the rate curve, the surface must be cleaned of CO. The time required to clean the surface of CO will be approximately equal to $a_m L_m / r_{SS} Q_o [CO]_o$. If $F_{CO,crit}$ is defined as the CO composition (in percent) at the point where the line between (CO,O_2) compositions of (0%,1%) and (2%,0%) intersects the low-to-high-conversion bifurcation curve, then, to a first

approximation,

$$\omega_{crit} = \left[2\tau_v \ln\left(\frac{F_{CO,crit}}{2-F_{CO,crit}}\right)\right]^{-1} + \frac{a_m L_m}{r_{ss} Q_o [CO]_o} \qquad (6.1)$$

For five of the seven cases in Table 6.1 (Cases I-V), the observed critical frequency was within 15% of that predicted by Eqn. (6.1). The largest difference was for case VI, where the predicted critical frequency was 55% higher than the experimental value (the steady-state conversion for Case VI is not negligible, thus violating the stated assumptions). Thus, the critical frequency is strongly related to the time required for the concentrations to cross the low-to-high-conversion bifurcation boundary on the steady-state multiplicity diagram (Figure 6.2).

In the low-frequency regions of Figure 6.4 the frequency-conversion curve is linear. The slope is primarily a function of flow rate, reactor volume and catalyst surface area. For long cycle periods (low frequencies), the conversion will be limited by the amount of CO_2 produced by the alternate cleaning of the surface of adsorbed carbon monoxide and oxygen (the two peaks per cycle behavior shown in Figure 6.3a). The first peak, associated with switching on the CO feed, will contain an amount of CO_2 limited by the sum of one monolayer of oxygen on the catalyst surface and the gas-phase oxygen contained in the reactor volume. The second peak, which occurs after the oxygen feed is switched on, will contain an amount of CO_2 approximately equal to the CO in one surface monolayer (most of the gas-phase CO has

left in the reactor effluent). The total CO_2 produced during the two peaks will thus be approximately equal to two monolayers plus twice (due to the stoichiometry) the feed oxygen concentration multiplied by the reactor volume. The time-average conversion of a single cycle is defined as the total CO_2 production divided by the total amount of CO in the feed stream during a complete cycle. The CO in a single cycle is the product of the flow rate, the average feed concentration, and the period of the cycle. Thus, at low frequencies:

$$r_{TA} \approx \left[\frac{2a_mL_m + 2V[O_2]}{Q_o[CO]_o}\right]\omega \tag{6.2}$$

Using experimentally determined values of $(r_{TA}Q_o[CO]_o/\omega)$ from the approximately linear portions of Cases I to VII in Figure 6.4, and values of (a_mL_m) from hydrogen adsorption measurements (as given in Chapter 4), a linear regression was performed to obtain

$$r_{TA} = \left[\frac{0.92a_mL_m + 2.57V[O_2]}{Q_o[CO]_o}\right]\omega \tag{6.3}$$

where the 95% confidence intervals for the constant terms are 0.92 ± 0.20 and 2.57 ± 0.83. The first constant in Eqns. (6.2) and (6.3) differs by more than a factor of two, but, considering the assumptions used to derive Eqn. (6.2), the agreement between these equations is quite good. The $(2a_mL_m)$ term in Eqn. (6.2) is an upper limit assuming that two complete monolayers react, and that the number of active

catalytic sites is the same for reaction as for hydrogen adsorption. If fewer than two monolayers react, or if the number of active sites for reaction is less than that for hydrogen adsorption, then this term will be replaced by a smaller one. Several factors could be responsible for fewer sites being active for CO oxidation than for hydrogen adsorption. The most obvious is that both oxygen and CO have smaller uptakes than hydrogen on platinum. As discussed in Chapter 5, CO uptakes can be less than 90% of hydrogen uptakes. Herz and Marin (1980) have summarized the data which show that oxygen uptakes are typically about half of hydrogen uptakes. Reduced uptakes of CO and oxygen relative to hydrogen would affect the first numerator term in Eqn. (6.2) by decreasing the value of the constant (i.e., 2). Because of these factors, it is postulated that fewer sites are available for CO oxidation than are active for hydrogen adsorption.

The second numerator term in Eqn. (6.2) is based on the assumption that no gas-phase CO replenishes the surface after the oxygen feed is switched on. It is more likely that a small fraction of the gas-phase CO adsorbs on the surface after the introduction of oxygen, so this term should be larger than given in Eqn. (6.2).

From Eqns. (6.2) and (6.3), it is seen that large catalyst charges lead to large slopes, while large flow rates lead to small slopes. Thus, for operating conditions with the same flow rate and catalyst charge, the slope in the low

frequency region should be the same, even if the steady-state behavior is different. This was observed for reactor operation at different temperatures (Cases I, IV, and V) and can be seen in Figure 6.4b.

The largest average conversion obtained during 180-degree out-of-phase cycling was 71% for Case VI with a frequency of 2.2 mHz. Although this is 4.5 times greater than the steady-state conversion for the same average feed composition, it is not greater than that which can be obtained from a combination of steady states with the same average feed composition. That is, this cycling strategy does not represent a global maximum. For example, by operating in the high-conversion region with a feed composition of 1% oxygen and 1.6% CO for one-half of the time, and in the low conversion regime with a feed composition of 0% oxygen and 0.4% CO for the other half of the time, the time-average conversion of CO to CO_2 will be 80%. This combination of steady-states is a higher conversion than any found using out-of-phase cycling.

6.4.2 Effect of Oxygen Phase Lead on Time-Average Conversion

Following the completion of the first set of experiments, the effects of the phase angle between the feed square waves were determined. The phase-angle experiments were performed at the base case (Case I) operating conditions. The time-average conversion is plotted against the oxygen phase lead for four frequencies in Figure 6.5. (The

solid lines represent model predictions which will be discussed later.)

At frequencies higher than those shown in Figure 6.5 (e.g., for ω = 10 mHz) the time-average conversion was approximately 5%, close to the steady-state conversion, for all values of oxygen phase lead. As cycle frequency was decreased, a small region of enhanced conversions appeared for oxygen phase leads of less than 180 degrees. For a period of 120 seconds, as shown in Figure 6.5a, this region spans from 45 degrees to 150 degrees. The maximum time-average conversion attained was greater than 90%, and this occurred for phase leads between 45 and 90 degrees. For phase leads less than 45 degrees or greater than 170 degrees the time-average conversion was approximately 5%. It is interesting to note that 180-degree out-of-phase cycling does not lead to rate enhancement for this frequency (see also Case I in Figure 6.4 with ω = 8.33 mHz).

As shown in Figure 6.5b, for ω = 5.56 mHz, the maximum time-average conversion is greater than 90%. This is greater than the highest time-average rate (55% for Case I conditions) obtained with 180 degree out-of-phase cycling. Thus, by varying the phase angle between inputs, it is possible to improve the conversion obtained during feed composition cycling.

The range of phase angles for which rate enhancement occurred increased as frequency was decreased, as shown in Figure 6.5. The maximum conversion increased and then

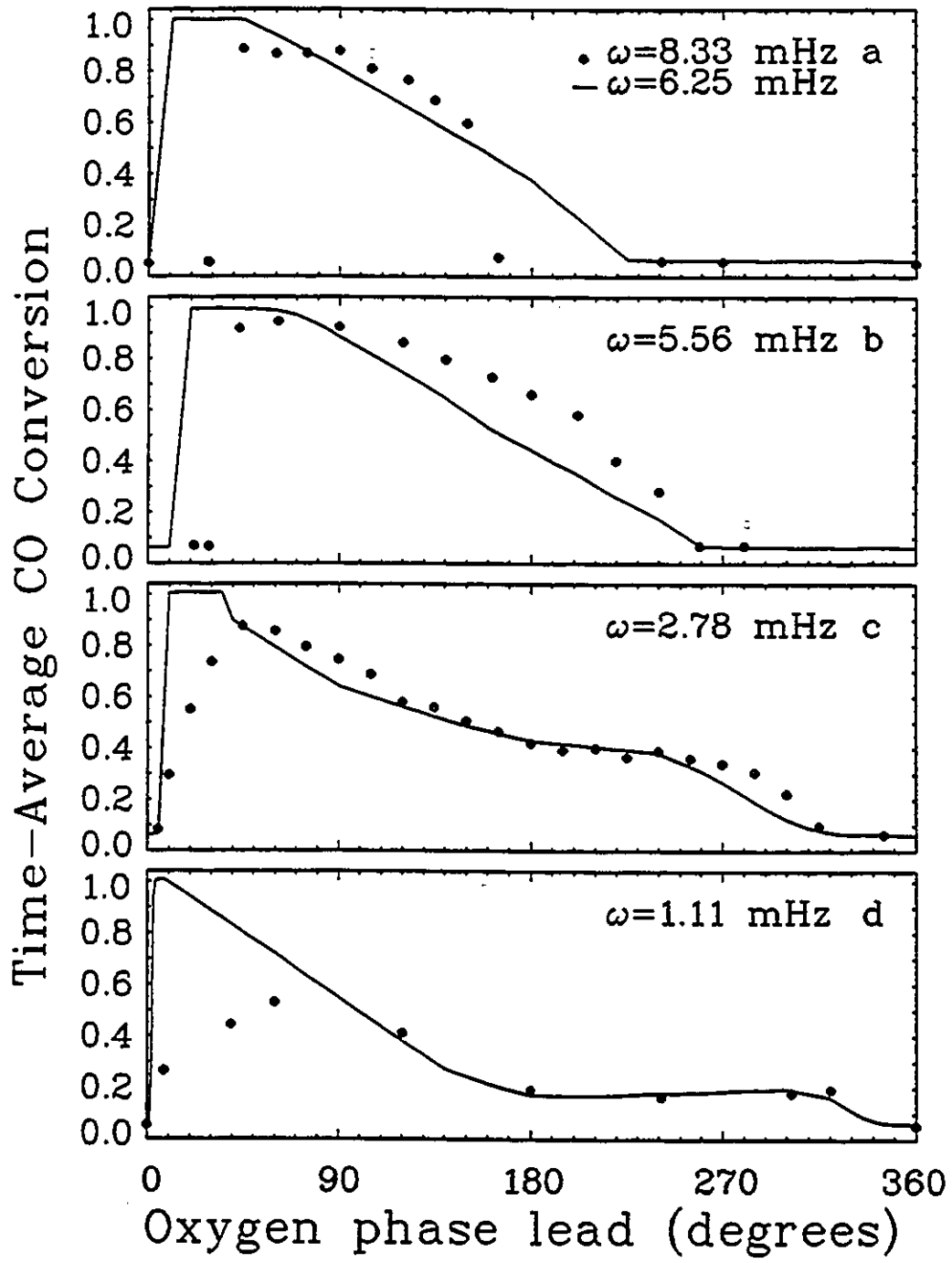

Figure 6.5 Effect of Phase Angle on Time-Average Conversion

decreased, and a plateau region appeared for large oxygen phase leads. The plateau region is shown clearly in Figure 6.5c (and 6.5d) for a frequency of 2.78 mHz (1.11 mHz) and extends from about 180 (180) to 270 (320) degrees of phase lead. The plateau conversion is related to the catalyst charge, reactor volume, feed flow rate, and frequency in the same way as the conversion in the low frequency regions of Figure 6.4 and can be described by Eqn. (6.3). Thus, the conversion of the plateau is not strongly affected by the reaction kinetics.

The achievement of greater than 90% conversions for high frequencies and low phase leads is of particular interest. The highest conversion attainable by combining Case I steady-state operating conditions is 62.5% (one-half the time operating with 1.25% CO in 1% O_2, one-half the time operating with 0.75% CO in 0% O_2). Hence, with cyclical operation it was possible to increase the maximum average reaction rate by more than 40%. This is an example of global rate enhancement.

Although there have been a number of experimental studies of out-of-phase feed composition cycling, this is apparently the first report of an experimental examination of the effect of phase angle during feed composition cycling. Cho (1983) reported a theoretical study of feed cycling to a single catalyst pellet, but even in that work only a very limited number of phase angles was investigated.

6.5 Model Details

The reaction was assumed to proceed via a Langmuir-Hinshelwood mechanism, as given by Eqns. (2.2)-(2.4). Two key assumptions were made which distinguish the mechanism from a standard LH mechanism. First, as described in detail in Chapter 5, it was assumed that CO self-exclusion occurs; that is, on average, each adsorbed CO molecule prevents adsorption of further CO from slightly more than the one surface site occupied by the adsorbed CO molecule. It was also assumed that the kinetic parameters are strong functions of CO surface coverage. Lynch *et al.* (1986) used a model incorporating adsorbate-induced surface phase transformations to describe oscillations in the rate of CO oxidation. In the present study, as in that of Lynch *et al.* (1986), the catalyst surface will be assumed to switch between two phases of different activity when critical values of CO surface coverages are reached. For high CO surface coverages, the oxygen sticking probability and the surface reaction rate constant will increase due to geometric effects associated with a phase change of the catalyst surface. This enhancement of oxygen adsorption and surface reaction disappears when the CO surface coverage drops below a critical value.

These effects are shown in Figure 6.6, where the fraction of the surface in each phase is shown as a function of fractional surface coverage of CO. For clean surfaces, the Pt(100) face reconstructs to a quasihexagonal (hex)

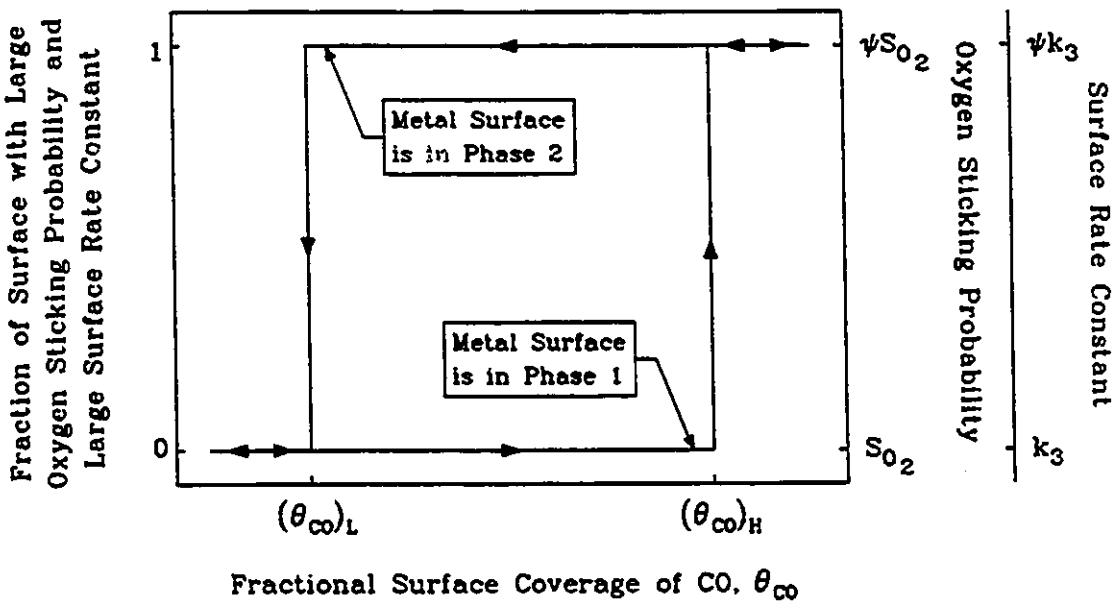

Figure 6.6 Effect of CO Coverage on Rate Constants

phase. This phase has a low sticking probability for oxygen adsorption. When the fractional surface coverage of CO exceeds a critical value, $(\theta_{CO})_H$, the entire surface will spontaneously transform to a (1×1) phase (i.e., the reconstruction is removed). The (1×1) phase has an oxygen sticking probability orders of magnitude higher than the hex phase. The metal surface will remain in the (1×1) phase until the fractional surface coverage of CO drops below a second critical value, $(\theta_{CO})_L$. The surface will then reconstruct to form the hex phase.

Platinum crystal faces other than the (100) face will also undergo phase transformations upon adsorption of CO. In the mathematical representation of this phenomenon the

surface is treated as a homogeneous surface, that is, the entire surface is either in Phase 1 (hex) or Phase 2 (1×1). In Phase 1, the oxygen sticking probability and the surface reaction rate constant have low values, as shown in Figure 6.6. When the catalyst surface transforms to Phase 2, the oxygen sticking probability and the surface reaction rate constant both increase by a factor of ψ, which for this work has been assigned a value of 250. When the surface transforms back to Phase 1, the oxygen sticking probability and the surface reaction rate constant both return to their initial values. (In Lynch *et al.* (1986), ψ was equal to 150 for the oxygen sticking probability, and the surface reaction rate constant was assumed to be unaffected by the surface phase transformation.) Although there are apparently no reports of the surface reaction rate constant being different in the hex and the (1×1) phases, there is no reason which precludes this possibility, and several arguments which support the possibility. In initial attempts to fit the feed cycling data, the surface reaction rate constant was kept at the same value for both phases, but it was found that much better agreement with the data could be obtained by allowing the surface reaction rate constant to change in the same manner as the oxygen sticking probability.

When these assumptions are incorporated into a mathematical model for an isothermal CSTR, the following equations result:

$$\frac{dX}{d\tau} = X_o - Q_n X - K_1 X(1-\theta_{co}-\theta_o)\frac{(1-N_{co}\theta_{co})}{(1-\theta_{co})} + K_{-1}\theta_{co} \qquad (6.4)$$

$$\frac{dY}{d\tau} = Y_o - Q_n Y - K_2 Y(1-\theta_{co}-\theta_o)^2 \qquad (6.5)$$

$$\frac{dZ}{d\tau} = Z_o - Q_n Z + K_3\theta_{co}\theta_o - K_4 Z(1-\phi_{co_2}) + K_{-4}\phi_{co_2} \qquad (6.6)$$

$$\frac{d\theta_{co}}{d\tau} = \alpha_m\{K_1 X(1-\theta_{co}-\theta_o)\frac{(1-N_{co}\theta_{co})}{(1-\theta_{co})} - K_{-1}\theta_{co} - K_3\theta_{co}\theta_o\} \qquad (6.7)$$

$$\frac{d\theta_o}{d\tau} = \alpha_m\{(2F_{o_2}/F_{co})K_2 Y(1-\theta_{co}-\theta_o)^2 - K_3\theta_{co}\theta_o\} \qquad (6.8)$$

$$\frac{d\phi_{co_2}}{d\tau} = \alpha_s\{K_4 Z(1-\phi_{co_2}) - K_{-4}\phi_{co_2}\} \qquad (6.9)$$

where $$Q_n = 1 - F_{co}\{K_1 X(1-\theta_{co}-\theta_o)\frac{(1-N_{co}\theta_{co})}{(1-\theta_{co})} - K_{-1}\theta_{co}\}$$

$$- F_{o_2}K_2 Y(1-\theta_{co}-\theta_o)^2 + F_{co}K_3\theta_{co}\theta_o$$

$$- F_{co}\{K_4 Z(1-\phi_{co_2}) - K_{-4}\phi_{co_2}\} \qquad (6.10)$$

These equations are identical to those used in Chapter 5 except that in this model the rate constants for oxygen adsorption and surface reaction are given by:

$$K_2 = 6.43\ a_m\ \psi\ S_{o_2}\ \sqrt{T}\ /\ Q_o \qquad (6.11)$$

$$K_3 = a_m\ L_m^2\ \psi\ k_3\ \exp(-E_3/RT)\ /\ Q_o\ [CO]_o \qquad (6.12)$$

where ψ is always unity for surface phase 1 (low CO coverage) and greater than unity for surface phase 2 (high CO coverage). It is noted that this model reduces to the CO self-exclusion model if ψ is always unity; to the surface phase transformation model of Lynch *et al.* (1986) if $N_{co} = 1$; and to the standard LH model if N_{co} and ψ are both

unity. For cycling of the type used in this study, X_o and Y_o both alternate between 0 and 2 (but not together unless the cycles are in phase), while Z_o is always zero.

Kinetic parameters for the model were chosen based on two criteria: the model predictions should match the experimental time-average behavior as closely as possible, and the model should describe the steady-state bifurcation behavior.

6.6 Model Predictions

The first attempts at describing the time-average behavior used the standard LH model and the CO self-exclusion model with rate parameters, tabulated in Chapter 5, which minimized the error in the predicted steady-state bifurcation behavior. The predicted base case (Case I) time-average conversions for these models are plotted in Figure 6.7. At low frequencies the initial slope of the predicted conversion-frequency curve was in agreement with the data. However, as previously mentioned, the slope of the initial linear region is determined by mass balance considerations. Thus, most kinetic models with correct values for volume, flow rate, and surface area will correctly predict the slope, so the ability to predict the conversion in the low frequency region is not an adequate test of a model. A better test is to examine the predicted behavior in the intermediate and high frequency regions. As shown in Figure 6.7, neither the standard LH model nor the CO self-exclusion model could describe the time-average conversion

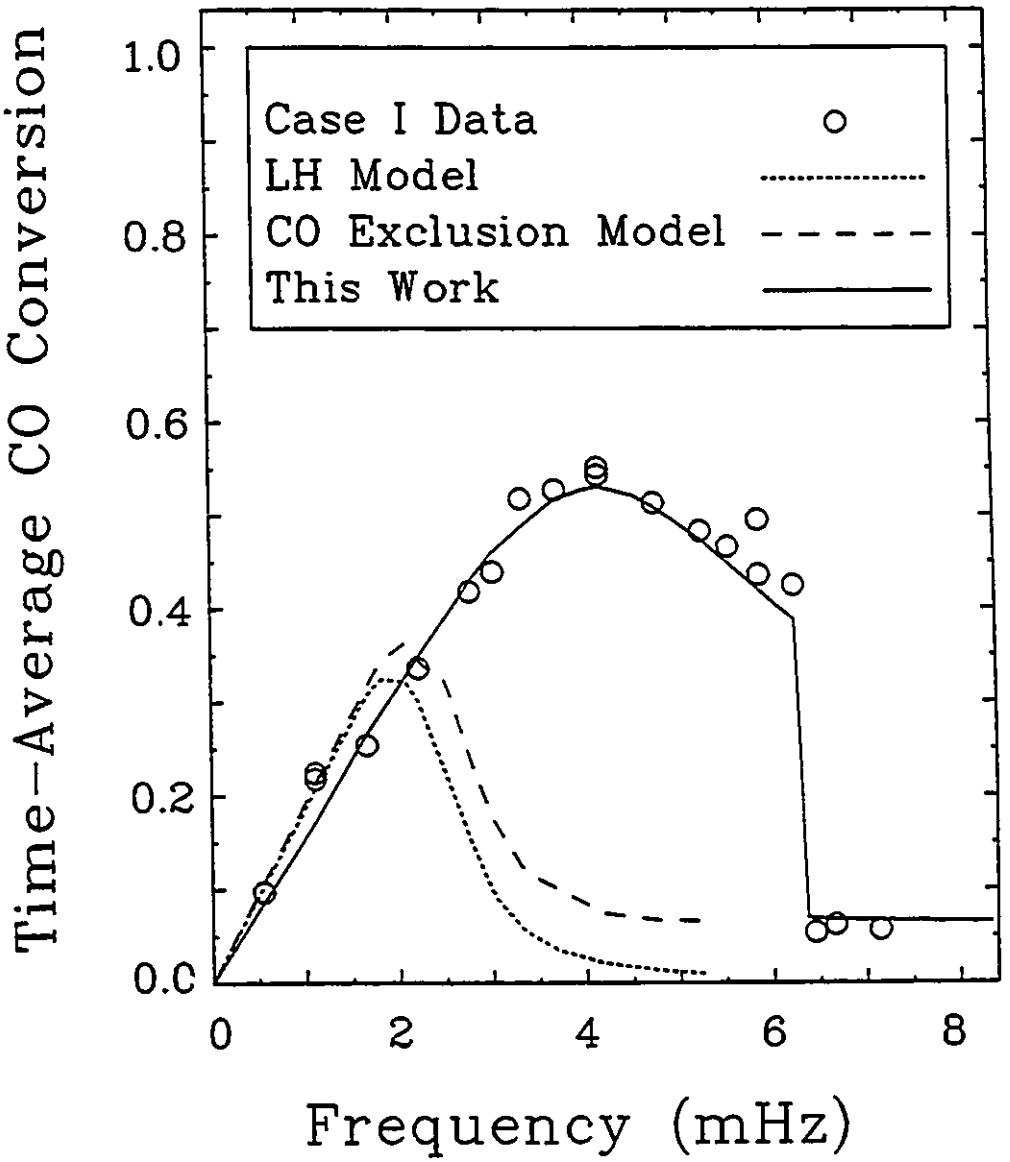

Figure 6.7 Comparison of Predicted Time-Average Conversions

for other than low frequencies. As frequency increases from low values, these models predicted a smooth transition to low time-average rates, unlike the data which showed an abrupt decrease in conversion at a critical frequency

related to the location of the steady-state bifurcation boundary. Larger values of K_2 and K_3 are required if these models are to adequately describe the time-average behavior. However, increasing K_2 and K_3 causes the error in the predicted steady-state behavior to increase (agreement with steady-state behavior shown in Figure 6.2 must be maintained). The error in the predicted low-to-high-conversion bifurcation points can be reduced by increasing the ratio of K_1 to K_{-1}, but the error in the predicted high-to-low bifurcation points will remain unacceptable. If, however, K_2 and K_3 are increased only in the low-conversion, high-CO-coverage region, then it is possible to describe both the steady-state and the time-average behavior of the system. This is precisely what occurs when the surface phase transformation model is used.

In the final modeling attempt a value of ψ greater than unity was used, in this case ψ=250. For the parameter values listed in the Nomenclature, the predicted steady-state behavior is shown in Figure 6.2. The model describes the steady-state data very well. This is an important point of agreement between the model and the experimental data, as a model which does not correctly describe the observed steady-state behavior should be discarded. The predicted Case I time-average conversions are shown in Figure 6.7, where they are compared to the standard LH model and the CO self-exclusion model. The new model is superior to both of the existing models and quantitatively describes all of the

major features of the conversion-frequency curve: the initial slope at low frequency, the magnitude and frequency of the maximum conversion, and the critical frequency above which significant rate enhancement does not occur.

The model was also used to predict the effects of temperature, catalyst charge, and flow rate on time-average conversion. As shown in Figure 6.4, the resulting predictions are in excellent agreement with the data, describing qualitatively and quantitatively all of the major features of the time-average conversion behavior.

The model predictions of the dynamic behavior are shown in Figure 6.8. The rate parameters used for CO_2 adsorption and desorption on the support are similar to those used by Lynch *et al.* (1986). These predictions are for case VI conditions. Each frame in Figure 6.8, except for 6.8e, can be compared directly with the corresponding frame in Figure 6.3. In Figure 6.8e a slightly higher frequency was used than in Figure 6.3e so that a low-conversion state was attained. Most of the important features in Figure 6.3 appear in Figure 6.8.

Apparently this is the first model of CO oxidation that has been shown capable of describing quantitatively both the steady-state bifurcation behavior and the time-average and dynamic behavior during 180-degree out-of-phase feed composition cycling. This model (in a simplified form, with $N_{CO}=1$) has already been used successfully to describe self-sustained oscillations during the catalytic oxidation of CO

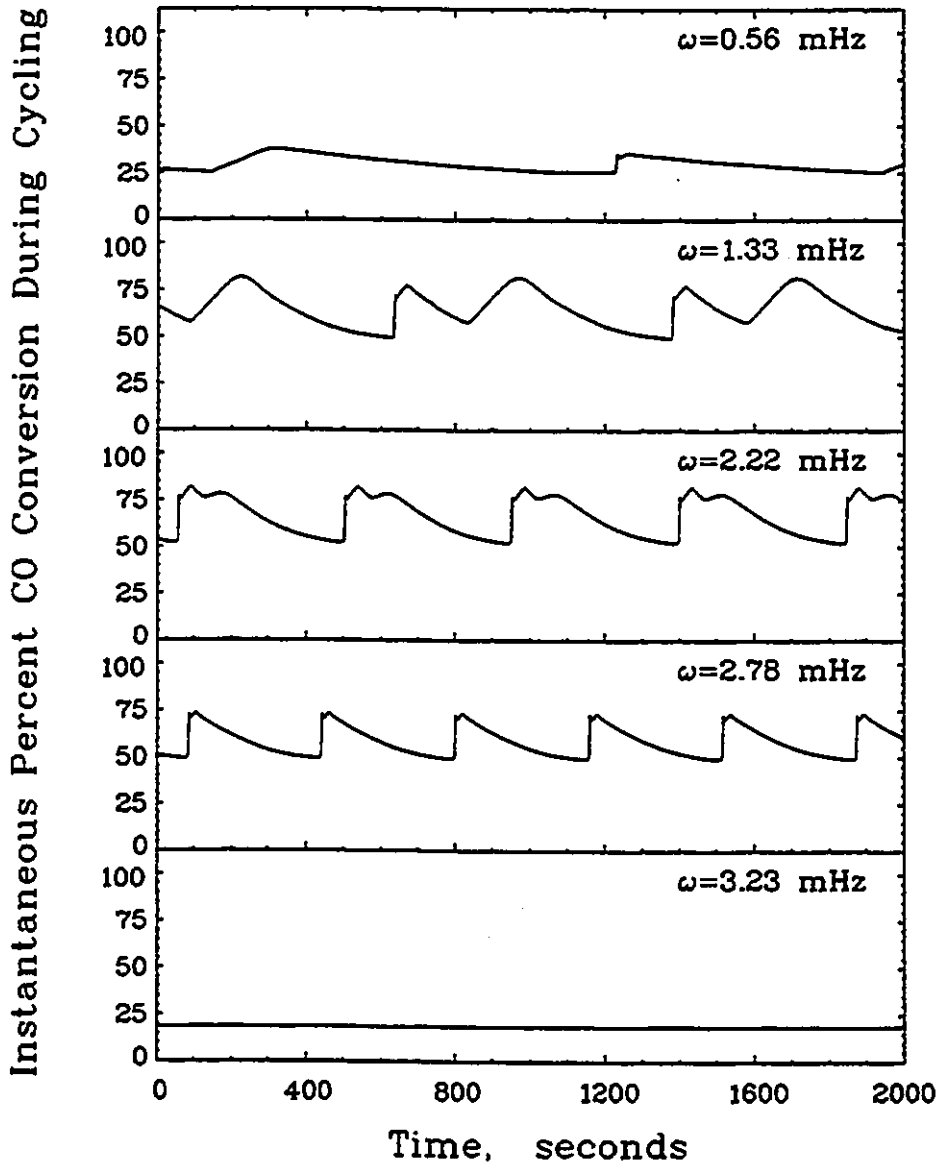

Figure 6.8 Predicted Dynamic Behavior

(Lynch *et al.*, 1986). Hence, this model gives a single, consistent explanation for three of the commonly observed complex phenomena displayed during CO oxidation on supported platinum.

The final test of the model was to determine if it could describe the effect of oxygen phase lead on the time-average rates. The predicted time-average rate behavior is shown in Figure 6.5, where it is compared with the experimental results. At intermediate frequencies, as shown in Figures 6.5b and 6.5c, there is very good agreement between the model predictions and the data. For higher frequencies, however, the model predicts that a low-conversion state will be reached at a lower frequency than was observed experimentally (model ceases to predict a region of high conversions at ω = 8.0 mHz whereas high experimental conversions were observed at frequencies as high as ω = 8.33 mHz). This can be seen in Figure 6.5a. At low frequencies (Figure 6.5d) the model predictions are very good for large values of oxygen phase lead (greater than 180 degrees), but for small oxygen phase leads the predicted time-average rate is significantly higher than the experimental rate.

There could be many reasons for the differences between the model predictions of the effect of phase-angle on time-average conversion and the experimental data, but several changes come quickly to mind which might bring the model predictions into closer agreement with the data. The first change is to require a finite time for the surface phase transformation to occur. In the model, the phase transformation takes place instantaneously and simultaneously on all active sites. If the model were changed so that, during a finite period of time following the crossing of the critical

surface coverage, the surface transformation occurred as a ramp between Phase 1 and Phase 2, then the model predictions of high conversions at low phase leads might be reduced.

A second change which might improve model predictions is to treat the platinum crystallites as a number of crystal faces of different activity rather than as a grouped average face. Another change with similar effects is to include coverage-dependent rate parameters (above and beyond the coverage dependence of the phase transformation assumption).

6.7 Conclusions

There are four main conclusions that can be made from this study of feed concentration cycling. First, rate enhancement occurs during forced feed composition cycling of the platinum-catalyzed CO oxidation reaction. Second, adjusting the phase angle between the oxygen and CO feed streams can cause increases in the time-average rates over and above those for out-of-phase cycling. The phase angle between inputs is an important parameter if maximum conversion is desired. Third, the standard Langmuir-Hinshelwood model, when forced to match the steady-state bifurcation behavior, is incapable of describing the observed rate enhancement. Finally, a surface phase transformation model with CO self-exclusion can describe both the steady-state data and the rate enhancement for this system. A simplified form of this model (Lynch *et al.*, 1986) has already been used to describe oscillatory behavior during CO oxidation,

thus, the surface phase transformation model with CO self-exclusion can quantitatively describe three of the commonly observed forms of complex behavior exhibited by the oxidation of CO on supported platinum catalysts.

6.8 References

Bailey, J. E., "Periodic Operation of Chemical Reactors: A Review", Chem. Eng. Comm. 1, 111-124 (1973).

Bailey, J. E., *in* "Chemical Reactor Theory, A Review", L. Lapidus and N. R. Amundson, (Eds.), Prentice-Hall, Englewood Cliffs, NJ (1977) p758.

Barshad, Y., and E. Gulari, "A Dynamic Study of CO Oxidation on Supported Platinum", AIChE J. 31, 649-658 (1985).

Behm, R. J., P.A. Thiel, P. R. Norton, and G. Ertl, "The interaction of CO and Pt(100). I. Mechanism of adsorption and Pt phase transition", J. Chem. Phys. 78, 7437-7447 (1983).

Cho, B. K., "Dynamic Behavior of a Single Catalyst Pellet. 1. Symmetric Concentration Cycling during CO oxidation of Pt/Al_2O_3", Ind. Eng. Chem. Fundam. 22, 410-420 (1983).

Cutlip, M. B., "Concentration Forcing of Catalytic Surface Rate Processes, Part 1. Isothermal Carbon Monoxide Oxidation Over Supported Platinum", AIChE J.25, 502-508 (1979).

Cutlip, M. B., C. J. Hawkins, D. Mukesh, W. Morton, and C. N. Kenney, "Modelling of Forced Periodic Oscillations of Carbon Monoxide Oxidation over Platinum Catalyst", Chem.

Eng. Commun. 22, 329-344 (1983).

Douglas, J. M., Process Dynamics and Control, Vol. 2, Prentice-Hall, Englewood Cliffs, NJ (1972).

Douglas, J. M., "Periodic Reactor Operation", Ind. Eng. Chem. Proc. Des. Dev.6, 43-48 (1967).

Douglas, J. M., and D. W. T. Rippin, "Unsteady State Process Operation", Chem. Eng. Sci. 21, 305-315 (1966).

Herz, R. K., and S. P. Marin, "Surface Chemistry Models of Carbon Monoxide on Supported Platinum Catalysts", J. Catal. 65, 281-296 (1980).

Lynch, D. T., "Modelling of Resonant Behavior during Forced Cycling of Catalytic Reactors", Can. J. Chem. Eng. 61, 183-188 (1983).

Lynch, D. T., "On the Use of Adsorption/Desorption Models to Describe the Forced Periodic Operation of Catalytic Reactors", Chem. Eng. Sci. 39, 1325-1328 (1984).

Lynch, D. T., G. Emig, and S. E. Wanke, "Oscillations during CO Oxidation over Supported Metal Catalysts: III. Mathematical Modeling of the Observed Phenomena", J. Catal. 97, 456-468 (1986).

Oh, S. E., K. Baron, J. C. Cavendish, and L. L. Hegedus, "Carbon Monoxide Oxidation in an Integral Reactor: Transient Response to Concentration Pulses in the Regime of Isothermal Multiplicities", ACS Symp. Ser. 65, 461-474 (1978).

Thiel, P. A., R. J. Behm, P. R. Norton, and G. Ertl, "The interaction of CO and Pt(100). II. Energetic and Kinetic

Parameters", J. Chem. Phys. 78, 7448-7458 (1983).

7. Oscillations and Multiplicity

7.1 Predicted Behavior

The surface phase transformation model was originally developed by Lynch *et al.* (1986) to describe oscillatory behavior observed during CO oxidation on a supported platinum catalyst. As was shown in Chapter 6, this model is also capable of describing steady-state multiplicity and transient behavior during feed composition cycling. For some values of rate parameters, the phase transformation model predicts a crossover from a region of oscillations to a region of multiplicity. The sequence in Figure 7.1 shows that, for the same intrinsic rate constants used in Chapter 6, decreasing the amount of catalyst in the reactor causes a change from predicted multiplicity to predicted oscillations. In Figure 7.1a, for a metal area of 6.92 m^2, the regions of unique steady states are separated by a region of multiplicity. In Figure 7.1b, for 0.5 m^2 of platinum, multiplicity and oscillations are both present. The high-to-low and low-to-high bifurcation points cross. A region of oscillations separates the unique steady states for a metal surface area of 0.1 m^2, as shown in Figure 7.1c.

As a final test of the surface phase transformation model an attempt was made to find behavior similar to that shown in Figure 7.1. Finding this behavior would result in experimental confirmation of model predictions, and not merely a description of data after they were collected. As

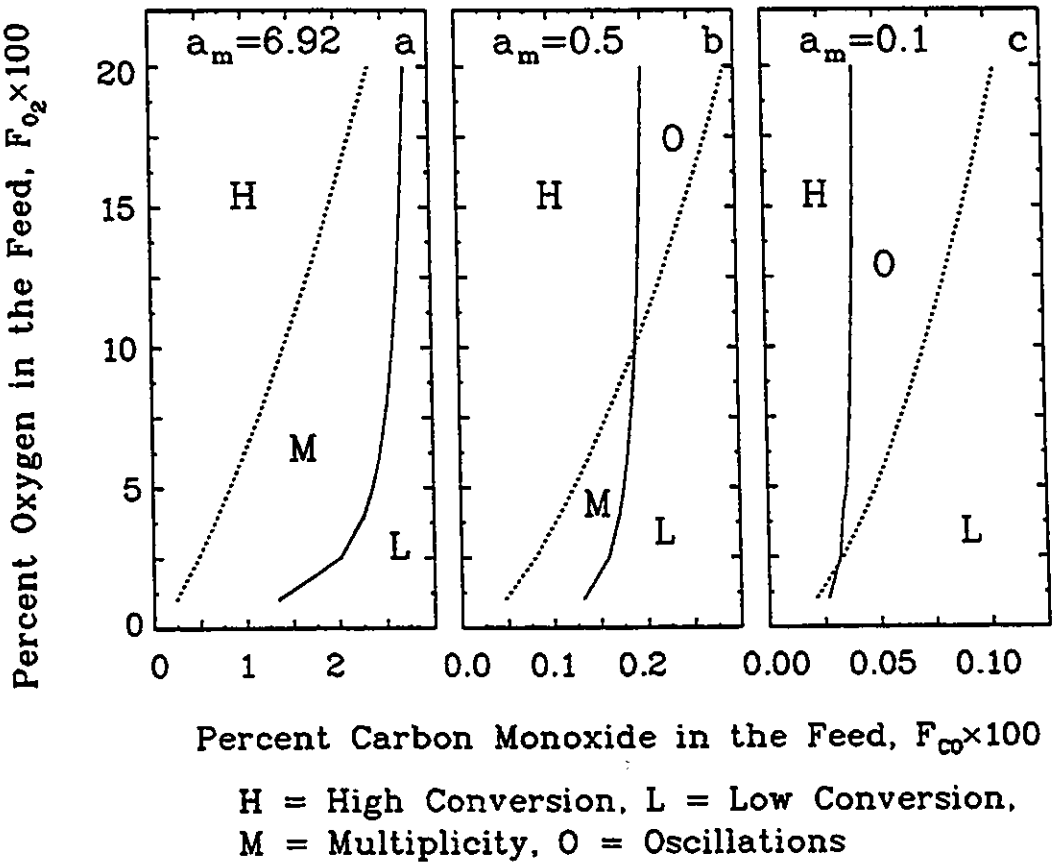

Figure 7.1 Transition from Multiplicity to Oscillations

such, finding a crossover between oscillations and multiplicity would be much stronger support of the surface phase transformation model with CO self-exclusion.

It should be noted that the phase transformation model is not alone in predicting a crossover between oscillations to multiplicity. Aluko and Chang (1986) have shown that the surface oxide model also predicts such a crossover. Thus the discovery of a crossover will not be sufficient to exclude all models except the phase transformation model.

However, taking into consideration the inability of the surface oxide model to accurately describe the steady-state behavior of Chapter 5, the discovery of a crossover would be strong evidence supporting the surface transformation model.

The predictions in Figure 7.1 indicate that, for operating conditions easily attained with the available equipment, a very small catalyst surface area, on the order of 0.5 m^2, is necessary for the existence of a crossover between multiplicity and oscillations. This amounts to approximately 1 gram of the 0.5% platinum on alumina catalyst used in the previous chapters. Using such a small mass of catalyst in the recycle reactor could result in significant flow bypassing problems leading to questionable data. To avoid this potential problem, a new recycle reactor, described in Chapter 4, was constructed for use with platinum gauze catalyst. A stack of gauze discs fit snugly in the 2.5 cm ID reactor, forcing the gas to flow through the catalyst. Flow distribution rings above and below the stacked gauze prevented bypass along the reactor walls. The gauze was 99.999% pure and was in the form of 2.5 cm discs. The 146 sheets of gauze had a combined mass of 51.95 g, for an average sheet mass of 0.356 g. The platinum wires comprising the gauze were nominally 0.1 mm diameter. The estimated total platinum surface area for 146 sheets of gauze was 0.1 m^2.

The catalytic characteristics of platinum wire are likely different from those of small supported platinum

crystallites. The wire will likely have larger crystals with better thermal contact than the supported catalyst. Thus, one would expect that the parameters used to describe the results of Chapters 5 and 6 will not be directly applicable to platinum gauze. However, the catalytic properties of the gauze and supported platinum should be similar enough so that the trends shown in Figure 7.1 should be the same for both gauze and supported platinum.

A series of tests, described in the following section, was performed. Unfortunately, the results were inconclusive. Although some of the results indicated that a crossover from multiplicity to oscillations was found, the results were not reproducible due to slow catalyst activity changes. The experimental results are presented in the following section.

7.2 Experimental Behavior

The reactor used in the work reported in this chapter was described in Chapter 4. The circular platinum wire mesh sheets, 2.5 cm in diameter and 146 in number, were loaded into the reactor. The experimental results are summarized in Table 7.1. Initially the feed to the reactor was set with a total flow of 250 cm^3/min. The CO feed composition ranged from 0 to 6% and the oxygen feed composition ranged from 0 to 100%. Initial experiments determined the general catalyst behavior with a constant feed. Oscillatory behavior was found in a region of intermediate CO concentrations.

Table 7.1 Summary of Platinum Gauze Behavior

Treat-ment	Temp °C	Gases	Multi-plicity	Oscilla-tions	Comments
1			NO	YES	as-received catalyst
2	220	H_2/O_2	NO	NO	only low conversion steady states
3	400	CO/O_2	NO	NO	only low conversion steady states
4	500	CO/O_2	NO	YES	
5	600	CO/O_2	YES	YES	originally only multi-plicity; oscillations found after prolonged use; crossover from oscillations to multi-plicity
6	650	CO/O_2	YES	YES	originally only multi-plicity; oscillations found after prolonged use
7	700	CO/O_2	YES	YES	crossover from oscilla-tions to multiplicity; long-term deactivation

High conversion steady states occurred at low CO concentrations. Low conversion steady states were found at high CO concentrations. No region of multiplicity was found using the as-received catalyst. A typical oscillation is shown in

Figure 2.3 for 200°C, 250 cm^3/min, 40% O_2 and 0.26% CO.

In an attempt to increase the activity of the catalyst, the catalyst was treated in an alternating feed of hydrogen and oxygen. The feed composition cycled between 10% oxygen and 10% hydrogen in nitrogen. The cycle period was 10 minutes, and the treatment temperature was 220°C. This treatment reduced the activity so that only low-conversion steady states were found. Neither high conversions nor oscillatory states were observed after the H_2-O_2 cycling treatment.

The catalyst was next treated in a tube furnace by switching the feed between CO in N_2 and O_2 in N_2. The feed composition alternated between 10% O_2 and 10% CO. The tube furnace temperature was set to 400°C. Cycle period was 10 minutes. After this treatment only low conversion steady states were observed.

The CO-O_2 cycling treatment was repeated at 500°C. After the treatment oscillatory behavior was observed. No multiplicity was observed after cycling at 500°C. Apparently the cycling treatment increased the catalyst activity. The regions of high and low conversion and oscillations were determined as functions of composition and temperature and are shown in Figure 7.2. The lines in Figure 7.2 show the limits of the high-conversion steady-state region and the low-conversion steady-state region as determined experimentally. As shown in Figure 7.2, the region of oscillations separated the regions of high and low

conversions, similar to the predictions shown in Figure 7.1c.

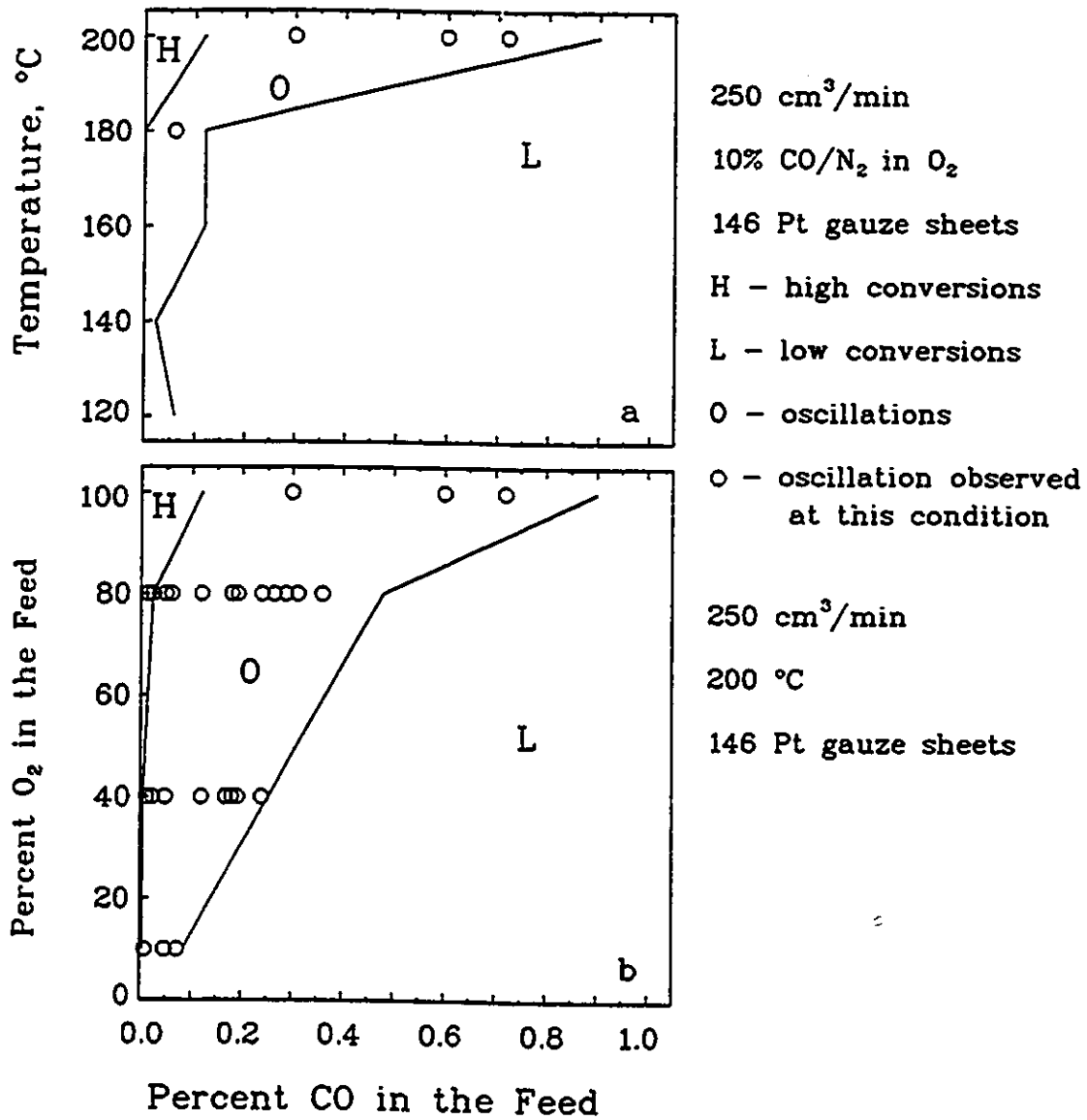

Figure 7.2 Region of Oscillations

Following catalyst characterization after 500°C CO-O_2 cycling, the catalyst was treated with the same cycling treatment at 600°C for 6 hours. After the 600°C treatment the catalyst showed both oscillatory and multiplicity

behavior. When 146 gauze discs were in the reactor, multiplicity was observed at 200°C for flow rates of 250 and 500 cm^3/min. Oscillations were then observed for 15 discs at 200°C and 250 cm^3/min. The feed composition of the observed oscillations ranged from 80% oxygen to 40% oxygen. Thirty gauze discs were then loaded into the reactor. For a flow rate of 500 cm^3/min, multiplicity was observed at 200 and 210°C for oxygen mole fractions of 1-20% and 1-10%, respectively. At 220°C and 500 cm^3/min, oscillations were observed at 4% oxygen. The temperature was reduced to 200°C, and oscillations were observed at 500 cm^3/min and 4-20% O_2. The flow rate was reduced to 250 cm^3/min and oscillations were observed between 40 and 80% oxygen. Finally, with 146 discs at 200°C and 500 cm^3/min only multiplicity was observed between 2 and 20% oxygen. The behavior described above (oscillations with 30 discs, multiplicity with 146 discs) is shown in Figure 7.3. The experimental limits of the high-conversion steady-state region and the low-conversion steady-state region are shown by the lines in Figure 7.3. The behavior shown in Figure 7.3 is similar to the predictions shown in Figures 7.1a and 7.1c. There should be a crossover from oscillations to multiplicity at a reactor catalyst loading between 30 and 146 discs of platinum gauze.

The crossover from multiplicity to oscillations was not located because it had become apparent that the catalyst activity was not constant but was decreasing with time.

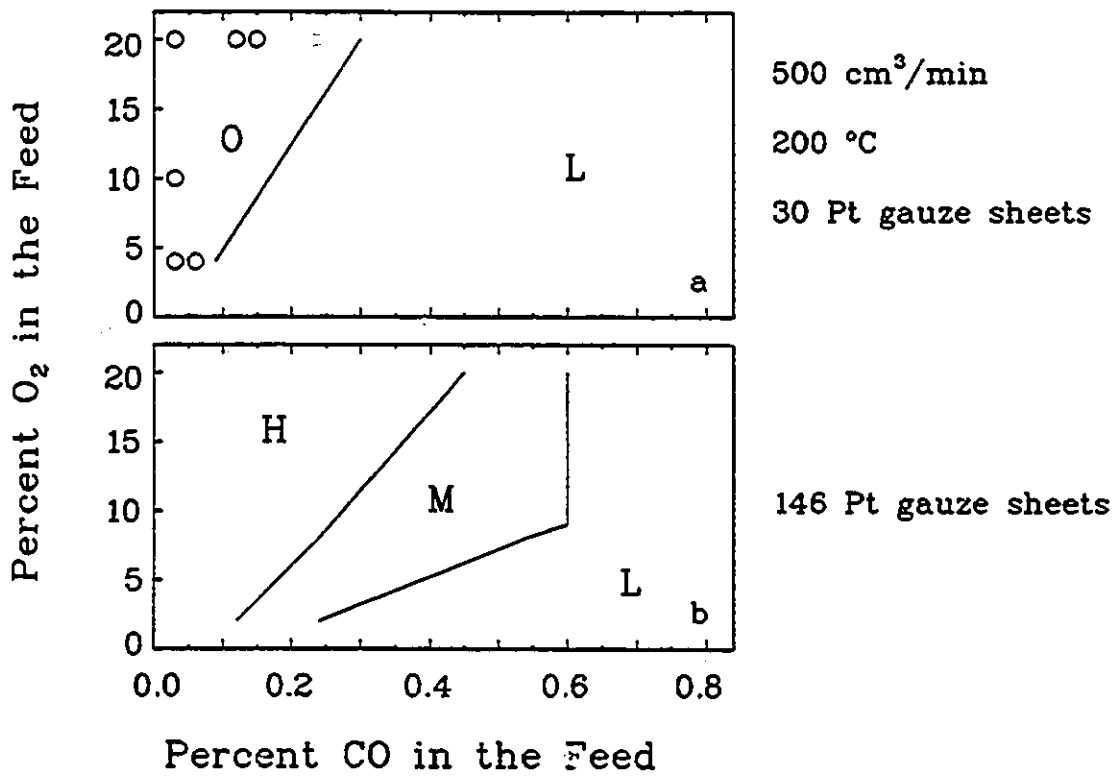

Figure 7.3 Multiplicity and Oscillations with Different Catalyst Charges

Before the 30 catalyst discs were used at 220°C, multiplicity was observed at 200°C between 1 and 20% oxygen, but after operating at 220°C oscillations were observed at 200°C in the same range of oxygen concentration.

Some studies have shown that a constantly decreasing catalytic activity can cause jumps from high-conversion to low-conversion branches of the rate curve, which could be confused with oscillatory behavior, thus further experimental work focussed on finding a constant catalytic activity crossover between oscillations and multiplicity.

The catalyst was next treated in an alternating flow of CO in N_2 and O_2 in N_2 at 650°C. After this treatment, multiplicity was found initially. However, after one day of operation, oscillations were found at the same operating conditions where multiplicity had been found previously. This indicated that the catalytic activity was decreasing.

It was hoped that higher temperature catalyst treatments would lead to more stable activity, so the catalyst was next treated at 700°C. Following this treatment, multiplicity was found with 146 discs of catalyst at temperatures between 160 and 220°C. Oscillations were then found with 15 and 45 sheets of catalyst at 200 and 220°C. With 15 catalyst discs no high-conversion steady states were observed, even at CO feed concentrations as low as 0.05%. All of the catalyst was then replaced in the reactor, and tests were run at temperatures ranging from 240 to 120°C. Only multiplicity was found at 140°C and above, but both multiplicity and oscillations were found at 120°C. Oscillations were found at 20% and 92% oxygen, and multiplicity was found at 4% O_2. At 140°C oscillations were found at 80% O_2 and multiplicity at 2% O_2. Multiplicity was then found at 160, 180 and 200°C. The observation of both oscillations and multiplicity at 120°C and 140°C was the only direct evidence collected that a crossover existed. The observed crossovers are shown in Figure 7.4. The experimental limits of the high-conversion steady-state region and the low-conversion steady-state region are shown by the lines in Figure 7.4.

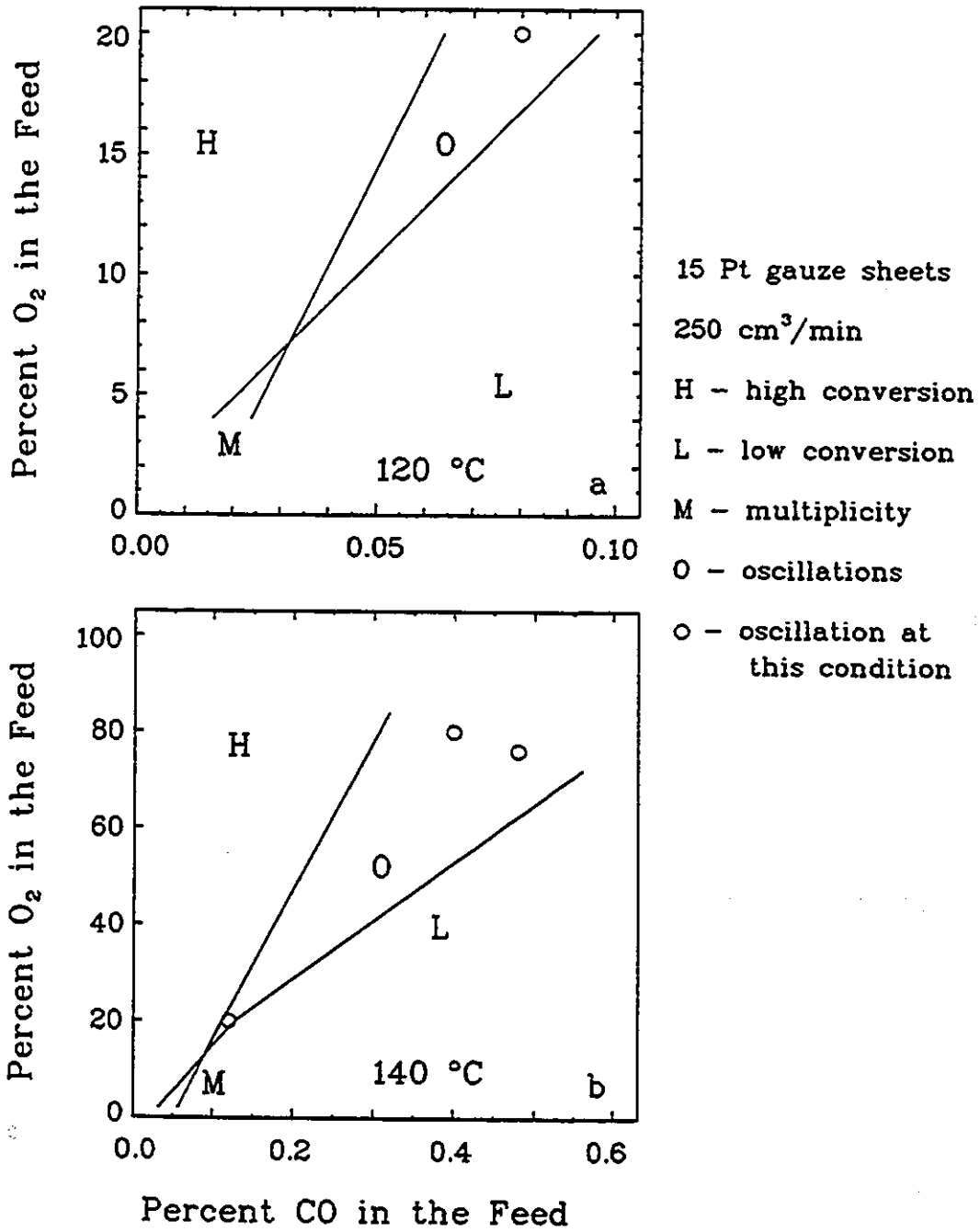

Figure 7.4 Experimental Transition from Multiplicity to Oscillations

The crossovers are similar to the predictions shown in Figure 7.1b. At 120°C the oscillations were observed before the multiplicity so, even if the catalyst was undergoing deactivation, the crossover was a valid observation. At 140°C the multiplicity was observed first, followed by oscillations. If the catalyst were slowly deactivating, the deactivation could have been responsible for the observed crossover at 140°C.

At 220°C, the catalyst activity began to fluctuate with time. A fixed transition between high and low conversions could not be found for oxygen feed compositions between 70 and 80%. At 20% oxygen oscillations were found. Oscillations were then found with a flow rate of 125 cm^3/min with 60-90% O_2. After this, oscillations were found with 250 cm^3/min at 70-80% oxygen, and with 500 cm^3/min at 80-90% oxygen.

A series of tests at 200°C and 250 cm^3/min with 75-100% oxygen was then performed to check the catalyst activity. Each day the reactor was heated to 200°C in a N_2-CO mixture. The flow was then switched to a mixture of pure O_2 and 10% CO-in-N_2. With 2% CO (80% O_2), the initial steady state was a high-conversion steady state. As the day progressed, the region of multiplicity moved to progressively lower CO concentrations. By the end of one day the high-to-low bifurcation point was at 0.9% CO, and most days it typically was between 1.2 and 1.6% CO. However, each morning after heating in CO there would be a high-conversion steady state

at about 2% CO. This interesting behavior indicates that during operation the catalyst was slowly being deactivated, likely by an oxidation process of some sort. During heating in CO, the catalyst was reactivated by a reduction of the poison by CO. Tests were then run in which the catalyst was heated in oxygen. During these tests oscillations were observed at 160 and 200°C at 250 cm^3/min between 20 and 99.4% oxygen. The oscillations occurred at CO concentrations much lower than the bifurcation points after heating in CO. These tests also indicate catalyst deactivation by oxygen: heating in oxygen may have decreased the active surface area, resulting in a change from multiple steady-state behavior to oscillatory behavior.

Thus, it is seen that a platinum gauze system displays the crossover behavior predicted by the surface phase transformation model with CO self-exclusion. Although the catalyst behavior was not constant, it appears that crossovers from multiplicity to oscillations were found. The catalyst activity decreased, possibly due to an oxidation process on the surface. The long-term deactivation occurred on a much longer time-scale than the oscillations, thus the deactivation is probably caused by a different process than that behind the oscillations. One possible explanation for the observed phenomena is that surface oxide formation causes the deactivation, while surface phase transformation is responsible for the oscillatory behavior. It seems unlikely that a surface oxide could form and be reduced quickly

enough to cause oscillations at the relatively low temperatures (120°C) where oscillations were found. Furthermore, the catalyst deactivation process was not observed at the low temperatures where oscillations were found, but only at temperatures of 200°C and higher.

7.3 References

Aluko, M., and H.-C. Chang, "Dynamic Modelling of a Heterogeneously Catalysed System with Stiff Hopf Bifurcations", Chem. Eng. Sci. 41, 317-331 (1986).

Lynch, D. T., G. Emig, and S. E. Wanke, "Oscillations during CO Oxidation over Supported Metal Catalysts: III. Mathematical Modeling of the Observed Phenomena", J. Catal. 97, 456-468 (1986).

8. The Effect of Model Assumptions on Predicted Bifurcation Behavior

8.1 Nomenclature

a_m = total surface area of the supported catalyst, m^2

$[CO]$ = CO concentration, mol/m^3

$[CO]_o$ = CO feed concentration, mol/m^3

$[CO-S]$ = CO surface concentration, mol/m^2

k_1 = CO adsorption rate constant, $m^3/mol \cdot s$

k_{-1} = CO desorption rate constant, s^{-1}

k_2 = O_2 adsorption rate constant, $m^5/mol^2 \cdot s$

k_{-2} = O_2 desorption rate constant, $m^2/mol \cdot s$

k_3 = surface reaction rate constant, $m^2/mol \cdot s$

K = parameter defined in Eqn. (8.11), $K_1^\dagger[CO]_o/(1+K_2^\dagger[O_2]^{0.5})$

K^* = parameter in Eqn. (8.27), $K_1/(K_2^*+1)$

K_1 = dimensionless CO adsorption rate constant, $a_m L_m k_1/Q$

K_1^* = dimensionless CO adsorption equilibrium constant, $k_1[CO]/k_{-1}$

$K_1^\dagger$ = CO adsorption equilibrium constant, k_1/k_{-1}, m^3/mol

K_{-1} = dimensionless CO desorption rate constant, $a_m L_m k_{-1}/Q[CO]_o$

K_2 = parameter defined in Eqn. (8.12) $K_3 K_2^\dagger [O_2]_0^{0.5}/(1+K_2^\dagger[O_2]_0^{0.5})$

K_2^* = dimensionless O_2 adsorption equilibrium constant, $\sqrt{k_2[O_2]/k_{-2}}$

$K_2^{\dagger}$ = O_2 adsorption equilibrium constant, $\sqrt{k_2/k_{-2}}$, $m^{1.5}/mol^{0.5}$

K_3 = dimensionless surface reaction rate constant, $a_m L_m^2 k_3/Q[CO]_o$

L_m = adsorption capacity of the metal surface, mol/m^2

$[O_2]$ = O_2 concentration, mol/m^3

$[O_2]_o$ = O_2 feed concentration, mol/m^3

[O-S] = oxygen surface concentration, mol/m^2

Q = feed volumetric flow rate, m^3/s

$-r_{CO}$ = dimensionless rate of disappearance of CO,

R = recycle ratio

[S] = concentration of empty surface sites, mol/m^2

t = time, s

V = volume of reactor, m^3

X = dimensionless CO concentration, $[CO]/[CO]_o$

Greek Symbols

α_m = ratio of bulk volume to metal surface capacitances, $[CO]_o V/a_m L_m$

θ_{CO} = fractional surface coverage of species CO on the metal surface, $[CO\text{-}S]/L_m$

θ_o = fractional surface coverage of species oxygen on the metal surface, $[O\text{-}S]/L_m$

τ = dimensionless time based on the reactor residence time, Qt/V

8.2 Introduction

There have been many experimental studies of bifurcation behavior in continuous stirred tank reactors (CSTRs) and in recycle reactors (Root and Schmitz, 1969; Hugo and Jakubith, 1972; Cutlip, 1979; Plichta and Schmitz, 1979; Herskowitz and Kenney, 1983). Most of the modeling studies of multiplicity in recycle reactors have made the implicit assumption that the recycle ratio was "high enough" that the reactor could be modeled as a CSTR (Herskowitz and Kenney, 1983; Mukesh *et al.*, 1984). However, apparently no report of the effect of the CSTR assumption on bifurcation behavior has been published. Reilly and Schmitz (1966, 1967), Schmeal and Amundson (1966) and Luss and Amundson (1967) presented numerical studies of recycle reactor multiplicity and stability. Root and Schmitz (1969) were able to predict the effect of recycle ratio on the bifurcation behavior for relatively low values of recycle ratio (experimental recycle ratios less than 2). There are many reports of the effect of recycle ratio on reactor behavior. Gillespie and Carberry (1966a,b) showed that recycle reactor behavior approaches CSTR behavior for recycle ratios of 20 or more. Berty (1979) claimed that the recycle reactor will usually approximate the limit condition of a CSTR at a recycle ratio of about 20 to 25, but cautioned that for high precision measurements, or systems with undiluted reactants, higher recycle ratios are needed. Wedel and Villadsen (1983) showed how the incorrect treatment of recycle reactor data

can lead to the falsification of kinetic parameters, where falsification is defined as the systematic determination of incorrect kinetic parameters, while Broucek (1983) presented simple criteria for estimating the upper limit of falsification that can be tolerated.

In this chapter a theoretical investigation of the effect of recycle ratio on the multiplicity behavior of CO oxidation will be presented. The derivation of the rate function requires the assumption that adsorption-desorption equilibrium exists for the surface species. It has been shown by Lynch (1981) that the equilibrium assumption can lead to incorrect predictions for Langmuir-Hinshelwood models. The effect which making the equilibrium assumption has on the bifurcation behavior will also be studied here.

8.3 Reaction Model

Consider the CO oxidation reaction system, where the desorption of oxygen from the surface is not neglected.

$$CO(g) + S \underset{k_{-1}}{\overset{k_1}{\rightleftharpoons}} CO\text{-}S \tag{8.1}$$

$$O_2(g) + 2\ S \underset{k_{-2}}{\overset{k_2}{\rightleftharpoons}} 2\ O\text{-}S \tag{8.2}$$

$$CO\text{-}S + O\text{-}S \xrightarrow{k_3} CO_2(g) + 2\ S \tag{8.3}$$

If reactions (8.1) and (8.2) are both considered to be at equilibrium, then

$$\theta_{co} = \frac{K_1^*(1-\theta_o)}{(K_1^*+1)} \tag{8.4}$$

$$\theta_o = \frac{K_2^*(1-\theta_{co})}{(K_2^*+1)} \tag{8.5}$$

Substituting Eqn. (8.5) into Eqn. (8.4) gives

$$\theta_{co} = \frac{K_1^*}{(1+K_1^*+K_2^*)} \tag{8.6}$$

Similarly, solving for θ_o gives

$$\theta_o = \frac{K_2^*}{(1+K_1^*+K_2^*)} \tag{8.7}$$

Substituting Eqns. (8.6) and (8.7) into the rate equation for the surface reaction (8.3) gives

$$-r_{co} = K_3\theta_o\theta_{co} = \frac{K_3K_1^*K_2^*}{(1+K_1^*+K_2^*)^2} \tag{8.8}$$

In terms of gas-phase reactant concentrations, Eqn. (8.8) can be rearranged to give

$$-r_{co} = \frac{K_3K_1^\dagger K_2^\dagger[CO][O_2]^{0.5}}{(1+K_1^\dagger[CO]+K_2^\dagger[O_2]^{0.5})^2} \tag{8.9}$$

If oxygen is in excess, so that the oxygen concentration is approximately constant, then Eqn. (8.9) can be rearranged to give

$$-r_{co} = \frac{K_2KX}{(1+KX)^2} \tag{8.10}$$

where

$$K = \frac{K_1^{\dagger}[CO]_o}{(1+K_2^{\dagger}[O_2]_0^{0.5})} \tag{8.11}$$

and

$$K_2 = \frac{K_3K_2^{\dagger}[O_2]_0^{0.5}}{(1+K_2^{\dagger}[O_2]_0^{0.5})} \tag{8.12}$$

Equation (8.10) is mathematically similar to one presented by Voltz *et al.* (1973), who, in an investigation of carbon monoxide and propylene oxidation on a platinum-alumina catalyst, found that the rate of CO oxidation could be written as:

$$r_{CO} = \frac{k_{r1}[O_2][CO]}{(1+k_{a1}[CO])^2} \tag{8.13}$$

If oxygen is in excess, so that the oxygen concentration is approximately constant, then the form of Eqn. (8.13) reduces to that of Eqn. (8.10).

Equation (8.10) is also similar in form to one presented for ethylene hydrogenation by Matsuura and Kato (1967) in an investigation of multiplicity in a CSTR. Their original rate expression was:

$$-r_{C_2H_4} = \frac{k[H_2][C_2H_4]}{(1+K[C_2H_4])^2} \tag{8.14}$$

If is assumed that hydrogen is in excess, then Eqn. (8.14) reduces to the form of Eqn. (8.11).

8.4 Bifurcation Behavior in a CSTR with Equilibrium

When Eqn. (8.10) is inserted into the design equation for a CSTR the following equation results:

$$\frac{dX}{d\tau} = 1 - X - \frac{K_2KX}{(1+KX)^2} \tag{8.15}$$

To solve for the steady-state solutions, the left-hand side of Eqn. (8.15) is set to zero, giving a cubic equation:

$$-K^2X^3 + (K^2 - 2K)X^2 + (2K - K_2K - 1)X + 1 = 0 \tag{8.16}$$

Solutions of Eqn. (8.16), plotted as conversion (1-X), are shown as functions of K for several values of K_2K in Figure 8.1. For values of K_2K less than 27, there is only one solution for each value of K, but for K_2K greater than 27 there is a range of K for which three solutions exist. The bifurcation points from one steady-state solution to three steady-state solutions must satisfy Eqn. (8.16) and the further condition that

$$\frac{dK}{dX} = 0 \tag{8.17}$$

Differentiating Eqn. (8.16) and setting the derivative to zero gives

$$-3K^2X^2 + (2K^2 - 4K)X + (2K - K_2K - 1) = 0 \tag{8.18}$$

Eliminating K_2 between Eqns. (8.16) and (8.18) gives

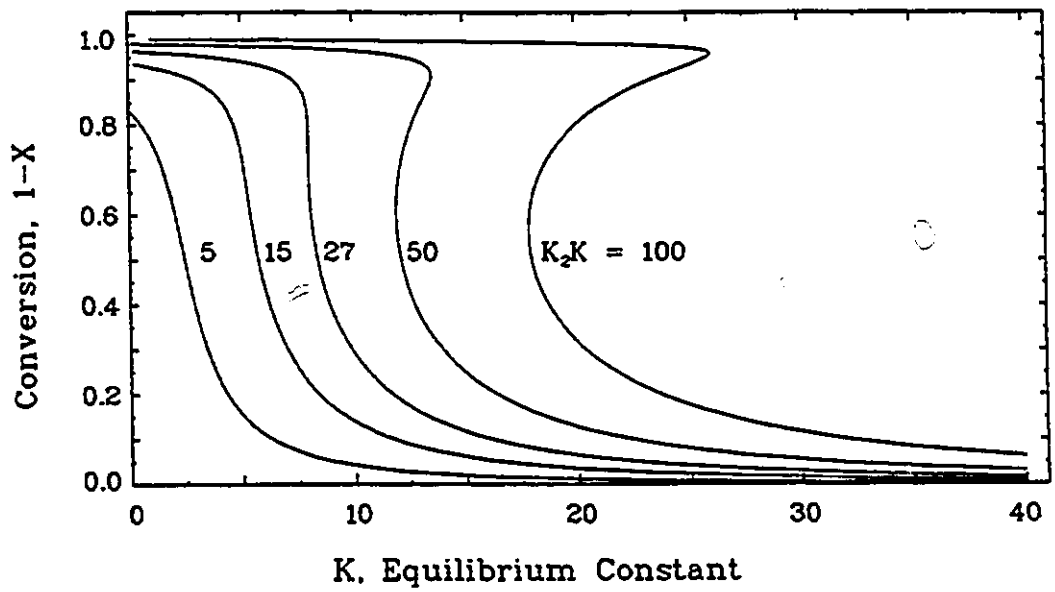

Figure 8.1 Multiplicity Behavior in a CSTR with Equilibrium

$$2K^2X^3 + (2K - K^2)X^2 + 1 = 0 \tag{8.19}$$

which has solutions of

$$X = -\frac{1}{K} \tag{8.20a}$$

and

$$X = 0.25 \pm 0.25\sqrt{1 - 8/K} \tag{8.20b}$$

Equation (8.20a) is a physically unrealizable solution (X is constrained between zero and unity). Equation (8.20b) has real solutions, between zero and unity, for $K \geq 8$. Thus, by substituting Eqns. (8.20b) into either Eqn. (8.16) or (8.18), the loci of bifurcation points can be determined in

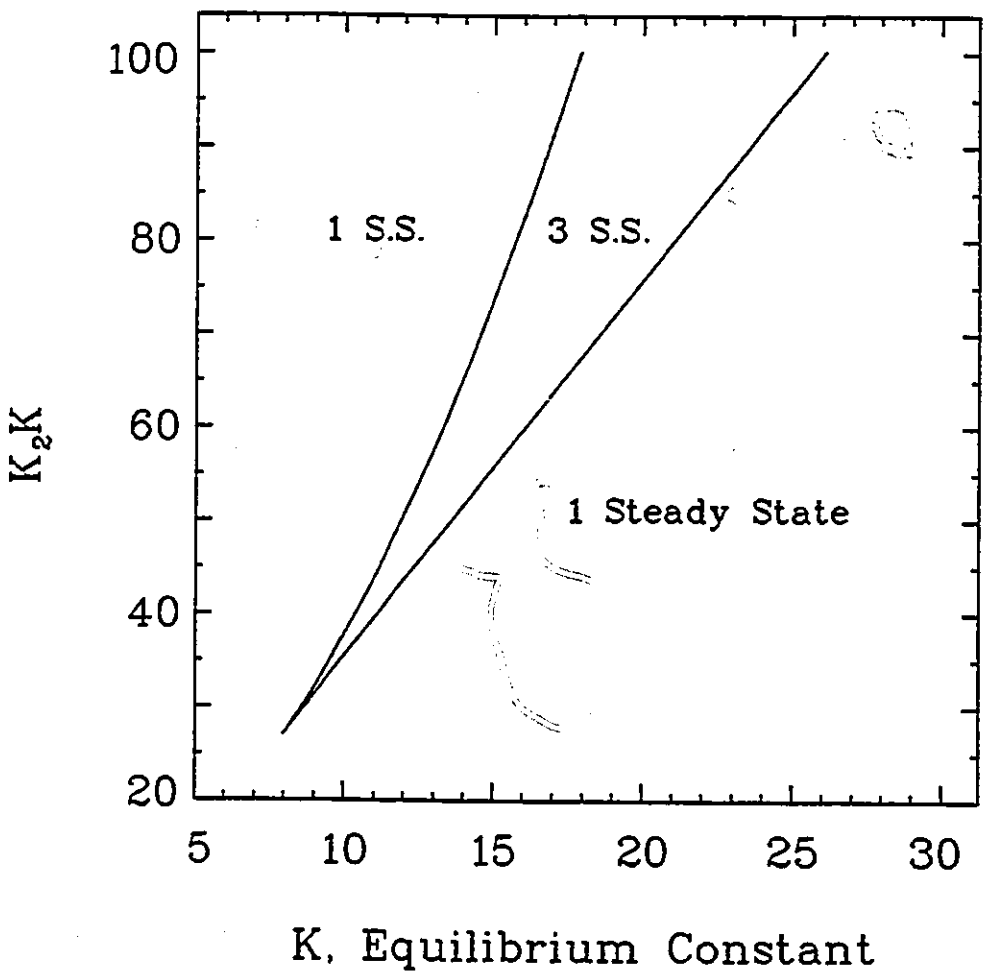

Figure 8.2 Bifurcation Behavior in a CSTR with Equilibrium

terms of K and K_2K. These were originally reported by Matsuura and Kato (1967). The multiplicity region is plotted on a K-K_2K diagram in Figure 8.2. There are three steady states (two stable, one unstable) inside the cusp-shaped region, and one stable steady state elsewhere. The conversion of A to B is higher to the left of the multiplicity region in Figure 8.2 (low values of K) than to the

right of the multiplicity region.

To interpret the bifurcation diagram in terms of CO oxidation, the K_2K axis can be thought of as a scaled oxygen feed concentration while the K axis can be thought of as a scaled carbon monoxide feed concentration. Thus, for CO oxidation, there are high-conversion steady states predicted for low CO feed concentrations, and low-conversion steady states predicted for high CO feed concentrations. This behavior is in qualitative agreement with the experimental data presented in Chapter 5.

8.5 Recycle Reactor Bifurcation Behavior (CO Adsorption at Equilibrium)

Modeling studies of bifurcation behavior in recycle reactors have often assumed that the recycle ratio is high enough to allow the reactor to be treated mathematically as a CSTR (Mukesh *et al.*, 1984). It is usually assumed that a recycle ratio of 20 or more is "high enough". To test the validity of this assumption the reaction rate function described above (Eqn. (8.10)) was used to determine the effect of recycle ratio on the location of the bifurcation points.

Consider the same reaction system as above (Eqns. (8.1)-(8.3)) with adsorption-desorption equilibrium in a recycle reactor. The rate function is again given by Eqn. (8.10), but the reactor design equation is now for a recycle reactor:

$$\frac{1}{(R+1)} = \int_{\frac{RX+1}{R+1}}^{X} \frac{dX}{-r_{co}} \tag{8.21}$$

Substituting Eqn. (8.10) for the r_{co} term in Eqn. (8.21) gives

$$\frac{1}{(R+1)} = -\int_{\frac{RX+1}{R+1}}^{X} \frac{(1+KX)^2 dX}{K_2 KX} \tag{8.22}$$

Integrating yields

$$\frac{K_2 K}{(R+1)} = -\left[\ln(X) + 2KX + \frac{K^2X^2}{2}\right]_{\frac{RX+1}{R+1}}^{X} \tag{8.23}$$

Evaluating this expression and rearranging gives

$$\frac{K_2 K}{(R+1)} = -\ln\left[\frac{(R+1)X}{RX+1}\right] + \frac{(2+K)K}{(R+1)}(1-X) - \frac{K^2(2R+1)}{2(R+1)^2}(1-X)^2 \tag{8.24}$$

The boundary of the multiplicity region will satisfy Eqns. (8.24) and (8.17). These equations were solved using homotopy-continuation methods as in Chapter 5, and the resulting cusps of multiplicity are shown in Figure 8.3 for recycle ratios of 1, 2, 10, and ∞ (limiting case of CSTR). It is seen that, for recycle ratios of 10 or greater, there is little change in the location of bifurcation points when compared to the CSTR case. For smaller values of recycle ratio, however, the bifurcation points move to lower values of K. This effect is shown more clearly in Figure 8.4, where the value of K at the bifurcation points is plotted against recycle ratio for two values of K_2. For comparison

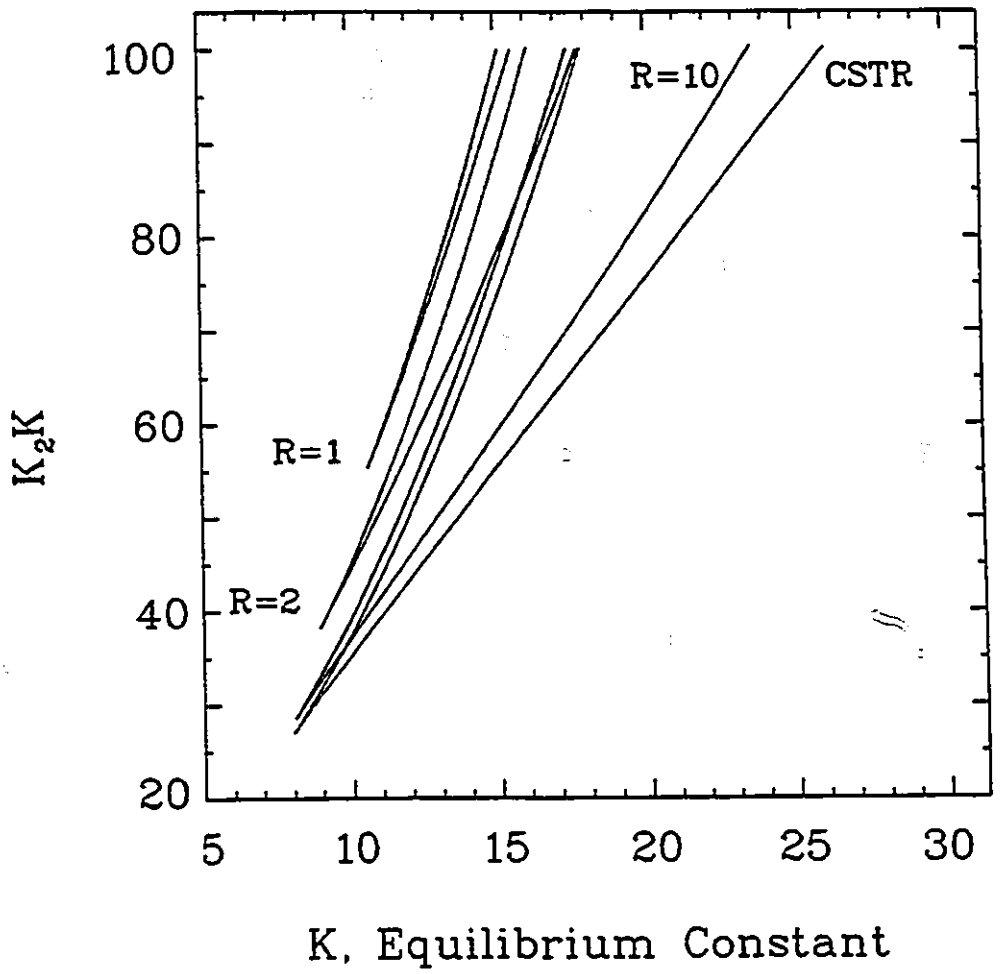

Figure 8.3 Recycle Reactor Bifurcation Behavior (Step 1 and 2 at Equilibrium)

the CSTR bifurcation points are shown on the right-hand axis of Figure 8.4. The low-to-high bifurcation point is less sensitive to recycle ratio than is the high-to-low bifurcation point. This is because the conversion at the low-to-high bifurcation point is less than that at the high-to-low bifurcation point. (High-conversion processes are affected more strongly by recycle ratio than are

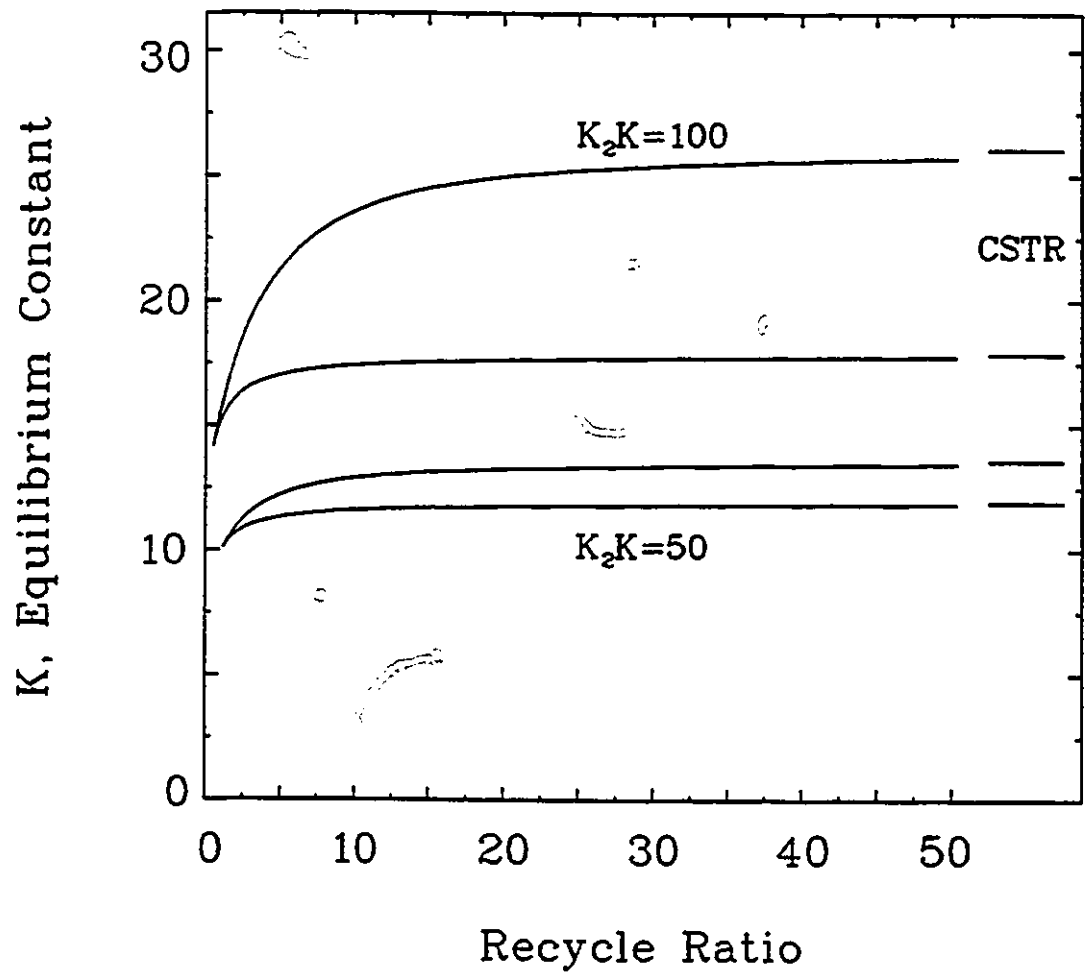

Figure 8.4 Effect of Recycle Ratio on Bifurcation Behavior: Equilibrium Assumption

low-conversion processes.) The low-to-high bifurcation points are within 5% of the CSTR values at a recycle ratio greater than 5 both for K_2K=50 and for K_2K=100. The high-to-low bifurcation points, which are at higher conversions and are thus more strongly influenced by the recycle ratio than are the low-to-high bifurcation points, are within 5% of the CSTR values for recycle ratios greater than

10 for $K_2K=50$, and for recycle ratios greater than 18 for $K_2K=100$.

Due to the dimensionalization that was used, the ordinate value is proportional to the product of the CO adsorption equilibrium constant $K_1^\dagger$ and the feed concentration $[CO]_o$. If the bifurcation behavior of an experimental system is being used to determine the kinetic parameters, the true value of $K_1^\dagger$ would not be known. Typically, to determine the rate constants, the value of $[CO]_o$ at the bifurcation points would be determined. The ratio of the CO feed concentrations at the high and low bifurcation points would then be used to determine K and K_2. For a CSTR, these ratios are shown as a function of K_2K in Figure 8.5. It is seen that for a CSTR the ratio is a monotonically decreasing function and thus can be used to uniquely determine the value of K_2K. The value of K can be determined in a similar manner from the bifurcation point ratio. If bifurcation data from a recycle reactor are treated as if they were from a CSTR, then the experimentally determined values of K and K_2 would not be the true values of K and K_2. The ratio of CO feed concentrations at the high and low bifurcation points for the finite recycle ratios shown in Figure 8.3 (i.e., 1, 2, and 10) are shown in Figure 8.5. These bifurcation point ratios were used to determine the apparent rate constants. A 'falsification ratio', defined as the ratio of the apparent rate constant to the true rate constant, can be

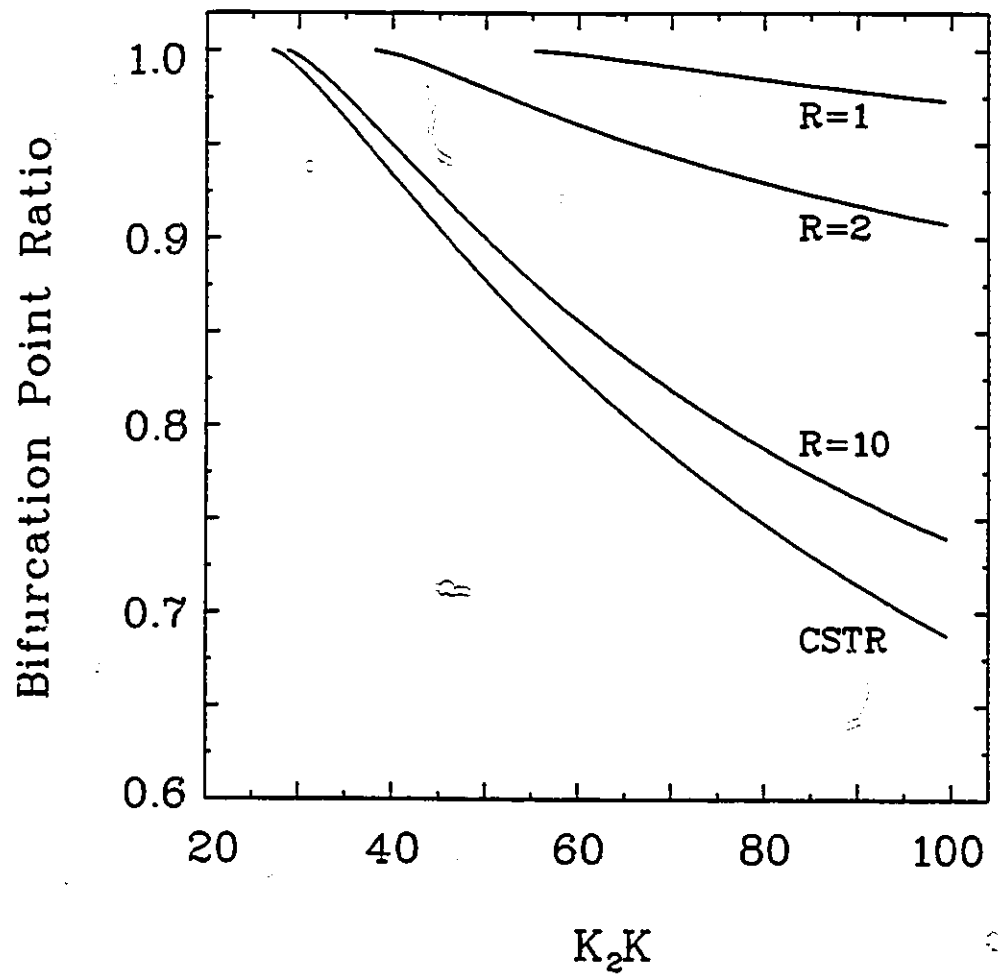

Figure 8.5 Ratio of Bifurcation Points

determined for both K and K_2K. The falsification ratio for K_2 at the three finite recycle ratios shown in Figure 8.3 are shown as functions of K_2 in Figure 8.6. There is greater falsification (the falsification ratio is further from unity) for small values of recycle ratio than for large values of recycle ratio. Similarly, there is greater falsification for large values of K_2 than for small values

of K_2.

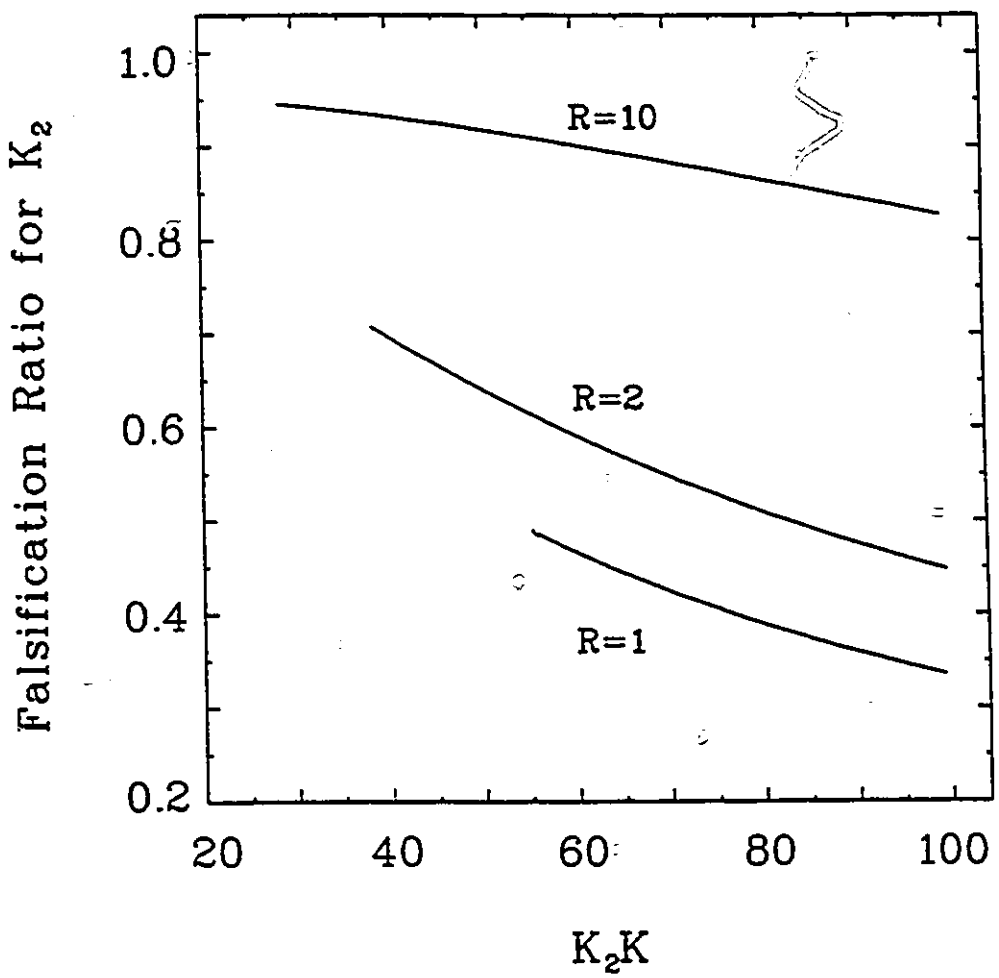

Figure 8.6 Falsification of Surface Rate Constant

The falsification ratio is shown as a function of the recycle ratio in Figure 8.7 for K_2K = 50 and K_2K = 100. For large values of recycle ratio, the falsification ratio is close to unity, indicating that the experimentally determined rate parameters are close to their true values. For small recycle ratios, the falsification ratio is much less than unity, indicating that the experimentally determined rate parameters are much less than the true values. The

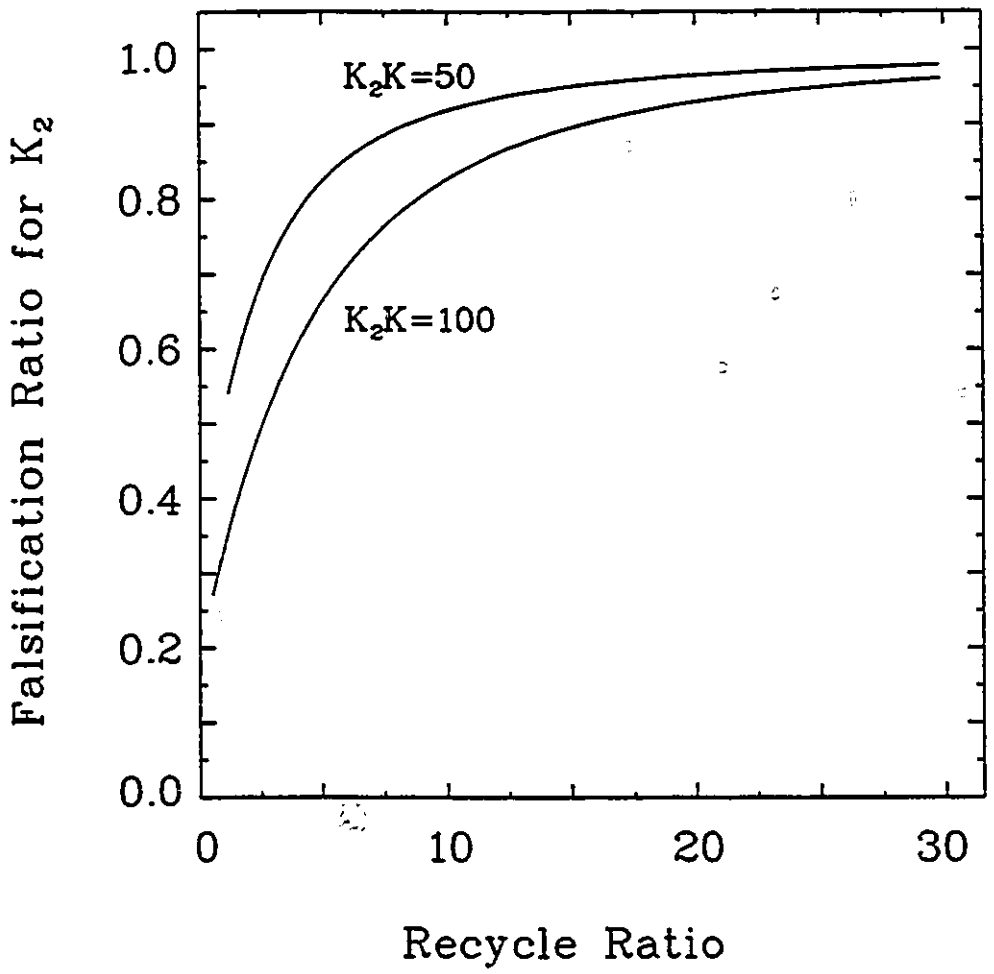

Figure 8.7 Effect of Recycle Ratio on Falsification of Surface Rate Constant

higher the true value of K_2, the greater the potential falsification of rate parameters. This is because higher values of K_2 have higher conversions at the bifurcation points and, as mentioned above, high conversion processes are affected more strongly than low conversion processes by recycle ratio. Thus, high values of K_2 lead to a greater falsification of the rate parameters.

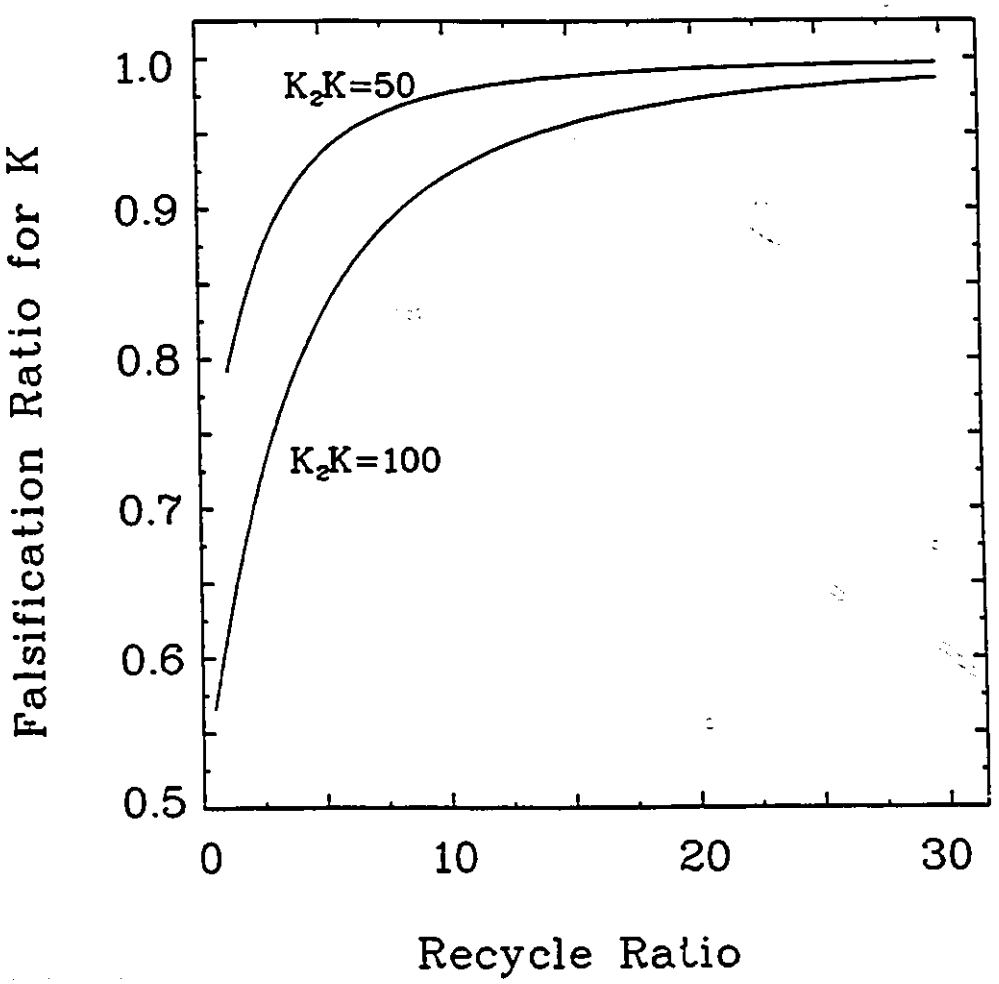

Figure 8.8 Effect of Recycle Ratio on Falsification of Equilibrium Constant

In Figure 8.8 the falsification ratio for K is shown as a function of recycle ratio. The behavior shown in Figure 8.8 is similar to what is shown in Figure 8.7 for falsification of K_2, except the falsification ratios are slightly closer to unity in Figure 8.8.

This study shows that if experimental bifurcation behavior is used to determine kinetic parameters, then

significant error can occur if a recycle reactor, even one with a large recycle ratio, is treated as a CSTR. Thus, the validity of the CSTR approximation cannot be established *a priori* by the existence of a large value for the recycle ratio, but instead must be verified after the kinetic parameters have been determined.

As a final examination of kinetic falsification in recycle reactors, the equation developed in Chapter 5 for CO oxidation (Eqn. (5.41)) was studied. The conversions predicted by Eqn. (5.41) are much higher (99.8% for Case I conditions with 0.5% O_2) than predicted by Eqn. (8.10) (96% for K_2K = 100) and therefore the parameters in Eqn. (5.41) should be more susceptible to falsification by low recycle ratios. To determine the falsification ratio the surface reaction rate constant, K_3, was adjusted to keep the recycle reactor high-to-low (upper) bifurcation point (for 0.5% O_2 and Case I conditions) at its experimental value. The CSTR and recycle-reactor rate constants were then compared to give the falsification ratio, which is plotted in Figure 8.9. As shown in Figure 8.9, the parameter falsification is significant even at recycle ratios as high as 1000. The experimental conversions at the high-to-low bifurcation points measured in Chapter 5 were typically about 99.9%, nearly the same as the 99.8% conversion predicted using Eqn. (5.41) (exact determination of the conversion was made difficult by the precision of the IR and the long times required to reach a true steady-state). For

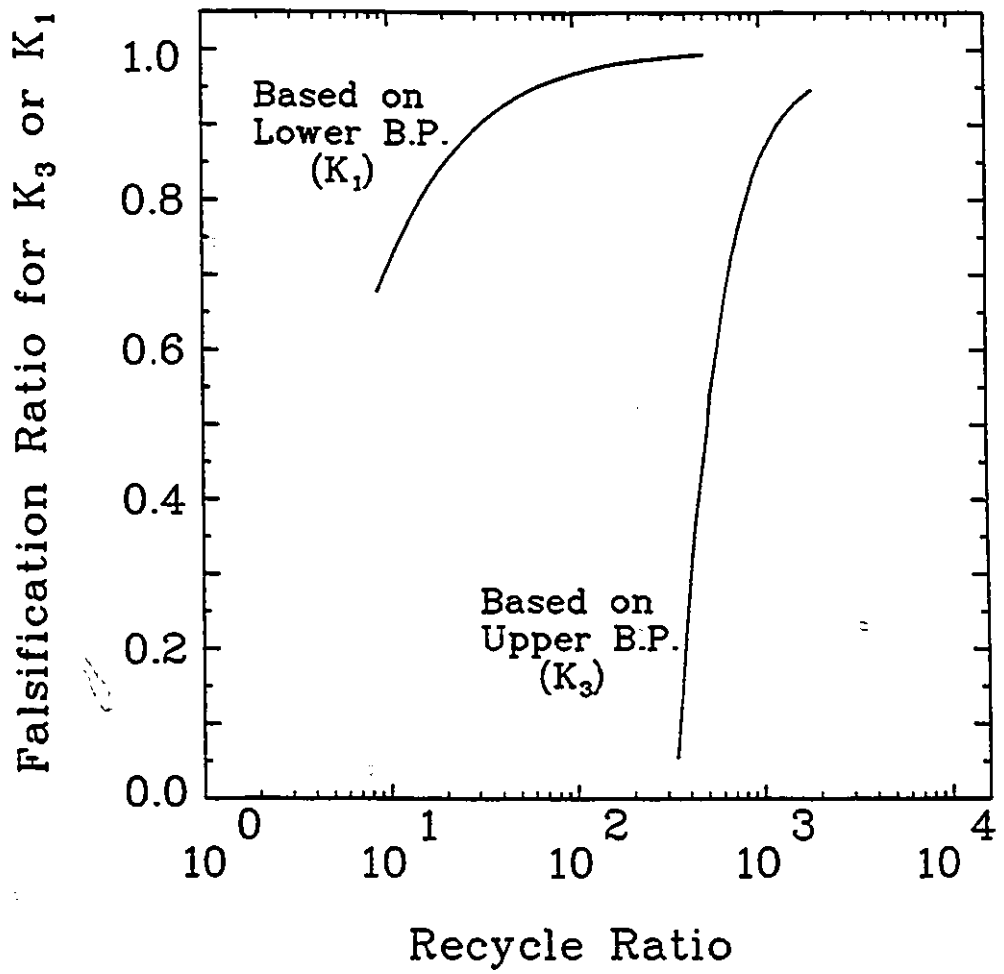

Figure 8.9 Effect of Recycle Ratio on Falsification of Surface Rate Constant

Case I operating conditions the recycle ratio was approximately 100. Thus, there could be significant falsification in the value of K_3 determined from the steady-state bifurcation behavior in Chapter 5. However, even with this potential falsification the model was able to describe the high to low bifurcation point data very well (the model predictions were not very sensitive to the value of K_3, which

could vary as much as 20% while the model predictions remained in the 95% confidence interval).

In Chapter 5 a major problem in fitting models to the data was that the effect of flow rate on the experimental low to high bifurcation point was greater than could be predicted by most kinetic models. Shown in Figure 8.9 is the falsification of $K_{\approx}$ associated with the Case I conditions, 0.5% O_2 feed, caused by treating the reactor as a CSTR. There is much less falsification associated with the lower bifurcation point than with the upper bifurcation point. For the Case I recycle ratio of 100, the falsification shown in Figure 8.9 is 0.97. Thus, the finite experimental recycle ratio is not responsible for the problems associated with matching the effect of flow rate on the low to high bifurcation point.

8.6 Bifurcation Behavior in a CSTR without Equilibrium

A number of recent studies (for example, Lynch, 1981; Mukesh *et al.*, 1984)) have shown that only elementary-step models should be used for modeling the dynamic behavior of CO oxidation; that is, no assumptions should be made concerning the rate determining step and/or equilibrium between the rates of adsorption and desorption. In sections 8.2-8.5 the model reaction was examined assuming equilibrium existed between the adsorption and desorption steps. In this section the effect of the CO equilibrium assumption on bifurcation behavior will be addressed.

If no assumption is made concerning equilibrium for CO adsorption and desorption (step (8.1)), then the surface concentration of CO must be taken into consideration. For the purposes of this derivation, oxygen adsorption-desorption equilibrium will be assumed. Thus, Eqn. (8.5) can still be used to describe the oxygen surface coverage. If the reaction is assumed to take place in a CSTR, then the equations which describe the reaction are:

$$\frac{dX}{d\tau} = 1 - X - K_1X(1-\theta_{CO}-\theta_O) + K_{-1}\theta_{CO} \tag{8.25}$$

$$\frac{d\theta_{CO}}{d\tau} = \alpha_m\{K_1X(1-\theta_{CO}-\theta_O) - K_{-1}\theta_{CO} - K_3\theta_{CO}\theta_O)\} \tag{8.26}$$

To solve for the steady-state solutions of Eqns. (8.25) and (8.26), the left-hand sides are set to zero.
Equation (8.26) can be solved for the surface concentration to give

$$\theta_{CO} = \frac{(K_2 + K_{-1} + K^*X) \pm \sqrt{(K_2 + K_{-1} + K^*X)^2 - 4K^*K_2X}}{2K_2} \tag{8.27}$$

where $K^* = K_1/(K_2^* + 1)$. Because θ_{CO} is constrained between zero and unity, only the negative square root solution of Eqn. (8.27) is feasible. At steady state, Eqn. (8.25) yields

$$X = \frac{(1 + K_{-1}\theta_{CO})}{(1 + K^* - K^*\theta_{CO})} \tag{8.28}$$

Equations (8.27) and (8.28) were solved using homotopy-continuation methods to determine the multiplicity behavior.

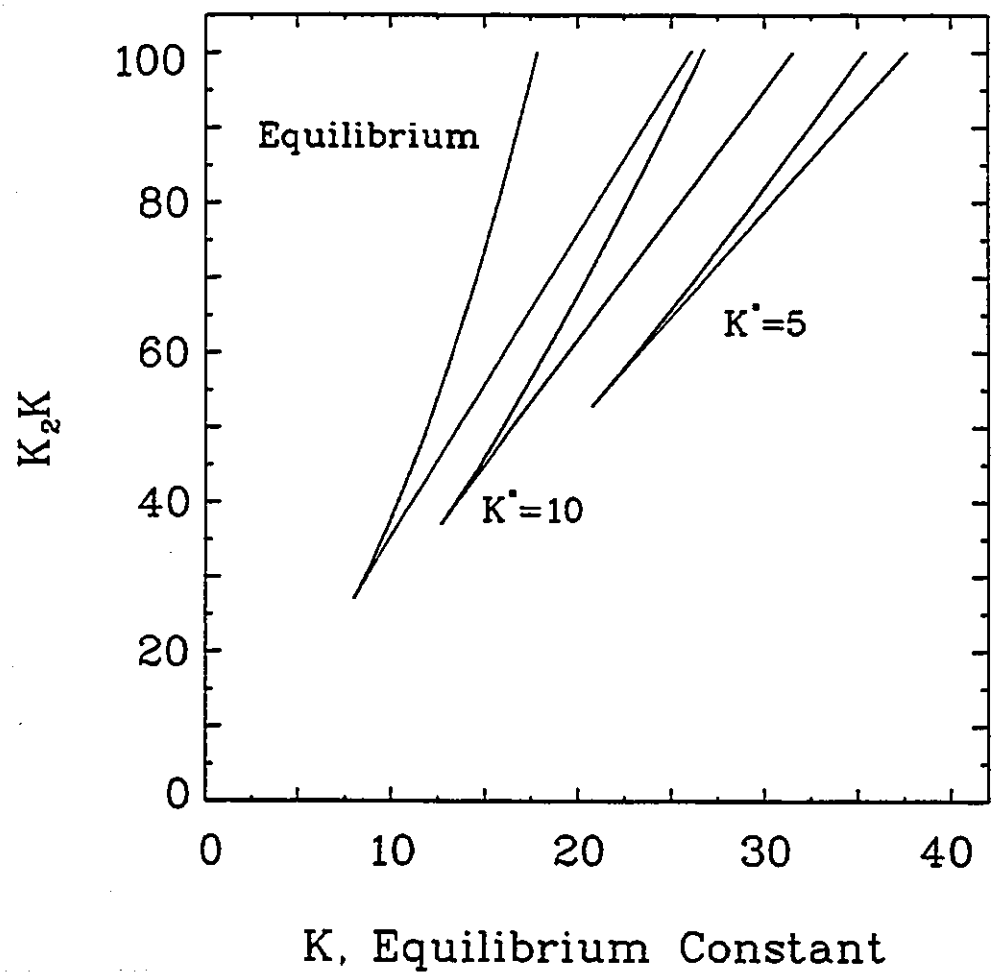

Figure 8.10 Bifurcation Behavior in a CSTR without Equilibrium

As in section 8.5, the multiplicity behavior can be represented as a family of cusps on a K-K_2K plot. This is shown in Figure 8.10. The parameter determining the cusp is K^*, a group proportional to the adsorption rate constant. As K^* approaches infinity, the cusp approaches the multiplicity cusp for the equilibrium assumption case discussed in section 8.4. This is shown more clearly in Figure 8.11 where

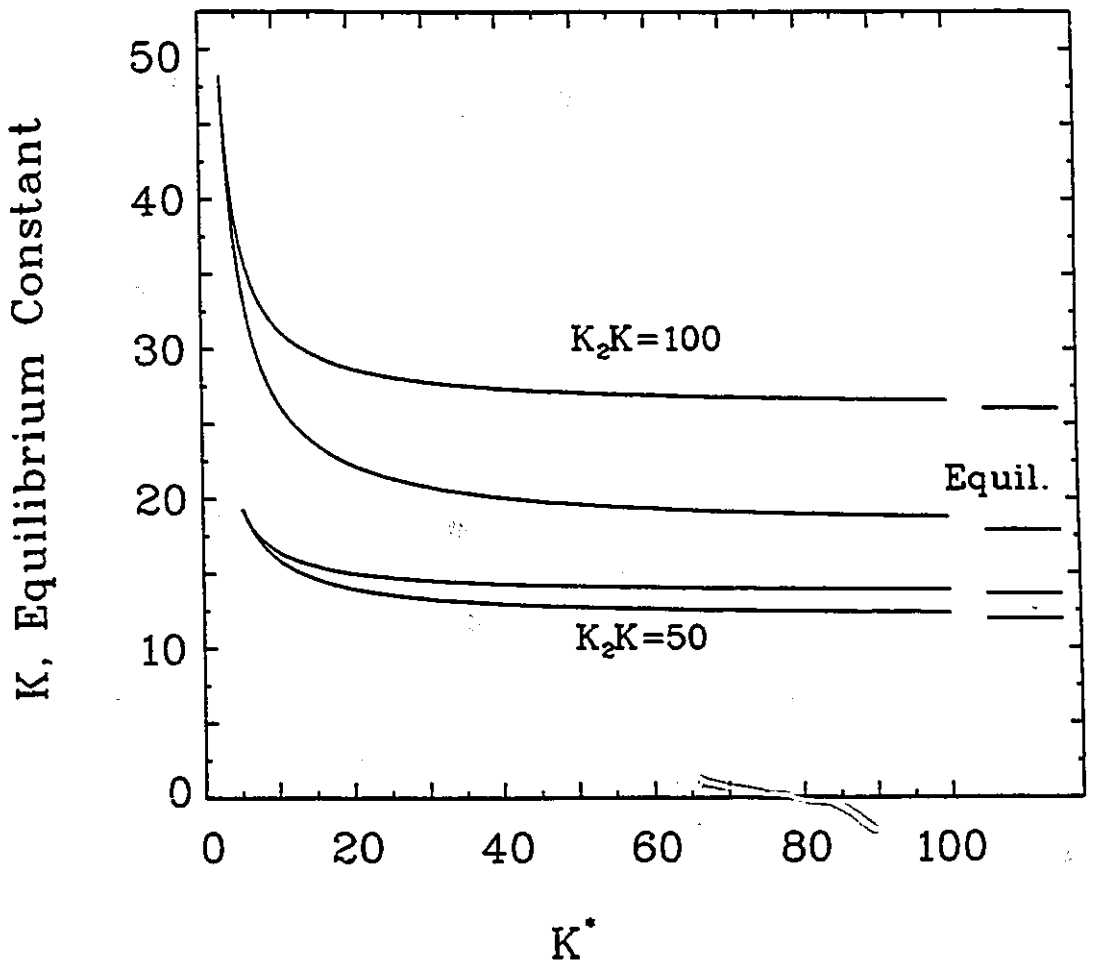

Figure 8.11 Effect of Equilibrium Assumption on Bifurcation Behavior in a CSTR

the upper and lower bifurcation points are plotted as a function of K^* for two different values of K_2K. The bifurcation points for the adsorption-desorption equilibrium case are shown at the right-hand axis. For small values of K^* the locations of the bifurcation points can increase by more than 100%.

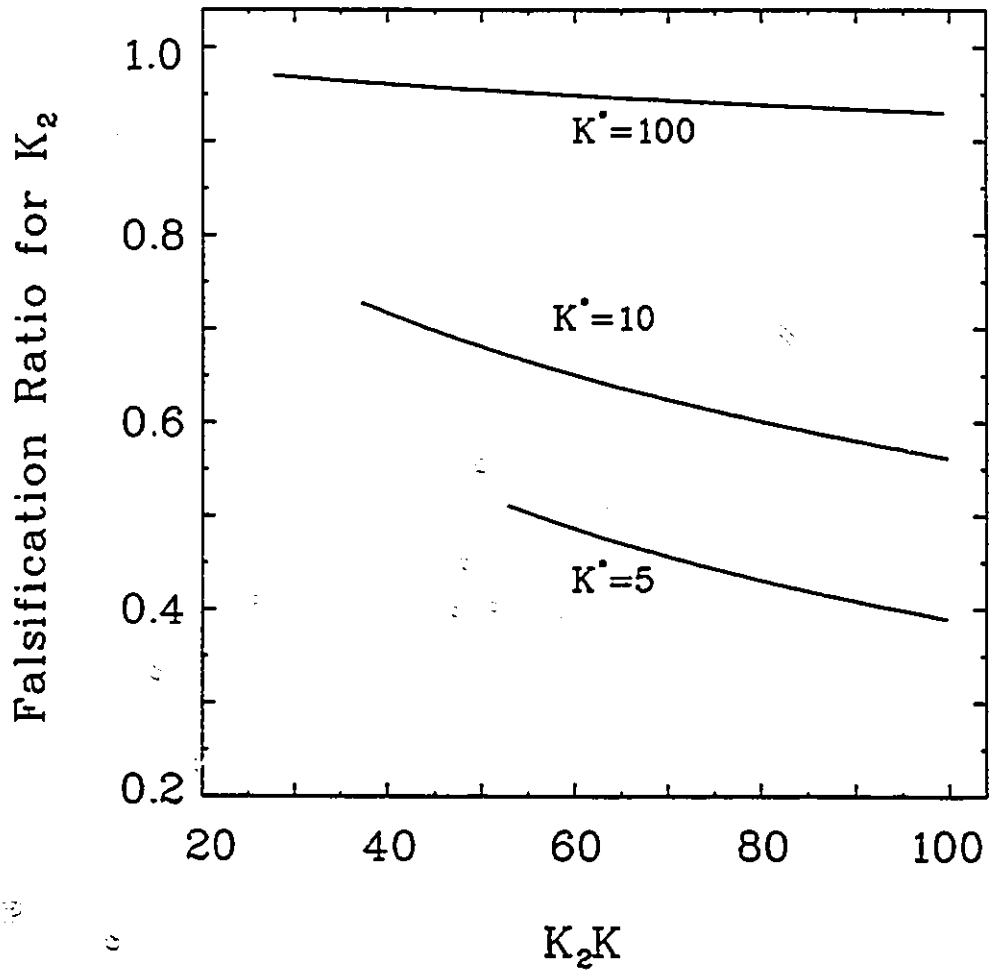

Figure 8.12 Falsification of Surface Rate Constant

The ratios of bifurcation points were determined and these were used to determine falsification ratios. The falsification ratio for K_2 is shown as a function of K_2K for fixed values of K^* in Figure 8.12, and as a function of K^* for fixed values of K_2K in Figure 8.13. The falsification ratio for $K_1^\dagger$ is shown as a function of K^* for fixed values of K_2K in Figure 8.14. For fixed K^* the falsification ratio

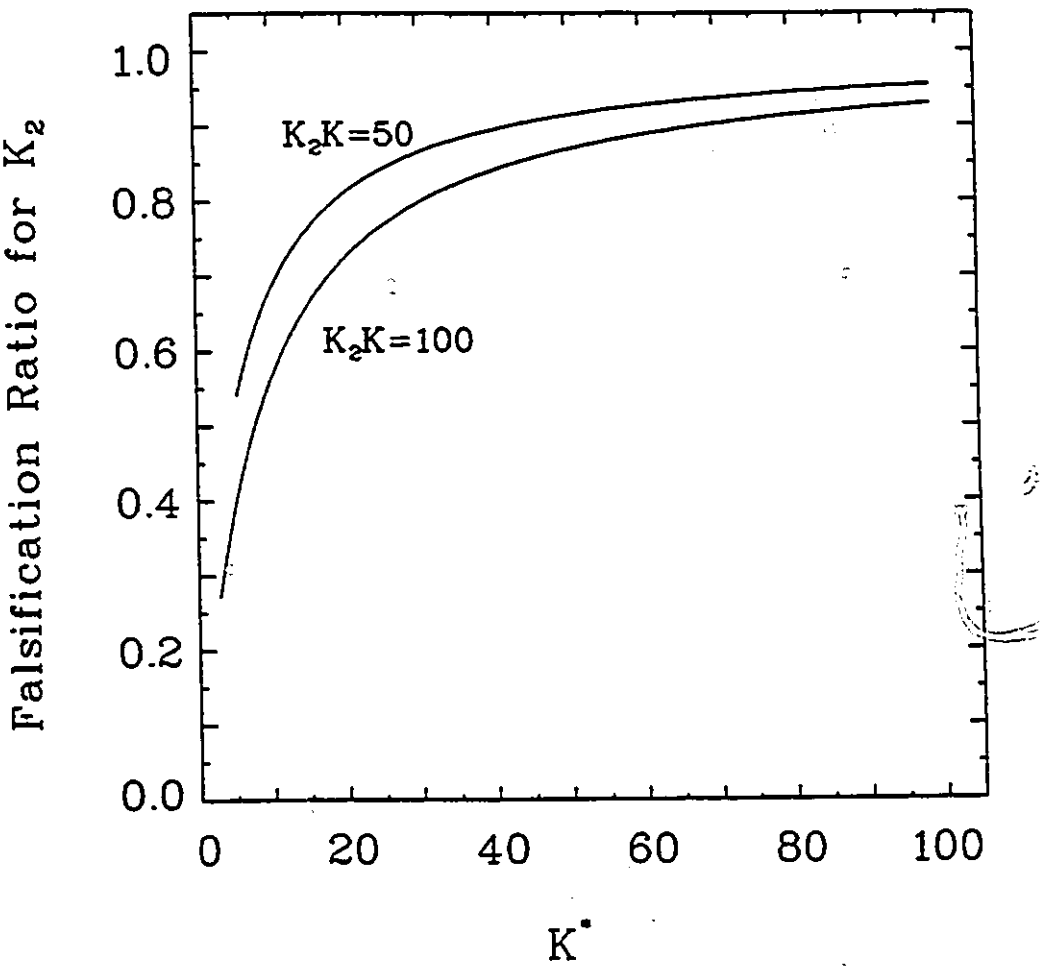

Figure 8.13 Effect of Equilibrium Assumption on Falsification of Surface Rate Constant

is relatively constant. However, as shown in Figures 8.13 and 8.14, for low values of K^* the falsification ratios for both K_2 and $K_1^\dagger$ become much smaller than unity.

Thus it is seen that, when using multiplicity behavior to determine rate constants, assumptions of adsorption-desorption equilibrium should not be made or significant error can result in the rate constant values. When modeling

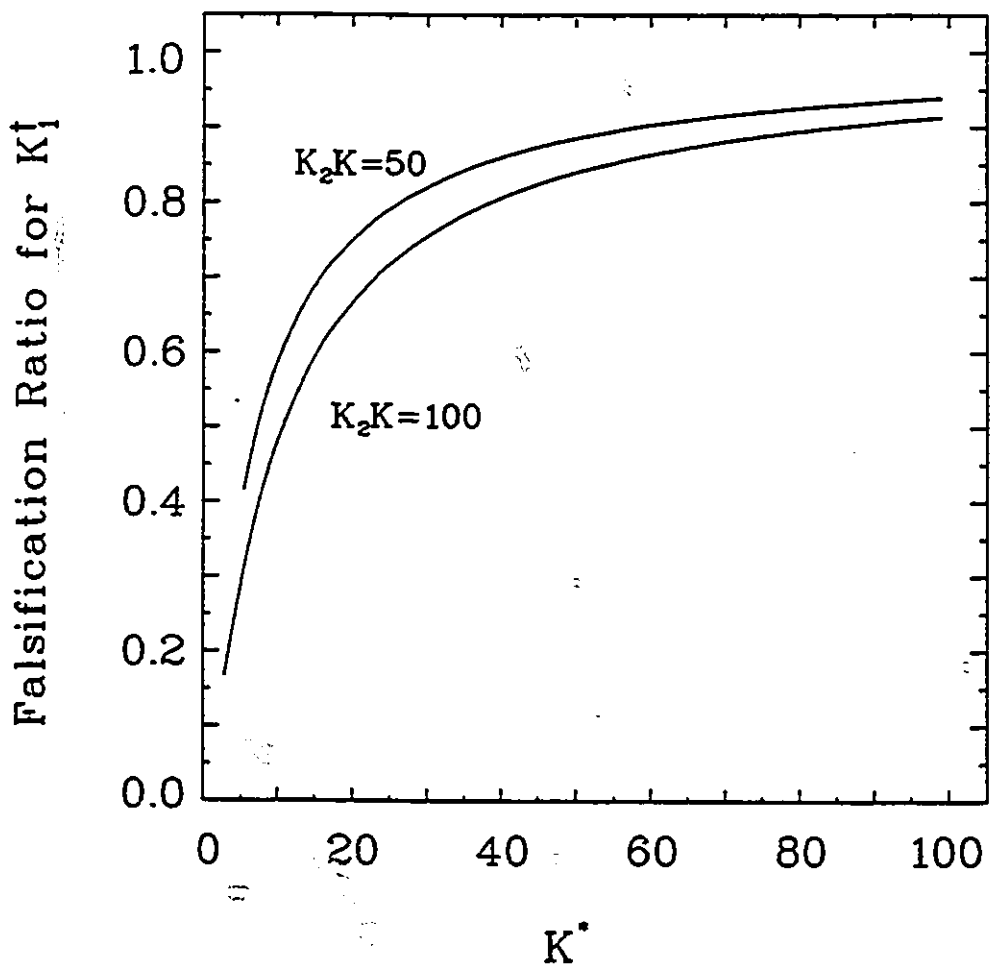

Figure 8.14 Effect of Equilibrium Assumption on Falsification of Equilibrium Constant

multiplicity behavior, it is better to use an elementary-step model to determine the kinetic parameters. After determining the parameters, it may be possible to use an equilibrium model to describe the results, but an equilibrium model should not be used *a priori* or falsification of parameters may occur.

8.7 References

Berty, J. M., "Testing Commercial Catalysts in Recycle Reactors", Catal. Rev.-Sci. Eng. 20, 75-96 (1979).

Broucek, R., "Falsification of Kinetic Parameters by Incorrect Treatment of Recirculation Reactor Data", Chem. Eng. Sci. 38, 1349-1350 (1983).

Cutlip, M. B., "Concentration Forcing of Catalytic Surface Rate Processes, Part 1. Isothermal Carbon Monoxide Oxidation Over Supported Platinum", AIChE J. 25, 502-508 (1979).

Gillespie, B. M., and J. J. Carberry, "Influence of Mixing on Isothermal Reactor Yield and Adiabatic Reactor Conversion", Ind. Eng. Chem. Fund. 5, 165-171 (1966a).

Gillespie, B. M., and J. J. Carberry, "Reactor Yield at Intermediate Mixing Levels - An Extension of Van de Vusse's Analysis", Chem. Eng. Sci. 21, 472-475 (1966b).

Herskowitz, H., and C. N. Kenney, "CO Oxidation on Pt Supported Catalysts. Kinetics and Multiple Steady States", Can. J. Chem. Eng. 61, 194-199 (1983).

Luss, D., and N. R. Amundson, "Stability of Loop Reactors", AIChE J. 13, 279-290 (1967).

Lynch, D. T., "Oscillatory Behavior in Catalytic Reactions: A Mathematical and Experimental Investigation", Ph.D. Thesis, University of Alberta (1981).

Matsuura, T., and M. Kato, "Concentration Stability of the Isothermal Reactor", Chem. Eng. Sci. 22, 171-184 (1967).

Mukesh, D., W. Morton, C. N. Kenney, and M. B. Cutlip,

"Island Models and the Catalytic Oxidation of Carbon Monoxide and Carbon Monoxide-Olefin Mixtures", Surface Sci. 138, 237-257 (1984).

Plichta, R. T., and R. A. Schmitz, "Oscillations in the Oxidation of Carbon Monoxide on a Platinum Foil", Chem. Eng. Commun. 3, 387-398 (1979).

Reilly, M. J., and R. A. Schmitz, "Dynamics of a Tubular Reactor with Recycle: Part I. Stability of the Steady State", AIChE J. 12, 153-161 (1966).

Reilly, M. J., and R. A. Schmitz, "Dynamics of a Tubular Reactor with Recycle: Part II. Nature of the Transient State", AIChE J. 13, 519-527 (1967).

Root, R. B., and R. A. Schmitz, "An Experimental Study of Steady State Multiplicity in a Loop Reactor", AIChE J. 15, 670-679 (1969).

Schmeal, W. R., and N. R. Amundson, "The Effect of Recycle on a Linear Reactor", AIChE J. 12, 1202-1211 (1966).

Voltz, S. E., C. R. Morgan, D. Liederman, and S. M. Jacob, "Kinetic Study of Carbon Monoxide and Propylene Oxidation on Platinum Catalysts", Ind. Eng. Chem. Prod. Res. Dev. 12, 294-301 (1973).

Wedel, S., and J. Villadsen, "Falsification of Kinetic Parameters by Incorrect Treatment of Recirculation Reactor Data", Chem. Eng. Sci. 38, 1346-1349, (1983).

9. Summary and Recommendations

In the previous chapters, two major subjects have been investigated. The first of these is CO oxidation on platinum catalysts. The second is reaction rate enhancement by operation of a catalytic reactor in a cyclic manner. In this chapter a brief summary of both of these topics will be presented. The summary will be followed by some recommendations for further work on these subjects.

9.1 CO Oxidation

CO oxidation on platinum catalysts has been the subject of many investigations. Numerous reports of complex behavior: multiplicity, oscillations, chaos, and resonance during feed cycling - have provided a wealth of information. Although much knowledge has been gained about this important reaction, there is still a lack of understanding of the basic mechanisms by which CO oxidation occurs. Many mechanisms have been proposed to explain the behavior, but none has yet successfully described all of the types of complex behavior. It was a goal of this work to develop a mechanism which could describe many of the complex phenomena.

The initial experiments determined the steady-state multiplicity behavior for CO oxidation on a supported platinum catalyst in a recycle reactor. Five kinetic models were evaluated by using the steady-state data to estimate kinetic parameters. The bifurcation cusps were described equally well by all five models, except for the effect of flow rate

on the low-conversion to high-conversion bifurcation points. In describing the effect of flow rate on the low-conversion to high-conversion bifurcation points, three models (standard Langmuir-Hinshelwood, standard surface island, and surface oxide) showed a dependence on the 0.33 power of flow rate, one model (modified surface island model) predicted an inverse dependence on the square root of flow rate, and only one model (the CO self-exclusion model) could describe the experimental dependence on the -0.67 power of flow rate. It was shown mathematically that the first four models could not describe the experimental dependence on flow rate, and that the CO self-exclusion model could describe the data. Based on the steady-state bifurcation modeling results, the CO self-exclusion model was selected as the basis for further modeling work. Because of the inability of the other four models to successfully describe the steady-state data, they were dropped from further consideration as models which could describe the behavior of CO oxidation on platinum catalysts.

Feed composition cycling experiments were then carried out and the predictions of the CO self-exclusion model were compared with the data. It was found that the CO self-exclusion model could not adequately describe the time-average conversion data if the model parameters were chosen to fit the steady-state bifurcation behavior. The CO self-exclusion model could not describe the high time-average conversions observed at high cycling frequencies. It was

also found that the standard Langmuir-Hinshelwood model, when forced to fit the steady-state bifurcation behavior, could not describe the dynamic behavior. The LH model produced poorer predictions of the time-average conversion behavior than did the CO self-exclusion model. To improve the CO self-exclusion model predictions, it was combined with the surface-phase transition model. The surface-phase transition model has been used by Lynch *et al.* (1986) to describe, in detail, the oscillatory behavior of CO oxidation on noble metal catalysts. By choosing to combine the CO self-exclusion model with the phase transition model, the resulting model would already be capable of describing steady-state multiplicity and self-sustained oscillations. Thus, if the new model could describe the behavior of CO oxidation during feed composition cycling, a comprehensive model of CO oxidation would result. The new model, which incorporated surface-phase transition into the CO self-exclusion model, was capable of describing the time-average conversion behavior, although the predictions for small oxygen lead phase angles were not quite right. When adsorption and desorption of CO_2 on the alumina support were added to the model, it was also able to describe most of the elements of transient behavior displayed by the experimental system. Thus, the new model seems to be a comprehensive model of CO oxidation on supported platinum catalysts, that is, it is capable of describing most of the patterns of behavior which have been observed for CO oxidation.

An interesting prediction made by the new model is that, for small amounts of catalyst, the high-to-low and the low-to-high bifurcation lines should cross. An experiment designed to find the cross-over point failed to do so conclusively, but the experiment was compromised by changing catalyst activity. The data do not rule out the possibility of the existence of the cross-over, and some of the data indicate that the cross-over was found. Further experiments, with a more stable catalyst, should be performed to search for the cross-over. The discovery of a cross-over between the high-to-low and the low-to-high bifurcation lines would provide important support of the model.

One aspect of CO oxidation not addressed in this work is chaotic oscillations. No attempt has been made with this model to predict regions of chaotic behavior, or even to determine if chaotic behavior is possible with this model. Lynch *et al.* (1986) did not address chaotic behavior when the surface phase transformation model was first presented. Some types of chaotic oscillations arise from the coupling of two oscillators with different frequencies. The surface transformation is effectively only a single oscillator, thus alone it will not lead to these types of chaos. If heat transfer between the gas phase and the catalyst is included in the model, it might be possible to obtain predictions of chaotic behavior. It is well-known that oscillations can result from the coupling of heat transfer and reaction. Introducing the catalyst surface temperature as a variable

would add another potential oscillator to the model, which might result in predictions of chaotic behavior. This would result in a model capable of predicting the four main types of complex behavior for CO oxidation.

Another interesting observation from this work is that the concentration of active sites for CO oxidation appears to be less than the concentration of active sites for H_2 adsorption. In fact, the value of surface area (a measure of active site concentration) used in the model had to be less than 50% of the value determined from hydrogen uptake measurements for the model results to match the experimental data. What this indicates is that not all sites are equal for all reactions: a site which can adsorb hydrogen is not necessarily a site which will catalyze the oxidation of carbon monoxide. This result has important implications for modeling catalytic reactions. These implications will be discussed in more detail in the next section.

9.2 Feed Composition Cycling

The most obvious conclusion that can be drawn from the feed composition cycling presented in this work is that significant increases over steady-state conversions can, in some cases, be achieved by cycling the feed composition in a catalytic reactor. This result is by no means new: a number of papers both by Douglas and co-workers and by Bailey and co-workers have demonstrated that enhancements in conversion and selectivity can be achieved by switching between two

reactants in the feed. For CO oxidation, Cutlip (1979) was the first to demonstrate reaction rate resonance. The 180 degree out-of-phase cycling done in this work is similar to Cutlip's work, although this work is a much more comprehensive investigation than Cutlip presented. At high cycling frequencies, the time-average conversion is close to the steady-state conversion. This is as expected because, in the limit of frequencies approaching infinity, the reactant concentrations will be unable to move far from their steady-state values so the reactor performance should be close to the steady state.

This is apparently the first experimental and modeling study of the effect of phase angle on reactor performance during feed composition cycling. The phase angle between reactants can be a very important parameter if maximum performance is desired. For example, in this work, global rate enhancement was only achieved when the phase angle was varied from 180 degrees. In previous studies, such as Cutlip (1979), the operating parameters leading to global rate enhancement would not have been found with the limitation of out-of-phase cycling. The demonstration of global rate enhancement by switching between feed gases is also a significant achievement. This is apparently the first such demonstration for CO oxidation.

Feed cycling can be used to discriminate among rival kinetic models, and to check the validity of models which correctly predict steady-state behavior. In this study, a

model which was in excellent agreement with the steady-state behavior was found to be incapable of describing the reaction behavior during feed composition cycling. Examination of the cycling data suggested changes in the model which improved the model description of the reaction. Without the feed composition cycling data, the model would have been an inadequate model for the oxidation of CO on supported platinum catalysts. Thus, it is seen that feed composition cycling can be an important tool in discriminating among rival kinetic models of a reaction.

With regard to the phase angle between inputs, it seems unlikely that optimum results will be obtained with a phase angle of exactly 180 degrees. If rate enhancement occurs during 180 degree out-of-phase cycling, it is likely that more rate enhancement can be found if the phase angle between inputs is varied a small amount in one direction or the other. For the frequencies surveyed in this study, the maximum conversion conditions never coincided with 180 degree out-of-phase cycling. As seen in this study, there can be significant rate enhancement for very small phase angles between inputs, even at frequencies where there is no enhancement for 180 degree out-of-phase cycling. To find the optimum operating conditions, a search of both frequency and phase angle should be conducted.

9.3 Recommendations for Future Work

The results presented in the previous chapters suggest a number of areas for future study. Investigation of the following areas is recommended.

1. One limitation of the experimental work in this thesis is the lack of a "surface probe" - there was no measurement of the state of the catalyst surface. It is recommended that further feed composition cycling be performed with a surface probe, such as Fourier Transform infrared spectroscopy (FTIR), to measure the transient concentration of surface species. Data concerning the surface species concentrations would facilitate further model development and validation.

2. It is recommended that feed concentration cycling to a well-defined surface (i.e., a single crystal) be carried out with low energy electron diffraction (LEED) monitoring of the surface structure. The dynamics of the phase transformation should be more fully characterized. The gathered data should be incorporated into the CO oxidation model. Related to these recommendations, predicted cycling dynamics should be examined for a model with a non-instantaneous phase transformation.

3. One prediction of the surface phase transformation model is the crossover from oscillations to multiplicity. This prediction was neither validated nor disproved in this work due to changing catalyst activity. It is recommended that further experimental work be performed to validate the

crossover prediction. A very stable catalyst should be used for this work.

4. The final model of this work (surface phase transformation with CO exclusion) may be capable of describing chaotic oscillations. It is recommended that the model be analyzed to determine the modifications necessary for it to predict chaotic oscillations. One suggested model modification is the inclusion of heat transfer between the catalyst and gas phase.

5. In the modeling work of Chapter 8, it was found that two of the eigenvalues of the recycle reactor Jacobian matrix had positive real parts in the neighborhood of the cusp. Two eigenvalues with positive real parts often indicate the existence of an oscillatory solution. Further mathematical analysis should be conducted to verify the existence of an oscillatory solution.

9.4 References

Cutlip, M. B., "Concentration Forcing of Catalytic Surface Rate Processes, Part 1. Isothermal Carbon Monoxide Oxidation Over Supported Platinum", AIChE J. 25, 502-508 (1979).

Lynch, D. T., G. Emig, and S. E. Wanke, "Oscillations during CO Oxidation over Supported Metal Catalysts: III. Mathematical Modeling of the Observed Phenomena", J. Catal. 97, 456-468 (1986).

Appendix A

The computer programs listed in this Appendix were used to solve for the steady-state solutions of the differential equations presented in this thesis.

```
      IMPLICIT  REAL*8(A-H,K,O-Z)
      PARAMETER  (NX=6)
C
C      THIS MODELS EXCLUSIVE O2 SITES   (N FOR CO ADSORPTION)
C    (CO SELF-EXCLUSION)
C
      REAL*8  X(NX+1),XLOW(NX+1),XUPP(NX+1),W(NX+1),HMAX(NX+1),
     *            PREF(NX+1),OUT(100,NX+2),F(NX),WKAREA(NX+1,3),
     *            B(NX+1),BETA(NX+1),J(NX,NX+1),DXDT(NX+1)
      INTEGER  NDIR(NX+1),IAREA(NX+1,2)
      CHARACTER  MARK(NX+1)
      COMMON  /TOL/ABSDX,RELDX
      READ(5,*)(X(I),I=1,NX+1)
      READ(5,*)(XLOW(I),I=1,NX+1)
      READ(5,*)(XUPP(I),I=1,NX+1)
      READ(5,*)(W(I),I=1,NX+1)
      READ(5,*)(HMAX(I),I=1,NX+1)
      READ(5,*)(PREF(I),I=1,NX+1)
      READ(5,*)(NDIR(I),I=1,NX+1)
      READ(5,*)EPS,HH,E
      READ(5,*)NCORR,NCRAD,MAXOUT,NPRNT,INITAL,ITIN
      READ(5,*)ABSDX,RELDX
      CALL  INPUT(NX)
      CALL  DERPAR(NX,X,XLOW,XUPP,EPS,W,INITAL,ITIN,HH,
     *            HMAX,PREF,NDIR,E,NCORR,NCRAD,NOUT,
     *            OUT,MAXOUT,NPRNT,MARK,
     *            WKAREA,IAREA,B,F,J,BETA,DXDT)
      WRITE(6,300)ITIN,NOUT,MAXOUT
 300  FORMAT(' ITIN = ',I5,'   NOUT = ',I5,'   MAXOUT = ',I5)
      STOP
      END
```

```
      SUBROUTINE  INPUT(N)
      IMPLICIT  REAL*8(A-H,K,O-Z)
      REAL*8  XX(N+1),F(N)
      REAL*8  PF(3),P(20)
      CHARACTER  MARK(N+1)
      EQUIVALENCE  (P(1),COP),(P(2),RKM1),(P(3),E1R),(P(4),O2P),
     *(P(5),RK3),(P(6),E3R),(P(7),A),(P(8),V),(P(9),RL),
     *(P(10),RMASS),(P(11),CP),(P(12),U),(P(13),TO),(P(14),PO),
     *(P(15),QMOL),(P(16),DH3),(P(17),FCO),(P(18),FO2),
     *(P(19),RN),(P(20),E2R)
      DATA  PF/3*0.D0/
      COMMON  /TOL/ABSDX,RELDX
      COMMON  /PAR/G1,G3,K1,K2,K3,KM1,A1,A2,TT,RNALSO
900   FORMAT(//,3D40.16,/)
901   FORMAT(//,4D40.16,/)
905   FORMAT(//,I20,I50,/)
      READ(5,900)  COP,RKM1,E1R
      READ(5,901)  O2P,E2R,RK3,E3R
      READ(5,900)  A,V,RL
      READ(5,900)  RMASS,CP,U
      READ(5,900)  TO,PO,QMOL
      READ(5,900)  DH3,FCO,FO2
      READ(5,901)  RN,RNCO,FFMT,PSI1
      RNALSO=RN
      READ(5,905)IPAR,IPF
      READ(5,*)PSI2,PSI3
      PF(IPF)=1.D0
      RETURN
      ENTRY  FCN(N,XX,F)
      X=XX(1)
      Y=XX(2)
      Z=XX(3)
      COS=XX(4)
      OS=XX(5)
      T=XX(6)
      P(IPAR)=PF(1)*DEXP(XX(N+1))+PF(2)*XX(N+1)+PF(3)*DLOG(XX(N+1))
      DH1=E1R*8.314D0
      DHR=(-66772.D0-4.4525D0*TO+6.035D-03*TO*TO-2.93D-06*TO**3
     *+5.395D-10*TO**4)*4.184D0*(-1.D0)
      DH2=DHR-(DH1+DH3)
      CONCT=PO/(8.314D0*TO)
      QO=QMOL/CONCT
      VQO=V/QO
      G1=E1R/TO
      G2=E2R/TO
      G3=E3R/TO
      RK1=6.87D0*COP*DSQRT(TO)/RL
      RK2=6.42D0*O2P*DSQRT(TO)/(RL*RL)
      K1=RK1*A*RL/QO*PSI1
      K2=RK2*A*RL*RL*PSI2*DEXP(-G2)/QO
      K3=RK3*A*RL**2*DEXP(-G3)/(QO*CONCT*FCO)*PSI3
      KM1=RKM1*A*RL*DEXP(-G1)/(QO*CONCT*FCO)
      B1=DH1*V*CONCT*FCO/(RMASS*CP*TO)
      B2=DH2*V*CONCT*FO2/(RMASS*CP*TO)
```

```
      B3=DH3*V*CONCT*FCO/(RMASS*CP*TO)
      B4=V*U*A/(RMASS*CP*QO)
      A1=V*CONCT*FCO/(A*RL)
      A2=2.D0*V*CONCT*FO2/(A*RL)
      RNALSO=RN
      SCO=0.D0
C      IF(COS.LT.1.D0/RNCO)
      IF(COS.NE.1.D0)
     *SCO=(1.D0-COS-OS)*(1.D0-RNCO*COS)/(1.D0-COS)
      SO2=0.D0
      IF(OS.LT.1.D0/RN)SO2=(1.D0-OS-COS)*(1.D0-RN*OS)/(1.D0-OS)
      TT=T/(T+1.D0)
      R1=K1*X*SCO-KM1*DEXP(G1*TT)*COS
      R2=K2*Y*SO2**2
      R3=K3*DEXP(G3*TT)*COS*OS
      QN=1.D0-FCO*(R1-R3)-FO2*R2
      F(1)=1.D0-QN*X-R1
      F(2)=1.D0-QN*Y-R2
      F(3)=-QN*Z+R3
      F(4)=A1*(R1-R3)
      F(5)=A2*R2-A1*R3
      F(6)=B1*R1+B2*R2+B3*R3-B4*T
      RETURN
      ENTRY  OUTPUT(XX,SQUAR,MARK,NPRP,IK,IWRITE)
      DO  160  I=1,N+1
      MARK(I)='  '
  160 CONTINUE
      MARK(IK)  ='*'
      ALPHA=PF(1)*DEXP(XX(N+1))+PF(2)*XX(N+1)+PF(3)*DLOG(XX(N+1))
      WRITE(6,800)NPRP,(XX(I),MARK(I),I=1,N),ALPHA,MARK(N+1),SQUAR
 800  FORMAT(1X,I2,7(1PD12.4,A1),2X,1PD6.0)
      RETURN
      END
```

```
      SUBROUTINE DERPAR(N,X,XLOW,XUPP,EPS,W,INITAL,ITIN,HH,
     * HMAX,PREF,NDIR,E,NCORR,NCRAD,NOUT,OUT,
     * MAXOUT,NPRNT,MARK,WKAREA,IAREA,B,
     * F,G,BETA,DXDT)
      IMPLICIT REAL*8(A-H,O-Z)
      DIMENSION X(N+1),XLOW(N+1),XUPP(N+1),W(N+1),HMAX(N+1),
     * PREF(N+1),NDIR(N+1),OUT(100,N+2),F(N),G(N,N+1),BETA(N+1),
     *   DXDT(N+1),B(N+1),WKAREA(N+1,3),IAREA(N+1,2),X2(4)
      COMMON /TOL/ABSDX,RELDX
      CHARACTER MARK(N+1)
      EXTERNAL FCN
C OBTAINING OF DEPENDENCE OF SOLUTION X(ALFA) OF EQUATION
C F ( X ,ALFA ) = 0
C ON PARAMETER ALFA BY MODIFIED METHOD OF DIFFERENTIATION
C WITH RESPECT TO PARAMETER
C N - NUMBER OF UNKNOWNS X(I)
C X(1),...,X(N) - INITIAL VALUES OF X(I),AFTER RETURN FINAL VALUES
C                       OF X(I)
C X(N+1) - INITIAL VALUE OF PARAMETER ALFA,AFTER RETURN FINAL VALUE
C              OF ALFA
C XLOW(1),...,XLOW(N) - LOWER BOUNDS FOR X(I)
C XUPP(1),...,XUPP(N) - UPPER BOUNDS FOR X(I)
C XLOW(N+1),XUPP(N+1) - LOWER AND UPPER BOUNDS FOR ALFA
C     IF XLOW OR XUPP IS EXCEEDED,THEN END OF DERPAR
C     AND MAXOUT=-2 AFTER RETURN
C EPS - ACCURACY DESIRED IN NEWTON ITERATION FOR
C     SUM OF (W(I)*DABS(XNEW(I)-XOLD(I))),I=1,...,N+1
C W(1),...,W(N+1) - WEIGHTS USED IN TERMINATION CRITERION OF NEWTON
C                           PROCESS
C INITAL - IF (INITAL.NE.0) THEN SEVERAL STEPS IN NEWTON ITERATION
C            ARE MADE BEFORE COMPUTATION IN ORDER TO INCREASE
C            ACCURACY OF INITIAL POINT-
C       IF (INITAL.EQ.1.AND.EPS-ACCURACY IS NOT FULFILLED IN ITIN
C       ITERATIONS) THEN RETURN.    IF (INITAL.EQ.2) THEN ALWAYS RETURN
C       AFTER INITIAL NEWTON ITERATION,RESULTS ARE IN X.
C       IF (INITAL.EQ.3) THEN CONTINUE IN DERPAR AFTER INITIAL NEWTON.
C       IF (INITAL.EQ.0) THEN NO INITIAL NEWTON ITERATION IS USED.
C ITIN - MAXIMAL NUMBER OF INITIAL NEWTON ITERATIONS. IF
C          EPS-ACCURACY IS NOT FULFILLED IN ITIN ITERATIONS THEN
C          ITIN=-1 AFTER RETURN.
C HH - INTEGRATION STEP ALONG ARC LENGTH OF SOLUTION LOCUS
C HMAX(1),...,HMAX(N+1) - UPPER BOUNDS FOR INCREMENTS OF X(I) IN
C                                 ONE INTEGRATION STEP (APPROXIMATION ONLY)
C PREF(1),...,PREF(N+1) - PREFERENCE NUMBERS (EXPLANATION SEE IN
C                                  SUBR.GAUSE)
C NDIR(1),...,NDIR(N+1) - INITIAL CHANGE OF X(I) IS POSITIVE ALONG
C       SOLUTION LOCUS (CURVE) IF NDIR(I)=1 AND NEGATIVE IF
C       NDIR(I)=-1.
C E - CRITERION FOR TEST ON CLOSED CURVE,IF
C     (SUM OF (W(I)*DABS(X(I)-XINITIAL(I))),I=1,...,N+1).LE.E)
C     THEN CLOSED CURVE MAY BE EXPECTED.
C MXADMS - MAXIMAL ORDER OF ADAMS-BASHFORTH FORMULA,
C              1.LE.MXADMS.LE.4.
C NCORR - MAXIMAL NUMBER OF NEWTON CORRECTIONS AFTER PREDICTION
```

```
C      BY ADAMS-BASHFORTH METHOD.
C NCRAD - IF (NCRAD.NE.0) THEN ADDITIONAL NEWTON CORRECTION
C      WITHOUT NEW COMPUTATION OF JACOBIAN MATRIX IS USED.
C NOUT - AFTER RETURN NUMBER OF CALCULATED POINTS ON THE CURVE
C            X(ALFA),NOUT.LE.MAXOUT.
C OUT(J,1),OUT(J,2),...,OUT(J,N+1) - J-TH POINT X(1),...,X(N),ALFA
C      ON CURVE X(ALFA)
C OUT(J,N+2) - VALUE OF DSQRT(SUM OF SQUARES OF F).
C      IF (OUT(J,N+2).LT.0.D0) THEN   DABS(OUT(J,N+2)) CORRESPONDS TO X
C      AND ALFA NOT EXACTLY,BECAUSE ADDITIONAL NEWTON CORRECTION WAS
C      USED (NCRAD.NE.0).
C      VALUES F(I) ARE NOT COMPUTED FOR X AND ALFA PRINTED AND/OR
C      STORED AND THEREFORE LAST TIME COMPUTED VALUE OF DSQRT(SUM OF
C      SQUARES OF F) IS ON OUR DISPOSAL ONLY.
C MAXOUT - MAXIMAL NUMBER OF CALCULATED POINTS ON CURVE X(ALFA).
C      IF MAXOUT AFTER RETURN EQUALS TO-
C               -1 - THEN CLOSED CURVE X(ALFA) MAY BE EXPECTED
C               -2 - THEN BOUND XLOW OR XUPP WAS EXCEEDED
C               -3 - THEN SINGULAR JACOBIAN MATRIX OCCURRED,ITS RANK IS
C                      .LT. N.
C NPRNT - IF (NPRNT.EQ.3) THEN RESULTING POINTS ON CURVE X(ALFA)
C      ARE IN ARRAY OUT( ,) AFTER RETURN. IF (NPRNT.EQ.1) THEN THESE
C      POINTS ARE PRINTED ONLY.   IF (NPRNT.EQ.2) THEN THESE POINTS ARE
C      BOTH PRINTED AND IN ARRAY OUT.
C SUBROUTINE FCTN MUST BE PROGRAMMED IN FOLLOWING FORM -
C    SUBROUTINE FCTN(N,X,F,G)
C    DIMENSION X(11),F(10),G(10,11)
C    F(I)= FI (X(1),X(2),...,X(N),ALFA) FOR I=1,...,N
C    G(I,J)= D FI (X(1),...,X(N),ALFA)/ D X(J) FOR   I,J=1,...,N
C    G(I,N+1)= D FI (X(1),...,X(N),ALFA)/ D ALFA   FOR I=1,...,N
C    RETURN
C    END
C LW IS PRINTER DEVICE NUMBER
        N1 = N + 1
        LW = 6
        IF (INITAL) 10,60,10
C INITIAL NEWTON ITERATIONS
   10 DO 40 L=1,ITIN
           CALL FCN(N,X,F)
           CALL NUJACX(FCN,X,N,G,ABSDX,RELDX,WKAREA,IFLAG)
        IF(IFLAG.GT.0)WRITE(6,*)'WARNING:    IFLAG FROM NUJACX =   ',IFLAG
           SQUAR = 0.D0
           DO 20 I=1,N
              SQUAR = SQUAR + F(I)**2
   20      CONTINUE
           LL = L - 1
           SQUAR = DSQRT(SQUAR)
           IF (NPRNT.NE.3) WRITE (LW,99999) LL,(X(I),I=1,N1),SQUAR
           CALL GAUSE(N,G,F,B,M,PREF,BETA,K,WKAREA,IAREA)
           IF (M.EQ.0) GO TO 310
           P = 0.D0
           DO 30 J=1,N1
              X(J) = X(J) - B(J)
              P = P + DABS(B(J))*W(J)
```

```
   30     CONTINUE
           IF (P.LE.EPS) GO TO 50
   40 CONTINUE
       WRITE (LW,99998) ITIN
       ITIN = -1
       IF (INITAL.EQ.1) RETURN
   50 IF (NPRNT.NE.3) WRITE (LW,99997) (X(I),I=1,N1)
       IF (INITAL.EQ.2) RETURN
C AFTER INITIAL NEWTON ITERATIONS
   60 IF (NPRNT.NE.3) WRITE (LW,99996)
       KOUT = 0
       NOUT = 0
       MADMS = 0
       NC = 1
       K1 = 0
   70     CALL FCN(N,X,F)
           CALL NUJACX(FCN,X,N,G,ABSDX,RELDX,WKAREA,IFLAG)
       IF(IFLAG.GT.0)WRITE(6,*)'WARNING:    IFLAG FROM NUJACX =   ',IFLAG
       SQUAR = 0.D0
       DO 80 I=1,N
           SQUAR = SQUAR + F(I)**2
   80 CONTINUE
           CALL GAUSE(N,G,F,B,M,PREF,BETA,K,WKAREA,IAREA)
       IF (M.EQ.0) GO TO 310
       IF (K1.EQ.K) GO TO 90
C CHANGE OF INDEPENDENT VARIABLE (ITS INDEX = K NOW)
       MADMS = 0
       K1 = K
   90 SQUAR = DSQRT(SQUAR)
       IF (NCRAD.EQ.1) SQUAR = -SQUAR
       P = 0.D0
       DO 100 I=1,N1
           P = P + W(I)*DABS(B(I))
  100 CONTINUE
       IF (P.LE.EPS) GO TO 130
       IF (NC.GE.NCORR) GO TO 120
       DO 110 I=1,N1
           X(I) = X(I) - B(I)
  110 CONTINUE
C ONE ITERATION IN NEWTON METHOD
       NC = NC + 1
       GO TO 70
  120 IF (NCORR.EQ.0) GO TO 130
       WRITE (LW,99995) NCORR,P
  130 NC = 1
       IF (NCRAD.EQ.0) GO TO 150
C ADDITIONAL NEWTON CORRECTION
       DO 140 I=1,N1
           X(I) = X(I) - B(I)
  140 CONTINUE
  150 NOUT = NOUT + 1
           CALL NUJACX(FCN,X,N,G,ABSDX,RELDX,WKAREA,IFLAG)
       IF(IFLAG.GT.0)WRITE(6,*)'WARNING:    IFLAG FROM NUJACX =   ',IFLAG
       CALL HSBG(N,G,N)
```

```
      CALL ATEIG(N,G,WKAREA(1,1),WKAREA(1,2),IAREA,N)
      NPRP=0
      DO 165 I=1,N
         IF(WKAREA(I,1).GT.0.D0)NPRP=NPRP+1
 165  CONTINUE
 163  IF (NPRNT.EQ.2) GO TO 170
C     WRITE (LW,99994)
      CALL OUTPUT(X,SQUAR,MARK,NPRP,K,IWRITE)
 170  IF (NPRNT.EQ.1) GO TO 200
      IF (NOUT.LE.100) GO TO 180
      WRITE (LW,99992)
      RETURN
 180  DO 190 I=1,N1
         OUT(NOUT,I)=X(I)
 190  CONTINUE
      OUT(NOUT,N+2)=SQUAR
      GO TO 210
 200  IF (NOUT.EQ.1) GO TO 180
 210  IF (NOUT.GE.MAXOUT) RETURN
      DO 220 I=1,N1
         IF (X(I).LT.XLOW(I) .OR. X(I).GT.XUPP(I)) GO TO 300
 220  CONTINUE
      IF (NOUT.LE.3) GO TO 240
      P = 0.D0
      DO 230 I=1,N1
         P = P + W(I)*DABS(X(I)-OUT(1,I))
 230  CONTINUE
      IF (P.LE.E) GO TO 290
C CLOSED CURVE MAY BE EXPECTED
 240  DXK2 = 1.D0
      DO 250 I=1,N1
         DXK2 = DXK2 + BETA(I)**2
 250  CONTINUE
      DXDT(K) = 1.D0/DSQRT(DXK2)*DFLOAT(NDIR(K))
C DERIVATIVE OF INDEPENDENT VARIABLE X(K) WITH RESPECT TO ARC LENGTH
C OF SOLUTION LOCUS IS COMPUTED HERE
      H = HH
      DO 270 I=1,N1
         NDIR(I) = 1
         IF (I.EQ.K) GO TO 260
         DXDT(I) = BETA(I)*DXDT(K)
 260     IF (DXDT(I).LT.0.D0) NDIR(I) = -1
         IF (H*DABS(DXDT(I)).LE.HMAX(I)) GO TO 270
         MADMS = 0
         H = HMAX(I)/DABS(DXDT(I))
 270  CONTINUE
      IF (NOUT.LE.KOUT+3) GO TO 280
      IF (H*DABS(DXDT(K)).LE.0.8D0*DABS(X(K)-OUT(1,K))) GO TO 280
      IF ((OUT(1,K)-X(K))*DFLOAT(NDIR(K)).LE.0.D0) GO TO 280
      MADMS = 0
      IF (H*DABS(DXDT(K)).LE.DABS(X(K)-OUT(1,K))) GO TO 280
      H = DABS(X(K)-OUT(1,K))/DABS(DXDT(K))
      KOUT = NOUT
 280  CONTINUE
```

```
      DO 239 III=1,N+1
            X(III)=DXDT(III)*H+X(III)
 239  CONTINUE
C 280 CALL ADAMS(N,DXDT,MADMS,H,X,MXADMS)
C 280 CALL RKF45(T,X,N,F2,H,DT,HMXFR,ABSER,RELER,IFLAG,
C     *      DXDT,K,BETA)
      GO TO 70
  290 WRITE (LW,99991)
      MAXOUT = -1
      RETURN
  300 MAXOUT = -2
      RETURN
  310 WRITE (LW,99990) (X(I),I=1,N1)
      MAXOUT = -3
      RETURN
99999 FORMAT (3X,7H DERPAR,I3,25H.INITIAL NEWTON ITERATION/22X,
     * 11HX,ALFA,SQF=,8(1PD15.7))
99998 FORMAT (/16H DERPAR OVERFLOW,I5,2X,18HINITIAL ITERATIONS/)
99997 FORMAT (3X,39H DERPAR AFTER INITIAL NEWTON ITERATIONS/22X,
     * 7HX,ALFA=,4X,5(1PD15.7)/(33X,5F15.7))
99996 FORMAT (/6X,45H DERPAR RESULTS (VARIABLE CHOSEN AS INDEPENDE,
     * 18HNT IS MARKED BY *)/)
99995 FORMAT (/37H DERPAR NUMBER OF NEWTON CORRECTIONS=,I5,
     * 31H  IS NOT SUFFICIENT,ERROR OF X=,1PD15.7/)
99994 FORMAT (6X,27H DERPAR RESULTS X,ALFA,SQF=)
99993 FORMAT(7(1PD12.5,A1),1X,1PD12.5,2X,I3)
99992 FORMAT (/28H DERPAR OUTPUT ARRAY IS FULL//)
99991 FORMAT (/36H DERPAR CLOSED CURVE MAY BE EXPECTED/)
99990 FORMAT (/48H DERPAR SINGULAR JACOBIAN MATRIX FOR X AND ALFA=,
     * 5F12.6/(48X,5F12.6))
      END
```

```
C          SUBROUTINE HSBG
C
C          PURPOSE
C              TO REDUCE A REAL MATRIX INTO UPPER ALMOST TRIANGULAR FORM
C
C          USAGE
C              CALL HSBG(N,A,IA)
C
C          DESCRIPTION OF THE PARAMETERS
C              N         ORDER OF THE MATRIX
C              A         THE INPUT MATRIX, N BY N
C              IA       SIZE OF THE FIRST DIMENSION ASSIGNED TO THE ARRAY
C                        A IN THE CALLING PROGRAM WHEN THE MATRIX IS IN
C                        DOUBLE SUBSCRIPTED DATA STORAGE MODE.   IA=N WHEN
C                        THE MATRIX IS IN SSP VECTOR STORAGE MODE.
C
C          REMARKS
C              THE HESSENBERG FORM REPLACES THE ORIGINAL MATRIX IN THE
C              ARRAY A.
C
C          SUBROUTINES AND FUNCTION SUBPROGRAMS REQUIRED
C              NONE
C
C          METHOD
C              SIMILARITY TRANSFORMATIONS USING ELEMENTARY ELIMINATION
C              MATRICES, WITH PARTIAL PIVOTING.
C
C          REFERENCES
C              J.H. WILKINSON - THE ALGEBRAIC EIGENVALUE PROBLEM -
C              CLARENDON PRESS, OXFORD, 1965.
C
C              SEE IBM SSP MANUAL FOR ADDITIONAL INFORMATION
C
C       ..........................................................
C
      SUBROUTINE HSBG(N,A,IA)
      IMPLICIT REAL*8(A-H,O-Z)
      REAL*8 A(1)
      L=N
      NIA=L*IA
      LIA=NIA-IA
C
C         L IS THE ROW INDEX OF THE ELIMINATION
C
   20 IF(L-3) 360,40,40
   40 LIA=LIA-IA
      L1=L-1
      L2=L1-1
C
C         SEARCH FOR THE PIVOTAL ELEMENT IN THE LTH ROW
C
      ISUB=LIA+L
      IPIV=ISUB-IA
      PIV=DABS(A(IPIV))
```

```
      IF(L-3) 90,90,50
   50 M=IPIV-IA
      DO 80 I=L,M,IA
      T=DABS(A(I))
      IF(T-PIV) 80,80,60
   60 IPIV=I
      PIV=T
   80 CONTINUE
   90 IF(PIV) 100,320,100
  100 IF(PIV-DABS(A(ISUB))) 180,180,120
C
C           INTERCHANGE THE COLUMNS
C
  120 M=IPIV-L
      DO 140 I=1,L
      J=M+I
      T=A(J)
      K=LIA+I
      A(J)=A(K)
  140 A(K)=T
C
C           INTERCHANGE THE ROWS
C
      M=L2-M/IA
      DO 160 I=L1,NIA,IA
      T=A(I)
      J=I-M
      A(I)=A(J)
  160 A(J)=T
C
C           TERMS OF THE ELEMENTARY TRANSFORMATION
C
  180 DO 200 I=L,LIA,IA
  200 A(I)=A(I)/A(ISUB)
C
C           RIGHT TRANSFORMATION
C
      J=-IA
      DO 240 I=1,L2
      J=J+IA
      LJ=L+J
      DO 220 K=1,L1
      KJ=K+J
      KL=K+LIA
  220 A(KJ)=A(KJ)-A(LJ)*A(KL)
  240 CONTINUE
C
C           LEFT TRANSFORMATION
C
      K=-IA
      DO 300 I=1,N
      K=K+IA
      LK=K+L1
      S=A(LK)
```

```
      LJ=L-IA
      DO 280 J=1,L2
      JK=K+J
      LJ=LJ+IA
  280 S=S+A(LJ)*A(JK)*1.0D0
  300 A(LK)=S
C
C           SET THE LOWER PART OF THE MATRIX TO ZERO
C
      DO 310 I=L,LIA,IA
  310 A(I)=0.0D0
  320 L=L1
      GO TO 20
  360 RETURN
      END
```

```
C
C     ..................................................................
C
C          SUBROUTINE ATEIG
C
C          PURPOSE
C              COMPUTE THE EIGENVALUES OF A REAL ALMOST TRIANGULAR MATRIX
C
C          USAGE
C              CALL ATEIG(M,A,RR,RI,IANA,IA)
C
C          DESCRIPTION OF THE PARAMETERS
C              M         ORDER OF THE MATRIX
C              A         THE INPUT MATRIX, M BY M
C              RR        VECTOR CONTAINING THE REAL PARTS OF THE EIGENVALUES
C                         ON RETURN
C              RI        VECTOR CONTAINING THE IMAGINARY PARTS OF THE EIGEN-
C                         VALUES ON RETURN
C              IANA     VECTOR WHOSE DIMENSION MUST BE GREATER THAN OR EQUAL
C                         TO M, CONTAINING ON RETURN INDICATIONS ABOUT THE WAY
C                         THE EIGENVALUES APPEARED (SEE MATH. DESCRIPTION)
C              IA        SIZE OF THE FIRST DIMENSION ASSIGNED TO THE ARRAY A
C                         IN THE CALLING PROGRAM WHEN THE MATRIX IS IN DOUBLE
C                         SUBSCRIPTED DATA STORAGE MODE.
C                         IA=M WHEN THE MATRIX IS IN SSP VECTOR STORAGE MODE.
C
C          REMARKS
C              THE ORIGINAL MATRIX IS DESTROYED
C              THE DIMENSION OF RR AND RI MUST BE GREATER OR EQUAL TO M
C
C          SUBROUTINES AND FUNCTION SUBPROGRAMS REQUIRED
C              NONE
C
C          METHOD
C              QR DOUBLE ITERATION
C
C          REFERENCES
C              J.G.F. FRANCIS - THE QR TRANSFORMATION---THE COMPUTER
C              JOURNAL, VOL. 4, NO. 3, OCTOBER 1961, VOL. 4, NO. 4, JANUARY
C              1962.  J. H. WILKINSON - THE ALGEBRAIC EIGENVALUE PROBLEM -
C              CLARENDON PRESS, OXFORD, 1965.
C
C              SEE IBM SSP MANUAL FOR ADDITIONAL INFORMATION
C
C     ..................................................................
C
      SUBROUTINE ATEIG(M,A,RR,RI,IANA,IA)
      IMPLICIT REAL*8(A-H,O-Z)
      REAL*8 A(1),RR(1),RI(1),PRR(2),PRI(2)
      INTEGER P,P1,Q,IANA(1)
C
      E8=1.0D-08
      E6=1.0D-06
      E10=1.0D-10
```

```
      DELTA=0.5D0
      MAXIT=30
C
C         INITIALIZATION
C
      N=M
   20 N1=N-1
      IN=N1*IA
      NN=IN+N
      IF(N1) 30,1300,30
   30 NP=N+1
C
C         ITERATION COUNTER
C
      IT=0
C
C         ROOTS OF THE 2ND ORDER MAIN SUBMATRIX AT THE PREVIOUS
C         ITERATION
C
      DO 40 I=1,2
      PRR(I)=0.0D0
   40 PRI(I)=0.0D0
C
C         LAST TWO SUBDIAGONAL ELEMENTS AT THE PREVIOUS ITERATION
C
      PAN=0.0D0
      PAN1=0.0D0
C
C         ORIGIN SHIFT
C
      R=0.0D0
      S=0.0D0
C
C         ROOTS OF THE LOWER MAIN 2 BY 2 SUBMATRIX
C
      N2=N1-1
      IN1=IN-IA
      NN1=IN1+N
      N1N=IN+N1
      N1N1=IN1+N1
   60 T=A(N1N1)-A(NN)
      U=T*T
      V=4.0D0*A(N1N)*A(NN1)
      IF(DABS(V)-U*E8) 100,100,65
   65 T=U+V
      IF(DABS(T)-DMAX1(U,DABS(V))*E6) 67,67,68
   67 T=0.0D0
   68 U=(A(N1N1)+A(NN))/2.0D0
      V=DSQRT(DABS(T))/2.0D0
      IF(T)140,70,70
   70 IF(U) 80,75,75
   75 RR(N1)=U+V
      RR(N)=U-V
      GO TO 130
```

```
   80 RR(N1)=U-V
      RR(N)=U+V
      GO TO 130
  100 IF(T)120,110,110
  110 RR(N1)=A(N1N1)
      RR(N)=A(NN)
      GO TO 130
  120 RR(N1)=A(NN)
      RR(N)=A(N1N1)
  130 RI(N)=0.0D0
      RI(N1)=0.0D0
      GO TO 160
  140 RR(N1)=U
      RR(N)=U
      RI(N1)=V
      RI(N)=-V
  160 IF(N2)1280,1280,180
C
C           TESTS OF CONVERGENCE
C
  180 N1N2=N1N1-IA
      RMOD=RR(N1)*RR(N1)+RI(N1)*RI(N1)
      EPS=E10*DSQRT(RMOD)
      IF(DABS(A(N1N2))-EPS)1280,1280,240
  240 IF(DABS(A(NN1))-E10*DABS(A(NN)))  1300,1300,250
  250 IF(DABS(PAN1-A(N1N2))-DABS(A(N1N2))*E6)  1240,1240,260
  260 IF(DABS(PAN-A(NN1))-DABS(A(NN1))*E6)1240,1240,300
  300 IF(IT-MAXIT)  320,1240,1240
C
C           COMPUTE THE SHIFT
C
  320 J=1
      DO 360  I=1,2
      K=NP-I
      IF(DABS(RR(K)-PRR(I))+DABS(RI(K)-PRI(I))-DELTA*(DABS(RR(K))
     1      +DABS(RI(K))))  340,360,360
  340 J=J+I
  360 CONTINUE
      GO TO (440,460,460,480),J
  440 R=0.0D0
      S=0.0D0
      GO TO 500
  460 J=N+2-J
      R=RR(J)*RR(J)
      S=RR(J)+RR(J)
      GO TO 500
  480 R=RR(N)*RR(N1)-RI(N)*RI(N1)
      S=RR(N)+RR(N1)
C
C           SAVE THE LAST TWO SUBDIAGONAL TERMS AND THE ROOTS OF THE
C           SUBMATRIX BEFORE ITERATION
C
  500 PAN=A(NN1)
      PAN1=A(N1N2)
```

```
      DO 520 I=1,2
      K=NP-I
      PRR(I)=RR(K)
  520 PRI(I)=RI(K)
C
C          SEARCH FOR A PARTITION OF THE MATRIX, DEFINED BY P AND Q
C
      P=N2
      IF (N-3)600,600,525
  525 IPI=N1N2
      DO 580 J=2,N2
      IPI=IPI-IA-1
      IF(DABS(A(IPI))-EPS) 600,600,530
  530 IPIP=IPI+IA
      IPIP2=IPIP+IA
      D=A(IPIP)*(A(IPIP)-S)+A(IPIP2)*A(IPIP+1)+R
      IF(D)540,560,540
  540 IF(DABS(A(IPI)*A(IPIP+1))*(DABS(A(IPIP)+A(IPIP2+1)-S)+
     1 DABS(A(IPIP2+2))) -DABS(D)*EPS) 620,620,560
  560 P=N1-J
  580 CONTINUE
  600 Q=P
      GO TO 680
  620 P1=P-1
      Q=P1
      IF (P1-1) 680,680,650
  650 DO 660 I=2, P1
      IPI=IPI-IA-1
      IF(DABS(A(IPI))-EPS)680,680,660
  660 Q=Q-1
C
C          QR DOUBLE ITERATION
C
  680 II=(P-1)*IA+P
      DO 1220 I=P,N1
      II1=II-IA
      IIP=II+IA
      IF(I-P)720,700,720
  700 IPI=II+1
      IPIP=IIP+1
C
C          INITIALIZATION OF THE TRANSFORMATION
C
      G1=A(II)*(A(II)-S)+A(IIP)*A(IPI)+R
      G2=A(IPI)*(A(IPIP)+A(II)-S)
      G3=A(IPI)*A(IPIP+1)
      A(IPI+1)=0.0D0
      GO TO 780
  720 G1=A(II1)
      G2=A(II1+1)
      IF(I-N2)740,740,760
  740 G3=A(II1+2)
      GO TO 780
  760 G3=0.0D0
```

```
  780  CAP=DSQRT(G1*G1+G2*G2+G3*G3)
       IF(CAP)800,860,800
  800  IF(G1)820,840,840
  820  CAP=-CAP
  840  T=G1+CAP
       PSI1=G2/T
       PSI2=G3/T
       ALPHA=2.0D0/(1.0D0+PSI1*PSI1+PSI2*PSI2)
       GO TO 880
  860  ALPHA=2.0D0
       PSI1=0.0D0
       PSI2=0.0D0
  880  IF(I-Q)900,960,900
  900  IF(I-P)920,940,920
  920  A(II1)=-CAP
       GO TO 960
  940  A(II1)=-A(II1)
C
C            ROW OPERATION
C
  960  IJ=II
       DO 1040 J=I,N
       T=PSI1*A(IJ+1)
       IF(I-N1)980,1000,1000
  980  IP2J=IJ+2
       T=T+PSI2*A(IP2J)
 1000  ETA=ALPHA*(T+A(IJ))
       A(IJ)=A(IJ)-ETA
       A(IJ+1)=A(IJ+1)-PSI1*ETA
       IF(I-N1)1020,1040,1040
 1020  A(IP2J)=A(IP2J)-PSI2*ETA
 1040  IJ=IJ+IA
C
C            COLUMN OPERATION
C
       IF(I-N1)1080,1060,1060
 1060  K=N
       GO TO 1100
 1080  K=I+2
 1100  IP=IIP-I
       DO 1180 J=Q,K
       JIP=IP+J
       JI=JIP-IA
       T=PSI1*A(JIP)
       IF(I-N1)1120,1140,1140
 1120  JIP2=JIP+IA
       T=T+PSI2*A(JIP2)
 1140  ETA=ALPHA*(T+A(JI))
       A(JI)=A(JI)-ETA
       A(JIP)=A(JIP)-ETA*PSI1
       IF(I-N1)1160,1180,1180
 1160  A(JIP2)=A(JIP2)-ETA*PSI2
 1180  CONTINUE
       IF(I-N2)1200,1220,1220
```

```
 1200 JI=II+3
      JIP=JI+IA
      JIP2=JIP+IA
      ETA=ALPHA*PSI2*A(JIP2)
      A(JI)=-ETA
      A(JIP)=-ETA*PSI1
      A(JIP2)=A(JIP2)-ETA*PSI2
 1220 II=IIP+1
      IT=IT+1
      GO TO 60
C
C          END OF ITERATION
C
 1240 IF(DABS(A(NN1))-DABS(A(N1N2))) 1300,1280,1280
C
C          TWO EIGENVALUES HAVE BEEN FOUND
C
 1280 IANA(N)=0
      IANA(N1)=2
      N=N2
      IF(N2)1400,1400,20
C
C          ONE EIGENVALUE HAS BEEN FOUND
C
 1300 RR(N)=A(NN)
      RI(N)=0.0D0
      IANA(N)=1
      IF(N1)1400,1400,1320
 1320 N=N1
      GO TO 20
 1400 RETURN
      END
```

```
      FUNCTION DET4(A,B,C,D)
      IMPLICIT REAL*8(A-H,K,O-Z)
      REAL*8 A(4),B(4),C(4),D(4)
      DET4=A(1)*DET3(B(2),C(2),D(2))
     *         -B(1)*DET3(A(2),C(2),D(2))
     *         +C(1)*DET3(A(2),B(2),D(2))
     *         -D(1)*DET3(A(2),B(2),C(2))
      RETURN
      END
```

```
      FUNCTION  DET3(A,B,C)
      IMPLICIT  REAL*8(A-H,K,O-Z)
      REAL*8  A(3),B(3),C(3)
      DET3=A(1)*DET2(B(2),C(2))
     *            -B(1)*DET2(A(2),C(2))
     *            +C(1)*DET2(A(2),B(2))
      RETURN
      END
```

```
FUNCTION  DET2(A,B)
IMPLICIT  REAL*8(A-H,K,O-Z)
REAL*8  A(2),B(2)
DET2=A(1)*B(2)-A(2)*B(1)
RETURN
END
```

```
      SUBROUTINE GAUSE(N,A,F,B,M,PREF,BETA,K,WKAREA,IAREA)
      IMPLICIT REAL*8(A-H,O-Z)
      DIMENSION A(N,N+1),B(N+1),PREF(N+1),BETA(N+1),WKAREA(N+1,3),
     * IAREA(N+1,2),F(N)
C SOLUTION OF N LINEAR EQUATIONS FOR N+1 UNKNOWNS
C BASED ON GAUSSIAN ELIMINATION WITH PIVOTING.
C N - NUMBER OF EQUATIONS
C A - N X (N+1) MATRIX OF SYSTEM
C B - RIGHT-HAND SIDES
C M - IF (M.EQ.0) AFTER RETURN THEN RANK(A).LT.N
C PREF(I) - PREFERENCE NUMBER FOR X(I) TO BE INDEPENDENT VARIABLE,
C 0.D0.LE.PREF(I).LE.1.D0,THE LOWER IS PREF(I) THE HIGHER IS
C PREFERENCE OF X(I).
C BETA(I) - COEFFICIENTS IN EXPLICIT DEPENDENCES OBTAINED IN FORM -
C             X(I)=B(I)+BETA(I)*X(K),I.NE.K.
C K - RESULTING INDEX OF INDEPENDENT VARIABLE
      N1 = N + 1
      ID = 1
      M = 1
      DO 10 I=1,N1
         IAREA(I,1) = 0
         IAREA(I,2) = 0
   10 CONTINUE
   20 IR = 1
      IS = 1
      AMAX = 0.D0
      DO 60 I=1,N
         IF (IAREA(I,2)) 60,30,60
   30    DO 50 J=1,N1
            P = PREF(J)*DABS(A(I,J))
            IF (P-AMAX) 50,50,40
   40       IR = I
            IS = J
            AMAX = P
   50    CONTINUE
   60 CONTINUE
      IF (AMAX.NE.0.D0) GO TO 70
C THIS CONDITION FOR SINGULARITY OF MATRIX MUST BE SPECIFIED
C MORE EXACTLY WITH RESPECT TO COMPUTER ACTUALLY USED
      M = 0
      GO TO 150
   70 IAREA(IR,2) = IS
      DO 90 I=1,N
         IF (I.EQ.IR .OR. A(I,IS).EQ.0.D0) GO TO 90
         P = A(I,IS)/A(IR,IS)
         DO 80 J=1,N1
            A(I,J) = A(I,J) - P*A(IR,J)
   80    CONTINUE
         A(I,IS) = 0.D0
         F(I) = F(I) - P*F(IR)
   90 CONTINUE
      ID = ID + 1
      IF (ID.LE.N) GO TO 20
      DO 100 I=1,N
```

```
      IR = IAREA(I,2)
      WKAREA(IR,1) = F(I)/A(I,IR)
      IAREA(IR,1) = 1
100 CONTINUE
    DO 110 K=1,N1
      IF (IAREA(K,1).EQ.0) GO TO 120
110 CONTINUE
120 DO 130 I=1,N
      IR = IAREA(I,2)
      WKAREA(IR,2) = -A(I,K)/A(I,IR)
130 CONTINUE
    DO 140 I=1,N1
      B(I) = WKAREA(I,1)
      BETA(I) = WKAREA(I,2)
140 CONTINUE
    B(K) = 0.D0
    BETA(K) = 0.D0
150 RETURN
    END
```

```
      SUBROUTINE  NUJACX(FOFX,X,NX,J,ABSDX,RELDX,WKAREA,IFLAG)
      IMPLICIT  REAL*8(A-H,K,O-Z)
      REAL*8  X(NX+1),J(NX,NX+1),WKAREA(NX+1,3)
      IFLAG=0
      P=1.D-13
      DO  10  IX=1,NX+1
          WKAREA(IX,1)=(DABS(X(IX))*RELDX+DABS(ABSDX))/2.D0
 10   CONTINUE
      DO  30  JCOL=1,NX+1
          XSAVE=X(JCOL)
          X(JCOL)=XSAVE-WKAREA(JCOL,1)
          CALL  FOFX(NX,X,WKAREA(1,2))
          X(JCOL)=XSAVE+WKAREA(JCOL,1)
          CALL  FOFX(NX,X,WKAREA(1,3))
          X(JCOL)=XSAVE
          DO  20  JROW=1,NX
              J(JROW,JCOL)=(WKAREA(JROW,3)-WKAREA(JROW,2))/
     *                                 (2.D0*WKAREA(JCOL,1))
           IF((DABS(WKAREA(JROW,3)-WKAREA(JROW,2)).LT.
     *      P*DMAX1(DABS(WKAREA(JROW,3)),DABS(WKAREA(JROW,2))))
     *      .AND.(WKAREA(JROW,3).NE.WKAREA(JROW,2)))
     *      IFLAG=JROW
 20       CONTINUE
 30   CONTINUE
      RETURN
      END
```

```
      SUBROUTINE  NUJAC(FOFX,X,NX,J,ABSDX,RELDX,WKAREA,IFLAG)
      IMPLICIT  REAL*8(A-H,K,O-Z)
      REAL*8  X(NX),J(NX,NX),WKAREA(NX,3)
      IFLAG=0
      P=1.D-13
      DO  10  IX=1,NX
          WKAREA(IX,1)=(DABS(X(IX))*RELDX+DABS(ABSDX))/2.D0
10    CONTINUE
      DO  30  JCOL=1,NX
          XSAVE=X(JCOL)
          X(JCOL)=XSAVE-WKAREA(JCOL,1)
          CALL  FOFX(NX,X,WKAREA(1,2))
          X(JCOL)=XSAVE+WKAREA(JCOL,1)
          CALL  FOFX(NX,X,WKAREA(1,3))
          X(JCOL)=XSAVE
          DO  20  JROW=1,NX
              J(JROW,JCOL)=(WKAREA(JROW,3)-WKAREA(JROW,2))/
     *                                 (2.D0*WKAREA(JCOL,1))
            IF((DABS(WKAREA(JROW,3)-WKAREA(JROW,2)).LT.
     *       P*DMAX1(DABS(WKAREA(JROW,3)),DABS(WKAREA(JROW,2))))
     *       .AND.(WKAREA(JROW,3).NE.WKAREA(JROW,2)))
     *       IFLAG=JROW
20        CONTINUE
30    CONTINUE
      RETURN
      END
```

This is a sample data file.

```
0.05D0,0.99D0,0.95D0,0.05D0,0.80D0,0.D0,0.10D-03,
0.D0,0.D0,0.D0,0.D0,0.D0,0.D0,-4.D0,
1.D1,1.D1,1.D1,1.D1,1.D1,1.D1,10.D0,
1.D0,1.D0,1.D0,1.D0,1.D0,1.D0,1.D0,
1.D-2,1.D-2,1.D-2,1.D-2,1.D-2,1.D-2,2.0D-4,
0.01D0,1.D0,1.D0,1.D0,0.01D0,0.01D0,0.001D0,
-1,1,1,1,-1,1,1,
1.D-12,1.D1,0.D0,
10,0,10000,1,1,100,0,
1.D-5,1.D-3,
CO STICK. PROB.;   CO DESORP. PRE-EXP. FACT.;   -E1/R FOR CO DESORP.
 (0.0 TO 1.0)                (1/SECOND)                        (KELVIN)
  100.0E-05,                500.E+13,                       1.390E+04,

O2 STICK. PROB.;   -E2/R O2 ADS.;   REAC. PRE-EXP FAC.;   REAC. -E3/R
 (0.0 TO 1.0)           (KELVIN)       (SQ. METRES/(MOL-S))     (KELVIN)
    1.22E-07,        0.000D+00,             81.E+9,        0.580D+04,

METAL SURFACE AREA;   REACTOR VOLUME;   NUMBER OF CATALYST SITES
 (SQUARE METRES)       (CUBIC METRES)    (MOL SITES/SQUARE METRE)
  6.92D+00,                1.90D-04,                    2.D-05,

MASS OF METAL;   METAL HEAT CAPACITY;   OVERALL HEAT TRANSFER COEFF.
 (KILOGRAM)      (JOULES/(KG.-KELVIN))    (WATTS/(SQ. METRE-KELVIN))
    75.D-06,                  188.D+00,                        1.D+03,

REACTOR TEMPERATURE;   REACTOR PRESSURE;   REACTOR FEED RATE
        (KELVIN)                (PASCALS)          (MOLES/SECOND)
        363.D+00,               1.000D+05,                205.D-06,

HEAT OF SURFACE REACTION;   FEED CO FRACTION;   FEED O2 FRACTION
        (JOULES/MOLE)               (0.0 TO 1.0)          (0.0 TO 1.0)
           15.0D+04,                      0.01D-00,             0.040D0,

CO ADSOPTION SITES   / O2 ADSORPTION SITES;   FFMT;   PSI1;
       ( 1.0 TO 2.0 )          Nco                          (1.0 TO 150.0)
              1.D0,   1.004D0,         100.D0,                    1.E0,

PARAMETER TO BE VARIED (SEE SUBROUTINE INPUT);IPF
          (1 - 20)                                      1=DEXP   2=NONE   3=DLOG
              17,                                   2,
   PSI2,PSI3
    1.D0,1.D0,
**************************************************
(X(I),I=1,NX+1)      INITIAL GUESSES
(XLOW(I),I=1,NX+1)
(XUPP(I),I=1,NX+1)
(W(I),I=1,NX+1)
(HMAX(I),I=1,NX+1)
```

```
(PREF(I),I=1,NX+1)
(NDIR(I),I=1,NX+1)
EPS,HH,E
NCORR,NCRAD,MAXOUT,NPRNT,INITAL,ITIN,IEVAL
ABSDX,RELDX
   1.0D0,1.0D0,0.D0,1.D0,0.D0,0.D0,1.0D-2,
   -1,1,1,1,1,1,-1,
0.0001D0,0.99D0,0.99D0,0.01D0,0.8D0,0.D0,1.0D-2,
-1,1,1,1,-1,1,1,
```

Appendix B

The programs listed in this Appendix were used to solve for the dynamic solutions of the differential equations in Chapter 6.

```
      PROGRAM DIM57
      IMPLICIT REAL (A-H,K,O-Z)
C
C     ..........................................................
C
C    MAIN PROGRAM DIM57
C
C   THIS IS THE MOST RECENT VERSION OF THE PROGRAM, AND IT
C   IS THE ONE WHICH SHOULD BE USED.
C
C    PURPOSE
C        THIS PROGRAM IS USED TO DETERMINE THE DYNAMIC
C        BEHAVIOR FOR THE OXIDATION OF CO IN A WELL-MIXED
C        REACTOR WHERE THE CATALYTIC MECHANISM IS GIVEN BY:
C
C                    CO + S <---> CO-S
C                   O2 + 2S ----> 2 O-S
C              O-S + CO-S ----> CO2 + 2S
C                 CO + O-S ----> CO2 +  S
C
C          (S)co = 1 - CO-S - O-S
C          (S)o2 = (1 - CO-S - O-S)(1 - (N)O-S)/(1 - O-S)      (1 <= N <= 2)
C
C         IN ADDITION, THE MODEL ALSO HAS THE FOLLOWING FEATURES:
C
C           1. CO2 ADSORPTION/DESORPTION ON/FROM THE ALUMINA SUPPORT
C           2. METAL CRYSTALLITE TEMPERATURES VARIATIONS ARE POSSIBLE
C           3. O2 STICKING PROBABILITY IS A DISCONTINUOUS FUNCTION
C               OF THE CO SURFACE COVERAGE.
C
C         PROGRAM CALCULATES CO, O2, CO2, COS, OS, CO2S, AND T
C         WHEN GIVEN ALL PARAMETERS FOR THE 5-7 ODE MODEL.
C         THE MODEL CONTAINS BETWEEN 5 AND 7 ORDINARY DIFFERENTIAL
C         EQUATIONS DEPENDING ON THE VALUE OF AN INPUT PARAMETER (ICODE).
C         THIS "SWITCH" ENABLES THE CO2 ADSORPTION/DESORPTION TO BE
C         INCLUDED OR NEGLECTED FROM THE MODEL. IN ADDITION, THE MODEL
C         CAN DETERMINE THE METAL CRYSTALLITE TEMPERATURE IN ONE OF
C         THREE WAYS:
C
C            1. ISOTHERMAL (VALUE IS SPECIFIED AS INPUT)
C            2. TEMPERATURE DETERMINED BY PSEUDO-STEADY-STATE APPROX.
C            3. TEMPERATURE DETERMINED BY INTEGRATION OF ODE.
C
C
C
C   SYMMETRICAL SQUARE WAVE CYCLING WITH ANY LAG BETWEEN THE
C   CO AND O2 IS POSSIBLE.  ON INPUT, VALUES OF THE PERIOD AND THE
C   LAG ARE REQUIRED, WHERE BOTH ARE RELATIVE TO (DIVIDED BY) THE
C   RESIDENCE TIME (V/Q) FOR THE REACTOR.
C
C   THE LAG IS DEFINED AS THE AMOUNT OF TIME WHICH PASSES AFTER
C   THE CO IS ON BEFORE THE O2 COMES ON.    INTERNALLY, MOST
C   CALCULATIONS USE THE LEAD WHICH IS THE AMOUNT OF TIME FOLLOWING
C   THE O2 TURNING ON BEFORE THE CO TURNS ON.
```

```
C
C       DESCRIPTION OF THE INPUT PARAMETERS
C           SEE SUBROUTINE INPUT FOR A DESCRIPTION OF THE INPUT PARAMETERS
C
C       DESCRIPTION OF THE OUTPUT QUANTITIES
C           CO=X(1)     NORMALIZED CO EXIT CONCENTRATION, (0 - 1)
C           O2=X(2)     NORMALIZED O2 EXIT CONCENTRATION, (0 - 1)
C           CO2=X(3)   NORMALIZED CO2 EXIT CONCENTRATION, (0 - 1+)
C           COS=X(4)   FRACTIONAL SURFACE COVERAGE BY CO, (0 - 1)
C           OS=X(5)     FRACTIONAL SURFACE COVERAGE BY OXYGEN, (0 - 1/RNY)
C           CO2S=X(6) FRACTIONAL SURFACE COVERAGE BY CO2 ON SUPPORT, (0 - 1)
C           T=X(7)   DIMENSIONLESS SURFACE TEMPERATURE, (0+)
C
C          SUBROUTINES AND FUNCTION SUBPROGRAMS REQUIRED
C             INPUT -   OBTAINS ALL INPUT PARAMETERS FROM DATA FILE
C             RKF45 -   RUNGE-KUTTA-FEHLBERG INTEGRATION OF SYSTEM OF ODE'S
C             DIFEQS - SUBROUTINE CONTAINING THE ODE'S TO BE INTEGRATED BY RKF45
C             CONVT   - SUBROUTINE USED TO DETERMINE PSEUDO-STEADY-STATE TEMPERATURE
C
C       ..........................................................
C
        PARAMETER (NDIM=880)
        DIMENSION Y(7)
        COMMON /P1/ COSH,COSL,K2H,K2L,K3H,K3L
        COMMON /P2/ K4,KM4,A3,RNY,RNX,VQO
        COMMON /P3/ K1,KM1,K2,K3,G1,G2,G3,A1,A2,B1,B2,B3,B4,KMA
        COMMON /P6/ X(7),IPSS(7),ILOC(7)
        EQUIVALENCE (X(1),CO),(X(2),O2),(X(3),CO2)
       *,(X(4),COS),(X(5),OS),(X(6),CO2S),(X(7),T)
        DIMENSION XS(NDIM),YS(NDIM),COSS(NDIM),OSS(NDIM)
        DIMENSION Z2PIS(NDIM),ZS(NDIM),CO2SS(NDIM),TIMES(NDIM)
        DIMENSION FACTCO(4),FACTO2(4),DT(4)
        INTEGER NI(4),NSTART(4),NSTOP(4)
        COMMON /COUNT/ NPINT,ICYLE,NDLAY,NCONV,ITERM
        COMMON /MAN/ AEC,REC,NCYLE,NINT,IPLOT
        COMMON /PARAM2/FCO,AMPCO,FO2,AMPO2,PERIOD,PLEAD
        COMMON /PRT/CONCT,QO,AREA
        COMMON /FCOO2/ FCOT,FO2T
        DATA Y/7*0.0D0/
        DATA Z2PIS/NDIM*0.0D0/
        DATA XS/NDIM*0.0D0/
        DATA YS/NDIM*0.0D0/
        DATA ZS/NDIM*0.0D0/
        DATA COSS/NDIM*0.0D0/
        DATA OSS/NDIM*0.0D0/
        DATA CO2SS/NDIM*0.0D0/
        DATA TIMES/NDIM*0.0D0/
C
C       THIS STATEMENT DISABLES FLOATING-POINT UNDERFLOW ERRORS
C       ON THE FPS ARRAY PROCESSOR
C
        CALL SYS$DISEXC(0,0,0,4)
C
C       THESE OPEN STATEMENTS ARE NECESSARY IF THE AP164 ARRAY
```

```
C       PROCESSOR IS TO BE USED, OTHERWISE, A "C" SHOULD BE
C       PLACED IN COLUMN #1 OF EACH OF THE THREE OPEN STATEMENTS.
C
C            UNIT #3 - DIMENSIONAL MODEL PARAMETERS (I.E. D.MULT6)
C            UNIT #4 - INPUT DEVICE CONTAINING ALL MODEL AND CONTROL PARAMETERS.
C            UNIT #7 - OUTPUT DEVICE RECEIVING TOTAL OUTPUT CONSISTING OF
C                          TIME, CO, O2, CO2, COS, OS, CO2S AND TEMPERATURE.
C            UNIT #8 - OUTPUT DEVICE RECEIVING THE CONVERGED CYCLE
C                          VALUES SUITABLE FOR USE BY THE PLOTTING PROGRAM.
C            UNIT #9 - OUTPUT DEVICE RECEIVING SURFACE CONCENTRATIONS FOR
C                          USE IN CO2 AD/DESORPTION PROGRAM
C
        OPEN(UNIT=3,FILE='D.MULT6',STATUS='OLD')
        OPEN(UNIT=4,FILE='D.BOTH',STATUS='OLD')
        OPEN(UNIT=7,FILE='TOTAL',STATUS='NEW')
        OPEN(UNIT=8,FILE='OUT',STATUS='NEW')
        OPEN(UNIT=9,FILE='SURFACE',STATUS='NEW')
C
C       OBTAIN THE INPUT PARAMETERS FROM THE DATA FILE
C
        CALL INPUT(TIME,H,HMXFR,AER,RER,N,Y)
        IF(NDLAY.GT.0) THEN
            NPINT=0
            NPRINT=0
        ELSE
            NPINT=1
            NPRINT=1
        ENDIF
        ICONV=0
        G2SAVE=G2
        IF(COS.GT.COSH) THEN
            K2=K2H
            K3=K3H
            G2=0.0D0
        ENDIF
            HS=H
            PREC=0.001D0
            IF(PLEAD.LE.PERIOD/2.D0) THEN
                CALL SIGNA(FACTCO,FACTO2,DT,PERIOD,PLEAD)
                IF(PLEAD.LT.PREC*PERIOD) THEN
                    NI(1)=0
                    NI(2)=NINT
                    NI(3)=0
                    NI(4)=NINT
                    DT(2)=PERIOD/2.D0
                    DT(4)=PERIOD/2.D0
                ELSEIF(PLEAD.GT.(1.D0-PREC)*PERIOD/2.D0) THEN
                    NI(1)=NINT
                    NI(2)=0
                    NI(3)=NINT
                    NI(4)=0
                    DT(1)=PERIOD/2.D0
                    DT(3)=PERIOD/2.D0
                ELSE
```

```
                IF(DT(1).LT.DT(2)) THEN
                    NI(1)=NINT
                    NI(3)=NINT
                    NI(2)=MIN(4,MAX(1,INT(DT(2)/(PREC+DT(1)))))*NINT
                    NI(4)=NI(2)
                ELSE
                    NI(2)=NINT
                    NI(4)=NINT
                    NI(1)=MIN(4,MAX(1,INT(DT(1)/(PREC+DT(2)))))*NINT
                    NI(3)=NI(1)
                ENDIF
            ENDIF
        ELSEIF(PLEAD.GT.PERIOD/2.D0) THEN
            CALL SIGNB(FACTCO,FACTO2,DT,PERIOD,PLEAD)
            IF(PLEAD.GT.(1.D0-PREC)*PERIOD) THEN
                NI(1)=0
                NI(2)=NINT
                NI(3)=0
                NI(4)=NINT
                DT(2)=PERIOD/2.D0
                DT(4)=PERIOD/2.D0
            ELSEIF(PLEAD.LT.(1.D0+PREC)*PERIOD/2.D0) THEN
                NI(1)=NINT
                NI(2)=0
                NI(3)=NINT
                NI(4)=0
                DT(1)=PERIOD/2.D0
                DT(3)=PERIOD/2.D0
            ELSE
                IF(DT(1).LT.DT(2)) THEN
                    NI(1)=NINT
                    NI(3)=NINT
                    NI(2)=MIN(4,MAX(1,INT(DT(2)/(PREC+DT(1)))))*NINT
                    NI(4)=NI(2)
                ELSE
                    NI(2)=NINT
                    NI(4)=NINT
                    NI(1)=MIN(4,MAX(1,INT(DT(1)/(PREC+DT(2)))))*NINT
                    NI(3)=NI(1)
                ENDIF
            ENDIF
        ENDIF
        NCOMP=NI(1)+NI(2)+NI(3)+NI(4)+1
        NSTART(1)=2
        DO 10 INS=1,3
            NSTART(INS+1)=NSTART(INS)+NI(INS)
            NSTOP(INS)=NSTART(INS)+NI(INS)-1
10      CONTINUE
        NSTOP(4)=NSTART(4)+NI(4)-1
    IF(ITERM.EQ.0) THEN
        WRITE(*,870) (NI(I),I=1,4)
        WRITE(*,870) (NSTART(I),I=1,4)
        WRITE(*,870) (NSTOP(I),I=1,4)
        WRITE(*,875) (FACTCO(I),I=1,4)
```

```
          WRITE(*,875)  (FACTO2(I),I=1,4)
          WRITE(*,875)  (DT(I),I=1,4)
      ENDIF
 870  FORMAT(4I5)
 875  FORMAT(4(1PG13.5))
      WRITE(9,500)TIME,COS,OS,K2,K3
      DO 200 ICYLE=1,NCYLE
          TIMES(1)=TIME
          XS(1)=Y(1)
          YS(1)=Y(2)
          ZS(1)=Y(3)
          COSS(1)=Y(4)
          OSS(1)=Y(5)
          CO2SS(1)=Y(6)
              DO 80 INI=1,4
                  IFLAG=1
                  H=HS
                  FO2T=(FO2+FACTO2(INI)*AMPO2)/FO2
                  FCOT=(FCO+FACTCO(INI)*AMPCO)/FCO
                  IF(FCOT.LT.0.0D0) FCOT=0.0D0
                  IF(FO2T.LT.0.0D0) FO2T=0.0D0
                  IF(NI(INI).GT.0) DTIME=DT(INI)/FLOAT(NI(INI))
                  DO 70 INS=NSTART(INI),NSTOP(INI)
C
C       IF IFLAG=1, TAKE A NORMAL STEP OF SIZE DTS=DTIME
C       IF IFLAG=-1, UPPER CO SURFACE LEVEL REACHED.  SWITCH K2
C                          VALUE TO K2H AND COMPLETE PREVIOUS STEP
C                          USING DTS VALUE AS DETERMINED BY RKF45.
C       IF IFLAG=-2, LOWER CO SURFACE LEVEL REACHED.  SWITCH K2
C                          VALUE TO K2L AND USE DTS TO COMPLETE STEP.
C
   30 CONTINUE
          IF(IFLAG.EQ.1) THEN
              DTS=DTIME
          ELSEIF(IFLAG.EQ.-1) THEN
              K2=K2H
              K3=K3H
              G2=0.0D0
          ELSEIF(IFLAG.EQ.-2) THEN
              K2=K2L
              K3=K3L
              G2=G2SAVE
          ENDIF
C
C       INTEGRATE ODE'S FROM "TIME" TO "TIME+DTS".
C       IF UPPER OR LOWER CO SURFACE LEVELS ARE REACHED, THEN
C       INTEGRATION IS STOPPED BEFORE "TIME+DTS" AND DTS IS
C       SET EQUAL TO THE REMAINING INTERVAL TO BE INTEGRATED.
C
          CALL RKF45(TIME,Y,N,DTS,H,HMXFR,AER,RER,IFLAG)
       WRITE(9,500) TIME,COS,OS,K2,K3
  500 FORMAT(' ',5(1PD16.7))
       IF(IFLAG.GT.1) GO TO 300
       IF(IFLAG.EQ.-1 .OR. IFLAG.EQ.-2) GO TO 30
```

```
C
                        TIMES(INS)=TIME
                        XS(INS)=Y(1)
                        YS(INS)=Y(2)
                        ZS(INS)=Y(3)
                        COSS(INS)=Y(4)
                        OSS(INS)=Y(5)
                        CO2SS(INS)=Y(6)
                  IF(ICYLE.GT.NDLAY.AND.NPRINT/IPLOT*IPLOT.EQ.NPRINT) THEN
                            WRITE(7,800) TIME,(Y(I),I=1,N)
800                     FORMAT(' ',12(1PD13.5))
810                     FORMAT(' ',7(1PD11.3))
                            IF(ITERM.EQ.0) WRITE(*,810) TIME,(Y(I),I=1,N)
                        ENDIF
                            NPINT=NPINT+1
                            NPRINT=NPRINT+1
 70                 CONTINUE
 80             CONTINUE
            RCO2=0.0D0
            CO2AVG=0.0D0
            DO 90 I=2,NCOMP
        S1=(1.D0-COSS(I-1)-OSS(I-1))*(1.D0-RNX*COSS(I-1))/(1.D0-COSS(I-1))
        S2=(1.D0-COSS(I)-OSS(I))*(1.D0-RNX*COSS(I))/(1.D0-COSS(I))
                RATE1=K1*XS(I-1)*S1-KM1*COSS(I-1)
                RATE2=K1*XS(I)*S2-KM1*COSS(I)
                RCO2=RCO2+0.5D0*(RATE1+RATE2)*(TIMES(I)-TIMES(I-1))
                CO2AVG=CO2AVG+0.5D0*(ZS(I-1)+ZS(I))*(TIMES(I)-TIMES(I-1))
  90        CONTINUE
            RCO2=RCO2/(TIMES(NCOMP)-TIMES(1))
            CO2AVG=CO2AVG/(TIMES(NCOMP)-TIMES(1))
            IF(ITERM.EQ.0) WRITE(*,850) ICYLE,RCO2,CO2AVG
            WRITE(7,850) ICYLE,RCO2,CO2AVG
 850        FORMAT(' CYCLE#',I3,'    RCO2=',1PD11.4,'    CO2AVG=',1PD11.4)
            IF(ICONV.EQ.0) GO TO 160
            ICONV=ICONV+1
            IF(ICONV.EQ.NCONV) GO TO 210
            GO TO 199
160         DO 170 ICOMP=1,NCOMP
            IF(DABS((ZS(ICOMP)-Z2PIS(ICOMP))/(REC*ZS(ICOMP)+AEC))
     *      .GE.1.0D0) GO TO 180
170         CONTINUE
            ICONV=1
            CALL CONV(ICYLE,NCOMP,TIMES,XS,YS,ZS,COSS,OSS,CO2SS,RCO2)
            IF(ICONV.EQ.NCONV) GO TO 210
180         DO 190 ISAVE=1,NCOMP
190         Z2PIS(ISAVE)=ZS(ISAVE)
199         CONTINUE
200     CONTINUE
210     IF(ITERM.EQ.0) WRITE(*,820) NPRINT
820     FORMAT(' ',' # OF POINTS =',I6)
         IF(ITERM.EQ.0) WRITE(*,825) RCO2
825     FORMAT(' ',' CO2 RATE = ',1PD13.5)
         WRITE(7,825) RCO2
         GO TO 310
```

```
300     IF(ITERM.EQ.0) WRITE(*,830) IFLAG,TIME,(Y(I),I=1,N)
830     FORMAT(' ',I3,7(D13.6,1X))
310     WRITE(7,840) NPRINT
840     FORMAT(I6)
          END
```

```
      SUBROUTINE INPUT(TIME,H,HMXFR,AER,RER,N,Y)
      IMPLICIT REAL (A-H,K,O-Z)
C
C     ..........................................................
C
C     SUBROUTINE INPUT
C
C     PURPOSE
C         THIS SUBROUTINE OBTAINS ALL OF THE PARAMETERS FOR
C         THE MODEL EQUATIONS (ODE'S IN SUBROUTINE DIFEQS)
C         AS WELL AS THE CONTROL PARAMETERS FOR DETERMINING
C         THE LENGTH AND THE ACCURACY OF THE INTEGRATION.
C         ALL INPUT PARAMETERS ARE ECHOED TO THE TERMINAL
C         AND TO THE TWO OUTPUT FILES.
C
C     USAGE
C         CALL INPUT(TIME,H,HMXFR,AER,RER,N,Y)
C
C     DESCRIPTION OF THE INPUT PARAMETERS
C     PARAMETER (ARRANGED ACCORDING TO ORDER OF READ STATEMENTS)
C
C         K1      DIMENSIONLESS CO ADSORPTION RATE CONSTANT
C         KM1     DIMENSIONLESS CO DESORPTION RATE CONSTANT
C         G1      DIMENSIONLESS CO DESORPTION ACTIVATION ENERGY
C
C         K2      DIMENSIONLESS O2 ADSORPTION RATE CONSTANT
C         G2      DIMENSIONLESS O2 ADSORPTION ACTIVATION ENERGY
C                  (G2=0 FOR 1X1 SITES AND G2>0 FOR 5X20 SITES)
C         K3      DIMENSIONLESS SURFACE REACTION RATE CONSTANT
C         G3      DIMENSIONLESS SURFACE REACTION ACTIVATION ENERGY
C
C         B1      DIMENSIONLESS DELTA T FOR CO ADSORPTION
C         B2      DIMENSIONLESS DELTA T FOR O2 ADSORPTION
C         B3      DIMENSIONLESS DELTA T FOR SURFACE REACTION
C
C         B4      DIMENSIONLESS HEAT TRANSFER COEFFICIENT
C         A1      RATIO OF VOLUME TO SURFACE CAPACITANCES FOR CO
C         A2      RATIO OF VOLUME TO SURFACE CAPACITANCES FOR O2
C
C         FCO     FRACTION OF CO IN THE REACTOR FEED, (0 - 1)
C         FO2     FRACTION OF O2 IN THE REACTOR FEED, (0 - 1)
C         RNY      CO ADSORPTION SITES / O2 ADSORPTION SITES, (1 - 2)
C
C         CO      INITIAL CO CONCENTRATION IN THE REACTOR (0-1)
C         O2      INITIAL O2 CONCENTRATION IN THE REACTOR (0-1)
C         CO2     INITIAL CO2 CONCENTRATION IN THE REACTOR (0-1+)
C         COS     INITIAL FRACTIONAL CO SURFACE COVERAGE (0-1)
C         OS      INITIAL FRACTIONAL OXYGEN SURFACE COVERAGE (0-1/RNY)
C         T        INITIAL TEMPERATURE OF THE METAL CRYSTALLITES (0-0+)
C
C         COSH   UPPER LEVEL OF CO SURFACE COVERAGE AT WHICH K2 BECOMES K2H
(0-1)
C         COSL   LOWER LEVEL OF CO SURFACE COVERAGE AT WHICH K2 BECOMES K2L
(0-1)
```

```
C            K2H    K2 VALUE USED AFTER COS REACHES COSH FROM BELOW.
C            K2L    K2 VALUE USED AFTER COS REACHES COSL FROM ABOVE.
C            K3H    K3 VALUE USED AFTER COS REACHES COSH FROM BELOW.
C            K3L    K3 VALUE USED AFTER COS REACHES COSL FROM ABOVE.
C            ICOS   ELEMENT LOCATION OF COS IN Y VECTOR (PRESENTLY 4).
C
C            TIME   INITIAL TIME FOR THE INTEGRATION (USUALLY 0)
C            H       INITIAL VALUE OF INTERNAL RKF45 INTEGRATION STEP.
C            HMXFR  MAXIMUM FRACTION OF STEPSIZE TO BE USED INTERNALLY BY RKF45.
C            AER     ABSOLUTE LOCAL ERROR TOLERANCE FOR RKF45.
C            RER     RELATIVE LOCAL ERROR TOLERANCE FOR RKF45.
C                     (IN RKF45, ABS(EST. ERROR) < RER*ABS(Y(I))+AER)
C
C           ITERM   0 - OUTPUT IS PRODUCED AT THE TERMINAL.
C                     1 - NO TERMINAL OUTPUT IS PRODUCED.
C           VQO    REACTOR RESIDENCE TIME (VOLUME/VOLUMETRIC FLOW RATE)
C
C           NINT   NUMBER OF INTEGRATION STEPS OF SIZE DTIME TO BE TAKEN
C           IPLOT  OUTPUT IS PRODUCED FOR EVERY "IPLOT-TH" INTEGRATION STEP
C           NDLAY  SUPPRESSES ALL OUTPUT FOR NDLAY INTEGRATION INTERVALS.
C
C           K4      DIMENSIONLESS CO2 ADSORPTION RATE CONSTANT (TO SUPPORT)
C           KM4    DIMENSIONLESS CO2 DESORPTION RATE CONSTANT (FROM SUPPORT)
C           A3      RATIO OF VOLUME TO SUPPORT SURFACE CAPACITANCES FOR CO2
C           CO2S   INITIAL CO2 FRACTIONAL SURFACE COVERAGE ON SUPPORT (0-1)
C
C       ..........................................................
C
        DIMENSION Y(7)
        COMMON /P1/ COSH,COSL,K2H,K2L,K3H,K3L
        COMMON /P2/ K4,KM4,A3,RNY,RNX,VQO
        COMMON /P3/ K1,KM1,K2,K3,G1,G2,G3,A1,A2,B1,B2,B3,B4,KMA
        COMMON /COUNT/ NPINT,ICYLE,NDLAY,NCONV,ITERM
        COMMON /MAN/ AEC,REC,NCYLE,NINT,IPLOT
        COMMON /PARAM2/FCO,AMPCO,FO2,AMPO2,PERIOD,PLEAD
        COMMON /P6/ X(7),IPSS(7),ILOC(7)
        EQUIVALENCE (X(1),CO),(X(2),O2),(X(3),CO2)
       *,(X(4),COS),(X(5),OS),(X(6),CO2S),(X(7),T)
C
C       OBTAIN INPUT FROM DATA FILE ATTACHED TO UNIT #4
C
        READ(4,*) IDIM
C
C     IF IDIM=0 THEN DIMENSIONLESS INPUT, BUT,
C     IF IDIM=1 THEN DIMENSIONAL INPUT (FROM D.MULT6)
C
        IF(IDIM.EQ.0) THEN
            READ(4,*) K1,KM1,G1
            READ(4,*) K2,G2,K3,G3
            READ(4,*) B1,B2,B3
            READ(4,*) B4,A1,A2
            READ(4,*) FCO,FO2,RNY,RNX,VQO
            VQO=VQO/60.D0
            READ(4,*) CO,O2,CO2,COS,OS,T
```

```
            READ(4,*) COSH,COSL,K2FAC,K3FAC,ERCOSH
            COSH=COSH*DEXP(ERCOSH/TO-ERCOSH/393.D0)
            K2L=K2
            K2H=K2*K2FAC
            K3L=K3
            K3H=K3*K3FAC
            READ(4,*) TIME,H,HMXFR,AER,RER
            READ(4,*) (IPSS(I),I=1,7)
            READ(4,*) NINT,IPLOT,NDLAY,ITERM
            IF(IPSS(6).EQ.1) THEN
                READ(4,*) K4,KM4,A3
                CO2S=K4*CO2/(K4*CO2+KM4)
            ELSE
                CO2S=0.0D0
            ENDIF
        ELSEIF(IDIM.EQ.1) THEN
C 900       FORMAT(//,3D40.16,/)
C 901       FORMAT(//,4D40.16,/)
C905       FORMAT(//,I20,I50,//)
C910       FORMAT(I8,D40.16)
C
C           READ THE VALUES OF THE PARAMETERS
C
C         READ(3,899)
C 899   FORMAT(/////////)
            READ(3,*) COP,RKM1,E1R
            READ(3,*) O2P,E2R,RK3,E3R
            READ(3,*) A,V,RL
            READ(3,*) RMASS,CP,U
            READ(3,*) TO,PO,QMOL
            READ(3,*) DH3,FCOOLD,FO2OLD
            READ(3,*) RNY,RNX,FFMT
            READ(4,*) CO,O2,CO2,COS,OS,T
            READ(4,*) TIME,H,HMXFR,AER,RER
            READ(4,*) (IPSS(I),I=1,7)
            READ(4,*) COSH,COSL,K2FAC,K3FAC,ERCOSH
            READ(4,*) NINT,IPLOT,NDLAY,ITERM
        READ(4,*) NCYLE,AEC,REC,NCONV
        READ(4,*) FCO,AMPCO,FO2,AMPO2,PERIOD,PLAG
        PERIOD=PERIOD/60.D0
        PLAG=PLAG/60.D0
        PLEAD=PERIOD-PLAG
C
C         UNLESS IT IS DESIRED TO VARY FO2 (E.G. ADDITION OF INERTS),
C         THE VALUE OF FO2 IS ADJUSTED TO BE CONSISTENT WITH THE
C         EXPERIMENTAL SET-UP (PURE O2 WITH 11%CO IN N2).
C
            IF(FCO+FO2.GT.1.0D0) FO2=1.0D0-100.D0*FCO/11.D0
C
C         THE ENTHALPY CHANGES ARE CALCULATED USING THE KNOWN
C         VALUE FOR CO OXIDATION (DHR), AND WITH THE ASSUMPTION:
C         DELTA H FOR CO DESORPTION = CO DESORPTION ACTIVATION ENERGY
C
            DH1=E1R*8.314D0
```

```
      DHR=(-66772.D0-4.4525D0*TO+6.035D-03*TO*TO-2.93D-06*TO**3
     *  +5.395D-10*TO**4)*4.184D0*(-1.D0)
      DH2=DHR-(DH1+DH3)
C
C     USE THE INPUT PARAMETERS TO DETERMINE VALUES FOR THE
C     DIMENSIONLESS PARAMETERS.
C
      CONCT=PO/(8.314D0*TO)
      QO=QMOL/CONCT
      VQO=V/(QO*60.D0)
      G1=E1R/TO
      G2=E2R/TO
      G3=E3R/TO
      RK1=6.87D0*COP*DSQRT(TO)/RL
      RK2=6.43D0*O2P*DSQRT(TO)/(RL*RL)
      K1=RK1*A*RL/QO
      K2=RK2*A*RL**2*DEXP(-G2)/QO
      K3=RK3*A*RL**2*DEXP(-G3)/(QO*CONCT*FCO)
      KM1=RKM1*A*RL*DEXP(-G1)/(QO*CONCT*FCO)
    KMA=0.0423*36.61*((1.3D-04)**0.641D0)*(TO**0.629D0)*FFMT
     *  /((PO**0.359D0)*QO)
      B1=DH1*V*CONCT*FCO/(RMASS*CP*TO)
      B2=DH2*V*CONCT*FO2/(RMASS*CP*TO)
      B3=DH3*V*CONCT*FCO/(RMASS*CP*TO)
      B4=V*U*A/(RMASS*CP*QO)
      A1=V*CONCT*FCO/(A*RL)
      A2=2.D0*V*CONCT*FO2/(A*RL)
      COSH=COSH*DEXP(ERCOSH/TO-ERCOSH/393.D0)
      K2L=K2
      K2H=K2*K2FAC
      K3L=K3
      K3H=K3*K3FAC
      IF(IPSS(6).EQ.1) THEN
          READ(4,*) CO2P,RKM4,E4R,ASUP,RLSUP
          G4=E4R/TO
          RK4=5.48D0*CO2P*DSQRT(TO)/RLSUP
          K4=ASUP*RLSUP*RK4/QO
          KM4=ASUP*RLSUP*RKM4*DEXP(-G4)/(QO*CONCT*FCO)
          A3=V*CONCT*FCO/(ASUP*RLSUP)
          CO2S=K4*CO2/(K4*CO2+KM4)
      ELSE
          CO2S=0.0D0
      ENDIF
    ELSE
      IF(ITERM.EQ.0) WRITE(*,*) '** ERROR ** IDIM MUST BE 0 OR 1'
    ENDIF
C
C   DETERMINE THE CORRECT INITIAL VALUES TO USE FOR
C   THE X VECTOR DEPENDING ON THE CHOICE OF THE VARIOUS
C   PSEUDO-STEADY-STATE APPROXIMATIONS.
C
    RKM1=KM1*DEXP(G1*T)
    RK2=K2*DEXP(G2*T)
    RK3=K3*DEXP(G3*T)
```

```
C
C       PROTECT AGAINST NEGATIVE SURFACE CONCENTRATIONS, AND
C       AGAINST POSSIBLE DIVISIONS BY ZERO.
C
        IF(1.D0-COS-OS .LT. 0.0D0) THEN
            SCO=0.0D0
            SO2=0.0D0
        ELSE
            SCO=1.D0-COS-OS
            IF(1.D0-OS .LE. 0.D0) THEN
                SO2=0.0D0
            ELSE
                SO2=(1.D0-COS-OS)*(1.D0-RNY*OS)/(1.D0-OS)
            ENDIF
        ENDIF
        IF(IPSS(7).EQ.-1) THEN
            T=0.0D0
        ELSEIF(IPSS(7).EQ.0) THEN
            CALL CONVT
        ENDIF
C
C     DETERMINE THE NUMBER OF ODE'E TO INTEGRATE, AND PLACE
C     THE INITIAL VALUES INTO THE CORRECT LOCATIONS IN THE
C     Y VECTOR WHICH WILL BE USED BY RKF45.
C
        N=0
        DO 10 I=1,7
            ILOC(I)=0
            IF(IPSS(I).GE.1) THEN
                N=N+1
                Y(N)=X(I)
                ILOC(I)=N
            ENDIF
   10   CONTINUE
C
C       ECHO INPUT PARAMETERS TO THE TERMINAL
C
        WRITE(*,800) K1,KM1,G1,KMA
        WRITE(*,805) K2,G2,K3,G3
        WRITE(*,810) B1,B2,B3
        WRITE(*,815) B4,A1,A2
        WRITE(*,820) FCO,FO2,AMPCO,AMPO2
        WRITE(*,822) RNY,RNX,VQO
        IF(IPSS(6).EQ.1) WRITE(*,825) K4,KM4,A3,CO2S
        WRITE(*,830) CO,O2,CO2
        WRITE(*,835) COS,OS,T
        WRITE(*,840) COSH,COSL,K2FAC,K3FAC  ,ERCOSH
        WRITE(*,842) PERIOD*60.,PLAG*60.
        WRITE(*,845) TIME,H
        WRITE(*,850) HMXFR,AER,RER
        WRITE(*,855) N,ITERM,NINT,IPLOT,NDLAY
        WRITE(*,890) (IPSS(I),I=1,7)
        WRITE(*,860)
C
```

```
C       ECHO INPUT PARAMETERS TO OUTPUT UNIT #8
C
        WRITE(8,800) K1,KM1,G1,KMA
        WRITE(8,805) K2,G2,K3,G3
        WRITE(8,810) B1,B2,B3
        WRITE(8,815) B4,A1,A2
        WRITE(8,820) FCO,FO2,AMPCO,AMPO2
        WRITE(8,822) RNY,RNX,VQO
        IF(IPSS(6).EQ.1) WRITE(8,825) K4,KM4,A3,CO2S
        WRITE(8,830) CO,O2,CO2
        WRITE(8,835) COS,OS,T
        WRITE(8,840) COSH,COSL,K2FAC,K3FAC  ,ERCOSH
        WRITE(8,842) PERIOD*60.,PLAG*60.
        WRITE(8,845) TIME,H
        WRITE(8,850) HMXFR,AER,RER
        WRITE(8,855) N,ITERM,NINT,IPLOT,NDLAY
        WRITE(8,890) (IPSS(I),I=1,7)
        WRITE(8,860)
C
C       ECHO INPUT PARAMETERS TO OUTPUT UNIT #7
C
        WRITE(7,800) K1,KM1,G1,KMA
        WRITE(7,805) K2,G2,K3,G3
        WRITE(7,810) B1,B2,B3
        WRITE(7,815) B4,A1,A2
        WRITE(7,820) FCO,FO2,AMPCO,AMPO2
        WRITE(7,822) RNY,RNX,VQO
        IF(IPSS(6).EQ.1) WRITE(7,825) K4,KM4,A3,CO2S
        WRITE(7,830) CO,O2,CO2
        WRITE(7,835) COS,OS,T
        WRITE(7,840) COSH,COSL,K2FAC,K3FAC  ,ERCOSH
        WRITE(7,842) PERIOD*60.,PLAG*60.
        WRITE(7,845) TIME,H
        WRITE(7,850) HMXFR,AER,RER
        WRITE(7,855) N,ITERM,NINT,IPLOT,NDLAY
        WRITE(7,890) (IPSS(I),I=1,7)
        WRITE(7,860)
        IF(NDLAY.GT.0) RETURN
        WRITE(7,870) TIME,(X(I),I=1,7)
        RETURN
  800   FORMAT(T4,'K1=',1PG12.4,T21,'K-1=',1PG12.4,T41,'G1=',1PG12.4,
       *T59,'KMA=',1PG12.4)
  805   FORMAT(T4,'K2=',1PG12.4,T22,'G2=',1PG12.4,T41,'K3=',1PG12.4,
       *T60,'G3=',1PG12.4)
  810   FORMAT(T4,'B1=',1PG12.4,T22,'B2=',1PG12.4,T41,'B3=',1PG12.4)
  815   FORMAT(T4,'B4=',1PG12.4,T22,'A1=',1PG12.4,T41,'A2=',1PG12.4)
  820   FORMAT(T3,'FCO=',1PG12.4,T21,'FO2=',1PG12.4,T38,'AMPCO=',1PG12.4,
       *T57,'AMPO2=',1PG12.4)
  822   FORMAT(T3,'RNY=',1PG12.4,T21,'RNX=',1PG12.4,T41,'VQO=',1PG12.4)
  825   FORMAT(T4,'K4=',1PG12.4,T21,'K-4=',1PG12.4,T41,'A3=',1PG12.4,
       *T58,'CO2S=',1PG12.4)
  830   FORMAT(T4,'CO=',1PG12.4,T22,'O2=',1PG12.4,T40,'CO2=',1PG12.4)
  835   FORMAT(T3,'COS=',1PG12.4,T22,'OS=',1PG12.4,T42,'T=',1PG12.4)
  840   FORMAT(T2,'COSH=',1PG12.4,T20,'COSL=',1PG12.4,T38,'K2FAC=',
```

```
     *1PG12.4,T57,'K3FAC=',1PG12.4,T77,'ERCOSH=',1PG12.4)
842  FORMAT(T2,'PERIOD=',1PG12.4,T21,'LAG=',1PG12.4)
845  FORMAT(T4,'TIME=',1PG12.4,T23,'H=',1PG12.4,T42,'    ',1PG12.4)
850  FORMAT(T3,'HMXFR=',1PG12.4,T21,'AER=',1PG12.4,T40,'RER=',1PG12.4)
855  FORMAT(' N=',I1,3X,'ITERM=',I1,3X,'NINT=',I4,3X,
     *'IPLOT=',I2,3X,'NDLAY=',I4)
860  FORMAT(' ')
870  FORMAT(12(1PG13.5,','))
890  FORMAT(' ICO=',I2,3X,'IO2=',I1,3X,'ICO2=',I1,3X,
     *'ICOS=',I1,3X,'IOS=',I1,3X,'ICO2S=',I1,3X,'IT=',I2)
      END
```

```
      SUBROUTINE RKF45(A,Y,N,DA,H,HMXFR,ABSER,RELER,IFLAG)
      IMPLICIT REAL (A-H,K,O-Z)
C
C     ..........................................................
C
C     SUBROUTINE RKF45
C
C     PURPOSE
C         INTEGRATION OF A SYSTEM OF N ORDINARY DIFFERENTIAL EQUATIONS
C         USING A RUNGE-KUTTA-FEHLBERG METHOD.  A FIFTH ORDER RUNGE-
C         KUTTA PROCEDURE IS USED FOR THE INTEGRATION, AND THE LOCAL
C         ERROR IS CONTROLLED BY ADJUSTING THE INTEGRATION STEP-SIZE.
C         THE LOCAL ERROR IS MEASURED AS THE DIFFERENCE BETWEEN THE
C         FIFTH ORDER SCHEME AND A FOURTH ORDER SCHEME.
C
C     USAGE
C         CALL RKF45(A,Y,N,DA,HMXFR,ABSER,RELER,IFLAG)
C
C     DESCRIPTION OF THE PARAMETER LIST
C
C        A      -ON INPUT THE INITIAL VALUE OF THE INDEPENDENT VARIABLE.
C                 ON OUTPUT THE LAST VALUE AT WHICH A SOLUTION WAS
C                 SUCCESSFULLY COMPUTED.  NORMAL OUTPUT HAS A INCREASED BY DA.
C        Y      -ON INPUT THE VECTOR OF INITIAL VALUES OF THE DEPENDENT
C                 VARIABLES.  ON OUTPUT THE VECTOR OF COMPUTED SOLUTIONS
C                 AT OUTPUT VALUE OF A.
C        N      -NUMBER OF EQUATIONS TO BE INTEGRATED.
C        F      -SUBROUTINE OF THE FORM  F(A,Y,YP)  WHICH ACCEPTS INDEPENDENT
C                 VARIABLE A AND A VECTOR OF DEPENDENT VARIABLES Y, AND
C                 FURNISHES A VECTOR OF VALUES OF THE DERIVATIVES YP.
C                 IN VECTOR FORM THE DIFFERENTIAL EQUATIONS SOLVED ARE:
C
C                        DY/DX = YP   ,    Y(A)=Y
C
C        DA    -INTEGRATION IS TO PROCEED FROM A TO A+DA. DA CAN BE NEGATIVE.
C        H      -NOMINAL STEP-SIZE ON INPUT.  ON OUTPUT IT IS REPLACED BY THE
C                 OPTIMAL VALUE CURRENTLY BEING USED.  H CAN BE NEGATIVE.
C        HMX   -UPPER BOUND ON STEP-SIZE TO BE USED. HMX CAN BE NEGATIVE.
C        HMXFR-MAXIMUM FRACTION OF STEP-SIZE TO BE USED.
C        ABSER-ABSOLUTE LOCAL ERROR TO BE TOLERATED.
C        RELER-RELATIVE LOCAL ERROR TO BE TOLERATED.
C
C                 ABS(EST. LOCAL ERROR) < ABS(H)*(RELER*ABS(Y(I))+ABSER)
C
C        IFLAG   -2  LOWER CO SURFACE VALUE REACHED FROM ABOVE (K2 NOW K2L)
C                  -1  UPPER CO SURFACE VALUE REACHED FROM BELOW (K2 NOW K2H)
C                   1  NORMAL RETURN, INTEGRATION REACHED A+DA
C                   2  HMX, H AND DA ARE NOT ALL OF THE SAME SIZE ON INPUT.
C                   3  RELER<0, OR ABSER<0, OR RELER+ABSER=0 ON INPUT
C                   4  DA IS TOO SMALL RELATIVE TO COMPUTER PRECISION.
C                   5  H HAS BECOME INSIGNIFICANT RELATIVE TO A (PRECISION
PROBLEM).
C        SUBROUTINES AND FUNCTION SUBPROGRAMS REQUIRED
C            F - SUBROUTINE CONTAINING ODE'S TO BE INTEGRATED
```

```
C                    THE "TRUE" NAME OF F MUST BE DECLARED EXTERNAL
C                    IN THE PROGRAM SEGMENT WHICH CALLS RKF45.
C                     IT IS NOW DIFEQS
C
C
C          REFERENCES
C              SHAMPINE, L.F. AND R.C. ALLEN, NUMERICAL COMPUTING:
C                    AN INTRODUCTION, SAUNDERS, TORONTO, 1973.
C              FEHLBERG, E., "CLASSICAL FOURTH- AND LOWER ORDER RUNGE-KUTTA
C                    FORMULAS WITH STEP-SIZE CONTROL AND THEIR APPLICATION TO
C                    HEAT TRANSFER PROBLEMS", COMPUTING 6, 61-71 (1970).
C
C       ..........................................................
C
        DIMENSION Y(7),YTEMP(7),TEMP(7),R(7),DOUT(8)
        DIMENSION FUN1(7),FUN2(7),FUN3(7),FUN4(7),FUN5(7),FUN6(7)
        COMMON /P1/ COSH,COSL,K2H,K2L,K3H,K3L
        COMMON /P2/ K4,KM4,A3,RNY,RNX,VQO
        COMMON /P3/ K1,KM1,K2,K3,G1,G2,G3,A1,A2,B1,B2,B3,B4,KMA
        COMMON /COUNT/ NPINT,ICYLE,NDLAY,NCONV,ITERM
        COMMON /MAN/ AEC,REC,NCYLE,NINT,IPLOT
        COMMON /P6/ X(7),IPSS(7),ILOC(7)
C
C       U IS APPROXIAMTELY EQUAL TO THE MACHINE PRECISION
C       B IS THE END-POINT OF THE INTEGRATION INTERVAL
C       IADJS IS SET TO 1 WHEN THE END OF THE INTERVAL IS REACHED
C
        U=1.0D-16
        HMX=HMXFR*DA
        HEXP=0.2D0
        HATMPT=0.75D0
        B=A+DA
        IADJS=0
        ASV=A
C
C       CHECK FOR THE ERROR CONDITIONS 2, 3 AND 4
C
        IF(HMX*DA.LE.0.0D0 .OR. HMX*H.LT.0.0D0) THEN
            IFLAG=2
            RETURN
        ENDIF
        IF(RELER.LT.0.0D0 .OR. ABSER.LT.0.0D0
     *      .OR. RELER+ABSER.EQ.0.0D0) THEN
            IFLAG=3
            RETURN
        ENDIF
        IF(IFLAG.GE.0 .AND. DABS(DA).LE.13.D0*U*DABS(A)) THEN
            IFLAG=4
            RETURN
C       ELSE
C           IFLAG=0
        ENDIF
C
C       ADJUST THE INITIAL AND THE MAXIMUM STEP-SIZES IF NECESSARY
```

```
C
      IF(DABS(HMX).GT.DABS(DA)) THEN
          HMAX=DA
      ELSE
          HMAX=HMX
      ENDIF
      IF(DABS(H).LE.13.0D0*U*DABS(A)) H=HMAX/100.D0
C
C     THIS IS THE BEGINNING OF THE INTEGRATION LOOP.
C     WHEN A PARTICULAR STEP IS ACCEPTED, THE CALCULATIONS FOR
C     THE NEXT STEP BEGINS HERE.
C
   10 CONTINUE
      IMAX=0
      IF(DABS(H) .GT. DABS(HMAX)) H=HMAX
      IF(DABS(B-A) .LE. DABS(H)/(HATMPT**HEXP)) THEN
C
C     SET PARAMETERS TO INDICATE THAT THE LAST STEP IS BEING TAKEN
C
          HKEEP=H
          IADJS=1
          H=B-A
      ENDIF
C
C     OBTAIN THE DERIVATIVE VALUES (IN FUN1) BASED ON THE
C     INDEPENDENT VARIABLE=A AND THE DEPENDENT VARIABLES=Y(I)
C
      CALL DIFEQS(A,Y,FUN1)
   20 CONTINUE
C
C     IF A STEP IS REJECTED DUE TO A LARGE ERROR, THE STEP
C     IS REPEATED WITH A SMALLER H STARTING AT THIS POINT.
C
      DO 30 I=1,N
          YTEMP(I)=Y(I)+0.25D0*H*FUN1(I)
   30 CONTINUE
      ARG=A+0.25D0*H
      CALL DIFEQS(ARG,YTEMP,FUN2)
      DO 40 I=1,N
          YTEMP(I)=Y(I)+H*(FUN1(I)*(3.D0/32.D0)+FUN2(I)*(9.D0/32.D0))
   40 CONTINUE
      ARG=A+H*(3.D0/8.D0)
      CALL DIFEQS(ARG,YTEMP,FUN3)
      DO 50 I=1,N
          YTEMP(I)=Y(I)+H*(FUN1(I)*(1932.D0/2197.D0)
     *                -FUN2(I)*(7200.D0/2197.D0)+FUN3(I)*(7296.D0/2197.D0))
   50 CONTINUE
      ARG=A+H*(12.D0/13.D0)
      CALL DIFEQS(ARG,YTEMP,FUN4)
      DO 60 I=1,N
          YTEMP(I)=Y(I)+H*(FUN1(I)*(439.D0/216.D0)-8.D0*FUN2(I)
     *                +FUN3(I)*(3680.D0/513.D0)-FUN4(I)*(845.D0/4104.D0))
   60 CONTINUE
      ARG=A+H
```

```
      CALL DIFEQS(ARG,YTEMP,FUN5)
      DO 70 I=1,N
          YTEMP(I)=Y(I)+H*(-FUN1(I)*(8.D0/27.D0)+2.D0*FUN2(I)
     *                 -FUN3(I)*(3544.D0/2565.D0)+FUN4(I)*(1859.D0/4104.D0)
     *                 -FUN5(I)*(11.D0/40.D0))
 70   CONTINUE
      ARG=A+0.5D0*H
      CALL DIFEQS(ARG,YTEMP,FUN6)
      DO 80 I=1,N
          TEMP(I)=FUN1(I)*(16.D0/135.D0)+FUN3(I)*(6656.D0/12825.D0)
     *                 +FUN4(I)*(28561.D0/56430.D0)-0.18D0*FUN5(I)
     *                 +FUN6(I)*(2.D0/55.D0)
C
C     YTEMP WILL NOW CONTAIN THE VALUES OF THE
C     INDEPENDENT VARIABLES AT THE END OF THE STEP.
C
          YTEMP(I)=Y(I)+H*TEMP(I)
 80   CONTINUE
C
C      THE R(I) TERMS ARE THE (LOCAL ERROR)/H ESTIMATES
C      FOR EACH OF THE VARIABLES.
C
      DO 90 I=1,N
          R(I)=FUN1(I)/360.D0-FUN3(I)*(128.D0/4275.D0)
     *     -FUN4(I)*(2197.D0/75240.D0)+FUN5(I)/50.D0+FUN6(I)*(2.D0/55.D0)
 90   CONTINUE
C
C      DETERMINE THE MAXIMUM RATIO BETWEEN THE ESTIMATED ERRORS
C      AND THE MAXIMUM ALLOWABLE (DESIRED) ERROR.
C
      RATIO=0.0D0
      DO 100 I=1,N
          TR=DABS(R(I))/(RELER*DABS(YTEMP(I))+ABSER)
          IF(RATIO.LT.TR) RATIO=TR
100   CONTINUE
C
C      IF RATIO>1, THEN THE STEP MUST BE REJECTED, AND THE INTEGRATION
C      MUST BE ATTEMPTED AGAIN WITH A SMALLER STEP-SIZE.
C
      IF(RATIO.GT.1.D0) THEN
          IF(RATIO.GT.4096.D0) RATIO=4096.D0
          H=H*(HATMPT/RATIO)**HEXP
          IADJS=0
C
C      IF H HAS BECOME SO SMALL THAT IT IS LESS THAN THE
C      COMPUTER'S PRECISION WHEN COMPARED TO A, THEN RETURN
C      WITH AN ERROR CODE.
C
C         IF(IFLAG.GE.0 .AND. DABS(H) .LE. 13.D0*U*DABS(A)) THEN
C             IFLAG=5
C             RETURN
C         ENDIF
          GO TO 20
      ELSE
```

```
C
C       IF RATIO<=1, THEN THE REQUESTED ACCURACY WAS ACHIEVED.
C
C       CHECK IF THE CO SURFACE CONCENTRATION HAS EXCEEDED THE
C       UPPER BOUND OR DECREASED BELOW THE LOWER BOUND.
C       IF IT HAS, THEN SET THE APPROPRIATE FLAG, AND DECREASE
C       H SO THAT THE BOUND IS MET EXACTLY.
C
            YOLD=Y(ILOC(4))
            YNEW=YTEMP(ILOC(4))
            IF(((YOLD.LT.COSH) .AND. (YNEW.GE.COSH)   .OR.
     *       (YOLD.GT.COSL) .AND. (YNEW.LE.COSL)) .AND. IFLAG.GE.0) THEN
                IF(IADJS.EQ.0 .AND. IFLAG.GE.0) HKEEP=H
                IADJS=0
                IF((YOLD.LT.COSH).AND.(YNEW.GE.COSH)) THEN
                     IFLAG=-1
                     COSHL=COSH
                ELSE
                     IFLAG=-2
                     COSHL=COSL
                ENDIF
                FRAC=(COSHL-YOLD)/(YNEW-YOLD)
                IF(FRAC.GE.1.D0-13.D0*U) THEN
                     DO 110 I=1,N
                          Y(I)=YTEMP(I)
 110                CONTINUE
                ELSEIF(FRAC*H.GT.13.D0*U*DABS(A)) THEN
                     H=H*FRAC
            IFLAG=0
                     GO TO 20
                ENDIF
                DA=B-A
                IF(DABS(DA).LT.13.D0*U*DABS(A)) DA=B-ASV+DA
                H=HKEEP/20.D0
                IF(IPSS(4).EQ.1) Y(ILOC(4))=COSHL
                RETURN
            ENDIF
            IF(IPINT.GT.NDLAY) THEN
C
C       DETERMINE IF THE CO OR CO2 CONCENTRATION HAS PASSED THROUGH
C       A MAXIMUM OR A MINIMUM DURING THE INTEGRATION STEP.
C       IF THIS HAS OCCURRED, THEN DETERMINE AND WRITE OUT THE
C       VARIABLES AT THE MAXIMUM.
C
            DO 130 I=3,3
                IF(FUN1(I)*FUN5(I) .LE. 0.0D0 .AND. DABS(FUN1(I)).GT.100.D0*U
     *          .AND. DABS(FUN1(I)-FUN5(I)).GT.100.D0*U .AND. IMAX.EQ.0) THEN
                     DOUT(1)=A*VQO
                     HMIMA=DABS(FUN1(I)/(FUN1(I)-FUN5(I)))
                     DO 120 JJ=1,N
                          DOUT(JJ+1)=Y(JJ)+HMIMA*(YTEMP(JJ)-Y(JJ))
 120                 CONTINUE
C                    WRITE(8,900) DOUT(1),(DOUT(JJ),JJ=2,4,2)
C                    IF(ITERM.EQ.0) WRITE(*,830) DOUT(1),(DOUT(JJ+1),JJ=1,N)
```

```
C900                FORMAT(11(1PG13.5,','))
C830                FORMAT(F8.3,6F9.6,F12.9)
                      NPINT=NPINT+1
                      IMAX=3
                  ENDIF
 130        CONTINUE
         ENDIF
C
C        ACCEPT THE VALUES OF THE STEP, AND RETURN IF THE ENTIRE
C        INTERVAL HAS BEEN COMPLETED.   OTHERWISE, PERFORM THE
C        INTEGRATION FOR THE NEXT STEP.
C
         DO 140 I=1,N
             Y(I)=YTEMP(I)
 140   CONTINUE
         A=A+H
         IF(IADJS.EQ.1) THEN
             IFLAG=1
             H=HKEEP
             RETURN
         ENDIF
         IF(IFLAG.GE.0) THEN
             IF(RATIO.LT.6.5536D-04) RATIO=6.5536D-04
             H=H*(HATMPT/RATIO)**HEXP
         ELSE
             IFLAG=0
         ENDIF
         GO TO 10
         ENDIF
         RETURN
         END
```

```
      SUBROUTINE DIFEQS(TIME,Y,YP)
      IMPLICIT REAL (A-H,K,O-Z)
C
C     ..........................................................
C
C     SUBROUTINE DIFEQS
C
C     PURPOSE
C         CALCULATES VALUES OF THE RIGHT-HAND SIDES OF THE
C         DIFFERENTIAL EQUATIONS WHEN SUPPLIED WITH VALUES
C         OF THE INDEPENDENT AND DEPENDENT VARIABLES.
C         IN VECTOR FORM, THE ODE'S ARE OF THE FORM:
C
C                YP(I) = FUNCTION(TIME,Y(I))
C
C     USAGE
C         CALL DIFEQS(TIME,Y,YP)
C
C     DESCRIPTION OF THE VARIABLES IN THE PARAMETER LIST
C         TIME   - VALUE OF THE INDEPENDENT VARIABLE
C         Y      - VALUES OF THE I INDEPENDENT VARIABLES
C         YP     - CALCULATED VALUES OF THE I DERIVATIVES
C
C     RESTRICTIONS
C         THE NAME DIFEQS MUST BE DECLARED EXTERNAL
C
C     FUNCTIONS AND SUBROUTINES REQUIRED
C         CONVT - SUBROUTINE USED TO DETERMINE THE PSEUDO-STEADY-STATE TEMPERATURE
C
C     ..........................................................
C
      DIMENSION Y(7),YP(7),XP(7)
      COMMON /P2/ K4,KM4,A3,RNY,RNX,VQO
      COMMON /P3/ K1,KM1,K2,K3,G1,G2,G3,A1,A2,B1,B2,B3,B4,KMA
      COMMON /P5/ NINT,IPLOT,N
      COMMON /FCOO2/ FCOT,FO2T
      COMMON /P6/ X(7),IPSS(7),ILOC(7)
      COMMON /PARAM2/FCO,AMPCO,FO2,AMPO2,PERIOD,PLEAD
      EQUIVALENCE (X(1),COB),(X(2),O2),(X(3),CO2)
     *,(X(4),COS),(X(5),OS),(X(6),CO2S),(X(7),T)
      EQUIVALENCE (XP(1),DCOB),(XP(2),DO2),(XP(3),DCO2)
     *,(XP(4),DCOS),(XP(5),DOS),(XP(6),DCO2S),(XP(7),DT)
C
C     ESTABLISH THE EQUIVALENCE BETWEEN THE QUANTITIES IN THE
C     Y-VECTOR AND THE PHYSICAL QUANTITIES CO, O2, CO2, COS, OS,
C     CO2S, AND T.  USE THE PSEUDO-STEADY-STATE RELATIONSHIPS
C     WHERE NECESSARY TO DETERMINE MISSING QUANTITIES.
C
      DO 10 I=1,7
          IF(ILOC(I).NE.0) THEN
              X(I)=Y(ILOC(I))
          ENDIF
   10 CONTINUE
      IF(IPSS(7).EQ.-1) THEN
```

```
            T=0.0D0
        ELSEIF(IPSS(7).EQ.0) THEN
            CALL CONVT
        ENDIF
C
C       PROTECT AGAINST NEGATIVE SURFACE CONCENTRATIONS, AND
C       AGAINST POSSIBLE DIVISIONS BY ZERO.
C
        S=1.D0-COS-OS
        IF(S .LT. 0.0D0) THEN
            SCO=0.0D0
            SO2=0.0D0
        ELSE
            IF(1.D0-OS .LE. 0.D0) THEN
                SO2=0.0D0
            ELSE
                SO2=S*(1.D0-RNY*OS)/(1.D0-OS)
            ENDIF
            IF(1.D0-COS .LE. 0.D0) THEN
                SCO=0.0D0
            ELSE
                SCO=S*(1.D0-RNX*COS)/(1.D0-COS)
            ENDIF
        ENDIF
C
C       CALCULATE THE RATE TERMS TO MINIMIZE ARITHMETIC OPERATIONS
C
        RCOD=KM1*DEXP(G1*T)*COS
        IF(IPSS(1).EQ.2) THEN
            CO=(KMA*COB+RCOD)/(KMA+K1*SCO)
        ELSE
            CO=COB
        ENDIF
        RCOA=K1*CO*SCO
        RO2A=K2*DEXP(G2*T)*O2*SO2*SO2
        RCO2=K3*DEXP(G3*T)*COS*OS
        RCOAD=RCOA-RCOD
        IF(IPSS(7).EQ.1) THEN
            OMT=1.D0-T
            DT=((B1*(RCOAD)+B2*RO2A+B3*RCO2)*OMT-B4*T)*OMT/VQO
        ENDIF
        IF(IPSS(6).EQ.0) THEN
            QN=1.D0-FCO*(RCOAD)-FO2*RO2A+FCO*RCO2
            DCO2=(-QN*CO2+RCO2 )/VQO
        ELSE
            RCO2A=K4*CO2*(1.D0-CO2S)
            RCO2D=KM4*CO2S
            QN=1.D0-FCO*(RCOAD)-FO2*RO2A
     *     +FCO*RCO2-FCO*(RCO2A-RCO2D)
            DCO2=(-QN*CO2+RCO2-RCO2A+RCO2D )/VQO
            DCO2S=A3*(RCO2A-RCO2D) /VQO
        ENDIF
        DCOB=(FCOT-QN*COB-RCOAD)/VQO
        DO2=(FO2T-QN*O2-RO2A )/VQO
```

```
      DCOS=A1*(RCOAD-RCO2)  /VQO
      DOS=(A2*RO2A-A1*RCO2  )/VQO
      DO  20  I=1,7
          IF(ILOC(I).NE.0)  THEN
              YP(ILOC(I))=XP(I)
          ENDIF
20    CONTINUE
      RETURN
      END
```

```
      SUBROUTINE CONVT
      IMPLICIT REAL (A-H,K,O-Z)
C
C     ..........................................................
C
C     SUBROUTINE CONVT
C
C     PURPOSE
C         USE THE PSEUDO-STEADY-STATE APPROXIMATION TO
C         DETERMINE THE VALUE OF THE TEMPERATURE BY SETTING
C         THE ODE FOR THE TEMPERATURE EQUAL TO ZERO, AND
C         THEN SOLVING ITERATIVELY FOR T USING NEWTON'S METHOD.
C
C     USAGE
C         CALL CONVT
C
C     DESCRIPTION OF THE PARAMETERS
C         X - VALUES OF THE DEPENDENT VARIABLES
C               THE ODE PARAMETERS ARE PASSED VIA THE NAMED COMMON BLOCKS.
C
C
C     ..........................................................
C
      COMMON /P2/ K4,KM4,A3,RNY,RNX,VQO
      COMMON /P3/ K1,KM1,K2,K3,G1,G2,G3,A1,A2,B1,B2,B3,B4,KMA
      COMMON /P6/ X(7),IPSS(7),ILOC(7)
      EQUIVALENCE (X(1),COB),(X(2),O2),(X(3),CO2)
     *,(X(4),COS),(X(5),OS),(X(6),CO2S),(X(7),T)
C
C     PROTECT AGAINST NEGATIVE SURFACE CONCENTRATIONS AND
C     POSSIBLE DIVISION BY ZERO.
C
          SCO=1.D0-COS-OS
      IF(SCO .LT. 0.0D0) THEN
          SCO=0.0D0
          SO2=0.0D0
      ELSE
          IF(1.D0-OS .LE. 0) THEN
              SO2=0.0D0
          ELSE
              SO2=(SCO)*(1.D0-RNY*OS)/(1.D0-OS)
          ENDIF
      ENDIF
      RCOD=KM1*DEXP(G1*T)*COS
      IF(IPSS(1).EQ.2) THEN
          CO=(KMA*COB+RCOD)/(KMA+K1*SCO)
      ELSE
          CO=COB
      ENDIF
      RCOA=K1*CO*SCO
      RCO2=K3*DEXP(G3*T)*COS*OS
      RO2A=K2*DEXP(G2*T)*O2*SO2*SO2
C
C     THIS WHILE-LOOP USES NEWTON'S METHOD TO ITERATIVELY
```

```
C       CONVERGE ON A VALUE OF T WHICH SATISFIES THE EQUATION
C
C           DT/DTIME = FUNCTION(TIME,X,T) = 0
C
C       IN THE FOLLOWING THE TERM DFTDT IS THE DERIVATIVE OF
C       THE ABOVE FUNCTION WITH RESPECT TO T.
C
        TS=T
   10   CONTINUE
             OMT=1.D0-T
             TDIFF=T-TS
             RCOD=RCOD*DEXP(G1*TDIFF)
             RCO2=RCO2*DEXP(G3*TDIFF)
             RO2A=RO2A*DEXP(G2*TDIFF)
             R1=B1*(RCOA-RCOD)
             R2=B2*RO2A
             R3=B3*RCO2
        R4=R1+R2+R3
             FT=((R4)*OMT-B4*T)*OMT
             DFTDT=(-2.D0*(R4)
       *              +OMT*(G3*R3-G1*B1*RCOD)-B4)*OMT+B4*T
             TS=T
             IF(DFTDT.EQ.0.0D0) THEN
                 T=TS
             ELSE
                 T=T-FT/DFTDT
             ENDIF
C
C       THE SAME ACCURACY IS REQUESTED AS IN THE INTEGRATION
C
             IF(DABS(T-TS) .GT. DABS(RER*T+AER)) GO TO 10
        RETURN
        END
```

```
SUBROUTINE SIGNA(FACTCO,FACTO2,DT,PERIOD,PLEAD)
IMPLICIT REAL (A-H,O-Z)
DIMENSION FACTCO(4),FACTO2(4),DT(4)
FACTCO(1)=-1.D0
FACTO2(1)=+1.D0
FACTCO(2)=+1.D0
FACTO2(2)=+1.D0
FACTCO(3)=+1.D0
FACTO2(3)=-1.D0
FACTCO(4)=-1.D0
FACTO2(4)=-1.D0
DT(1)=PLEAD
DT(2)=PERIOD/2.D0-PLEAD
DT(3)=PLEAD
DT(4)=PERIOD/2.D0-PLEAD
RETURN
END
```

```
SUBROUTINE SIGNB(FACTCO,FACTO2,DT,PERIOD,PLEAD)
IMPLICIT REAL (A-H,O-Z)
DIMENSION FACTCO(4),FACTO2(4),DT(4)
FACTCO(1)=-1.D0
FACTO2(1)=+1.D0
FACTCO(2)=-1.D0
FACTO2(2)=-1.D0
FACTCO(3)=+1.D0
FACTO2(3)=-1.D0
FACTCO(4)=+1.D0
FACTO2(4)=+1.D0
DT(1)=PERIOD-PLEAD
DT(2)=PLEAD-PERIOD/2.D0
DT(3)=PERIOD-PLEAD
DT(4)=PLEAD-PERIOD/2.D0
RETURN
END
```

```
      SUBROUTINE  CONV(ICYLE,NCOMP,TIME,X,Y,Z,COS,OS,CO2S,RCO2)
      IMPLICIT  REAL  (A-H,K,O-Z,$)
      DIMENSION  Z(NCOMP),COS(NCOMP),OS(NCOMP),X(NCOMP),Y(NCOMP)
      DIMENSION  CO2S(NCOMP),TIME(NCOMP)
      COMMON  /P3/  K1,KM1,K2,K3,G1,G2,G3,A1,A2,B1,B2,B3,B4,KMA
      COMMON  /PARAM2/FCO,AMPCO,FO2,AMPO2,PERIOD,PLEAD
      WRITE(8,800)  ICYLE,NCOMP
800   FORMAT(' ',I4,2X,I4)
      DO  20  I=1,NCOMP
      RATE=(K3*COS(I)*OS(I))
      WRITE(8,810)  TIME(I),X(I),Y(I),Z(I),COS(I),OS(I),RATE
810   FORMAT(9(1PD10.3))
 20   CONTINUE
      RCO2=0.0D0
      CO2AVG=0.0D0
      DO  30  I=2,NCOMP
      RATE1=(K3*COS(I-1)*OS(I-1))
      RATE2=(K3*COS(I)*OS(I))
      RCO2=RCO2+0.5D0*(RATE1+RATE2)*(TIME(I)-TIME(I-1))
      CO2AVG=CO2AVG+0.5D0*(Z(I-1)+Z(I))*(TIME(I)-TIME(I-1))
 30   CONTINUE
      RCO2=RCO2/(TIME(NCOMP)-TIME(1))
      CO2AVG=CO2AVG/(TIME(NCOMP)-TIME(1))
      WRITE(8,810)  RCO2,CO2AVG
      RETURN
      END
```

Appendix C

Steady-state multiplicity data from Chapter 5 are listed in the tables in this Appendix.

Flow rate = 205×10^{-6} mol/s

Catalyst mass = 14.6 g

Temperature = 110°C

	Increasing F_{CO}		Decreasing F_{CO}	
Feed $\%O_2$	Feed %CO	Conversion %	Feed %CO	Conversion %
1.0	0.6	52	1.	100
	.58	53	1.4	100
	.56	50	1.5	100
	.54	51	1.55	100
	.52	56	1.6	100
	.48	65	1.65	100
	.46	100	1.7	9
0.75	.5	50	1.	100
	.47	52	1.2	100
	.45	55	1.35	100
	.43	59	1.4	100
	.41	65	1.45	15
	.4	100		
0.5	.7	31	.9	100
	.4	41	.92	100
	.36	50	.94	100
	.34	33	.96	100
	.32	57	.98	16
	.3	100		
0.25	.28	38	.4	100
	.26	41	.5	100
	.24	48	.52	25
	.22	51		
	.20	59		
	.18	100		

Flow rate = 205×10^{-6} mol/s

Catalyst mass = 14.6 g

Temperature = 70°C

	Increasing F_{CO}		Decreasing F_{CO}	
Feed $\%O_2$	Feed %CO	Conversion %	Feed %CO	Conversion %
1.	.5	15.	.7	100
	.2	25	.73	100
	.18	27	.75	100
	.16	30	.78	100
	.14	34	.8	100
	.12	39	.83	100
	.1	52	.85	29*
	.09	64		
	.09	100		
.75	.2	24	.65	100
	.1	46	.68	100
	.09	55	.7	7
	.09	100		
.5	.2	17	.5	100
	.1	31	.52	100
	.09	41	.55	100
	.08	48	.57	10
	.07	59		
	.06	100		
.25	.2	19	.25	100
	.1	26	.28	100
	.08	35	.3	100
	.07	39	.32	100
	.06	42	.34	100
	.05	68	.36	70*
	.04	100		

* The conversion at this point was still falling.

Flow rate = 615×10^{-6} mol/s

Catalyst mass = 14.6 g

Temperature = 90°C

	Increasing F_{CO}		Decreasing F_{CO}	
Feed $\%O_2$	Feed %CO	Conversion %	Feed %CO	Conversion %
1.	.333	15	.4	100
	.167	33	.5	100
	.15	34	.55	100
	.14	33	.6	low*
	.13	38		
	.12	41		
	.1	100		
0.75	.167	27	.4	100
	.12	38	.45	100
	.1	52	.5	10
	.09	100		
0.5	.12	26	.25	100
	.1	30	.3	100
	.09	38	.35	100
	.08	45	.4	35*
	.07	54		
	.06	100		
0.25	.167	15	.2	100
	.1	22	.25	100
	.07	35	.3	25*
	.06	44		
	.05	61		
	.04	100		

* The conversion at this point was still falling.

Flow rate = 68×10^{-6} mol/s

Catalyst mass = 14.6 g

Temperature = 90°C

	Increasing F_{CO}		Decreasing F_{CO}	
Feed $\%O_2$	Feed %CO	Conversion %	Feed %CO	Conversion %
1.	.7	38	1.2	100
	.6	41	1.3	100
	.55	45	1.4	100
	.5	52	1.5	100
	.45	61	1.6	100
	.4	100	1.7	100
			1.8	49*
.75	.6	41	1.	100
	.5	45	1.2	100
	.4	62	1.3	100
	.35	100	1.35	15
.5	.5	34	.7	100
	.4	40	.75	100
	.35	55	.8	100
	.3	100	.9	100
			.95	100
			1.0	45*
.25	.35	35	.5	100
	.3	39	.6	33*
	.25	51		
	.2	77		
	.18	100		

* The conversion at this point was still falling.

Flow rate = 615×10^{-6} mol/s

Catalyst mass = 43.6 g

Temperature = 90°C

	Increasing F_{CO}		Decreasing F_{CO}	
Feed $\%O_2$	Feed %CO	Conversion %	Feed %CO	Conversion %
.9	.5	20	1.	100
	.33	33	1.02	100
	.28	40	1.04	100
	.26	41	1.09	50*
	.23	49		
	.21	62		
	.19	100		
.65	.28	35	.77	100
	.23	39	.83	100
	.21	48	.87	61*
	.19	59		
	.17	100		
.4	.22	46	.56	100
	.2	42	.61	100
	.18	42	.67	55*
	.16	52		
	.13	100		
.15	.22	30	.22	100
	.17	34	.28	100
	.13	38	.31	100
	.11	46	.33	54*
	.09	100		

* The conversion at this point was still falling.

Flow rate = 68×10^{-6} mol/s

Catalyst mass = 4.95 g

Temperature = 90°C

	Increasing F_{CO}		Decreasing F_{CO}	
Feed $\%O_2$	Feed %CO	Conversion %	Feed %CO	Conversion %
1.09	.5	37	1.2	100
	.4	53	1.3	100
	.35	58	1.4	100
	.3	100	1.5	100
			1.6	16
0.85	.28	33	1.	100
	.22	41	1.1	100
	.19	100	1.2	100
			1.3	5
0.61	.4	29	.8	100
	.3	30	.9	100
	.25	30	1.	10
	.2	57		
	.15	100		
.36	.25	22	.5	100
	.19	35	.6	100
	.16	49	.7	low*
	.13	100		

* The conversion at this point was still falling.

Flow rate = 205×10^{-6} mol/s

Catalyst mass = 14.6 g

Temperature = 90°C

	Increasing F_{CO}		Decreasing F_{CO}	
Feed $\%O_2$	Feed %CO	Conversion %	Feed %CO	Conversion %
1.	.5	24	1.	100
	.4	30	1.05	100
	.3	45	1.1	100
	.25	56	1.15	100
	.2	100	1.2	100
			1.25	100
			1.3	14
0.75	.5	24.	.8	100
	.3	40	.85	100
	.25	44	.9	100
	.22	54	.95	100
	.2	100	1.	100
			1.05	13
0.5	.25	38	.5	100
	.2	45	.7	100
	.18	53	.725	100
	.16	62	.75	100
	.14	100	.775	100
			.8	19
0.25	.2	30	.36	100
	.16	38	.4	100
	.14	43	.44	100
	.12	58	.48	100
			.5	100
			.51	low*

* The conversion at this point was still falling.

Appendix D

Time-average conversion data for 180-degree out-of-phase cycling as presented in Chapter 6 are tabulated in this Appendix.

The transient data (instantaneous CO_2 concentration versus time, at 1 s intervals) from this thesis are available as a set of MS-DOS compatible diskettes from Professor D. T. Lynch of the Department of Chemical Engineering of the University of Alberta. The set of diskettes contains dynamic data from approximately 250 runs, including both 180-degree out-of-phase experiments and experiments to determine the effect of phase angle between inputs. These data are available for a charge of $150 to cover the cost of the diskettes, copying, shipping and handling.

Temperature = 90°C

Flow rate = 205×10^{-6}

Catalyst mass = 14.6 g

Feed O_2 = 0.5 ± 0.5 %

Feed CO = 1.0 ∓ 1.0 %

Cycle Period (s)	Time-Average Fractional Conversion
300.	.517
240.	.543
210.	.513
270.	.527
900.	.224
900.	.218
240.	.551
190.	.483
600.	.254
180.	.466
1800.	.097
170.	.495
450.	.336
170.	.436
160.	.425
150.	.062
155.	.054
360.	.418
330.	.439
140.	.057

Temperature = 90°C

Flow rate = 68×10^{-6}

Catalyst mass = 14.6 g

Feed O_2 = 0.5 ± 0.5 %

Feed CO = 1.0 ∓ 1.0 %

Cycle Period (s)	Time-Average Fractional Conversion
360.	.552
300.	.171
280.	.169
1800.	.294
2400.	.228
1200.	.400
450.	.711
600.	.677
400.	.650
380.	.618
420.	.634
500.	.671
550.	.667
750.	.584
900.	.519
320.	.138
340.	.156
600.	.669

Temperature = 90°C

Flow rate = 615×10^{-6}

Catalyst mass = 14.6 g

Feed O_2 = 0.5 ± 0.5 %

Feed CO = 1.0 ∓ 1.0 %

Cycle Period (s)	Time-Average Fractional Conversion
180.	.302
150.	.329
120.	.379
90.	.444
80.	.425
70.	.365
60.	.028
100.	.403
110.	.380
65.	.032
360.	.148
300.	.174
240.	.205
75.	.411

Temperature = 110°C

Flow rate = 205×10^{-6}

Catalyst mass = 14.6 g

Feed O_2 = 0.5 ± 0.5 %

Feed CO = 1.0 ∓ 1.0 %

Cycle Period (s)	Time-Average Fractional Conversion
180.	.634
110.	.500
120.	.571
105.	.130
150.	.628
600.	.270
360.	.407
270.	.492
190.	.575
170.	.599
115.	.486
130.	.578
180.	.597
360.	.384
600.	.205
110.	.472

Temperature = 70°C

Flow rate = 205×10^{-6}

Catalyst mass = 14.6 g

Feed O_2 = 0.5 ± 0.5 %

Feed CO = 1.0 ∓ 1.0 %

Cycle Period (s)	Time-Average Fractional Conversion
650.	.220
650.	.214
260.	.384
250.	.375
330.	.389
420.	.356
360.	.371
600.	.189
300.	.375
240.	.381
1200.	.149
270.	.382
230.	.336
210.	.032

Temperature = 90°C

Flow rate = 615×10^{-6}

Catalyst mass = 43.6 g

Feed O_2 = 0.5 ± 0.5 %

Feed CO = 1.0 ∓ 1.0 %

Cycle Period (s)	Time-Average Fractional Conversion
900.	.051
300.	.354
180.	.582
150.	.671
100.	.625
600.	.168
90.	.547
80.	.525
70.	.410
60.	.069
65.	.363
62.	.072
450.	.242
200.	.535
240.	.482
270.	.412
360.	.319
110.	.650
120.	.665
130.	.702
120.	.668

Temperature = 90°C

Flow rate = 68×10^{-6}

Catalyst mass = 4.95 g

Feed O_2 = 0.5 ± 0.5 %

Feed CO = 1.0 ∓ 1.0 %

Cycle Period (s)	Time-Average Fractional Conversion
1200.	.262
2400.	.145
600.	.377
700.	.368
500.	.072
800.	.338
900.	.314
550.	.383
1000.	.267
520.	.390
510.	.091

Appendix E

Time-average conversion data for variable phase angle cycling as presented in Chapter 6 are tabulated in this Appendix.

The transient data (instantaneous CO_2 concentration versus time, at 1 s intervals) from this thesis are available as a set of MS-DOS compatible diskettes from Professor D. T. Lynch of the Department of Chemical Engineering of the University of Alberta. The set of diskettes contains dynamic data from approximately 250 runs, including both 180-degree out-of-phase experiments and experiments to determine the effect of phase angle between inputs. These data are available for a charge of $150 to cover the cost of the diskettes, copying, shipping and handling.

Temperature = 90°C

Flow rate = 205×10^{-6}

Catalyst mass = 14.6 g

Feed O_2 = 0.5 ± 0.5 %

Feed CO = 1.0 ∓ 1.0 %

Period = 100 s

Oxygen Phase Lead (fraction of cycle, degrees/360))	Time-Average Fractional Conversion
.5	.054
.6	.052
.7	.056
.8	.04
.9	.055
1.	.06
0.	.06
.4	.064
.2	.056

Temperature = 90°C

Flow rate = 205×10^{-6}

Catalyst mass = 14.6 g

Feed O_2 = 0.5 ± 0.5 %

Feed CO = 1.0 ∓ 1.0 %

Period = 120 s

Oxygen Phase Lead (fraction of cycle, degrees/360))	Time-Average Fractional Conversion
.75	.878
.833	.867
.92	.057
.0	.052
1.	.052
.25	.058
.33	.061
.792	.87
.875	.887
.922	.059
.708	.81
.66	.765
.625	.687
.583	.597
.542	.075

Temperature = 90°C

Flow rate = 205×10^{-6}

Catalyst mass = 14.6 g

Feed O_2 = 0.5 ± 0.5 %

Feed CO = 1.0 ∓ 1.0 %

Period = 160 s

Oxygen Phase Lead (fraction of cycle, degrees/360))	Time-Average Fractional Conversion
.5	.558
.375	.301
.25	.05
.125	.042
0.	.038
1.	.038
.875	.76
.75	.896
.625	.798
.562	.679
.81	.779

Temperature = 90°C

Flow rate = 205×10^{-6}

Catalyst mass = 14.6 g

Feed O_2 = 0.5 ± 0.5 %

Feed CO = 1.0 ∓ 1.0 %

Period = 180 s

Oxygen Phase Lead (fraction of cycle, degrees/360))	Time-Average Fractional Conversion
.5	.66
.44	.58
.94	.07
.55	.727
.61	.796
.666	.862
.75	.923
.83	.944
.88	.917
.92	.068
.39	.402
.333	.282
.222	.07
.28	.070

Temperature = 90°C

Flow rate = 205×10^{-6}

Catalyst mass = 14.6 g

Feed O_2 = 0.5 ± 0.5 %

Feed CO = 1.0 ∓ 1.0 %

Period = 240 s

Oxygen Phase Lead (fraction of cycle, degrees/360))	Time-Average Fractional Conversion
.5	.555
.42	.505
.33	.42
.25	.252
.167	.06
.58	.638
.667	.737
.75	.85
.83	.893
.92	.77
.958	.08
.938	.61
.0	.06
1.	.06
.083	.054

Temperature = 90°C

Flow rate = 205×10^{-6}

Catalyst mass = 14.6 g

Feed O_2 = 0.5 ± 0.5 %

Feed CO = 1.0 ∓ 1.0 %

Period = 360 s

Oxygen Phase Lead (fraction of cycle, degrees/360))	Time-Average Fractional Conversion
.5	.419
.25	.34
.125	.097
.375	.366
.75	.745
.875	.876
.916	.736
.944	.55
.972	.295
.986	.083
.666	.579
.208	.306
.792	.795
.833	.855
.583	.505
.625	.558
.541	.466
.708	.687
.333	.39
.166	.223
.416	.401
.041	.065
.292	.360
.458	.393

Temperature = 90°C

Flow rate = 205×10^{-6}

Catalyst mass = 14.6 g

Feed O_2 = 0.5 ± 0.5 %

Feed CO = 1.0 ∓ 1.0 %

Period = 900 s

Oxygen Phase Lead (fraction of cycle, degrees/360))	Time-Average Fractional Conversion
.5	.19
.33	.165
.16	.18
.11	.192
.0	.054
1.	.054
.666	.41
.833	.530
.89	.444
.978	.266